CHEMICAL REVIEWS

Review

Cite This: *Chem. Rev.* 2019, 119, 5461−5533

pubs.acs.org/CR

Bio-Integrated Wearable Systems: A Comprehensive Review

Tyler R. Ray,[†,∥] Jungil Choi,[†,∥] Amay J. Bandodkar,[†,∥] Siddharth Krishnan,[†] Philipp Gutruf,[‡] Limei Tian,[§] Roozbeh Ghaffari,[†] and John A. Rogers*[,†]

[†] Northwestern University, 2145 Sheridan Road, Evanston, Illinois 60208, United States

[‡]Department of Biomedical Engineering University of Arizona Tucson, Arizona 85721, United States

[§]Department of Biomedical Engineering, Texas A&M University, College Station, Texas 77843, United States

ABSTRACT: Bio-integrated wearable systems can measure a broad range of biophysical, biochemical, and environmental signals to provide critical insights into overall health status and to quantify human performance. Recent advances in material science, chemical analysis techniques, device designs, and assembly methods form the foundations for a uniquely differentiated type of wearable technology, characterized by noninvasive, intimate integration with the soft, curved, time-dynamic surfaces of the body. This review summarizes the latest advances in this emerging field of "bio-integrated" technologies in a comprehensive manner that connects fundamental developments in chemistry, material science, and engineering with sensing technologies that have the potential for widespread deployment and societal benefit in human health care. An introduction to the chemistries and materials for the active components of these systems contextualizes essential design considerations for sensors and associated platforms that appear in following sections. The subsequent content highlights the most advanced biosensors, classified according to their ability to capture biophysical, biochemical, and environmental information. Additional sections feature schemes for electrically powering these sensors and strategies for achieving fully integrated, wireless systems. The review concludes with an overview of key remaining challenges and a summary of opportunities where advances in materials chemistry will be critically important for continued progress.

CONTENTS

Received: September 18, 2018
Published: January 28, 2019

DOI: 10.1021/acs.chemrev.8b00573
Chem. Rev. 2019, 119, 5461−5533

1. INTRODUCTION

Natural physiological processes create a diverse range of biophysical (temperature, biopotential, motion) and biochemical (electrolytes, metabolites) signals that can be measured and quantified with body-integrated sensors. The resulting information is critically valuable in developing insights into health status, quantifying human performance, and in establishing bidirectional communication channels for human/machine control interfaces. The most advanced noninvasive physiological monitoring systems utilize sophisticated electronic recording hardware with wired interfaces to sensors that couple to the skin via straps/tapes. Operation typically involves expert personnel in clinical or laboratory settings. Although capable of precise measurements of parameters that have well-established, deep clinical significance, such systems are cumbersome and generally cannot be used for long-term, continuous monitoring outside of specialized facilities.

Wearable devices, typically in the form of small, rigid blocks of wireless electronic/sensing components loosely coupled to the wrist, offer some potential to address these limitations as a paradigm shift in physiological monitoring. These devices, which owe their existence primarily to the relentless miniaturization of integrated circuits via Moore's Law scaling,[1] can yield estimates of certain basic vital signs (heart rate, skin temperature) and they can record physical motions, typically of the wrist or chest, all without the wired, bulky hardware of clinical systems. Even though the parameters that can be measured with such systems are narrow in scope and have low levels of clinical relevance/accuracy, the established commercial market for consumer health wearables is large, and it is projected to grow to $30 billion annually by 2020.[2] Continued advances in electronics, optoelectronics, sensing components, wireless communication hardware, and battery technology will drive progress in this segment, although in a largely linear, predictable fashion with limited potential for qualitative improvements in functionality.

The inability to form stable, intimate skin interfaces with the classes of planar, rigid components that constitute these wearable systems remains a fundamental constraint in their measurement capabilities. For applications in fitness and wellness, where regulatory oversight is minimal, these restrictions do not impede the public adoption of such consumer health wearables for simple measurements of basic parameters such as heart rate.[3] For example, heart rate monitoring in laboratory environments with such devices offer acceptable performance in recreational applications.[4,5] Some products (Apple Watch in particular) can achieve accuracy comparable to clinical chest-mounted monitors for patients at rest or during low intensity exercise. The latest version of this platform, in fact, offers electrocardiogram recording capabilities that are approved by the US Federal Drug Administration, although only for momentary measurements due to requirements for touching the rim of the device with the opposite hand. Nevertheless, even the most accurate wrist-mounted systems fail during moderate daily physical activities or in continuous monitoring,[5−7] due largely to motion induced artifacts that arise from loose coupling to the body.[6−8] Most studies focus on device function rather than clinical performance[7,9] and lack standardized evaluation methodologies.[9,10] The development of technologies that overcome limitations associated with loose skin interfaces and incorporate advanced biochemical/biophysical sensing have the potential to transform consumer wearables from recreational novelty devices into body-worn, clinical-grade physiological measurement tools that yield physician actionable information.

Recent advances in material science, chemical analysis techniques, device designs, and manufacturing methods form the foundations for a distinctly different type of wearable technology, characterized their noninvasive, intimate integration with the curved surfaces of the body, from the skin and the cornea to the fingernails and the tissues of the mouth. The consequences are significant in terms of both the types of measurements that are possible and the accuracy/reliability of the resulting data.[11] These modes of deployment follow naturally from the soft, flexible form factors of these systems, as robust, nonirritating interfaces for clinical quality capabilities in biophysical and biochemical measurements. When taken together with advanced modalities for noninvasive biosensing, widespread adoption of smartphones, and the availability of low-power wireless communication systems and high capacity energy storage technologies, this type of bio-integrated platform is at the cusp of an inflection point toward broad adoption, with significant potential for societal benefit.

This review highlights the latest advances in this emerging field of "bio-integrated" technologies, with particular emphasis on materials and chemistry concepts that have the potential to shape the directions of future developments. Other reviews examine the field in the context of specific applications (biophysical[12−14] or biochemical[15−18] monitoring, medicine[19]), form factors,[20−23] sensing technologies (general,[24−26] strain,[27−29] electrochemical,[30−33] temperature[34]), power sources (general,[35] supercapacitors,[36−39] energy harvesting,[40,41] biofuel cells[42]), wireless communication technologies,[43] material systems (polymers,[44,45] carbon,[46−48] graphene,[49] hydrogels,[50,51] liquid metal,[52] bio-inspired,[53] and biological[54,55]), and fabrication methods (electrodes,[56,57] sensors,[58−60] and components[61,62]). By contrast, this review examines advances in bio-integrated technologies in a comprehensive manner that connects fundamental developments in material science and engineering with modalities in sensing physiological signals that have the potential for widespread deployment and societal benefit in human healthcare. A short introductory section on the chemistries and materials for the active electronic components of these systems contextualizes essential design considerations for sensors and associated platforms that appear in subsequent sections. The second part highlights the most advanced biosensors, classified according to their ability to measure biophysical, biochemical, and environmental information. Additional sections feature schemes for electrically powering these sensors and strategies for achieving fully integrated, wireless systems. The review concludes with an overview of key remaining challenges and a summary of opportunities where advances in materials chemistry will be critically important for continued progress.

2. MECHANICS AND MATERIALS FOR BIO-INTEGRATED WEARABLE SYSTEMS

The direct integration of sensors with the soft and curvilinear surfaces of the human body demands careful attention to materials design to ensure seamless, noninvasive interfaces that

DOI: 10.1021/acs.chemrev.8b00573
Chem. Rev. 2019, 119, 5461−5533

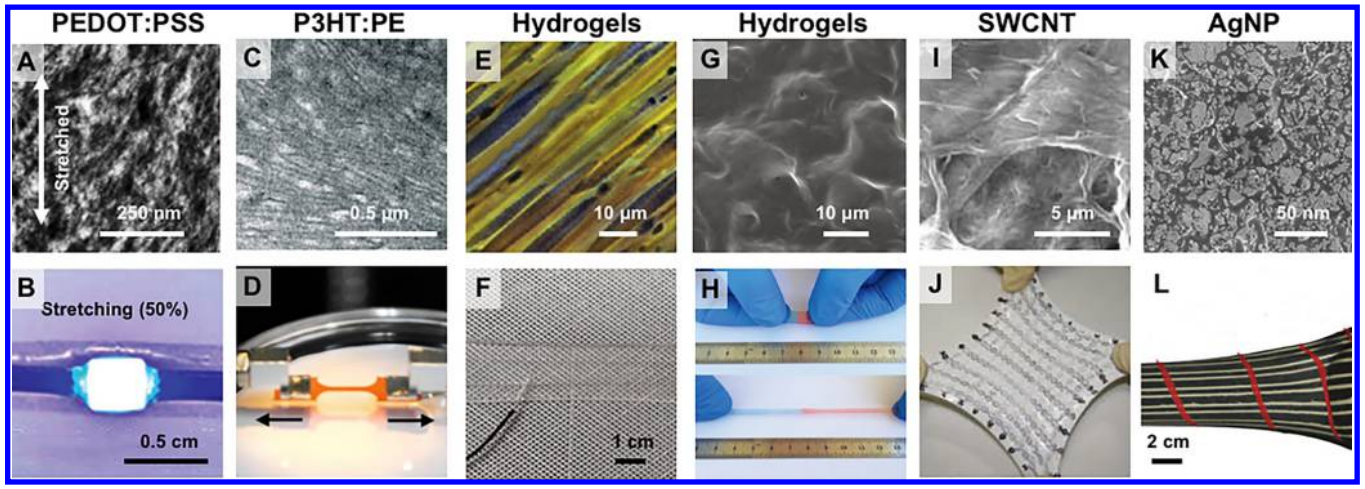

Figure 1. Concepts in materials synthesis for stretchable electronics and bio-integrated wearable sensors. (A) AFM height images of a stretched (25%) PEDOT:PSS film containing 1% polytetrafluoroethylene resin on PDMS. Reprinted with permission from ref 71. Copyright 2011 American Chemical Society. (B) Optical image of a stretchable device fabricated with PEDOT:PSS containing a nonvolatile surfactant plasticizer on a PDMS substrate. Reprinted with permission from ref 72. Copyright 2015 Wiley-VCH Verlag GmbH & Co. KGaA. (C) TEM image of P3HT:PE showing PE single-crystal-like entities that form when the insulating block crystallizes first. Reprinted with permission from ref 73. Copyright 2007 Wiley-VCH Verlag GmbH & Co. KGaA. (D) Optical image of a stretchable film of P3HT containing poly(2-vinylpyridine. Reprinted with permission from ref 74. Copyright 2014 American Chemical Society. (E) Optical micrographs of a microgel-reinforced hydrogel film stretched by 100%. Reprinted with permission from ref 75. Copyright 2012 Elsevier. (F) Optical image of a slime-type poly(vinyl alcohol) material cross-linked with sodium borate and stretched by 700%. Reprinted with permission from ref 76. Copyright 2017 Wiley-VCH Verlag GmbH & Co. KGaA. (G) SEM image of poly(vinylidene fluoride-*co*-hexafluoropropylene) with 43 wt % 1-ethyl-3-methylimidazolium trifluoromethanesulfonate and (H) optical image of a healed sample from an undeformed to a stretched (500%) state. (G,H) Reprinted with permission from ref 77. Copyright 2017 Wiley-VCH Verlag GmbH & Co. KGaA. (I) SEM image of a film composed of SWCNTs, polymer matrix, and ionic liquid, and (J) optical image of biaxially stretched organic transistor-based active matrix with 19-by-37 unit cells. (I,J) Reprinted with permission from ref 78. Copyright 2008 the American Association for the Advancement of Science. (K) Surface SEM images of elastic conductors formed from silver flakes and rubber with surfactant and (L) sensor networks on textiles stretched by 120%. (K,L) Reprinted with permission from ref 79. Copyright 2017 Springer Nature.

are robust during natural movements and associated biological processes. The most well-developed materials for conventional planar electronic devices are inorganic, and their high modulus, brittle mechanical properties are inherently ill-suited for bio-integration.[63] Broad research efforts seek to establish alternative materials and device designs that bypass these limitations in form and mechanics but without sacrificing options in functionality or performance. Flexible devices, as defined by those that can bend in a reversible fashion, are useful in this context. Such mechanics can be achieved in any material simply through reductions in thickness due to associated cubic and linear decreases in the bending rigidity and the linear bending induced strain, respectively.[64] Materials ranging from nanomembranes/nanowires/nanoribbons of monocrystalline silicon to polycrystalline thin films of conjugated small-molecule organics represent options in the semiconductor components of such types of thin, flexible devices. Many other materials, from electrical conductors to dielectrics and responsive elements of biosensors, can be deployed in similar thin film formats to yield complete systems on lightweight, plastic foils.[65] Although the ability to flex enables effective integration across small regions of the body or onto those with simple, gradual curvature, the complex textures of the skin and its natural motions cannot be accommodated in a general sense by bending alone. Here, stretchability, as defined by linear elastic responses to large strain deformations, is critically important. This mechanical characteristic requires advanced materials and designs, beyond those that simply rely on thickness reduction.

The most successful strategies to stretchable functional materials rely on specialized synthetic materials/composites or on heterogeneous collections of material micro/nanostructures. The first, as a chemical synthetic strategy, involves materials that are intrinsically stretchable based on specially formulated organic or inorganic chemistries. The second, as an engineering approach, exploits deterministic composites that combine ultrathin, typically nanoscale, wires, membranes, ribbons, or platelets of established, high performance materials (e.g., silicon, metals) with soft substrates/superstrates to yield systems with effective stretchability. This section illustrates these two schemes through some of the most recent examples and the most widely adopted platforms, with an emphasis on electronically conducting and semiconducting materials. Other contemporary reviews provide related, complementary content.[22,53,56−58,61,66,67] An additional discussion highlights the various locations on the body that can serve as points for integration of devices constructed with these materials.

2.1. Functional Electronic Materials for Stretchable Electronics and Bio-Integrated Wearable Sensors

2.1.1. Materials: Synthesis. The synthetic approach to stretchable electronic materials exploits specialized chemistries and their composites, as classified into one of three main categories: (1) intrinsically stretchable polymers, (2) conductive hydrogels and ionogels (a colloid of ionic liquid in a polymeric network), and (3) bulk or laminar composites of active materials and dielectric elastomers such as, silicones,[68] polyurethanes (PU),[69] and copolymers (e.g., styrene−butadiene−styrene block copolymer[70]).

By comparison to high modulus inorganics, organic materials such as conducting and semiconducting polymers are attractive due to their ability to combine soft, biocompatible characteristics with a range of chemical functionality for electronic transport and tailored mechanical and optical properties. A well-

DOI: 10.1021/acs.chemrev.8b00573
Chem. Rev. 2019, 119, 5461−5533

studied conductive polymer of interest in this context is poly(3,4-ethylenedioxythiophene) polystyrenesulfonate (PEDOT:PSS)[44] Although the neat polymer is not itself deformable to an appreciable extent,[80] plasticizing additives such as nonionic surfactants[72,82] and ionic liquids,[82] impart an effective level of stretchability when the material is coupled to a supporting elastomer substrate to provide an elastic restoring force. As an example, PEDOT:PSS plasticized with polytetrafluoroethylene resin, a fluoropolymer additive, bonded to a silicone substrate maintains conductivity and an elastic mechanical response for strains up to ∼188%[71] without adhesive failure or delamination (Figure 1A). Similarly, polyethylene glycol *tert*-octylphenyl ether, a nonionic additive, yields a deformable, "dough-like" form of PEDOT:PSS[72] that can be reversibly molded with minimal degradation of electrical performance, even under extreme deformations (Figure 1B). One disadvantage of such additives is that they reduce the conductivity relative to that of the neat polymer. Ionic liquid additives avoid this drawback[82] to yield stretchable materials with conductivities over 4100 S cm^{-1}, higher than the values for commercial PEDOT:PSS (∼1000 S cm^{-1}), with the additional ability to endure strains of up to 100%.

The toxicity of common fluoropolymer surfactants and ionic liquids impedes utilization of conductive polymers in bio-integrated platforms. Block copolymer scaffolds offer an alternative, biocompatible route to stretchable forms of PEDOT.[83] One example combines soft segments of poly(polyethylene glycol methyl ether acrylate) and hard segments of polystyrenesulfonate (PSS) to form an appropriate copolymer by a reversible addition−fragmentation chain transfer polymerization. This block elastomer serves as a matrix for the polymerization of PEDOT. Although the conductivity of the resulting material (∼0.046 S cm^{-1}) is much lower than that of commercial PEDOT:PSS (without dopant, ∼7.4 S cm^{-1}; with dopant, ∼1000 S cm^{-1}), this additive-free system accommodates strains up to 128%, which is more than a factor of 10 higher than that of the neat PEDOT.[84,85] The addition of 5 wt % glycerol as a biocompatible, secondary dopant[83] increases the conductivity of the PEDOT:copolymer scaffold by more than an order of magnitude, to ∼0.63 S cm^{-1}.

Intrinsically stretchable semiconducting polymers represent another important class of material.[86] Primary routes to stretchable mechanics include copolymerization[73] and introduction of side chain chemical moieties.[87] These methods disrupt the order of the crystalline structure of the semiconducting polymer, thereby increasing deformability, but at the expense of reducing the field-effect mobility. A representative example of an intrinsically stretchable semiconducting polymer follows from copolymerization of poly(3-hexylthiophene) (P3HT) and polyethylene (PE) to obtain a material with high deformability (up to 600%) and a mobility comparable to pristine P3HT (0.02 cm^2 V^{-1} s^{-1} for 10:90 P3HT:PE; 0.01 cm^2 V^{-1} s^{-1} for pristine P3HT with a stretchability of ∼13%) (Figure 1C).[73] Others leverage similar strategies to synthesize block copolymers of P3HT with poly(2-vinylpyridine),[74] poly(methyl acrylate),[88] and poly(3-octylthiophene-2,5-diyl)[89] (Figure 1D). Incorporating side chain moieties represents an alternative approach.[87] In one example, binding 2,6-pyridine dicarboxamide (10 mol %) to a 3,6-di(thiophen-2-yl)-2,5-dihydropyrrolo[3,4-*c*]pyrrole-1,4-dione-based semiconducting polymer introduces weak intrapolymer hydrogen bonding without significantly degrading the mobility.[90] The hydrogen bonds break under strain and absorb most of the energy with minimal deformation of the semiconducting polymer backbone. These broken bonds heal rapidly, thereby largely restoring the original polymer properties. This unique energy dissipation mechanism leads to high field-effect mobility performance (>1 cm^2 V^{-1} s^{-1}) even after a hundred cycles of stretching to 100% strain. Recent review articles highlight these and other related strategies to stretchable semiconducting polymers.[91,92]

Hydrogels and ionogels form a second category of stretchable active materials, noteworthy because they closely mimic the mechanical, chemical, and optical properties of biological tissues.[93] These types of systems exploit ionic mobility to achieve conduction, similar to that in biology. Conductive hydrogels are of particular interest, relative to ionogels, due to their biocompatibility. Recent advances in gel synthesis provide access to materials with Young's moduli from kilopascals to megapascals, suitable for a wide range of wearable applications, with levels of physical toughness that satisfy requirements for practical applications. Most chemical strategies to such systems use designs that facilitate rapid, isotropic dissipation of energy generated during mechanical deformation with minimal damage to the polymeric network.[94] Double-network hydrogels,[94,95] one class of tough hydrogels, rely on two polymers. The first provides a highly cross-linked network for structural integrity. The second, a loosely cross-linked polymer, offers sufficient fluidity to accommodate stress without damage to the structural network. A rich variety of polymer combinations can be used, including collagen or agarose as the first network and poly(2-hydroxyethyl methacrylate) or poly(*N*,*N*′-dimethyl acrylamide) as the second.[75] A double network hydrogel of poly(2-acrylamido-2-methylpropanesulfonic acid) (4 mol %) and polyacrylamide (2 mol %) is a representative example, where the tensile strength of 17.2 MPa is almost 20 times higher than that of hydrogels from individual polymers.[96] Although such gels contain ∼90 wt % water, the tearing energy is ∼4400 J/m^2, several thousand times that of single network hydrogels from individual polymers (Figure 1E,F).[75]

Alternative routes to tough, conductive hydrogels utilize a rich library of polymers, including polyacrylamide,[97] poly(*N*,*N*-dimethylacrylamide),[98] poly(vinyl alcohol),[99] poly(acrylic acid)/alginate,[100] and poly acrylic acid-*co*-3-dimethyl (methacryloyloxyethyl) ammonium propanesulfonate.[101] One approach cross-links poly(vinyl alcohol) with sodium borate to yield a slime-type, highly stretchable, transparent conductive gel that can accommodate strains as high as 700% (Figure 1G,H).[76] Supramolecular chemistry approaches offer means to realize tough hydrogels with skin-like, self-healing features. A recent example includes a bio-inspired supramolecular mineral hydrogel of amorphous calcium carbonate nanoparticles physically cross-linked by poly(acrylic acid) and alginate chains.[100] The rapid cross-linking by the poly(acrylic acid) and alginate chains enable rapid self-healing (within 20 min) and the ability to maintain conductivity for strains as large as 1000%. An additional example is in supramolecular chemistry-based stretchable, self-healing polyelectrolyte hydrogels of poly acrylic acid-*co*-3-dimethyl (methacryloyloxyethyl) ammonium propanesulfonate.[101] In contrast to the traditional polyacrylamide tough hydrogels, this system offers attractive material properties for bio-integrated devices including autonomous self-healing capability and recyclability.

Key challenges with hydrogels are in achieving strong adhesion to other materials and in avoiding gradual changes in properties due to evaporation of water. Recent work seeks chemical routes to adhesion energies that can reach values

DOI: 10.1021/acs.chemrev.8b00573
Chem. Rev. 2019, 119, 5461−5533

within the range of the material fracture energies (>1000 J m^{-2}).[102] Promising chemistries for bonding to silicone elastomers include UV/plasma treatment of the elastomer[103] and cyanoacrylate,[104] benzophenone,[105] or silanes[106] to form covalent interfacial linkages.[104] To slow evaporation, humectants can be added to the hydrogels, and traditional elastomers can be used as encapsulants. Advanced approaches replace water with room temperature ionic liquids, as exceptionally low vapor pressure liquids, to yield conductive gels (ionogels) with stability against evaporative drying. Common approaches for synthesizing conductive, stretchable ionogels include encapsulating ionic liquids such as ethylammonium nitrate,[107,108] 1-ethyl-3-methylimidazolium trifluoromethanesulfonate,[77] and 1-ethyl-3-methylimidazolium bis(trifluoromethylsulfonyl)-imide[109] into elastomeric networks such as poly(ethylene oxide)−poly(propylene oxide)−poly(ethylene oxide) triblock copolymer[107] and poly(vinylidene fluoride-*co*-hexafluoropropylene),[77,109] as discussed elsewhere.[110] As mentioned previously, the toxicity of most ionic liquids represents a major limitation to their use in bio-integrated applications. A recently reported choline-based ionogel offers a biocompatible alternative via the encapsulation of a synthesized choline ionic liquid and gelatin methacryloyl within a polycaprolactone polymer network.[111] This biocompatible material exhibits a conductivity of ∼5.16 × 10^{-5} S cm^{-1} and can withstand strains up to 40% with negligible degradation of conductivity.

Composite materials represent the third, and most research active, approach. Stretchable composites adopt either a bulk fill or laminar form. In bulk, charge transport occurs through percolation pathways within a material or a collection of material micro/nanostructures that serves as a conductive filler embedded in an insulating elastomeric matrix. Here, the former supports the electronic functionality and the latter defines the elastic mechanics. The compositional ratio between these two components determines the percolation threshold, which dictates the point at which the bulk material becomes conductive[112] and is inversely related to the aspect ratio, surface area, and dispersion of the conductive filler.[113,114] Anisotropic nanoparticle fillers can increase the conductivity of bulk polymer materials by ∼10^{8}−10^{12} S cm^{-1} at low volume concentrations (<1%) relative to those with spherical geometries owing to this decrease in the percolation threshold.[115] Functional nanoparticles,[116−121] nanowires/tubes/ribbons,[122−126] membranes/sheets,[127−129] and 3D networks[130−132] of carbonaceous, metallic nanomaterials and/or conducting polymers[133,134] represent the most widely explored conductive filler materials.

Foundational work in the context of stretchable electronics[78,123,135,136] relies on highly conductive, single-walled carbon nanotubes (SWCNTs). The high aspect ratios of supergrowth SWCNTs (>1 mm in length, and 3 nm in diameter) support long, highly flexible conductive pathways with superior properties compared to conventional low aspect ratio (length, ∼1 μm; diameter, <1 nm) SWCNTs grown using methods such as the high-pressure carbon monoxide process. The original materials use thick bucky gels of supergrowth SWCNTs in an ionic liquid 1-butyl-3-methylimidazolium bis(trifluoromethanesulfonyl)imide formed by a grinding process. Subsequent dispersion into a vinylidene fluoride−hexafluoropropylene copolymer suspension and casting onto a flat glass plate yields films that are highly conductive (∼53 S cm^{-1}) and stretchable to strains up to 38% (Figure 1I,J).[78] Although commercially available carbon-based elastomers exhibit much higher stretchability (∼150%), their conductivity is comparatively low (∼0.1 S cm^{-1}). Specialized formulations of this composite yield screen-printable elastomeric inks[123] with enhanced conductivities (102 S cm^{-1}) and levels of stretchability (up to 29%). Other bulk fill composite materials rely on multiwalled carbon nanotubes (MWCNTs),[137,138] graphene,[129] and graphene/CNT blends.[139,140]

These same materials can also be used as the primary conductive constituent in laminar composites. Such designs can offer superior electrical properties compared to bulk counterparts due to the absence of an insulating component within the active layer and ability to support thin film geometries. A popular approach embeds thin films of carbon nanomaterials between layers of elastomeric material by either the physical transfer or direct deposition of prefabricated films onto elastomeric membranes.[141−143] Studies of such laminar composites reveal that reversible, nonlinear buckling of the nanomaterials is an important feature in the mechanics of most such systems, where well-defined sinusoidal structures of SWNTs on elastomeric substrates represent examples[124,144,145] that can be predictively modeled using Newtonian mechanics.[146] The laminar approach to composites is especially favorable for obtaining thin film stretchable semiconductor based on carbon nanomaterials for transistors and other devices.[141,143]

The use of nanostructures of metals, such as silver, in place of carbon nanomaterials, can yield composites with improved properties as conductors.[147,148] An exemplary case uses silver nanoparticles (AgNP) in a bulk fill composite to yield high stretchability (strains up to 400%) and conductivity (935 S cm^{-1}) (Figure 1K,L).[79] The synthesis yields nanoparticles (∼8 nm diameter) from a precursor of microscale silver flakes, in situ, in a vinylidene fluoride/hexafluoropropylene fluorine rubber with a hydrophilic ethylene oxide group and a fluorophyllic perfluoroalkyl group-based surfactant. The fluorine rubber provides excellent stretchability, environmental stability, and a high polarity to attract metal ions. The fluoro-surfactant ensures a homogeneous suspension of the flakes. Dissolution in methylisobutylketone yields a printable ink (14.5 Pa s at a shear rate of 10 s^{-1}). The result is a material with an exceptionally high conductivity for a stretchable composite (4000 S cm^{-1} at 0% strain, 935 S cm^{-1} at strains up to 400%), significantly larger than that possible by direct dispersion of silver nanoparticles into an elastomeric matrix.

In addition to nanoparticles, silver nanowires (AgNW) offer a promising filler material for stretchable conductive composites due to the aspect ratio-induced lowered percolation threshold and the high ductility of bulk silver, resulting in superior electrical properties under strain.[149] Although several AgNW-based bulk composites exist,[150,151] most work focuses on laminar designs.[152−154] In one example of a bulk system, AgNWs form via the common polyol process with a subsequent ligand exchange reaction to partially replace the polyvinylpyrrolidone capping agent with hexylamine for homogeneous dispersion into a nonpolar styrene−butadiene−styrene elastomer suspension. A 20 vol % dispersion of AgNWs within the elastomer yields optimized conductivities of ∼11000 S cm^{-1}. An impressive example of a laminar system[154] involves formation of thin (up to several micrometer thick) films of AgNWs, followed by casting of a liquid prepolymer to PDMS, to yield an elastomer membrane with an embedded film of AgNWs. The resulting conductivity reaches ∼8130 S cm^{-1} at 0% strain and decreases to a stable value of ∼5285 S cm^{-1} after a few cycles of stretching/releasing to strains in the range of a few tens of percent. Gradual oxidation and resultant reductions in conductivity is a drawback

DOI: 10.1021/acs.chemrev.8b00573
Chem. Rev. 2019, 119, 5461−5533

Table 1. Stretchability and Electrical Performance Properties of Representative Materials via Synthetic Approaches for Bio-Integrated Devices

material	maximum stretchability (%)	electrical performance	ref
PEDOT:PSS with glycol *tert*-octylphenyl ether as surfactant	57	1.7×10^{-2} S (for 50 μm thick film with 0.7 weight fraction of surfactant)	72
PEDOT:PSS with polytetrafluoroethylene resin as surfactant	10	150 Ω sq^{-1} (for 1 wt % surfactant)	81
PEDOT:PSS with sulfonate or sulfonimide-based ionic liquids as surfactant	100	3600 S cm^{-1}	82
PEDOT blended with copolymer of poly(polyethylene glycol methyl ether acrylate) and PSS	20	0.046 S cm^{-1}	83
P3HT-PE	600 (break point)	0.02 cm^2 V^{-1} s^{-1}	73
P3HT-poly(methyl acrylate)	140 (break point)	9×10^{-4} cm^2 V^{-1} s^{-1}	88
3,6-di-2-thienyl-pyrrolo[3,4-*c*]pyrrole-1,4-dione cross-linked with PDMS	20	0.40 cm^2 V^{-1} s^{-1}	87
3,6-di(thiophen-2-yl)-2,5-dihydropyrrolo[3,4-*c*]pyrrole-1,4-dione cross-linked with 2,6-pyridine dicarboxamide	100	1 cm^2 V^{-1} s^{-1}	90
PEO_{106}–PPO_{70}– PEO_{106} triblock copolymer encapsulating ethylammonium nitrate	500	0.015 S cm^{-1}	107
poly-(vinylidene fluoride-*co*-hexafluoropropylene) encapsulating 1-ethyl-3-methylimidazolium trifluoromethanesulfonate	50	7.06×10^{-5} S cm^{-1}	77
polycaprolactone polymer network encapsulating choline-based ionic liquid	40	5.16×10^{-5} S cm^{-1}	111
SWCNTs and 1-butyl-3-methylimidazolium bis(trifluoromethanesulfonyl)imide dispersed in vinylidene fluoride–hexafluoropropylene copolymer; paste prepared by mechanical mixing	38	53 S cm^{-1}	78
SWCNTs and 1-butyl-3-methylimidazolium bis(trifluoromethanesulphonyl)imide dispersed in vinylidene fluoride–hexafluoropropylene copolymer). Ink mixed with jet milling.	29	102 S cm^{-1}	123
MWCNTs and 1-butyl-3-methylimidazolium bisaimide in polyurethane	200	1000 S cm^{-1}	137
graphene laminated on PDMS	30	280 Ω sq^{-1}	127
MWCNTs/graphene aerogel backfilled with PDMS	20	2.8 S cm^{-1}	139
SWCNTs laminated on PDMS	25	2200 S cm^{-1}	124
in situ synthesis of AgNPs in vinylidene fluoride/hexafluoropropylene copolymer with fluorophyllic perfluoroalkyl group-based surfactant	400	935 S cm^{-1}	79
AgNWs laminated on PDMS	50	5285 S cm^{-1}	154
AuNPs layer-by-layer film laminated on polyurethane	110	2400 S cm^{-1}	155

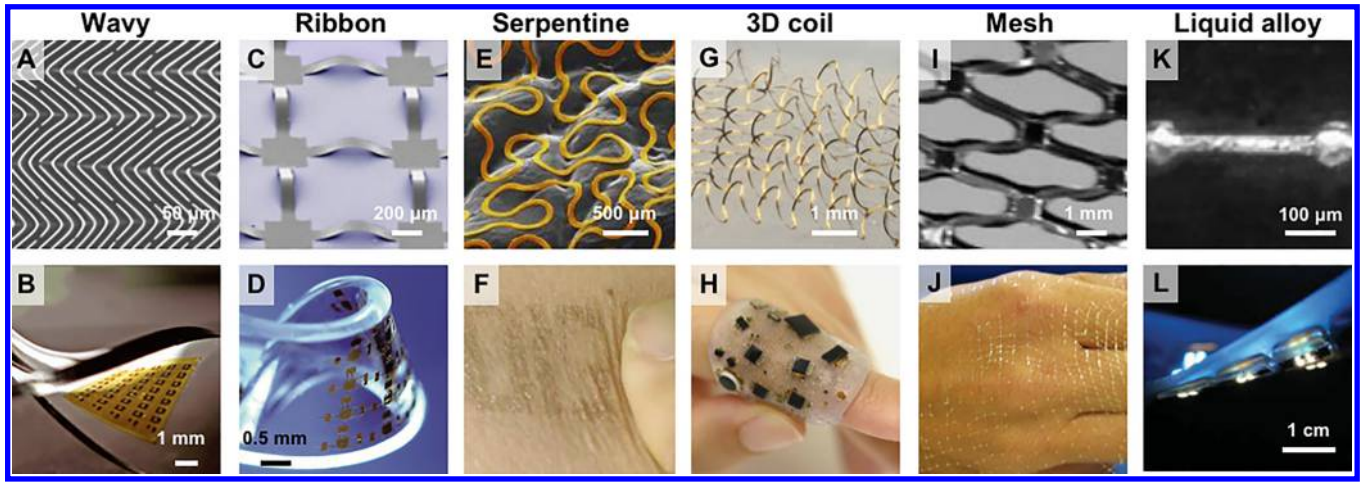

Figure 2. Concepts in materials engineering for stretchable electronics and bio-integrated wearable sensors. (A) Optical micrographs of 2D "wavy" Si nanomembranes on PDMS. Reprinted with permission from ref 161. Copyright 2007 American Chemical Society. (B) Optical image of a twisted Si-CMOS circuit in a "wavy" layout. Reprinted with permission from ref 162. Copyright 2008 the American Association for the Advancement of Science. (C) SEM image of a stretchable silicon nanomembrane (~100 nm thickness) patterned into a mesh geometry and bonded to a rubber substrate and (D) optical image of a device in a complex deformation mode. (C,D) Reprinted with permission from ref 163. Copyright 2008 National Academy of Sciences. (E) SEM image of similar traces on a skin-replica (colorized metal wires), showing the conformal attachment to the substrate and (F) optical image of skin-interfaced, serpentine metal traces with fractal design layouts. (E,F) Reprinted with permission from ref 164. Copyright 2014 Springer Nature. (G) Angled optical image of 3D helical coils bonded to a silicone substrate and (H) image of a device deformed on a finger. (G,H) Reprinted with permission from ref 165. Copyright 2017 Springer Nature. (I) Optical image of a mesh-shape plastic film with organic transistors and pressure-sensitive rubber. Reprinted with permission from ref 166. Copyright 2005 National Academy of Sciences. (J) Optical image of an expanded functional conductive network mounted on a hand. Reprinted with permission from ref 167. Copyright 2010 Wiley-VCH Verlag GmbH & Co. KGaA. (K) Optical images of a microchannel filled with liquid metal alloy. Reprinted with permission from ref 168. Copyright 2008 AIP Publishing LLC. (L) Optical image of arrays of LEDs connected by liquid metal on deformable substrates, in a strained state due to external force. Reprinted with permission from ref 169. Copyright 2014 Wiley-VCH Verlag GmbH & Co. KGaA.

DOI: 10.1021/acs.chemrev.8b00573
Chem. Rev. 2019, 119, 5461–5533

of silver-based materials. Several reports demonstrate the successful use of gold nanoparticles (AuNP) and nanowires (AuNW) in this context.[155,153] An attractive feature of the composite strategy is that multiple filler components can be combined to improve the performance beyond that achievable with the individual constituents. Examples include carbon nanomaterials/metallic nanomaterials,[156−158] conducting polymer/carbon nanomaterials,[159] and hydrogel/magnetic nanoparticle[160] stretchable composites and the resulting improvements in material performance.

These and other chemical synthesis approaches support considerable versatility in systems design for bio-integrated devices. Intrinsically stretchable conductive polymers, conductive composite materials, and hydrogels exhibit electrical properties sufficient for use as interconnects in simple electronic circuits and in certain types of sensors as shown in Table 1. Stretchable semiconductors are improving rapidly, although certain levels of function, particularly in radio frequency (RF) electronics, remain difficult to achieve due to limitations in charge transport through these materials.

2.1.2. Materials: Engineering. The engineering approach to stretchable electronic materials exploits principles of structural mechanics associated with well-defined micro/nanoscale elements of high performance inorganic semiconductors or conductors that embed into or onto elastomeric matrices. The result is a deterministic type of composite analogous to those described in the preceding section, but where the conducting/semiconducting pathways are defined directly at the engineering level, thereby bypassing the statistical aspects of percolation transport. In general, micro/nanofabrication processes define large-scale collections of semiconducting or conducting nanomembranes/ribbons/wires from the most sophisticated sources of thin-film or wafer-scale materials. Here, the structural shapes can respond to applied strains through controlled, nonlinear buckling and/or in-plane bending processes in a way that provides large effective levels of stretchability while avoiding significant strains in the active materials. As in Figure 2, various designs, each applicable to wide-ranging classes of materials including brittle inorganics that form the foundations of conventional electronic devices, can be classified according to geometric layouts.

"Wavy" ribbons/membranes of advanced electronic materials, including monocrystalline silicon created lithographically from wafer-based sources, represent the earliest examples of this strategy applied to high performance semiconductors (Figure 2A).[161] The structures result from uniformly bonding flat ribbons/membranes against uniaxially or biaxially prestrained elastomers and then relaxing the prestrain to form, spontaneously, "wavy" layouts through a controlled buckling process. The hard/soft composite materials formed in this way can support biaxial/uniaxial stretching with physics similar to that of an accordion bellows, where the wavelengths and amplitudes of the wave structures change to accommodate applied strain. In the example shown here, the active material consists of a nanomembrane (20−500 nm in thickness) of device-grade silicon, bonded to an underlying substrate of PDMS through condensation reactions associated with −OH functionality on the contacting surfaces. This concept can apply not only to active or passive electronic materials but also to completed electronic devices such as ultrathin silicon complementary metal-oxide semiconductor (Si-CMOS) integrated circuits (Figure 2B).[162] Here, a film of polyimide (PI) serves as the substrate and a bilayer of Cr (∼3 nm) and SiO_2 (∼30 nm) on the reverse side facilitates bonding to the PDMS via condensation reactions. Lithographically patterning the −OH surface chemistry allows for advanced control over the geometry of the bonded regions. Optimization that includes structuring the membranes into mesh-like architectures with joining ribbons and strategic bonding locations yields arc-shaped, noncoplanar configurations that increase the stretchability to values much greater than 100% (Figure 2C,D).[163]

Advanced designs use filamentary serpentine (FS) structures bonded in a similar manner to underlying elastomer substrates, such that both out-of-plane and in-plane buckling responses play roles in the responses to applied strains.[163,170−172] Thin (0.5 μm), narrow (∼100 μm), large amplitude (0.5 mm) networks of FS can serve as the basis for fully integrated, active electronic systems that, when supported by thin, soft elastomeric substrates, offer skin-like moduli (∼140 kPa) and ultralow bending stiffnesses (∼0.3 nNm). Such types of FS structures exhibit purely elastic stress−strain responses for strains to 30%, with only modest mechanical loading effects on the elastomeric substrate.[173] In advanced embodiments that use finite element deformation models as design tools, the FS architecture can be configured to extend in a manner that leads to a well-defined, enhanced tangential moduli at targeted strain levels.[174−176] The resulting J-shaped stress−strain curves can be matched precisely to those of biological tissues (e.g., skin) in a way that also mechanically protects the structures from excessive strains. A triangular lattice network of FS structures (PI) on a soft silicone elastomer experimentally demonstrates that the strain response begins with the bending-dominated deformations of the FS structures and ends with the stretching of the FS structures where the modulus in this phase reaches values several orders of magnitude higher than those in the initial phase.[175]

Further sophistication in this general design approach follows from the use of fractal mathematics. Here, self-similar, repeating geometrical shapes create structures that behave as nested collections of springs in two-dimensional arrays that release in sequence as the applied strain increases. The result is an interesting class of engineered metamaterials, applicable to single or multiple layers of active materials in the FS structures with effective properties that can be tailored to desired values (Figure 2E,F).[164,170]

The most recent strategies exploit these same core ideas in mechanically assembled 3D structures. Helical coils (Figure 2G,H)[165] provide examples that represent qualitative extensions of buckling processes used to form the simple arc-shaped structures of Figure 2C. Deformations of 2D FS shapes induce acute and predetermined stress concentrations at the arc regions due to their 2D formats and their physical coupling to the substrate. Helical coils avoid these stress concentrations due to the 3D structure that provides a uniform distribution of deformation-induced stresses. This absence of stress concentrations leads to elastic stretchabilities in 3D helices that exceed those for otherwise similar but 2D layouts by a factor of ∼3 for a strain of 50% and ∼10 for 300% without localized crack formation.

Other approaches use related mesh designs where in-plane rotations of 2D interconnecting bridges, rather than out-of-plane deformations, dominate the response to applied strain such that elastomeric materials are not required. In one example, polymer films (PI, for pressure sensor; poly(ethylene-naphthalate), for temperature sensor) in such a mesh structure serve as the support for an array of interconnected organic transistors and pressure/temperature sensors, where the entire

DOI: 10.1021/acs.chemrev.8b00573
Chem. Rev. 2019, 119, 5461−5533

system can accommodate strains of up to 25% (Figure 2I).[166] In a representative application, the use of a metal-coated, open mesh network of microscale PI wires and nodes formed via an oxygen plasma dry etch provides a highly stretchable conductor that can be patterned to yield addressable electrodes and other devices. This type of material can stretch uniaxially to strains of up to 1400% with strains in the constituent fibers remaining below ~5%. Full extension occurs at strains of 1600%, without microcracks. The material, after a fatigue test of a half million loading/unloading cycles (stress of 100 MPa), exhibits no degradation in performance (Figure 2J).[167]

An additional noteworthy engineering approach, applicable to conducting structures, involves liquid metals in microchannels formed within an elastomeric substrate. Such systems achieve stretchability not from deformation of the active materials but from physical flow (Figure 2K,L).[168] Table 2 highlights the stretchability that this class of structure exhibits in comparison to the aforementioned systems. The elastomeric microfluidic system provides guides for the liquid metal, as the electrical conductor and an overall elastic restoring force as first reported with eutectic alloys of Ga and In (EGaIn) and structures of PDMS.[177] Measurements indicate negligible changes in conductivity for strains of 70%.[169] EGaIn in the cores of hollow fibers formed using a triblock copolymer, poly[styrene-*b*-(ethylene-*co*-butylene)-*b*-styrene] (SEBS) resin results in ultra-stretchable conducting wires with the ability to maintain electrical continuity with strains of up to 700%.[178,179] By comparison to liquid metal in a defined microchannel structure, droplets of EGaIn within a soft, silicone elastomer establish conductivity through the rupture and fusion of droplets in response to local pressure, thereby providing high electrical conductivity and mechanical stretchability. This form factor also yields autonomous self-healing behaviors in response to damage through the in situ formation of new electrical pathways.[180] A recent review provides a thorough discussion of the various properties and applications of Ga-based liquid metals for stretchable electronics.[52]

Table 2. Stretchability and Conductivity of Representative Materials via Engineering Approaches for Bio-Integrated Devices

material	structure	maximum stretchability (%)	conductivity	ref
Si	wavy	5.7	mobility 290 (n-), 140 (p-) $cm^2 V s^{-1}$	162
Si	ribbon	140	mobility 370 (n-), 130 (p-) $cm^2 V s^{-1}$	163
Au	serpentine	100		164
Au	3D coil	150		165
Au	mesh	1600		167
EGaIn	liquid alloy	70		169

The material synthesis and the materials engineering approaches offer direct routes to all of the key constituent materials needed for highly stretchable electronics in bio-integrated sensing systems. The use of multiple strategies in a single device platform can mitigate trade-offs associated with any particular method. A widespread design technique combines flexible or even rigid functional device components and sensors in "islands" electrically and mechanically interconnected by stretchable conductors to yield systems with overall stretchability. The most advanced examples use self-similar fractal or 3D helical interconnects in skin-like wearable platforms that leverage off-the-shelf microcomponents.[164,165]

2.2. Interfacing Bio-Integrated Wearable Systems with the Body

2.2.1. Introduction to Bio-Integration. The seamless integration of wearable devices with the body necessitates consideration of not only the device composition (materials) and structure (design) but also the requirements prescribed by the device/body interface. This section provides a general overview of the critical requirements for bio-integration. Subsequent sections describe specific considerations for interfacing with the epidermis (section 2.2.2) or other body locations (section 2.2.3).

The biocompatibility of materials in direct contact with the body is of critical importance for ensuring not only an irritation-free interface[173,181−183] but also eliminating risks of allergic or toxic reactions.[184] Often, bio-integrated wearable devices utilize noble metals (primarily gold) and medical-grade silicones (e.g., PDMS) to define the interfaces.[185] Advances in material compositions, such as those described in section 2.1, primarily focus on performance rather than on biocompatibility and suitability for long-term wear.[186] Biological reactions to materials at the skin interface are topics of increasing academic interest, especially in understanding the toxicity effects of nanoscale materials to both humans and the environment.[187−192] Materials that were previously considered to be benign may in fact be less so, as recently shown with EGaIn.[193] Potential strategies for mitigating toxicity risks include use of biocompatible adhesives[194,195] and encapsulating layers[196,197] and in designs and modes of use that restrict direct skin contact to medical-grade materials.[198]

A key feature of bio-integrated wearable devices is their ability to interface with the body over both short (minutes to hours) and long-term (days to weeks) durations of continuous wear under a variety of environmental conditions.[186,199,200] These devices typically maintain such interfaces via adhesive coupling,[201] which in turn demands careful attention to adhesion strength,[202] strategies for mitigating physical damage during device application or removal[203,204] (e.g., skin removal), and designs to eliminate interfacial contaminants[205] (e.g., oils) or trapped moisture[186,206] (e.g., sweat). This integral aspect of bio-integrated wearable devices is of intense research interest, as detailed in a comprehensive topical review.[207]

2.2.2. Interfacing with the Epidermis. Emerging classes of wearable devices, enabled by the materials and device designs outlined in the previous sections, support a type of interface to the body that is qualitatively different than that of the loose mechanical coupling that is typical of commercially available wearable devices (Figure 3A,B). Characterized by intimate, conformal contact, the resulting configuration eliminates artifacts associated with relative motions and it supports many clinically relevant measurement modalities that demand physical interfaces to the skin, such as electroencephalography (EEG),[173] electromyography (EMG),[173,208] and electrocardiography (ECG).[209] Precision skin thermography,[210] arterial tonometry[211−216] and vital sign monitoring[217] from the skin represent additional examples of measurements that demand intimate coupling, as even small air gaps can prevent data collection and/or introduce significant errors (Figure 3C). Lightweight, highly breathable interface materials with elastic, low modulus mechanical responses to large strain deformations are important in this context. Ultrathin, gas-permeable devices that directly

DOI: 10.1021/acs.chemrev.8b00573
Chem. Rev. 2019, 119, 5461−5533

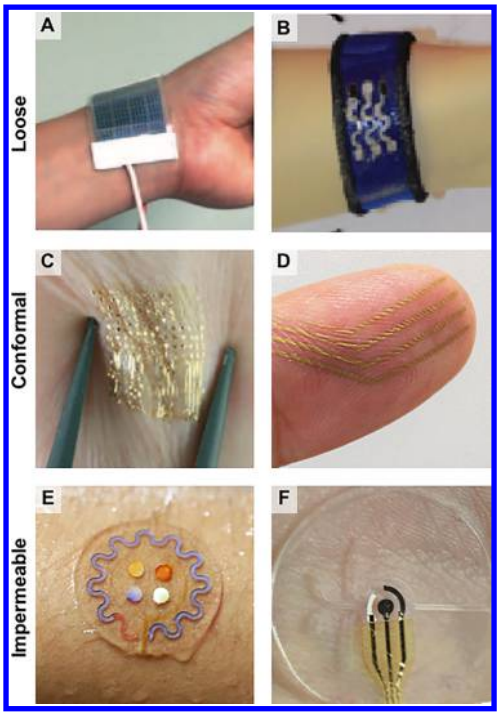

Figure 3. Interfacing with the epidermis. (A) Photograph of a sensor loosely coupled to the wrist. Reprinted with permission from ref 218. Copyright 2012 Springer Nature. (B) Optical image of stretchable sensors printed on a common textile mounted on the wrist. Reprinted with permission from ref 219. Copyright 2016 Wiley-VCH Verlag GmbH & Co. KGaA. (C) Optical image of an 8 × 8 array of Si nanomembrane diode sensors conformally mounted on the skin during a twisting motion. Reprinted with permission from ref 210. Copyright 2013 Springer Nature. (D) Optical image of nanomesh conductors attached to a finger. Reprinted with permission from ref 186. Copyright 2017 Springer Nature. (E) Optical image of a water-tight, soft microfluidic device sealed onto the forearm. Reprinted with permission from ref 220. Copyright 2016 the American Association for the Advancement of Science. (F) Optical image of a similar device with an integrated electrochemical detector. Reprinted with permission from ref 221. Copyright 2014 American Chemical Society.

laminate onto the skin can serve as the basis for wide ranging types of measurements, continuously for extended periods without inflammation or constraint on natural motions or body processes (Figure 3D).[186]

Impermeable interfaces represent an extension of this type of conformal contact, of particular interest in the capture, transport, storage, and chemical analysis of biofluids directly as they emerge from the epidermis. Specifically, impermeable interfaces to thin, soft microfluidic devices serve as water-tight seals for analysis of microliter quantities of sweat with sufficient spatiotemporal resolution to characterize instantaneous sweat rates (Figure 3E).[220] Electrochemical or colorimetric sensors integrated within such platforms can provide rapid and efficient measurements of the concentrations of important biomarkers, ranging from electrolytes to metabolites such as glucose and lactate (Figure 3F).[221]

2.2.3. Interfacing with Other Areas of the Body. Although the epidermis is an attractive interface point for physiological monitoring, natural processes of exfoliation of dead cells from the uppermost layer of the skin, the stratum corneum, limit the time for integration to a few weeks in the most favorable circumstances. Potential for irritation, inflammation, and other adverse reactions from sensitive skin types represent additional disadvantages. Alternatives, such as the surfaces of the fingernails, the outer ear, the inner mouth, the teeth, and the cornea, are of interest in certain complementary scenarios. The teeth and fingernails, as examples, represent hard, stable substrates for long-term monitoring without risks of irritation, with capabilities for measuring biochemical markers and biophysical signals, respectively. For example, miniaturized devices that exploit battery-free, near-field communication (NFC) technologies can support optical sensors that wirelessly capture photoplethysmogram (PPG) waveforms, blood oxygenation, and heart rate for up to three months, where the fingernails serve as optical windows for spectroscopic characterization of the underlying tissue bed (Figure 4A).[222] Earbud-style

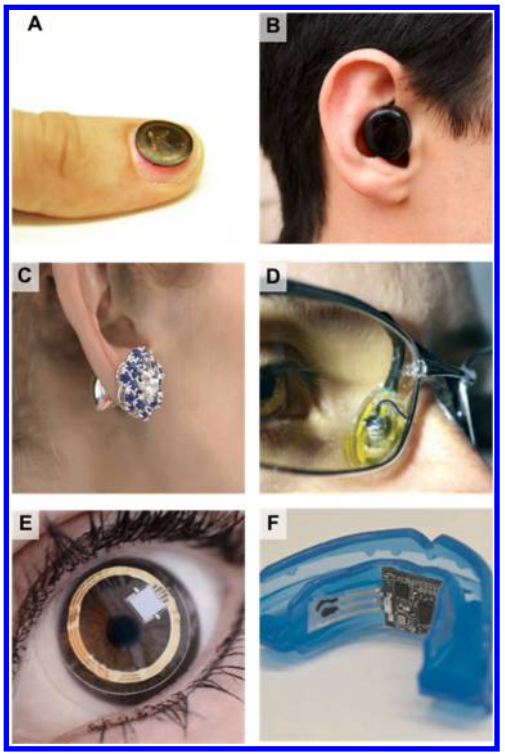

Figure 4. Interfacing with other areas of the body. (A) Optical image of an NFC enabled pulse oximeter device mounted on a thumbnail. Reprinted with permission from ref 222. Copyright 2016 Wiley-VCH Verlag GmbH & Co. KGaA. (B) Optical image of an earbud-style wearable device. Reprinted with permission from ref 232. Copyright 2018 Bragi GmbH. (C) Optical image of an earring-type pulse oximeter. Reprinted with permission from ref 233. Copyright 2016 BioSensive Technologies Inc. (D) Photograph of eyeglasses with an integrated electrochemical sensor and a wireless circuit board. Reprinted with permission from ref 225. Copyright 2017 The Royal Society of Chemistry. (E) Optical image of a biosensor in the form of a contact lens. Reprinted with permission from ref 234. Copyright 2018 Sensimed SA. (F) Photograph of a mouthguard with an integrated electrochemical sensor. Reprinted with permission from ref 231. Copyright 2015 Elsevier BV.

wearable devices ("earphones," "earables," "hearables"), by comparison to those that mount on more conventional locations of the skin, eliminate the need for adhesives and they largely avoid detrimental effects of hair follicles (Figure 4B).[223,224] Ear-based pulse oximeters can be realized in anatomically matching form factors and also in sizes and geometries similar to those of earrings (Figure 4C). Eyeglasses can support additional interfaces, where examples include electrochemical sensors

DOI: 10.1021/acs.chemrev.8b00573
Chem. Rev. 2019, 119, 5461−5533

that integrate into nose bridge pads with wireless communication modules supported by the arms of the eyewear (Figure 4D).[225] Further embodiments mount directly on the cornea to allow biochemical analysis of tears. Correlation of glucose levels in tears to those blood samples could, potentially, allow for a noninvasive means to manage diabetes.[226] Here, contact lenses provide an ideal substrate (Figure 4E).[227−230] Saliva, as an alternative to sweat, can be analyzed for hormones, electrolytes, and metabolites using devices that mount inside the mouth.[32] In one example, a soft mouth guard instrumented with electrochemical sensors and a wireless communication systems (Bluetooth Low Energy, BLE) performs continuous amperometric monitoring of uric acid in saliva (Figure 4F).[231] Although these various points of integration are not as widely studied as the epidermis, they provide useful capabilities for certain applications.

3. BIO-INTEGRATED WEARABLE SENSORS

Technologies that interface with the epidermis exploit soft functional materials, as described previously, and can include a broad range of biosensors for biophysical, biochemical, and environmental signals. This section summarizes the materials and technologies that serve as the foundations for these systems through discussions of many of the most significant, recently developed devices for continuous, real-time monitoring of important parameters for physiological health.

3.1. Biophysical Signals

Soft, skin-interfaced sensors are now available for noninvasively measuring biopotentials, absolute or relative physical motions and thermal signals associated with activity of the heart, brain, peripheral nervous system, skeletal muscles, and vascular tree. The following subsections present a critical evaluation of major advances in measuring these signals, broadly classified as electrophysiological, kinematic, and thermoregulatory, and highlight sensor utility in characterizing skin properties and recording biophysical signals generated by vascular dynamics (Figure 5).

3.1.1. Electrophysiological. The most advanced electrophysiological skin-integrated sensors combine ultrathin conformal electrode interfaces with capabilities in wireless communication and low power electronics suitable for monitoring over long periods of time.[165,173,235−237] This section summarizes recent work in materials and designs for the electrodes, and it includes comparisons of performance against conventional systems designed for use in the clinic and which require conductive gels, adhesive tapes, and hard-wired connections to external data acquisition electronics. Progress in materials science and structural design form the basis of various types of gel-free, dry electrodes that interface directly and conformally with the skin without limitations associated with evaporative drying and skin irritation associated with clinical standards, as highlighted in the following.

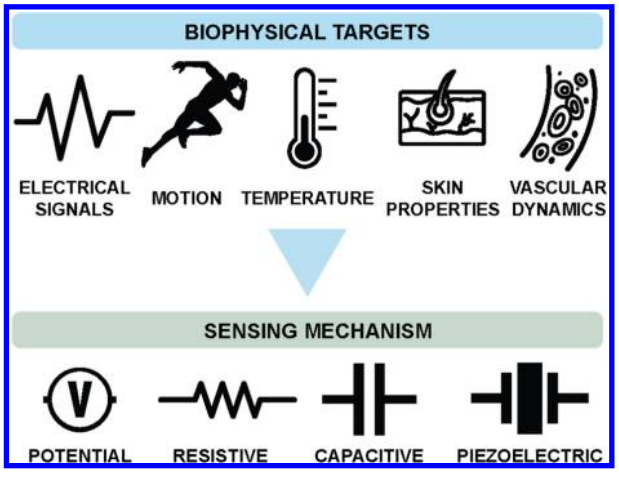

Figure 5. Schematic illustration of the main components of biophysical sensors.

The electrical impedance of the electrode−skin interface can be approximated as a complex expression $Z(\omega) = R/(1 + j\omega CR)$ in a RC-circuit models, where R and C represent the resistance and capacitance of the skin layer, ω is angular frequency, and j is the imaginary unit. The magnitude and stability of electrode−skin impedance largely affect the quality of electrical recordings. High and unstable impedance can cause low signal quality. In multiple electrode systems, high interelectrode impedance also causes a reduction in efficacy of common mode noise rejection due to amplified differences between electrodes. Certain of the materials synthesis and engineering approaches described in section 2 are relevant in this context. Optimized choices in the geometries and materials compositions of soft, skin-like electrodes enable irritation-free, conformal contact to the skin and a low impedance measurement interface.[200,235,241−244] Several classes of electrodes utilize low modulus elastomeric composites based on silicones with conductive fillers such as CNTs, graphene, or metallic nanowires.[238,240,245−251] Electrode contact impedance can be affected by the conductivity of the composites and the dimension of electrodes.[252] Highly conductive electrodes provide low interface impedance by reducing the contact resistance. Electrodes with large sizes decrease the interface impedance by decreasing the resistance and increasing the capacitance, although they reduce spatial resolution in multichannel sensors.[253] As a specific example, a formulation of PDMS in which the methyl groups are replaced with vinyl groups (sometimes referred to as adhesive PDMS) serves as a skin-adherent matrix material with CNTs as the conductive filler for electrodes that can support long-term continuous recording of electrophysiological signals such as ECG, even during movement (Figure 6A−C).[238] Improvements in signal stability and comfort follow from enhancements of breathability and from reductions in the thicknesses of the electrodes.[254] A recent extreme demonstration uses conductive nanomesh structures formed by depositing thin films of Au (70−100 nm) on a mat of fibers of poly(vinyl alcohol) (PVA) formed by electrospinning. The open architecture and ultrathin geometry lead to high levels of permeability to gases and biofluids, without compromising the ability to perform electrophysiological measurements and other forms of sensing, with performance that compares favorably to that of conventional Ag/AgCl gel electrodes (Figure 6D-F).[186]

A conceptually related alternative approach relies on micrometer-scale mesh constructs formed using photolithographically defined thin metal filaments in serpentine or fractal layouts, as introduced in section 2.[164,173] Generally, filaments with widths in the range of 10 μm or less and with areal coverages of ∼20% can yield sufficiently low effective moduli and bending stiffnesses to enable soft, conformal contact with the skin in ways that can be difficult to reproduce using mesh structures with wider, denser filamentary networks.[209] Increasing the area fill factor of these mesh electrodes reduces their impedances, but it also reduces their stretchability and, by consequence, their ability to

DOI: 10.1021/acs.chemrev.8b00573
Chem. Rev. 2019, 119, 5461−5533

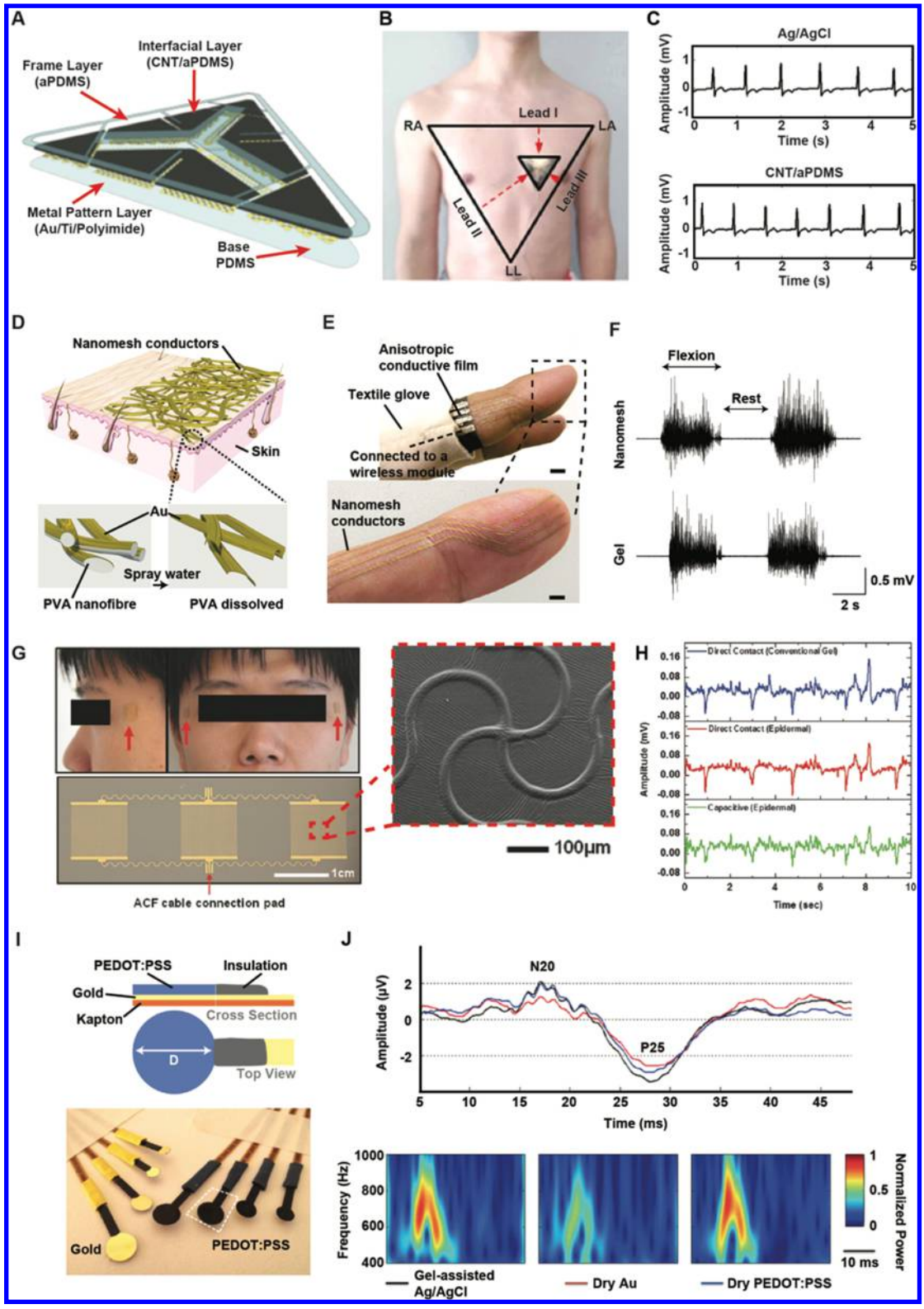

Figure 6. Electrophysiological sensors. (A) Schematic illustration of a self-adhesive form of carbon nanotube electronics. (B) Photograph of the device on the chest for continuous ECG recording. (C) ECG signal measured with the device compared to that collected with Ag/AgCl gel electrodes. (A–C) Adapted with permission from ref 238. Copyright 2014 Springer Nature. (D) Schematic illustration of nanomesh electrodes. (E) Photograph of the electrode array as a tactile sensor (scale bar, 3 mm). (F) EMG signals measured with the nanomesh electrode on the forearm compared to that collected with Ag/AgCl gel electrodes. (D–F) Adapted with permission from ref 186. Copyright 2017 Springer Nature. (G) Photograph of epidermal electrodes (bottom) attached near the eyes for EOG recording and an SEM image (inset) showing the FS electrode design. (H) EOG signals recorded from conventional electrodes (blue) with comparison to direct contact (red) and capacitive (green) epidermal electrodes. (G,H) Adapted with permission from ref 239. Copyright 2013 Wiley-VCH Verlag GmbH & Co. KGaA. (I) Schematic illustration and photograph of PEDOT:PSS

DOI: 10.1021/acs.chemrev.8b00573
Chem. Rev. 2019, 119, 5461–5533

Figure 6. continued

electrodes for EEG recording. (J) EEG signals and time-frequency analysis plots of EEG signals collected with the electrodes, compared to that obtained with Ag/AgCl gel electrodes. (I,J) Adapted with permission from ref 240. Copyright 2014 Wiley-VCH Verlag GmbH & Co. KGaA.

form intimate contact with the skin (Figure 6G).[209,239,255,256] Figure 6H shows as a representative example the collection of electrooculography (EOG) signals with these types of electrodes.[239] Continuous EEG recordings captured in a similar manner form the basis of persistent brain−computer interface systems with wear times of up to 2 weeks.[257] More recent demonstrations exploit graphene in similar filamentary serpentine designs but in forms that are also optically transparent (∼85% across the visible range).[258]

Further improvements are possible by forming coatings of conducting polymers, such as PEDOT:PSS, onto these or other types of metal electrodes,[240] to yield performance that exceeds that of bulk metal electrodes (Figure 6I,J). Here, the combined ionic and electronic transport through the polymer leads to reductions in the contact impedance. Likewise, the addition of ionic liquid gels, such as 1-ethyl-3-methylimidazolium ethyl sulfate, onto Au electrodes can further improve performance by maintaining a low impedance over longer periods of time than standard Ag/AgCl gel electrodes.[259,260] Although cholinium cation-based ionic liquids have relatively low toxicity compared to others, the long-term health effects of direct interfaces to the skin based on such materials requires further examination.

The need for direct contact between the skin and the electrodes can be avoided entirely by introducing thin insulating coatings and using capacitive approaches for electrophysiological sensing. Materials for such insulators include acylate-based adhesive tape, epoxy film, cotton fabric, latex rubber, and silicone.[200,239,261,262] Capacitive schemes are attractive in part because they eliminate the potential for irritation and allergic reactions to the electrode materials, and they also improve the safety by avoiding the possibility for any direct current pathways between the skin and the electrodes and associated electronics.[263] Although conventional capacitive electrodes suffer from motion artifacts, the sorts of conformal interfaces enabled by skin-like device designs highlighted in this article avoid this limitation. A prominent example combines electrodes in engineered composite designs as described above with thin overcoats of silicone elastomers as the insulating coating.[239] Systematic studies show that such electrodes can offer large capacitive coupling to the skin and an ability to capture electrophysiological data with high signal-to-noise ratio. The ultrathin construct of electrodes (5 μm soft silicone as insulating layer; 10 μm total electrode thickness) provides robust, intimate contact with the skin during movements without relative motions or slippage. Stray capacitances can be addressed by use of actively shielded amplifiers. Active circuit designs and lead-wire shielding that minimize effects of electromagnetic interference, triboelectric charging, and common-mode noise can be particularly valuable in this context.

3.1.2. Kinematic. Soft, wearable sensors that capture dynamic motions of the human body can provide critical insights across a broad range of applications, from clinical diagnostics (movement disorders,[264−268] neurological disorders[269]) to athletic performance monitoring.[264,270] The inertial and strain-based sensors integrated in the most common systems of this type[264,271−273] provide continuous monitoring capabilities and also support sensory and feedback controls in smart prosthetics and robotic limbs.[159,274] This section highlights advances in highly sensitive strain and motion sensors that are comprised of soft materials and thin film designs that allow intimate coupling with human skin. Other contemporary reviews provide related, complementary perspectives on strain sensing technologies[27,114,275−277] and on the deployment of discrete accelerometer and gyroscope-based multiaxial motion sensing systems.[278,279]

Recent demonstrations of skin-interfaced sensors exploit peizoresistive,[280−282] piezocapacitive,[283] piezoelectric,[284,285] piezophototronic,[286] and triboelectric[287] properties of functional materials that react to strains, vibrations, deformations, and applied pressures. Devices that measure changes in resistance and capacitance are commonly used in body-interfaced applications because of their simple designs and straightforward mode of data acquisition.[27] Typical constructs of resistive sensors include micro/nanoscale sheets of metals,[79,157] graphene,[288−290] CNTs,[270,291] nanowires,[121,292] and/or nanoparticles[120,293] encapsulated in soft elastomeric substrates (e.g., silicones). These sensors have a sufficiently broad dynamic range to characterize applied pressures, motions, and deformations noninvasively on the skin. Their simple architecture provides both robustness in operation and insensitivity to variations in stray capacitances and in the dielectric properties of the surroundings.

Resistive strain sensors that use solid metals typically operate on the basis that an applied mechanical stress causes a change in the geometry of the material structure, which in turn gives rise to changes in electrical resistance. Here, thin film metal traces can commonly serve as sensing resistors in a Wheatstone bridge configuration. These designs often exploit metal foils due to their low reactivity and the linear, low hysteresis changes in resistance that they exhibit under small strain deformations.[118] Implementation of such sensors in wearable formats often involves lamination of FS metallic traces on soft elastomer substrates (e.g., PDMS).[173] Alternative approaches use GaIn alloys as liquid metals in microchannels embedded in elastomeric PDMS sheets.[294,295] These liquid metal approaches offer intrinsically stretchable gauges capable of accommodating large external strains without loss of electrical conductivity. Interfacial oxide layers that form in these systems (in a few ppm of oxygen[296,297]) facilitate poor wetting of the GaIn-based metal to most surfaces (due to strong adhesion of the oxide layer), thereby restricting the spatial resolution of micropatterned structures.[298,299] A recent strategy to avoid this limitation uses selectively wetting of GaInSn on prepatterned traces of Au (50 μm width) on PDMS substrates that follows the removal of the oxide layer through exposure to dilute NaOH (a reducing agent).[300] This work demonstrates the use of GaInSn traces formed in this manner as stretchable antennas and resistive strain sensors capable of supporting strains up to 30% (Figure 7A,B).

Most device designs involve trade-offs between sensitivity and stretchability. The gauge factor (GF) is an important metric of sensor performance, defined by the relative change in resistance ($\Delta R/R_0$), where ΔR is the resistance change and R_0 is the unstrained resistance, for a given change in applied strain (ε).[118] For sensors that transduce strain via geometrically induced changes in resistance, the GF depends on changes in length and

DOI: 10.1021/acs.chemrev.8b00573
Chem. Rev. 2019, 119, 5461−5533

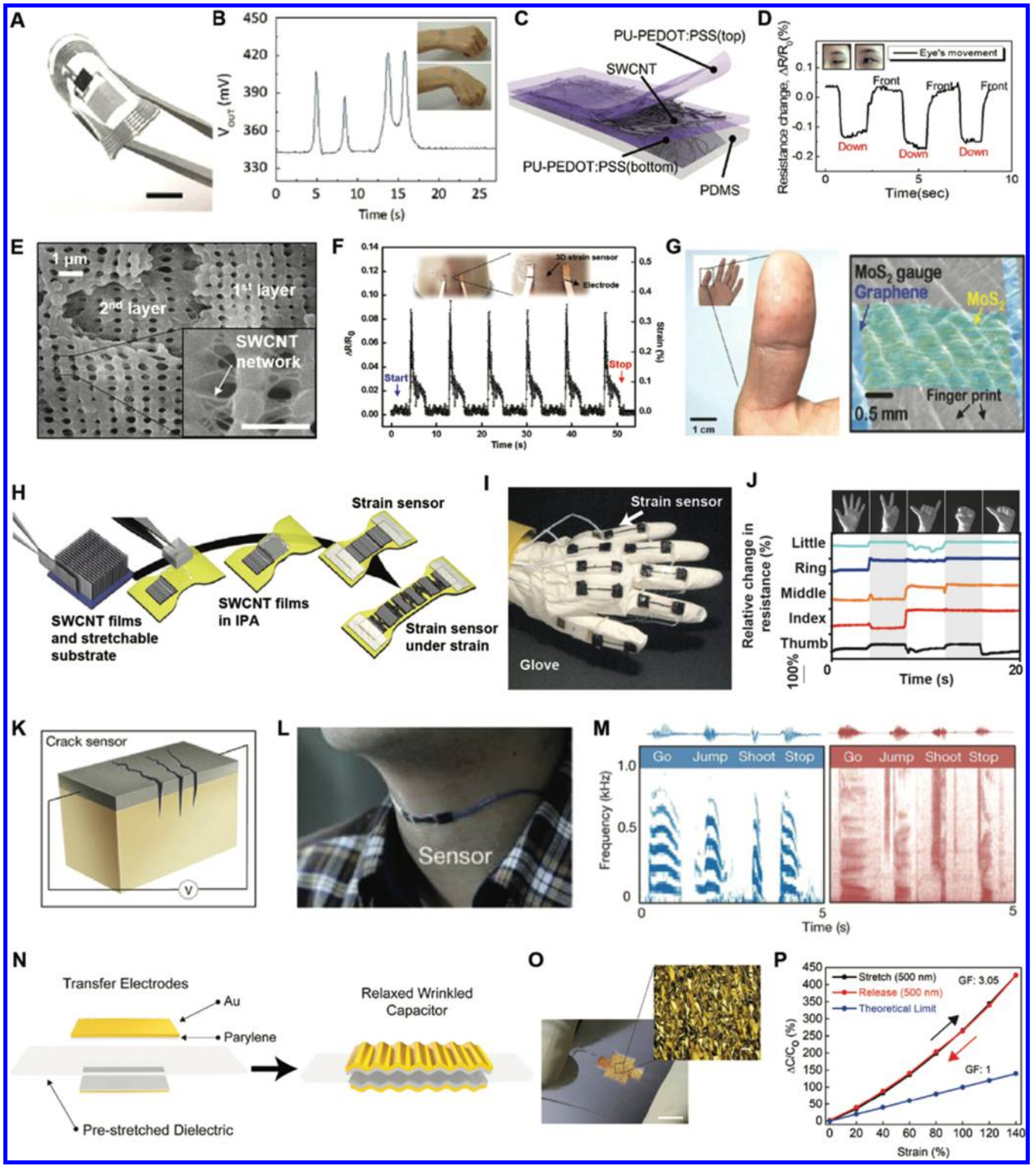

Figure 7. Strain sensors. (A) Optical image of an NFC-based wireless resistive strain sensor that uses GaInS (scale bar, 4 mm). (B) Wireless recording of wrist motion (inset: optical image of corresponding movement. (A,B) Adapted with permission from ref 300. Copyright 2017 Springer Nature. (C) Schematic illustration of a SWCNT-based stretchable strain sensor and (D) demonstration of sensitivity in recording subtle eye movements. (C,D) Adapted with permission from ref 159. Copyright 2015 American Chemical Society. (E) SEM image of nanoporous PDMS and percolating network of SWCNTs (inset scale bar, 1 μm). (F) Demonstration of a strain sensor designed to record phonation. (E,F) Reproduced with permission from ref 301. Copyright 2017 American Chemical Society. (G) Optical image of a transparent MoS_2 strain sensor with graphene electrodes mounted on the thumb (left) and false-colored SEM image of the sensor on a skin phantom (right). Adapted with permission from ref 302. Copyright 2016 Wiley-VCH Verlag GmbH & Co. KGaA. (H) Schematic illustration of a resistive strain sensor based on precracked, random networks of CNT. (I) Optical image of integrated sensors on a glove to (J) record fingers movements. (H–J) Adapted with permission from ref 270. Copyright 2011 Springer Nature. (K) Schematic illustration of the operation of a thin-film crack-based strain sensor. (L) Optical image of a throat-worn strain sensor to capture phonation (M) with comparison of the sensor performance (left) to that of a microphone (right). (K–M) Adapted with permission from ref 303. Copyright 2014

DOI: 10.1021/acs.chemrev.8b00573
Chem. Rev. 2019, 119, 5461–5533

Figure 7. continued

Springer Nature. (N) Schematic illustration of the assembly and final structure of a Au thin film capacitive strain sensor. (O) Optical image of the sensor in a relaxed (0% strain) state (scale bar, 1 cm). (P) Demonstration of sensor performance exceeding the simple theoretical limit for a capacitive strain gauge. (N−P) Adapted with permission from ref 304. Copyright 2018 Springer Nature.

cross-sectional area (GF for metal thin films, 2−5; liquid metals, ∼2) at low strains (ε < 5%).[114] By comparison, piezoresistive semiconductor-based devices offer significantly greater GFs as changes in resistance involve additional contributions from strain-induced variations in interatomic spacing.[305] For example, the intrinsic GF for p-type doped monocrystalline Si can approach 200.[306] Foundational work[282] uses Si nanomembranes on plastic substrates (e.g., PI) as a highly sensitive (GF = 43, ε ∼0.1%) flexible strain sensor. Refinements of this basic approach use silicone elastomeric substrates and sophisticated materials engineering approaches (section 2.1.2) to realize enhanced sensitivity (GF ∼97) and stretchability (ε ∼6%).[307] Although devices with modest GF are suitable for measuring large dynamic motions (e.g., arm bending), monitoring physiologically relevant strains at the surface of the skin (e.g., wound healing, emotional expression) require sensors with high GF.[308] Highly stretchable (ε > 50%) strain sensors with high GF represent the ideal.

Stretchable conductive composites provide an alternative route to this ideal. The designs have similarities to those outlined in section 2.1.1 but with the conductive filler at loadings near the percolation threshold. Strain-induced changes in the micro/nanostructural features of the percolation network (e.g., changes in the contact resistances between a pair of nanostructures or creation of electrical disconnections between them or along either) or in the intrinsic resistivity of nanomaterials that have piezoresistivity of some nanomaterials (CNTs) give rise to changes in the overall electrical conductivity of the composite.[27,114,309] CNTs are a widely utilized conductive filler for piezoresistive composite strain sensors due to their excellent mechanical and electrical properties.[310] A representative example[159] uses SWCNTs as a conductive network between two sheets of a surface functionalized ((3-aminopropyl)-triethoxysilane, APTES) binary elastomeric composite of PEDOT:PSS and PU bonded via thermal annealing (Figure 7C). The bonding process partially embeds the SWCNTs within the elastomeric sheets, thereby promoting a strong, electrically conductive interface between the SWCNTs and PEDOT. Sensors with this design demonstrate high sensitivity (GF of 62.3, ε > 100%) and the capability for detecting subtle strains on the skin associated with facial expressions (Figure 7D). However, cyclic loading (1000 cycles at 20% strain) degrades sensor performance due to structural damage to the percolating network.

Recent work[301] indicates that deterministically structuring the percolating network by patterned etching can increase the durability (Figure 7E,F). Here, infiltrating an aqueous solution of SWCNTs (0.9 v%) into a nanostructured porous PDMS matrix (10:1 ratio, structure lithographically defined) results in a uniform, 3D continuous percolation network. Repeating the infiltration process increases the number of contact junctions, providing a route to tuning the sensitivity and stretchability of the sensor (3 times, GF 134, ε < 40%; 4 times, GF 61, ε < 80%; 5 times, GF 24, ε < 160%). Under cyclic loading (>1000 cycles, ε = 40%), the sensors exhibit negligible hysteresis, independent of the number of infiltration cycles, due to the elastic recovery facilitated by the nanoporous structure.

Percolating networks of metallic nanoparticles can offer comparable performance. For example, one scheme uses a stacked construction of a patterned thin film of AgNWs infiltrated with a liquid precursor to PDMS and cured such that solid layers of PDMS encapsulate both sides of the thin film to obtain a skin-interfaced sensor with highly sensitive (GF 2−14), stretchable (ε < 70%), and linear (R^2 = 0.986) properties.[125] The GF, stretchability, and linearity depend on the density of the AgNWs in these thin films, thereby providing a simple way to form sensors optimized for operation in regimes of high or low strains. Additionally, infiltration of the percolating network with liquid PDMS precursor and subsequent curing reduces out-of-plane buckling of the AgNWs to ensure a reversible sliding dislocation strain transduction mode of the AgNW positions. This physics results in high linearity with negligible change in electrical properties after low strain cyclic loading (225 cycles, ε = 0−10%) and only a modest (6.25%) change in electrical properties after 1000 cycles at large strains (ε = 10−40%). Integrated into a glove, these sensors can record individual finger movements and finger positions in real time.

The use of 2D material systems, such as graphene, in percolating networks is also of significant interest. Because of the limited stretchability of graphene itself (elastic limit, ε_{EL}, 7%), stretchable designs typically exploit percolating networks of multilayer graphene (e.g., graphene flakes, ε_{EL} = 350%;[311] platelets, ε_{EL} = 25%[312]) or hybrid systems (graphene/AgNW, ε_{EL} = 200%[313]) in elastomeric matrices. Recent work[302] includes demonstrations using other 2D material systems, such as transition metal dichalcogenides (e.g., MoS_2). Ultrathin (1.4 nm) layers of MoS_2 grown by chemical vapor deposition (CVD) on SiO_2 and mounted onto graphene electrodes yield optically transparent, wearable strain sensors with high GFs (∼80), although with limited stretchability (ε < 2%) (Figure 7G).

Crack-based sensors exploit an alternative transduction method to realize, simultaneously, extremely high gauge factors and large stretchability.[303] By contrast to the percolating networks highlighted in the preceding examples, these systems often use laminar composites of thin films of carbon[128,314,315] or metallic[316] nanomaterials on elastomeric substrates. Early examples rely on precracked horizontal arrays of SWCNTs mounted on PDMS substrates as the sensing material (Figure 7H−J).[270] Here, the uncracked portions form distinct islands along the array, allowing for system-level stretching in a manner similar to the island−bridge configuration of section 2.1.2 The resistance increases monotonically as a function of applied strain due to crack propagation across the films, limited only by ultimate mechanical failure (ε = 280%). Remarkably, this mechanism can support good cyclic performance, including negligible degradation after 10000 cycles of 100% strain, although with low sensitivity (GF 0.82, ε = 0−40%; GF 0.06, ε = 60−200%). A subsequent embodiment of this same underlying concept[303] uses nanoscale cracking of a Pt thin film (20 nm) deposited onto a polyurethane acrylate (PUA) substrate as a highly sensitive (GF 2000) strain sensor (Figure 7K), albeit with limited stretchability (ε_{EL} < 2%) and durability (performance degradation after 500 cycles, ε = 2%). The high sensitivity results from the use of nanoscale cracks preformed

DOI: 10.1021/acs.chemrev.8b00573
Chem. Rev. 2019, 119, 5461−5533

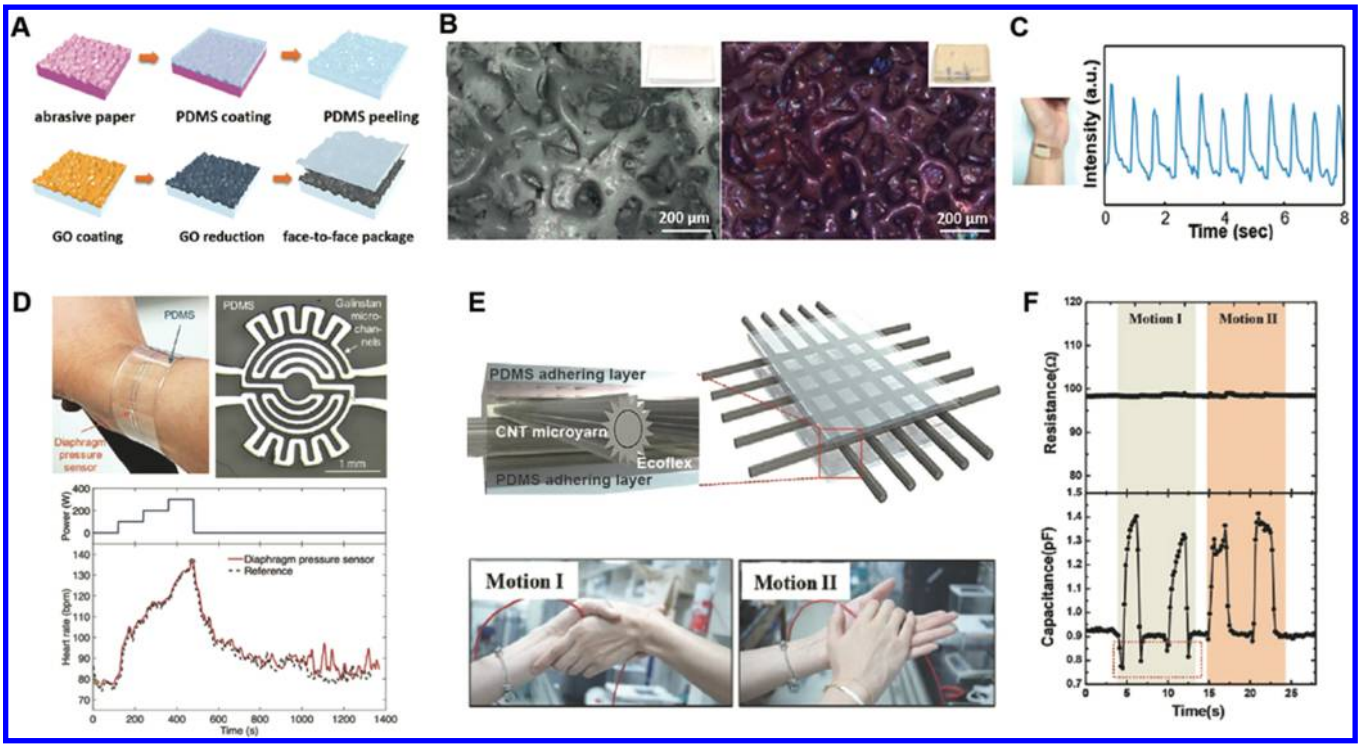

Figure 8. Pressure sensors. (A) Illustration of the process for fabricating a resistive pressure sensor and (B) optical images of the patterned PDMS and GO coating before (left) and after (right) high-temperature processing. (C) Optical image of a wrist-worn pressure sensor (left) designed to record the pulse rate (right). (A–C) Adapted with permission from ref 326. Copyright 2018 American Chemical Society. (D) Optical image of the GaIn-based pressure sensor as worn on the wrist (left) with a magnified view (right) of the diaphragm. (bottom) Comparison of sensor performance in recording pulse rate to that of a commercial monitor during exercise. Adapted with permission from ref 381. Copyright 2017 Wiley-VCH Verlag GmbH & Co. KGaA. (E) Schematic illustration of the sensor construction (top) and two types of movements recorded by the sensor (bottom) as worn on the palm of the hand with (F) comparisons of the sensitivity between resistive and capacitive modes of operation. (E,F) Adapted with permission from ref 327. Copyright 2015 Wiley-VCH Verlag GmbH & Co. KGaA.

within the Pt film by bending the films over a prescribed curvature. Upon application of strain, these cracks reopen in a repeatable manner; however, the absence of FS structuring or utilization of an open-mesh design limits system-level stretchability such that strains in excess of 2% result in mechanical failure of the metallic film. Such sensors can measure vibratory signatures of speech when mounted on the throat (Figure 7L,M), bending of limbs when located on the joints, and gestures of the hands when integrated into robotic gloves. Later work refines the cracking process with the application of a controlled tensile force to the film during bending resulting in a dramatically increased sensitivity (GF 16000, ε = 2%).[317]

A key drawback of resistive sensors that rely on changes in conductive contacts in percolating composites or across cracked films is that many tend to suffer from drift, nonlinear responses and hysteretic behaviors as a result of irreversible, deformation-induced variations in the microstructure of the conductive component and/or the viscoelasticity of the polymeric matrix/substrate. Capacitive effects represent an alternative basis of sensors for detecting local strains, small vibrations, and even acoustic waves propagating through soft biological tissues.[318] Parallel-plate capacitive sensors exploit changes in thickness or area of a soft, deformable dielectric material sandwiched between compliant electrodes.[264,319−321] An important figure of merit is the capacitive gauge factor (cGF), defined by the relative change in capacitance ($\Delta C/C_0$), where ΔC is the relative capacitance change and C_0 is the unstrained capacitance for a given applied strain (theoretical limit: cGF = 1).[321] Silicone elastomers, in flat slabs or textured sheets, often serve as the dielectric materials in such systems. As with resistive sensors, conductive composite materials comprised of CNT[124,264,319,320,322,323] or metallic nanoparticles[154,321,324,325] can be used as the stretchable electrodes. One example[320] exploits two films of CNTs (mixture of single- and double-wall, continuously grown by floating catalyst vapor deposition), infiltrated with silicone, and subsequently cured as electrodes laminated onto a dielectric layer of silicone (0.5 mm thickness) to obtain a highly stretchable (ε ∼300%) and transparent capacitive strain gauge with a high cGF (0.97). The high durability, negligible performance degradation and lack of hysteresis under cyclic loading (∼10000 cycles to failure, ε = 100%) allows for monitoring, in real-time, dynamic movements of the body such as the extension of a finger. A recent noteworthy example[304] uses an ultrathin wrinkled Au metal/poly *para*-xylylene (50 nm/500 nm) electrode and prestrained acrylate adhesive dielectric layer (500 μm) in a highly stretchable sensor with one of the highest reported cGF (3.05, ε ∼140%). The inherent stretchability results from the ultrathin electrode construction and spontaneous wrinkle formation after the relaxation of the prestrained elastomeric substrate, according to the same principles outlined in section 2 (Figure 7N,O). The out-of-plane deformation enhances the sensitivity to values that can exceed the simple theoretical limit (Figure 7P). Durable sensors of this type show minimal performance degradation under cyclic loading (1000 cycles at ε = 30%, 50%) and offer capabilities in measuring finger movements with high accuracy.

Wearable touch/pressure sensors that exploit both resistive and capacitive sensing modalities have broad utility in soft

DOI: 10.1021/acs.chemrev.8b00573
Chem. Rev. 2019, 119, 5461−5533

robotics and biosensing applications, resulting in widespread interest.[27,328] Popular classes of resistive sensors transduce pressure through changes in contact resistance between two electrodes. Typically, this basis of operation necessitates the use of stretchable electrodes with micropatterned[291,326,329−338] or porous[339−344] (as opposed to planar) features to obtain high sensitivity. An early representative demonstration[329] uses a slab of PDMS with micropyramidal features of relief on its surface, conformally coated with a stretchable conductive composite (PEDOT:PSS and PU blend), paired with a flat, stretchable counter electrode. The result is a stretchable (ε_{EL} = 40%) pressure sensor with high sensitivity (10.3 kPa^{-1}). When tuned to respond in the low pressure regime (13−200 Pa; 56.8 kPa^{-1} sensitivity), such sensors can detect small pressures (23 Pa) while stretched (ε = 40%). A recent example[326] replaces the micropyramids with random texture formed by use of an abrasive paper as a template for casting and curing PDMS (Figure 8A). Two conductive electrodes, prepared by first dip-coating the molded PDMS substrate in a solution of graphene oxide (GO) and subsequently reduced (RGO) in high temperature (Figure 8B), exhibit high contact resistance due to the randomized microstructural features of the roughened surfaces (hills and valleys, 20−200 μm height range). The resulting pressure sensor (Figure 8C) exhibits high sensitivity (25.1 kPa^{-1}) across a wide range of pressures (0−2.6 kPa), with capability of detecting the pressure associated with the weight of a single grain of rice (16 Pa).

The utilization of conductive materials with intrinsic structural features (porosity) provides another path to similar devices. One example[339] uses a Ni foam as a porous template for the CVD deposition of a multilayer graphene film, which, after infiltration of PDMS and subsequent removal of the Ni template by immersion in hydrochloric acid (HCl, 15%), results in a stretchable conductive composite. The graphene porous network in this PDMS matrix serves as the basis of a sensitive (0.09 kPa^{-1}) pressure sensor with a wide linear range (0−1000 kPa) suitable for monitoring human motions.

GaIn-based liquid metals offer yet another pathway to resistive pressure sensors by harnessing pressure-induced geometry deformations of microfluidic channels formed in elastomeric materials and filled with liquid metals. A recent notable example[281] exploits GaInSn microchannels as a highly sensitive microfluidic pressure diaphragm (Figure 8D). With the resistive sensor in a Wheatstone bridge circuit, this design exploits tangential and radial strain fields to obtain a sensitivity of (0.0835 kPa^{-1}). This construction also provides temperature compensation (between 20 and 50 °C), with a limit of detection of 100 Pa with sub-50 Pa resolution.

Capacitance-based devices are among the most prevalent pressure sensors in wearable and commercial applications due to their good sensitivity, low hysteresis, and low power requirements. The operating principals are similar to those for previously mentioned capacitive strain sensors. For example, CNTs embedded in two sheets of PDMS serve as electrodes with a separating layer of a low modulus formulation of silicone as a dielectric to yield a pressure sensor with a parallel plate capacitor design (Figure 8E,F).[327] Subtle changes in pressure (<0.4 Pa) lead to measurable changes in capacitance (sensitivity of 0.034−0.05 kPa^{-1} below 0.1 kPa; 0.5 MPa^{-1} above 10 kPa). In a related approach,[345] a silicone sheet separates two identical layers of FS thin film electrodes of Ag, supported on a patterned frame of polyethylene terephthalate (PET) and coated by a PDMS film, to form an addressable array of capacitive sensors. The resulting sensitivity (1.45 MPa^{-1}) compares favorably against other skin-interfaced capacitive pressure sensors (e.g., Ag nanowires, 1.62 MPa^{-1}; CNT, 0.23 MPa^{-1}; FS gold thin film, 0.48 MPa^{-1}), and the device has a detection limit of 6 Pa. Cyclic loading (1000 cycles at 50% tensile strain) results in negligible decreases in performance. Advanced designs use micropatterned dielectric layers to improve the performance. An early demonstration[346] leverages an ultrathin (10 μm thickness) sheet of PDMS with micropyramidal features of relief, as discussed previously, as a highly sensitive capacitance-based pressure sensor. Here, the molded sheet of PDMS laminates onto an ITO-coated substrate of PET; a second ITO-coated PET substrate completes the sensor. The device is highly sensitive to pressures <2 kPa (0.55 kPa^{-1}) and shows negligible performance degradation after 10000 cycles of compression (1.5 kPa applied pressure) and >15000 cycles of bending (4 mm bend, 1 Hz).

Piezoelectric sensors represent an additional approach to pressure transduction. Piezoceramics (lead zirconate titanate, PZT[347]), zinc oxide (ZnO) nanowires,[348] piezoelectric polymer polyvinylidene fluoride (PVDF),[349,350] and its copolymer trifluoroethylene, P(VDF-TrFE),[285,351] represent common choices for the active materials. Such sensors generate electrical charges under the application of external pressure or strain.[352] These devices exhibit fast response times, low power consumption, and high sensitivity.[376] One embodiment[353] utilizes ZnO nanowires, grown through a hydrothermal method from a seed layer of ZnO (~200 nm) on a PET substrate and encapsulated by a PDMS layer (thickness of 20 μm) as the piezoelectric medium. An Au metal thin film (~120 nm) and a layer of poly(methyl methacrylate) (~2 μm, PMMA) serve as the top electrode and packaging material, respectively. Strain induces changes in the Schottky barrier height of the ZnO/Au interface, thereby modifying the resistance of the sensor. The exponential current dependence of the Schottky barrier results in a strain sensor with a high sensitivity (GF = 1813) and fast response time (<100 ms). Another example exploits electrospinning to produce fibers of P(VDF-TrFE) (average diameter, 260 nm) that, when delivered to a fast rotating collector, form free-standing and mechanically robust piezoelectric sheets with a thicknesses up to ~40 μm.[354] This material offers ultrahigh sensitivity for measurements of pressures as small as 0.1 Pa, with simple routes to body integration for detecting human motion.

3.1.3. Thermoregulatory. Thermoregulation, a remarkable physiological process, ensures that the human body maintains a core temperature between 36 and 37 °C, an extraordinarily narrow range. The physiological responses of sweating, changes in blood perfusion, and modulation of exposed skin surface area represent the primary means for temperature regulation. Abnormal body temperature signatures, either globally as a core measurement or through local, spatiotemporal patterns, can indicate sickness or the failure of any of the above mechanisms. As such, temperature is a critical biomarker for determining overall human health.

The ability to capture subtle, time-dynamic changes in temperature (~0.05 °C) over relatively short time scales (~1−5 s) and in a spatially resolved manner provides important information related to these key thermoregulatory processes. Precision infrared (IR) thermography represents the most sophisticated tool for measuring temperature, with additional utility in diagnosing cancer[355,356] and diabetes.[357] Traditional medical thermometers (e.g., liquid-filled or electronic) reliably record temperature variations of 0.1 °C;[358] however, due to their

DOI: 10.1021/acs.chemrev.8b00573
Chem. Rev. 2019, 119, 5461−5533

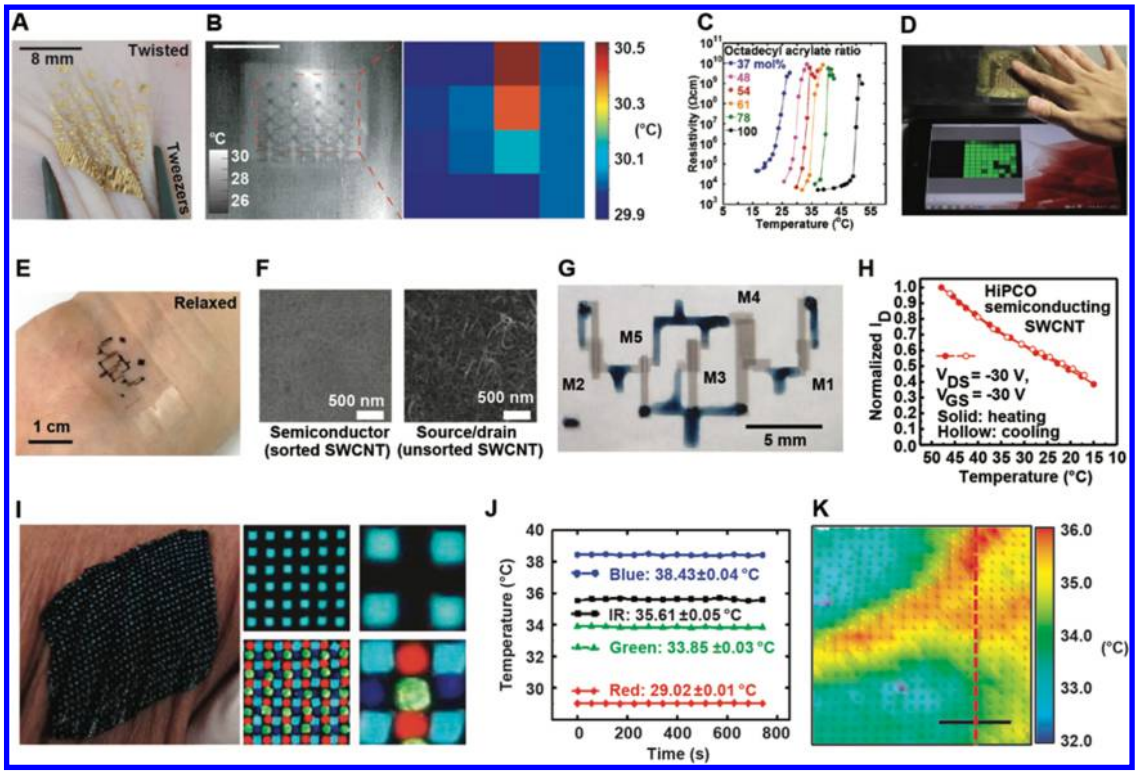

Figure 9. Temperature sensors. (A) Optical image of an array of temperature sensors, based on the temperature coefficient of resistance (TCR) of gold, highlighting their conformal, epidermal contact to the skin and (B) quantitative correlations between measurements with such devices and those with an IR camera (scale bar, 10 mm). (A,B) Reproduced with permission from ref 210. Copyright 2013 Springer Nature. (C) Acrylate-based block copolymer composites offer changes in resistance by many orders of magnitude across a narrow temperature band, with (D) strong signals demonstrated on a biological subject. (C,D) Adapted with permission from ref 377. Copyright 2015 National Academy of Sciences. (E) Optical image of a carbon nanotube-based thin-film transistor (TFT) on an elastomeric substrate, mounted on skin. (F) SEM images showcasing the types of CNTs used in the embodiment. (G) Optical image of a device architecture for motion noise rejection and (H) quasilinear temperature performance over a biologically relevant range of temperatures. (E–H) Adapted with permission from ref 365. Copyright 2018 Springer Nature. (I) Optical image of a colorimetric temperature sensor based on thermochromic liquid crystals on black PDMS, mounted on skin, with insets that show colorimetric dots and reference markers. (J) Calibrations for pigments used in this embodiment. (K) Image processed data that clearly show the presence of an artery (scale bar, 1 cm). (I–K) Adapted with permission from ref 378. Copyright 2014 Springer Nature.

relatively large thermal masses, these thermometers require long equilibration times (~2 min), thereby limiting the ability for tracking time-dependent processes.[210] In contrast to these methods, emerging classes of ultrathin, skin-integrated sensors exploit advances in materials science and microfabrication to enable highly sensitive, time-resolved measurements of temperature across nearly any region of the body, in a mode that has the additional advantage of enabling continuous monitoring of temperature, as a wearable.

Measurements of temperature typically rely on changes in the resistive, semiconducting, or optical properties of a material. Examples include metals (gold[359,360]), block copolymer composites,[361] conducting polymers,[117,362,363] liquid metals,[364] carbon nanomaterials,[365] 2D materials (e.g., graphene,[366−369] graphene oxide[370]), crystalline semiconducting molecules (e.g., pentacene[371]), silk,[372] and hydrogels.[373,374] Most published studies on skin-integrated devices involve a relatively narrow subset set of these materials options.

Devices that incorporate thin, FS structures of metal provide a widely used and versatile type of sensor whose response follows from the temperature-coefficient of resistance (TCR) of the metal. Several publications[210,375] highlight the utility of sensors of this type in performing precise temperature measurements on the skin by engineering them into ultrathin, skin-like forms. Gold is a common choice of metal due to its chemical inertness and linear response over a range of temperatures that include physiologically relevant values. The TCR of bulk gold is 0.0025 Ω ohm^{-1} °C^{-1}, although in practice an empirical calibration process connects temperature to resistance, to account for slight variations in device geometry and subtle thickness related variations in the TCR value. The extremely low thermal mass of these devices represents a key feature that allows for a rapid response to changes in the temperature of the skin in a manner that also does not affect the natural temporal dynamics of these changes. A typical Au-based sensor has a thermal mass per unit area of <150 μJ cm^{-2} K^{-1} in its isolated state and a thermal mass per unit area of ~7 mJ cm^{-2}K^{-1} with the addition of a < 100 μm thick silicone substrate and encapsulation layer.[210] Temperature response times of this latter construction are below 15 ms. The sensitivity is ~1 Ω °C^{-1} (corresponding to a temperature resolution of ~20 mK) with negligible hysteresis and quantitative correlation to IR imaging. Open-mesh FS interconnects impart effective levels of stretchability that exceed requirements for integration on the skin, with the additional capability of accommodating arrays of sensors for spatial thermal mapping as shown in (Figure 9A,B). When coupled with advanced thermal models, multilayer stacks of such sensors can also measure heat flux and, therefore, core body temperature.[376]

Advanced materials can greatly enhance the equivalent TCR values over those possible with simple metals. The electrical

DOI: 10.1021/acs.chemrev.8b00573
Chem. Rev. 2019, 119, 5461−5533

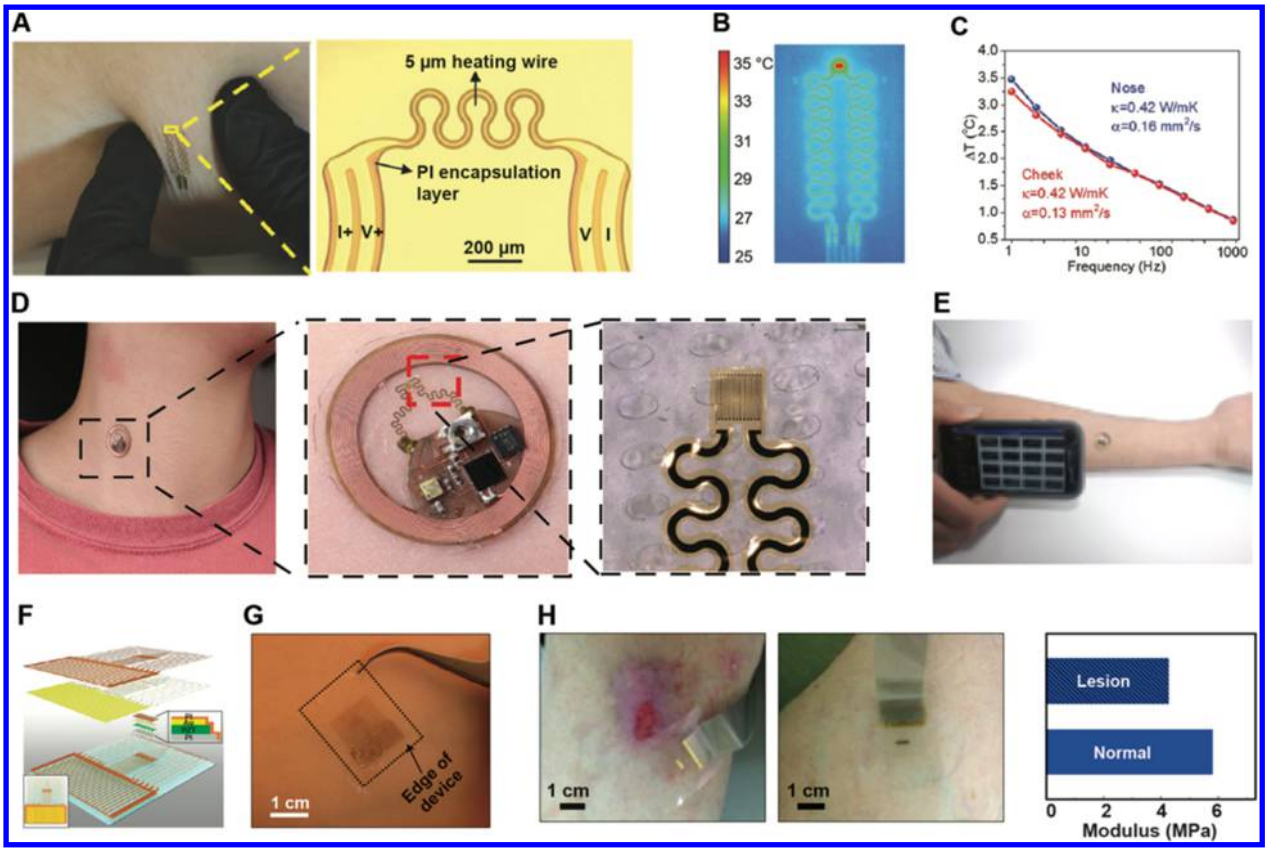

Figure 10. Sensors for measuring skin properties. (A) Optical image of a stretchable 3ω sensor on the skin, with inset that shows an optical micrograph of the 4-wire measurement. (B) IR thermograph showing local actuation at the 3ω element. (C) Frequency sweep of the amplitude of the thermal wave from which both thermal conductivity (k) and thermal diffusivity (α) of the skin can be determined. (A−C) Adapted with permission from ref 388. Copyright 2017 Wiley-VCH Verlag GmbH & Co. KGaA. (D) Optical images and enlarged views of transient plane-source systems for measuring the thermal properties of skin and (E) simulation of smartphone readout from an NFC-based sensor. (D,E) Adapted with permission from ref 389. Copyright 2018 Wiley-VCH Verlag GmbH & Co. KGaA. (F) Schematic illustration of a piezoelectric measurement system that incorporates PZT sensing/actuating elements connected via stretchable serpentine wires. (G) Optical image of a sensor on healthy skin. (H) Optical images of sensors on skin with lesions, with data that illustrate strong differences in Young's modulus between the lesion and healthy skin. (F−H) Adapted with permission from ref 390. Copyright 2015 Springer Nature.

resistivity of conductive polymer composites, such as a binary polymer composite of PE and poly(ethylene oxide) (PEO) with a Ni microparticle filler[361] or PDMS with graphite,[117] is highly dependent on temperature.[379] Recent work demonstrates that a semicrystalline acrylate copolymer with conductive graphite particles (2−3 μm diameter) exhibits an octadecyl acrylate concentration-dependent phase change (to an amorphous structure) across a physiological temperature range (25−50 °C). Tuning the concentration results in a sensor with a resistivity change more than 6 orders of magnitude in response to a temperature change less than 5 °C (sensitivity, 0.1 Δ°C; response time, 100 ms; Figure 9C,D).[377] Particularly noteworthy is that the sensor maintains at least 4 orders of magnitude resistivity change over 1800 temperature loading cycles (29.8−37.0 °C) in contrast to the significant performance degradation typical of polymer composite sensors after ∼100 thermal cycles. By contrast to metal TCR sensors, the promise of enhanced sensitivity is offset by the highly nonlinear response that limits the broad utility of this material class for skin-interfaced temperature sensing.

An important parameter for TCR-based sensors is their response to mechanical strain, a potentially confounding effect in the practical operation of these devices. As detailed in section 3.1.2, in simple metals, strain induces a geometry-based change in electrical resistance. For skin-interfaced stretchable temperature sensors, deconvolution of strain from temperature-induced resistance changes is critical for robust function while undergoing motion and deformation. Typical strategies include utilization of multiple sensors and signal processing[380] or sophisticated structural engineering schemes (section 2.1.2) to reduce strain effects.[375,381] For example, the FS interconnects and silicone layers for metal temperature sensors can absorb almost entirely a 10% uniaxial strain in a manner that induces <0.02% strain in the responsive materials of the sensors. This strain corresponds to a relative temperature error of <50 mK due to a change in electrical resistance.[210] Additional methods for further decoupling use metallic bilayers with distinct strain and temperature responses or multilayer sensor configurations or active responsive material sensors.

As responsive materials, semiconducting elements are attractive alternatives to metals due to their capacity to support active addressing across large arrays of temperature sensors. A common approach exploits the strong temperature dependence of turn-on voltage in P−I−N diodes.[173,210] More recent work[365] demonstrates that the use of SWCNTs as the semiconductor components of thin film transistors (TFTs, Figure 9E−H) allows the implementation of differential voltage readout circuits (formed with these TFTs) to reject signals associated with

DOI: 10.1021/acs.chemrev.8b00573
Chem. Rev. 2019, 119, 5461−5533

mechanical strain. Here, semiconducting SWCNTs form the channel while unsorted SWCNTs (as produced, mixture of semiconducting and metallic) form the source and drain electrodes. Laminating these sensors onto a hydrogenated SEBS elastomer yields a soft, stretchable system capable of robust operation on the skin. Here, the differential readout methods (static, dynamic) suppress strain-induced errors to enable accurate measurement of temperatures ranging from 15 to 55 °C with an absolute uncertainty of ±1 °C (ε < 60%).

An alternative to electrical sensing uses changes in color associated with thermochromic materials. One example[378] uses thermochromic liquid crystals patterned into arrays and embedded in a matrix of PDMS doped with carbon black and pigmented, fixed-color dots for calibration (Figure 9I,J). With thicknesses <50 μm, these platforms have low thermal mass and low modulus, elastic mechanical properties. Color extraction algorithms applied to digital images of such devices yields spatiotemporal information on temperature of the skin, with a resolution <50 mK, sufficient to image, as an example, vasculature at the near surface regions of the skin (Figure 9K).

3.1.4. Skin Properties. Human skin is a complex, heterogeneous biomaterial that serves as a protective barrier to pathogens, toxins, and other environmental hazards,[382] modulates transepidermal water loss,[383] and is essential to many physiological processes.[384] The basic physical properties of skin enable these vital functions and are themselves indicators of overall human health. This section introduces recent advances in soft, skin-interfaced sensors that elucidate the intrinsic thermal, electrical, and mechanical properties of skin, critical for disease diagnostics and evaluation of medical therapeutics.

The structure of skin dictates its thermal properties. The outermost layer, the stratum corneum, is avascular and keratinized.[383] The vascularized underlying epidermal and dermal layers reject warm arterial blood to the surface as a key thermoregulatory mechanism. These features result in diverse, depth dependent thermal properties that, taken together with clinical diagnosis or other indicators, provide compelling insights into skin physiology. The electrical sensors of temperature outlined in section 3.1.3 can serve simultaneously as precise thermal actuators. When used in this manner, these platforms can induce and measure transient temperature responses in a way that enables determination of skin transport properties. The two measurement approaches include epidermal adaptations of the transient plane source[385,386] and 3ω[387,388] technique. The former supplies short pulsed or step-function heating (several seconds) to the skin while simultaneously recording the temperature. Quantitative analysis of the measured response can yield both the thermal conductivity (k) and diffusivity (α) of the skin.[359] The 3ω technique uses an applied voltage at a frequency of ω to generate heating at a frequency of 2ω and, therefore, a change in resistance at a frequency of 3ω (Figure 10A−C). The amplitude and phase of this data can yield k and α.[388]

The proper function of the epidermis as a mechanical and diffusion barrier for ambient airborne toxins relies, in part, on the proper amount of free and bound water in this layer.[383] The two layers of the epidermis, the stratum corneum and stratum granulosum, consist of a layer of corneocytes and a lipid matrix in a lamellar structure. The transport of free water between these layers results in a "brick and mortar structure" and is, therefore, critical to maintaining the structure. A decrease in water content (<10%) dehydrates the outer layers to weaken the skin barrier property. A typical hydration level is ∼20%.[391−401] As a result, accurately measuring the skin hydration is important for disease diagnostics (e.g., eczema, psoriasis, atopic dermatitis), and for evaluating abnormal skin responses (e.g., stress, hormone) and the effectiveness of medical therapies.[402,403]

Measuring skin thermal transport properties or electrical impedance enables the rapid assessment of skin hydration. The dependence of thermal measurements on hydration state arises from the difference between the thermal properties of water and the tissue itself.[389] For example, an epidermal thermal sensor/actuator combination can determine the thermal conductivity, which serves as a proxy for free-water content in skin and, therefore, skin hydration.[210] As demonstrated by measurements on human subjects, this approach yields results that quantitatively match those obtained from a commercial moisture meters.

By contrast, electrical impedance measurements exploit the dependence of the electrical conductivity and permittivity of the skin on hydration state as a result of the influence of free and bound water in the skin.[392,404] A skin-interfaced device that includes concentric ring electrodes of Au metal FS traces can provide insights into the hydration profile of the stratum corneum by monitoring hydration-dependent impedance changes at either a sweeping or fixed frequency.[403,405]

Integration of both methods into a single epidermal platform[402] yields greater insight into overall hydration state. Thermal conductivity measurements, in contrast to those based on electrical impedance, typically probe to depths beyond the stratum corneum, as deep as several millimeters, depending on the device design.[406] Recent work[389] offers an entirely battery-free, wireless (NFC) embodiment that combines the advantages of ultrathin, soft epidermal electronics, namely low thermal masses and intimate thermal coupling to skin, with those afforded by flexible circuit board structuring in a miniaturized form factor for long-term skin hydration monitoring (Figure 10D,E).

As a material system, the skin exhibits complex, nonlinear, strain-limiting, and viscoelastic mechanical behaviors.[407] Monitoring the biomechanical properties of skin can aid in tracking processes associated with wound healing[408] and in detecting skin diseases.[390] For example, the viscoelastic responses of skin relate to the pathology of systemic sclerosis.[409] Conventional measurement methods such as those based on nanoindentation and pressure-based suction are well suited to basic studies, but they do not offer capabilities as a wearable system for continuous tracking.[390] Recent work illustrates that PZT nanoribbons joined by stretchable interconnects into arrays of millimeter-scale mechanical sensors and actuators on thin substrates of PDMS can induce and subsequently measure deformations in the skin (Figure 10F−H).[390] When combined with constitutive models of skin and finite element modeling of the response,[410] the resulting data can determine the Young's modulus of skin. Such platforms can be applied in a noninvasive manner to nearly any region of the skin, in a variety of healthy and pathologic states, before and after topical application of lotions or salves. The results have relevance not only in clinical aspects of skin health but in consumer oriented skin care and cosmetics.

3.1.5. Vascular Dynamics. Biophysical signals generated by vascular dynamics, such as pulse wave pressure waveforms, pulse wave velocity, and blood pressure (BP), serve as informative, noninvasive parameters of utility in the diagnosis of cardiovascular conditions such as arrhythmias,[411] pulmonary hypertension,[412] or pericardial disease.[413,414] BP, captured using a cuff sphygmomanometer, is one of the most common clinical

DOI: 10.1021/acs.chemrev.8b00573
Chem. Rev. 2019, 119, 5461−5533

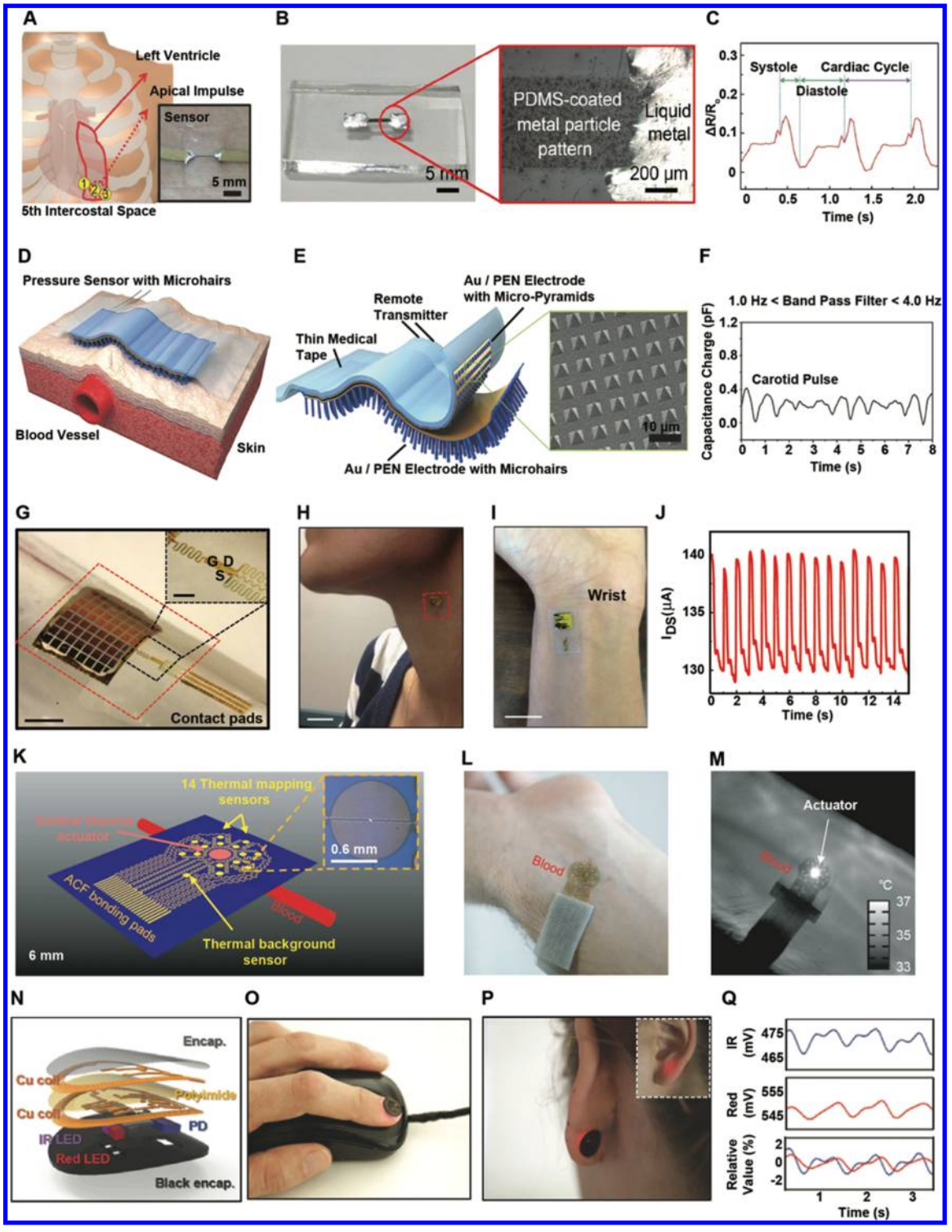

Figure 11. Sensors for analyzing vascular dynamics. (A) Schematic illustration of the locations of the resistive sensor (inset: an optical image of the sensor), (B) optical image of the patterned AuNPs and liquid metal contacts on a PDMS substrate, and (C) apexcardiogram contours that exclude the respiration wave in the normal state. (A–C) Adapted with permission from ref 280. Copyright 2016 Wiley-VCH Verlag GmbH & Co. KGaA. (D) Schematic illustration of a capacitive pressure sensor with microhairs for detecting the pulse rate from the skin. (E) Cross-sectional diagram of the microhair-structured sensor and (F) extracted waveforms associated with pulses measured at the carotid artery from the capacitive response of the sensor. (D–F) Adapted with permission from ref 212. Copyright 2014 Wiley-VCH Verlag GmbH & Co. KGaA. (G) Optical images of a thin conformable piezoelectric pressure sensor on a cylindrical glass support (scale bar, 5 mm; inset scale bar, 200 μm), (H) neck, and (I) wrist (H–I scale bar, 1 cm). (J) Current between drain and source (I_{DS}) as a function of time due to the response of the sensor from blood pressure from the neck. (G–J) Adapted with permission from ref 211. Copyright 2014 Springer Nature. (K) Schematic illustration of an ultrathin blood flow sensor, including a blood vessel near the skin surface and (L) an optical image and (M) an infrared image of a device on the skin over a vein. (K–M) Adapted with permission from ref 386. Copyright 2015 the American Association for the Advancement of Science. (N) Schematic illustration of a millimeter-scale, NFC-enabled pulse oximeter device and optical images of device on (O) the fingernail and (P) the back of the earlobe. (Q) Extracted signals from

DOI: 10.1021/acs.chemrev.8b00573
Chem. Rev. 2019, 119, 5461–5533

Figure 11. continued

operation in the IR and red and relative values at these two wavelengths. (N−Q) Adapted with permission from ref 222. Copyright 2016 Wiley-VCH Verlag GmbH & Co. KGaA.

measurements and is indicative of the critical role of these biophysical signals in assessing overall health status. This section highlights soft, skin-interfaced systems that are capable of recording these signals and their potential use in continuous monitoring.

The pulsatile nature of vascular dynamic signals can be captured using resistive,[218,281,291,292,316,415,416] capacitive,[212,216,283] or piezoelectric[213,214] skin-interfaced sensors. In general, accurate measurements require sensors with high sensitivity, fast response times, and minimal hysteresis due to the fast, subtle nature of strains induced by blood flow at the surface of the skin. Here, as with the kinematic sensors described in section 3.1.2, the unique advantages and trade-offs of each sensing modality dictate use, as highlighted in the following embodiments.

Resistive sensors represent a popular choice. As an example, a patterned composite material that involves AuNPs in a PDMS matrix allows recordings of the apexcardiogram (ACG), which is the time-related volume and pressure changes in the heart (Figure 11A).[280] Here, strain induced changes in the percolation pathways through the AuNPs offer high sensitivity (GF: 8) to small strains (ε < 2%) induced by apex palpitation, with negligible hysteresis for strains below 10% (Figure 11B). The device measures ACG contours when interfaced onto the skin in the fifth intercostal space, the ideal location for apical impulse detection. These waveforms contain information about heart operation (e.g., opening/closing valves) as a noninvasive means for diagnosing coronary artery disease. A representative mechanocardiogram (Figure 11C) captures changes in the temporal volumes and pressures associated with cardiac function.[280] Another type of device, known as a flexible piezoresistive pulse sensor (FPS), uses a fabric decorated with carbon black epidermal ECG electrodes for cuffless measurements of blood pressure measurements.[417] The FPS sensor allows measurement of the pulse waveform due to its fast response time (4 ms at ΔP = 28 mmHg) with low hysteresis. The pulse transit time (PTT) recorded by an ECG sensor located away from the FPS sensor enables an estimation of blood pressure from the following logarithmic relation: $P = a(\ln(\mathrm{PTT})) + b$, where a and b are subject-dependent coefficients. This integrated skin-interfaced sensor, by combining PZT-based mechanical pulse and ECG measurements through well-established mathematical models,[418] offers a promising solution for cuffless and real-time BP monitoring.

Capacitive pressure sensors can also be used in related applications. One interesting platform[212] exploits a unique microhair interfacial structure to improve epidermal interfacing and enhance sensor signal-to-noise ratio (Figure 11D). The pressure sensor is a gold/polyethylene naphthalene (Au/PEN) electrode conformally deposited on a micropyramidal-shaped PDMS dielectric layer. The microhair interfacial structure, consisting of a regular array of circular pillars (30 μm diameter; aspect ratio of 3, 6, and 10; PDMS), maximize the effective contact between the sensors and the irregular surface of the epidermis, yielding a sensor with a sensitivity of ∼0.5 kPa^{-1} and a response time of ∼30 ms (Figure 11E). Demonstrations include use of this type of device to track pulse waves associated with blood flow through the radial artery and the jugular vein (Figure 11F). Another example[419] involves ultrathin (1.9 μm) devices that include a transparent (85% optical transmission) electrode layer (PEDOT:PSS-coated PET sheet, 1.9 μm) coated with an ionic material (a perfluorosulfonate linear ion-exchange polymer). The skin, itself electrically conductive, serves as the second electrode in the capacitive pressure sensor. The sensor, separated from the skin by an air gap (50 μm), forms a capacitive electric double layer (EDL) interface between the ionic layer and the epidermis upon contact. Capacitance changes arise from pressure-induced variations in the EDL to enable pressure measurements with high sensitivity (5 nF kPa^{-1} for <5 kPa; 0.15 nF kPa^{-1} for 10−30 kPa) and fast response times (<1 ms) in detection of pressure waveforms from the temporal, carotid, radial, and dorsalis pedis artery. Measurements of the pulse wave velocity can yield information on arterial stiffness.

More advanced embodiments use piezoelectric pressure sensors for high sensitivity to dynamic stimuli, with wide frequency response range.[121] One example utilizes a PZT element to modulate the field across the channel of an adjacent SiNM n-MOSFET (Figure 11G).[211] This construction yields a stretchable, ultrathin (25 μm), compact (∼1 cm^2) device capable of softly laminating to the skin to obtain very low limits of detection (0.005 Pa) and response times of ∼0.1 ms. Designed to measure the blood pressure waves at either the wrist or neck, this device uses the measured wave peaks to generate the radial artery augmentation index and time differentials between peaks as a measure of arterial stiffness (Figure 11H−J).

Patterns of blood flow through microvascular and macrovascular vessels represent additional biophysical signals with relevance to diagnosing many pathologies in cardiovascular disease, atherosclerosis,[420] diabetes, inflammation, and aging.[421] Arterial and venous blood vessels serve key mechanistic roles in thermoregulation by providing the requisite flow rates for efficient heat exchange.[422,423] These flows alter thermal transport rates in well-defined ways for efficient thermal management.[424] The measurement of spatial anisotropies of thermal transport properties discussed in the preceding section (section 3.1.4) in the context of determining the skin hydration level can also yield quantitative information on vascular flow dynamics.[359,425,426] By using the thin metallic temperature sensors introduced in section 3.1.3, together with one or more thermal actuators, these devices provide continuous, high-quality mapping of macrovascular blood flow.[386] In a typical design, a thermal actuator locally increases the temperature of the adjacent tissue via measured, low-power DC heating at a rate governed by the thermal diffusivity of the skin (Figure 11K). The presence of local near-surface blood vessels induces changes in the skin thermal diffusivity along the direction of flow. Temperature sensors upstream and downstream of the actuator capture this thermal anisotropy. With sufficient density, sensor networks of this type can yield data for 2D spatial mapping as shown in (Figure 11L,M). Similar devices can monitor changes in the rates of isotropic thermal spreading to determine alterations in microvascular flow induced, for example, by vasoconstriction or vasodilation of capillary beds.[386]

By contrast to thermal and electrical, optical measurements of hemodynamics benefit from but do not require physical contact with the skin. Measurements of heart rate and heart rate

DOI: 10.1021/acs.chemrev.8b00573
Chem. Rev. 2019, 119, 5461−5533

variability (HRV)[427] can be extracted from temporal variations in absorption associated with hemoglobin in the blood.[428] Optical sensors measure the amount of light either transmitted or scattered after passing through tissue of interest.[429] Simultaneous illumination and absorbance measurements at two different wavelengths (red and infrared) can yield blood oxygenation levels.[427] In PPG,[430,431] the signals of interest correspond to the cardiac pulse and associated oscillatory variation in blood volume. Here, device geometry, specifically the configuration of the illumination source and optical detectors, is an important consideration. Most setups exploit a transmission mode of measurement where the light source and detector lie on opposite sides of a target body part such as the fingertip or earlobe.[432] The strong signal produced by this geometry results from light transmission exclusively through the tissue of interest and a large, often considerable, optical path.[433] A key limitation of this geometry is that it does not provide a straightforward route to miniaturization.[434] Co-location of the light source and detector on the same plane represents an alternative geometry well suited for miniaturization and, therefore, frequently adapted for skin-interfaced devices. The main challenge is in susceptibility to motion artifacts arising from changes to the optical path length induced by the relative motion of optical components and the underlying tissue.[433] Signal conditioning via digital and analogue filters can reduce much of this motion-induced noise,[435] particularly when performed in digital filters aided by accelerometer data.[436] Increasing the intensity of the light source and the size and sensitivity of the detector[437] can also yield improvements; however, unavoidable changes in the vascular structure relative to the light source/detector inhibits the ability for chronic, uninterrupted recording.

Polymer/organic light-emitting diodes and organic photodetectors are attractive choices for pulse oximetry.[215,438] High performance alternatives based on inorganic electronic and optoelectronic components in soft, skin-like form factors represent contemporary device embodiments.[439] A recent successful demonstration of an entirely battery-free wearable device based on NFC protocols demonstrates the potential this approach in sensor sizes and geometries optimized for wearability.[440] The example[222] in Figure 11N features a red and infrared LED activated by a microcontroller powered by the NFC technology available in almost all modern smartphones. This platform, with a mass of only 0.15 g, conforms intimately to the fingernail (Figure 11N−Q). The stable interface, coupled with the low mass, allows for a motion-artifact-free PPG and arterial oxygenation readout. The battery free nature of this device also enables continuous readout, offering a new tool set for at-home and remote monitoring. Another embodiment integrates an organic phototransistor composed of poly(*N*-alkyl diketopyrrolo-pyrrole dithienylthieno[3, 2-*b*]thiophene) (DPP-DTT) and a fullerene derivative, [6,6]-phenyl-C61-butyric acid methylester (PCBM), with an commercially available inorganic light-emitting diode to form an epidermal PPG sensor that encompasses a finger.[431] The HRV from the epidermal PPG sensor correlates favorably (correlation coefficient of 0.88) with data from ECG-derived HRV for 10 human volunteers. The PPG signal from the sensor, when combined with the ECG signal from the commercial device, enables calculation of BP values using a pulse transit time (PTT) method with a mean absolute difference to the reference BP of ∼3 mmHg.

3.2. Biochemical Signals

Monitoring biophysical responses provides only a partial window into the health status of an individual; a comprehensive assessment requires the additional consideration of biochemical signals.[17,275,441−444] Traditional biochemical measurements require expensive analytical instruments operated by trained personnel in centralized laboratory facilities.[445−447] A typical workflow involves sample collection (a biofluid, commonly blood), pretreatment, and subsequent analysis using specialized tools for detecting and quantifying the concentrations of biochemical targets of interest.[448,449] The advent of inexpensive, hand-held biochemical sensing devices for rapid, point-of-care biochemical detection promises to bypass these and other limitations of conventional testing.[450−452] Figure 12 illustrates

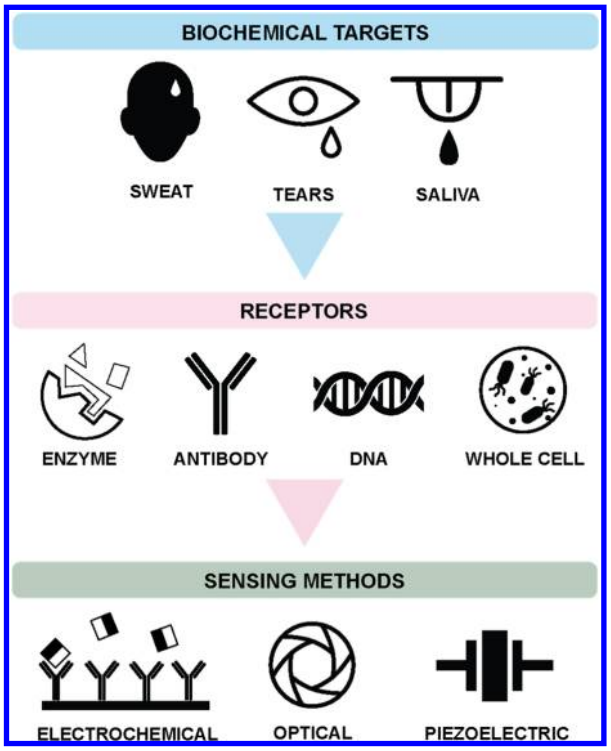

Figure 12. Schematic illustration of the main components of biochemical sensors.

the major components and working principles of a typical biochemical sensor. The receptor layer generates physicochemical signals in the presence of a chemical analyte present in the sample; the transducer converts the signal into an electrical or optical response that can be rendered into quantitative form for the user. Hand-held chemical sensors designed to detect blood analytes have two main drawbacks. First, collection of samples of blood is an invasive, painful process, especially for newborns, the elderly, and trypanophobics. Second, testing of blood with current technology (blood draws) is impractical for applications that require high sampling rates. These drawbacks pose particular problems for diabetics,[453] the critically ill,[454] athletes,[455] and people in demanding work environments (e.g., laborers,[456] active military personnel[457]).

Biofluids such as sweat, saliva, and tears represent potential alternatives to blood and are of interest due to their noninvasive modes for sample collection and to the rich library of biochemical targets that they contain. For example, the concentration of chloride in sweat represents the standard of

DOI: 10.1021/acs.chemrev.8b00573
Chem. Rev. 2019, 119, 5461−5533

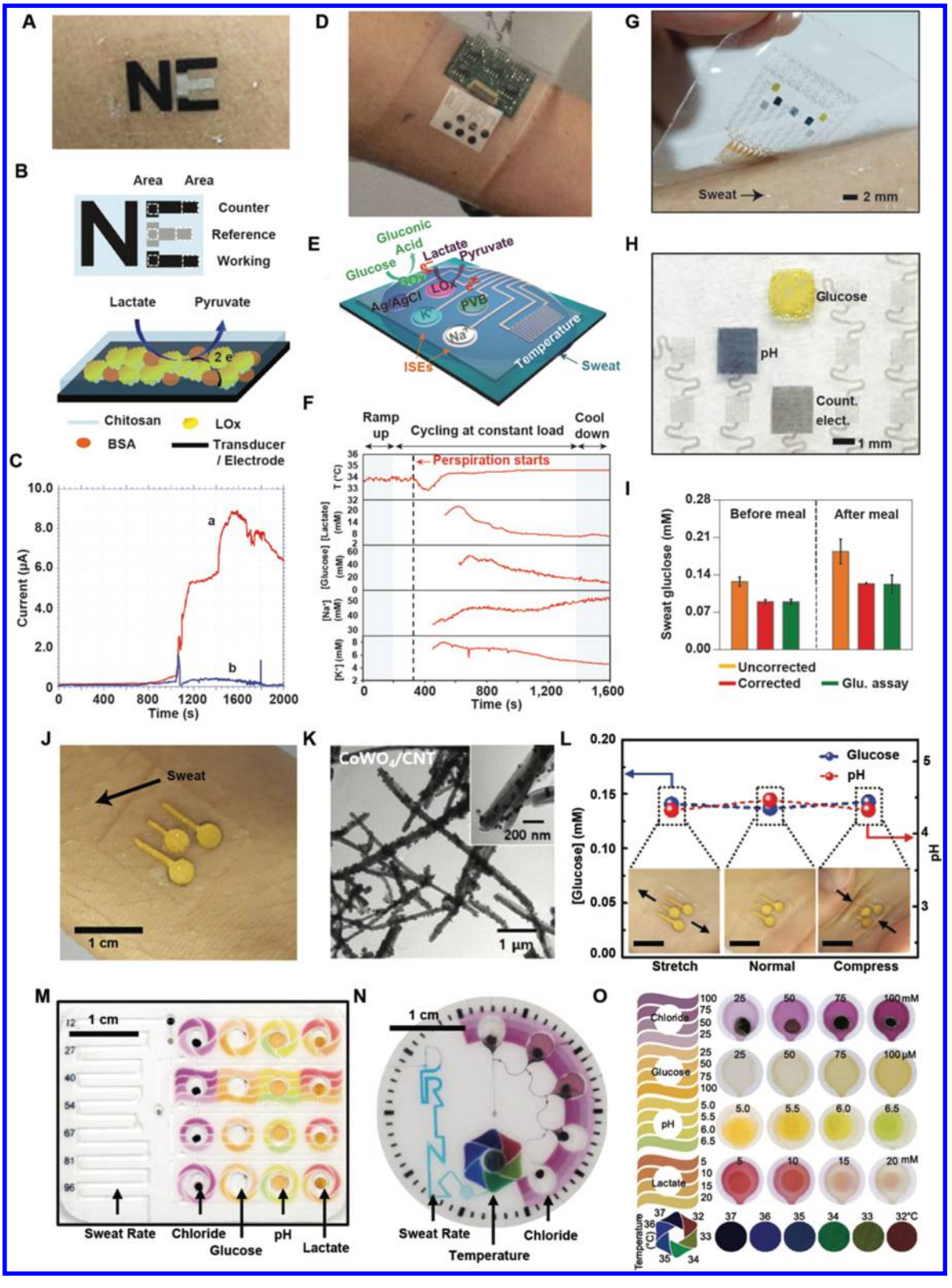

Figure 13. Skin-integrated metabolite sensors. (A) Photograph and (B) schematic illustration of sensor components and enzymatic reactions and (C) human trials showing real-time data collected using a temporary tattoo-based lactate sensor. (A–C) Adapted with permission from ref 462. Copyright 2013 American Chemical Society. (D) Photograph and (E) schematic illustration of sensor components and enzymatic reactions and (F) human trials showing real-time data collected on multiple analytes in sweat. (D–F) Adapted with permission from ref 494. Copyright 2016 Springer Nature. (G) Image showing the process for application of a soft, stretchable glucose sensor on the skin. (H) Close-up view of different electrodes for the sensor patch. (I) Sensor response before and after meal consumption. (G–I) Adapted with permission from ref 495. Copyright 2016 Springer Nature. (J) Image of a stretchable AuNS-based electrode ensemble for sweat glucose monitoring and (K) SEM of $CoWO_4$/CNT as a catalyst for glucose detection. (L) Data acquired from a nonenzymatic glucose sensor during field tests. (J–L) Adapted with permission from ref 496. Copyright 2018 American

DOI: 10.1021/acs.chemrev.8b00573
Chem. Rev. 2019, 119, 5461–5533

Figure 13. continued

Chemical Society. (M,N) Photographs of multiparameter colorimetric sweat sensors. (O) Concentration dependent color evolution associated with this colorimetric sweat sensor. (M−O) Adapted with permission from ref 220. Copyright 2018 American Association for the Advancement of Science.

care in screening of infants for cystic fibrosis.[458] When used in conjunction with the sodium concentration, this parameter is additionally useful in monitoring for electrolyte imbalance and the onset of hyponatremia.[459,460] Multiple reports indicate that the concentration of lactate in sweat can be used to identify both the transition of the human body from an aerobic to anaerobic state during physical activities[461−466] and onset of pressure-induced ischemia.[467] Similarly, analyzing the loss of minerals such as iron[468] and zinc[469,470] through sweat can provide insights into recovery after physical stress. Recent studies also demonstrate the utility of sweat glucose for noninvasively detecting blood glycemic transitions, of critical importance in diabetes management[15,471−473] or prevention of exercise-induced hypoglycemic shock.[474] Beyond sweat, the permeation of blood constituents into saliva via transcellular or paracellular pathways make saliva interesting for diagnosis of hormonal, metabolic, emotional, and nutritional health status.[475] Although comparatively nascent in development, interest in tear analysis continues to grow due to the complex biological pathways by which blood constituents diffuse into tears.[476]

Body-interfaced platforms that sample these biofluids may provide a path toward completely noninvasive, continuous measurement of physiologically important chemical biomarkers for health monitoring. As with biophysical sensing technologies, recent developments in chemistry, materials science, bioengineering, and electronics create opportunities for flexible and stretchable chemical sensing platforms suitable for use on the skin. The following subsections summarize major advances in such systems.

3.2.1. Metabolites. The rich variety of metabolites in sweat, saliva, and tears are potential indicators of health state. Most skin-interfaced metabolic sensors leverage amperometric measurement techniques due to their inherent sensitivity, selectivity, and low power requirements and their capacity for miniaturization. A limited number of examples exploit electrochemical transistors.[464,477,478] Amperometric sensors are either first-[479] or second-[462] generation enzymatic biosensors, with recent examples illustrating noninvasive routes to body-interfaced metabolic sensing.[480] In first-generation biosensors, electrons transfer to molecular oxygen and the measurement is of the resulting decrease in the oxygen concentration and/or the produced hydrogen peroxide. Second-generation biosensors use artificial mediators or nanomaterials to transport the electrons between enzyme active sites and the electrode. As with traditional electrochemical sensors, both types of devices incorporate a biorecognition element (enzyme or a transition metal oxide for nonenzymatic sensing) to catalyze the oxidation/reduction of an analyte to produce an electrical current that is proportional to concentration.[481,482]

Two interrelated factors govern metabolic sensor performance in epidermal applications: (1) the sensitivity and (2) the bio-interface. High sensitivity is required for detecting most analytes of interest, as they typically appear in low concentrations in noninvasively sampled biofluids. Intimate, conformal device interfaces to targeted tissues, typically the skin, are essential for high fidelity capture of biofluids in a way that avoids irritation and sample contamination. Bio-integrated metabolic sensors utilize the designs and materials strategies outlined in section 2 to realize soft, compliant sensors on substrates that range from textiles[483−486] and flexible plastic sheets[443,463,487] to stretchable silicone membranes[483,488] as the basis of epidermal,[30] salivary,[489] and lachrymal[476] metabolic sensing. Many systems rely on nano/microscale materials for improved sensitivity. Specifically, nano/microstructuring sensor electrode surfaces in 1D,[490] 2D,[491] or 3D[492] architectures can significantly increase the surface area which, in turn, enhances the loading of chemical reagents and improves the electrical pathways between reagents and underlying current collector. Moreover, such nano/microstructures often exhibit higher catalytic properties compared to their bulk counterparts, thereby augmenting sensor performance for the detection of analytes at low concentrations.[493]

As mentioned, sweat is of significant recent interest as a noninvasively sampled biofluid due its ready access via eccrine glands in the skin and the wide range of possible mounting locations across the body.[497] Although sweat contains many metabolites of interest, most work focuses on detecting glucose and lactate. An early example[462] uses a flexible, thin tattoo paper substrate with a backbone of screen printed conductive carbon and silver/silver chloride ink electrodes for continuously monitoring lactate concentrations in human perspiration (Figure 13A). The 3-fold functionalization of the carbon-based working electrode with (1) tetrathiafulvalene/CNT complex, where the CNTs increase the sensor surface area and help adsorb tetrathiafulvalene via $\pi-\pi$ bonding and the tetrathiafulvalene promotes electron transfer between the active sites of the enzyme and the CNTs, (2) lactate oxidase enzyme to selectively detect the analyte, and (3) chitosan (a biocompatible polymer) to minimize reagent leaching and to extend the detection range to physiologically relevant concentrations of lactate in sweat (1−30 mM), with negligible interference from other chemical species such as, glucose, uric acid, ascorbic acid, and creatinine (Figure 13B).

The real-time detection of sweat biomarkers is important as the concentrations of constituents in sweat can dynamically vary depending on physiological status. Continuous analysis requires that newly produced sweat immediately interacts with and subsequently transports away from the sensor surface to permit a constant reaction/analysis process. In one case,[462] a channel defined by the adhesive layer routes analyzed sweat away from the sensor surface. On-body evaluations of control (without enzyme) and fully functional devices on perspiring human subjects demonstrate a high selectivity to lactate (Figure 13C) and stable performance without motion artifacts due to the conformal skin interface.

Advanced metabolic sensing systems incorporate multiple chemical sensors onto a single platform and utilize epidermal electronic designs with integrated BLE wireless communication capabilities to eliminate the necessity for wired, benchtop electrochemical analyzers as used in the example described above. Figure 13D illustrates one such technology.[494] Here, the device simultaneously monitors sweat lactate and glucose as well as electrolytes (potassium and sodium) via amperometric and potentiometric techniques, respectively. The sensing elements use photolithographically patterned Au metal electrodes on a flexible PET sheet. Functionalization of the glucose and lactate

DOI: 10.1021/acs.chemrev.8b00573
Chem. Rev. 2019, 119, 5461−5533

working electrodes with Prussian Blue and corresponding enzymes (glucose oxidase and lactate oxidase) imparts selectivity (Figure 13E). The sensors exhibit linear responses to respective species within the physiological concentration range for sweat (lactate, up to 25 mM; glucose, 250 μM). A built-in temperature sensor allows for automated compensation for variations in skin temperature. On-body trials validate performance in real-life scenarios with participants riding stationary bikes while wearing sensors on their foreheads. The device transmits real-time data wirelessly to a smartphone for the user to analyze sweat composition (Figure 13F). The results correlate well with those from sweat samples collected and analyzed with conventional techniques.

Another recent example[495] uses a graphene-functionalized device with capabilities in sweat glucose monitoring and transcutaneous drug release for diabetes management (Figure 13G). The device exploits a soft, stretchable silicone membrane as a substrate and a sensing element based on glucose oxidase functionalized electrodes of a nanocomposite of Au-graphene with FS Au metal interconnects in a mesh structure. This nanocomposite increases the sensor surface area and establishes efficient electronic routes between the enzyme and the electrode surface in a stretchable form factor that results from the mesh construction. The device detects micromolar concentrations of glucose (0.1−0.5 mM) in human perspiration with high sensitivity and electrochemical performance that does not depend on mechanical deformation (up to 30% strain) (Figure 13H). The inclusion of a potentiometric polyaniline-based pH sensor and a temperature sensor enables pH and temperature correction of the glucose sensor data. Benchtop characterization under varying pH and temperature conditions as well as in the presence of interfering chemical species demonstrates robust performance for glucose sensing. Field trials highlight the practical application of this device for noninvasive tracking of blood glucose levels. Measurements of sweat glucose and blood glucose levels at regular intervals over several hours show strong correlations with time lags of ~30 min (Figure 13I). A prototype that combines glucose sensing with an array of bioresorbable microneedles for drug delivery foreshadows a possible scheme for glycemic level management.

The reliance on labile biological components, such as enzymes, antibodies, nucleic acids, or tissues, as receptors for analytes represents a key impediment to robust chemical biosensors. Such materials deteriorate if exposed to temperatures, pressures, or humidity levels that lie outside of a narrow range or if stored with (or without) certain chemical species. Skin-interfaced applications demand robust operation in a relatively uncontrolled environment with time varying ambient and skin temperatures, oxygen levels, and humidity and with biofluid that can involve varying ionic strengths and the presence of interfering chemistries. Utilizing certain stabilizers, such as polyelectrolytes and polyols, can minimize degradation and improve sensor stability,[30,498,499] but their use fails to completely solve challenges in sensor lifetimes.

Replacing bioreceptors with synthetic materials offers a promising alternative solution.[482] Recent work in this direction[496] involves a nonenzymatic, skin-interfaced electrochemical glucose sensor that uses cobalt wolframite ($CoWO_4$) (Figure 13J). Device fabrication involves vacuum filtering a solution of Au nanosheets through a template to define the electrode structure, followed by transfer printing onto a soft, stretchable silicone substrate. Such electrodes offer stretchability up to strains of 30% with minimal impact on sensing performance. Layer-by-layer assembly of positively and negatively charged CNTs increases the surface area of the electrode current collectors and improves the sensitivity from 3.73 to 10.89 $\mu A\ cm^{-2}\ mM^{-1}$. Dip coating the working electrode with a $CoWO_4$/CNT (Figure 13K) composite forms the basis of the nonenzymatic glucose detection capability. Specifically, the glucose selectively oxidizes at the $CoWO_4$ interface, even in the presence of other electroactive species (ascorbic acid, uric acid, urea, and acetaminophen) common to sweat, thereby producing a linear signal with glucose concentrations up to 0.3 mM (Figure 13L). Comparing sweat glucose levels in human volunteers recorded by the device (via a portable potentiostat) during repeated exercise sessions (cycling) over a single day to levels obtained using a commercial colorimetric glucose assay demonstrates the promise of nonenzymatic glucose monitoring.

Sensors of the type described above measure biochemical signals in human perspiration during athletic activity or during exposure to high temperatures and humidity levels. These requirements cannot be satisfied in many scenarios such as patient monitoring under ambient, sedentary conditions. Localized sweat stimulation provides a means to generate adequate sweat volumes for biochemical sensing. Here, transcutaneous delivery of sweat-inducing drugs such as acetylcholine, pilocarpine, bethanechol, methacholine, and carbachol via iontophoresis induces a localized sweat response for subsequent detection and analysis by skin-interfaced sensors.[500] As a long-established clinical method, this technique serves as the means for generating sweat in cystic fibrosis screening tests based on sweat chloride.[458] A recent demonstration[471] illustrates the use of this approach for nonclinical diagnostics in a device that integrates wireless, skin-interfaced sensors for sweat glucose and chloride with an iontophoretic system for the transdermal delivery of the sweat-inducing drug methacholine.

The platform includes two Au-based iontophoretic electrodes and electrochemical glucose and chloride sensors. Utilizing the device involves placing a gel with cholinergic agonist over the iontophoretic electrodes followed by 10 min of iontophoresis (current: 1 mA) to induce sweating. The glucose and chloride sensors analyze the composition of the resulting sweat. The construction and performance of the glucose sensor is similar to that described previously in this section.[494] Human subject studies indicate the potential for monitoring increases in sweat glucose after food consumption. A similar bio-integrated platform can electrochemically detect alcohol in sweat by use of Ag/AgCl-based iontophoretic electrodes for sweat generation and alcohol oxidase-functionalized amperometric sensors for selective detection.[501] A recent demonstration utilizes this approach for long-term (>3 h) monitoring of sweat ethanol concentrations.[502]

Although most metabolic sensors for skin-interfaced applications utilize electrochemical sensing modalities, challenges due to complexity, weight, and cost represent fundamental constraints. Moreover, as highlighted previously,[462] continuous monitoring requires a constant exchange of sweat at the sensor surface, therefore necessitating efficient approaches to fluid handling. A recent demonstration offers a path to circumvent these challenges by leveraging simple colorimetric assays with advanced microfluidic designs for electronics-free quantitative capture, storage, and biomarker analysis of sweat.[220] This class of skin-interfaced sensor involves a soft, stretchable epidermal microfluidic device (an "epifluidic" platform) with integrated assay chambers for the colorimetric

DOI: 10.1021/acs.chemrev.8b00573
Chem. Rev. 2019, 119, 5461−5533

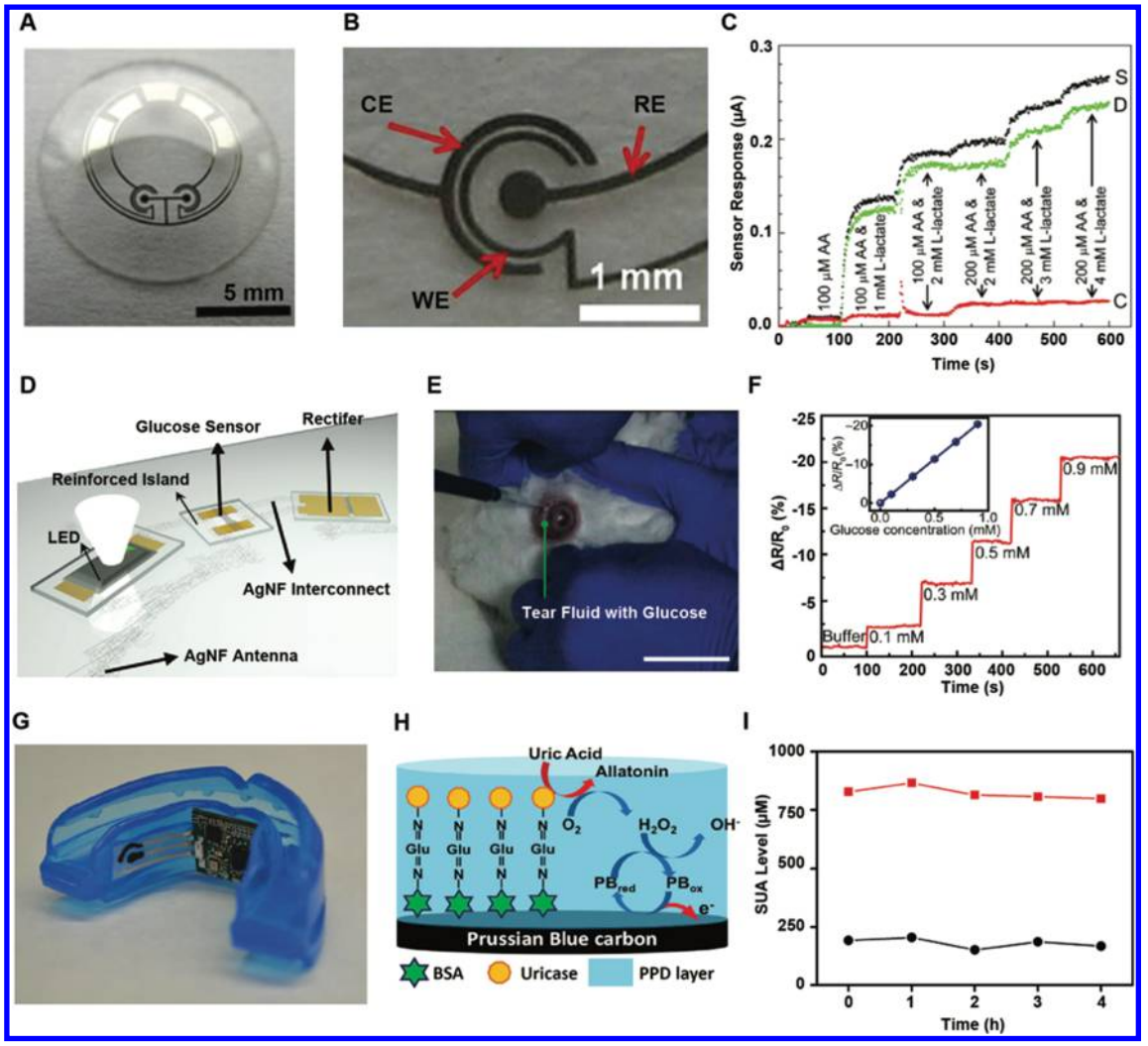

Figure 14. Metabolite sensors interfaced to other areas of the body. (A) Photograph of an electrochemical lactate sensing contact lens. (B) Close-up image of the three-electrode contingent. (C) Real-time benchtop response of the device to lactate and various interfering chemicals. (A–C) Adapted with permission from ref 228. Copyright 2012 Elsevier. (D) Schematic illustration of important components of a soft, stretchable, and transparent contact lens for glucose sensing and display. (E) Image of the glucose contact lens mounted on the eye of a rabbit while introducing a known concentration of glucose fluid as artificial tears. (F) Benchtop studies of the sensor response to increasing glucose concentration. (D–F) Adapted with permission from ref 506. Copyright 2018 American Association for the Advancement of Science. (G) Image of a wireless mouthguard-based electrochemical device for salivary uric acid sensing. (H) Scheme showing different reagents of the uric acid sensor and the enzymatic reaction responsible for selective detection. (I) Diurnal signals recorded by the uric acid sensor using saliva samples collected from healthy and uremic patient. (G–I) Adapted with permission from ref 231. Copyright 2015 Elsevier.

detection of sweat glucose, lactate, chloride, and pH as well as a method for measuring sweat rate (Figure 13M).[220] Sweat enters the device via the natural pressure generated by the sweat glands where embedded microfluidic channels direct sweat to separate chambers, each of which contains a commercially available colorimetric assay for a particular analyte. The sweat components interact with the colorimetric reagents and develop distinct colors quantitatively linked to the concentration of the target of interest. Using a smartphone to capture an image of the device allows for color analysis of each assay chamber as a simple route to measure the concentrations of sweat components.

One drawback is that the color changes associated with certain of the assays are irreversible. To capture dynamic changes in sweat composition, passive capillary bursting valves (CBVs) can be incorporated into the microfluidic designs to allow for time (or volume) sequenced capture and analysis of sweat (Figure 13N).[503,504] Here, the device consists of a series of reaction chambers and colorimetric assays, separated by CBVs. Incoming sweat enters the device and routes in such a manner that the chambers fills in a sequential manner. By using such microfluidic architectures, epifluidic devices can simultaneously detect sweat glucose, lactate, pH, chloride, and temperature in a time-sequential fashion (Figure 13O).[505]

As detailed in section 2.2.3, alternative surfaces such as the cornea and the inside of the mouth enable biochemical assessments of tears and saliva. Design challenges, however, are more significant compared to those associated with skin-interfaced devices. For example, the highly curvilinear, soft, and delicate surface of the cornea demands careful device layouts and material selections to avoid any risk of injury or harm. Similarly, component selection for mouthguard/teeth integrated biochemical sensors require special attention to toxicity and contamination. As a result, only a few demonstrations of such devices exist in the literature. Early ocular embodiments rely on simple designs in which sensors in the form of narrow strips detect a specific chemical of interest.[507−509] Recent

DOI: 10.1021/acs.chemrev.8b00573
Chem. Rev. 2019, 119, 5461−5533

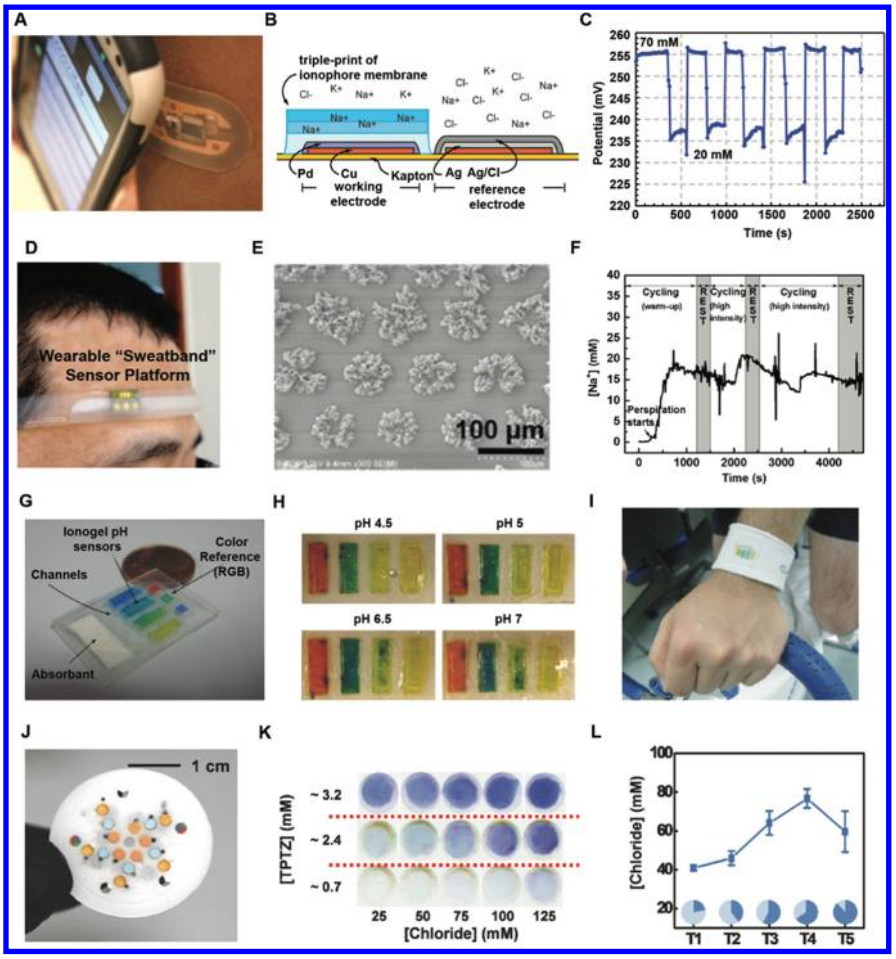

Figure 15. Sweat electrolyte sensors. (A) Image of a smartphone acquiring data wirelessly from a battery-free NFC-based wearable patch for sodium sensing. (B) Schematic illustration of different chemical reagents for the potentiometric sodium sensor. (C) Plot showing the reversible operation of the sodium sensor. (A–C) Adapted with permission from ref 521. Copyright 2015 Institute of Electrical and Electronics Engineers. (D) Image a subject wearing a headband-based potentiometric chloride sensor. (E) SEM image of Au nanodendrites as a solid contact for a potentiometric sensor. (F) Real-time measurements of chloride concentration for a human subject during perspiration. (D–F) Adapted with permission from ref 522. Copyright 2017 American Chemical Society. (G) Image of an ionogel-based colorimetric sensor for sensing the pH of sweat. (H) Evolution of color with pH. (I) Image of a patch worn on the wrist of a subject while cycling. (G–I) Adapted with permission from ref 523. Copyright 2012 Elsevier. (J) Image of a soft, microfluidic patch with hydrophobic and superabsorbent valves for time-sequenced sensing of chloride concentration. (K) Evolution of the colorimetric sensor with increasing chloride concentration. (L) Data acquired during human trials while wearing the sweat patch. (J–L) Adapted with permission from ref 441. Copyright 2018 Wiley-VCH Verlag GmbH & Co. KGaA.

publications report significant advances.[227−229,510] For example, one case uses a RF-powered wireless, contact lens-based chemical sensing architecture to detect glucose[510] and lactate[228] in tears (Figure 14A–C). Another similar sensor utilizes hard-wired glucose sensors based on a sol−gel matrix-based material deposited on curvilinear PET substrates.[229] Subsequent refinements yield completely wireless RF-powered glucose sensors[510] and demonstrator devices with a dual sensor architecture to compensate for signals generated by interfering chemical species.[227]

Although technically impressive, these devices rely upon opaque, brittle sensor components that can negatively affect vision. Furthermore, the mechanical mismatch between the device components and soft tissue surfaces greatly hinders suitability for long-term use. Recent work[506] attempts to address these issues with a soft, stretchable, transparent, wireless contact lens-based device for resistive-based glucose sensing along with display pixels to visualize sensor readouts. This platform integrates a glucose oxidase functionalized p-type graphene-based glucose sensor and micro-LED with stretchable interconnects and antennas formed from highly transparent and electrospun silver nanofiber-based conductors (Figure 14D). The enzymatic glucose reaction results in the formation of hydrogen peroxide. The decomposition of hydrogen peroxide produces protons which, in turn, modulate the resistance of the p-type graphene transducer. By selecting an appropriate resistor and by using external antenna for power harvesting, the device activates the LED when the glucose concentration exceeds a predetermined limit. The intrinsic transparency and stretchability of the device minimizes adverse impact on vision while permitting long-term use. Validated by benchtop analysis, this type of sensor exhibits a linear response across the physiologically relevant range of glucose concentrations (Figure 14E,F). Use of a rabbit eye model, when injected with known glucose solution, highlights the potential of this device for noninvasive glucose monitoring in tears.

The most recent devices for sialochemistry exploit designs that include tattoo[511] and mouthguard[231,489,512−514] form factors. For example, a mouthguard lactate[512] sensor monitors physical stress; a subsequent refinement uses a uric acid[231]

DOI: 10.1021/acs.chemrev.8b00573
Chem. Rev. 2019, 119, 5461−5533

sensor (Figure 14G) to monitor hyperuricemic, gout, Lesch–Nyhan syndrome, and renal syndrome patients. The device fabrication involves screen printing Prussian Blue-based carbon ink and Ag/AgCl ink on flexible PET substrates to realize a three-electrode contingent. Biofunctionalization with uricase or lactate enzyme renders the sensor signal specific to the analyte, as shown in interference studies (Figure 14H). Finally, bonding the sensor to the curved surface of the mouthguard completes the fabrication. In vitro evaluations to monitor uric acid levels in undiluted saliva samples regularly collected from a healthy and a hyperuricemia patient over a 5 h period demonstrates the efficacy and potential of this platform (Figure 14I).

3.2.2. Electrolytes. As with metabolic sensors, skin-interfaced electrolytic sensors primarily leverage electrochemical methods (potentiometry) for detection.[515] A typical potentiometric sensor includes an ion-selective electrode (ISE), referred to as the indicator electrode, and a reference electrode. The ISE potential is proportional to the ion activity and follows the Nernst equation. On the other hand, the potential of the reference electrodes (usually Ag/AgCl or Hg/Hg_2Cl_2) is independent of sample composition. The potential difference between these two electrodes is therefore proportional to ion activity, which approximates the ion concentration.[516] Such sensors for wearable applications commonly utilize solid-state polyvinyl chloride (PVC)-based ion selective membranes; less common is the use of a pH-sensitive conducting polymer as the membrane for pH sensing. In the former type, the ion selective membrane comprises an ionophore for selectivity, ionic additives for charge transport, and a plasticizer dispersed in a polymer matrix (typically PVC) for flexibility. In the latter, conducting polymer-based pH sensors rely on their direct electrodeposition or solution casting onto noble metals or carbon electrodes. Polyaniline[517] and polypyrrole[518] are two common pH sensitive conducting polymers. Other reviews provide complementary discussions on potentiometric sensors in significant detail.[519,520]

Skin-interfaced potentiometric devices based on benchtop/hand-held multimeters for recording represent the earliest demonstrations of sensors for real-time detection of sodium,[524] ammonium,[525] and pH of sweat.[526] Subsequent advances in materials science now allow for the full integration of hardware for wireless data communication for wearable BLE-based electrolytic sensors capable of continuous monitoring of sodium,[442,494] potassium,[225] pH,[527] chloride,[471] and calcium.[527] These devices utilize conventional solid-state PVC-based ISEs formed by the deposition of ion-selective membranes onto Au or screen-printed carbon-based electrodes.

As with all BLE-based devices, the advanced wireless functionality requires relatively large, bulky hardware and batteries for power supply. A recent demonstration circumvents these trade-offs by utilizing NFC, rather than BLE, communication technology, resulting in an ultralight, flexible, and battery-free sodium sensor capable of conformal interfacing to the epidermis (Figure 15A).[521] The sensor utilizes palladium current collectors: one coated with a sodium sensitive membrane and the other with Ag/AgCl (first plated with Ag with subsequent conversion to Ag/AgCl) as the reference electrode (Figure 15B). Preliminary studies reveal near-Nernstian behavior (57 mV/decade) and reversible response (coefficient of variance = 0.8%) (Figure 15C).

Signal stability is of critical importance for potentiometric sensors.[516,528] Minute drifts in voltage lead to significant errors in the ion concentration. Pretreating the solid-state potentiometric sensors with a conditioning solution[529] can mitigate some of these effects, but such a procedure is not well suited for skin-interfaced platforms, especially for consumer applications. An alternative approach to minimizing signal drift in the indicator electrode relies on a thin, ion-to-electron transducing solid contact layer between the electrode surface and ion-selective membrane.[530,531] Typical ion-to-electron transducers include conducting polymers (e.g., polypyrrole, poly(3-octylthiophene), poly(vinyl ferrocene), polyindole, polyaniline, and PEDOT)[519,532] and nanomaterials (e.g., CNTs,[530,531,533] graphene[534]). The use of chloride-saturated printable ink,[526] polyvinyl butyral,[219,535] polyvinyl acetate,[522] and poly(2-hydroxyethyl methacrylate)[536] as a polymeric matrix improves the stability of the solid-state reference electrode, which is equally important for potentiometric sensing.

Recent work combines nanomaterials as a stable solid contact for the indicator electrode and polyvinyl acetate as a solid-state reference electrode in a headband-based wearable sodium sweat sensor with stable response (Figure 15D).[522] A PVC membrane containing a sodium ionophore drop cast onto an electrochemically deposited gold electrode with dendritic structures forms the sodium selective indicator electrode (Figure 15E). The reference electrode structure is a drop cast layer of Ag/AgCl ink on a bare gold electrode subsequently coated with a polyvinyl acetate membrane saturated with KCl. The sensor exhibits a near-Nernstian response (56.43 ± 1.17 mV/decade). Comparisons with a similar sensor that uses a bare Au electrode reveal that the dendritic structures improve signal stability (signal drift: 0.22 mV/h compared to 4.66 mV/h), likely due to enhanced ion-to-electron transduction at the membrane/solid contact interface that results from the electrical double layer capacitor associated with the dendrites. Stability studies of the reference electrode reveal that the KCl-saturated polyvinyl acetate membrane has a drift of only 0.056 mV over 15 h. Human subject studies during indoor cycling confirm expected performance (Figure 15F).

As with amperometric metabolic sensors, colorimetric options for sensing of electrolytes can be attractive.[537] In addition to simplicity of design and operation, this transduction method does not require pretreatment or sensor calibration. Although typically less accurate than potentiometric sensors, colorimetric assays are adequate for many applications. One of the earliest colorimetric skin-interfaced electrolytic sensors mounts on the wrist to measure sweat pH with integrated red–blue–green (RGB) reference markers for accurate color analysis (Figure 15G).[523] A fluidic network transports sweat to the sensor and purges analyzed sweat via an adsorbent-based sink. pH-sensitive dyes (methyl red, bromophenol blue, bromocresol green, bromocresol purple, and bromothymol blue) in ionogels reside in assay chambers. The ionogels, prepared by encapsulating trihexyltetradecylphosphonium dicyanoamide ionic liquid in an arcylamide polymer network, provide a low vapor pressure liquid environment that maintains the pH sensitivity of the dyes. The assays develop colors that correspond to sweat pH level (Figure 15H,I).

As detailed in section 3.2.1, the irreversibility of the response requires additional concepts to allow monitoring of transient changes in electrolyte levels. As described previously, CBVs positioned at strategic locations in a microfluidic network provides one solution for routing sweat into separate assay chambers in a sequential manner. An alternative design (Figure 15J)[441] achieves a similar result by use of superabsorbent valves to direct incoming sweat, with demonstrations in colorimetric

DOI: 10.1021/acs.chemrev.8b00573
Chem. Rev. 2019, 119, 5461–5533

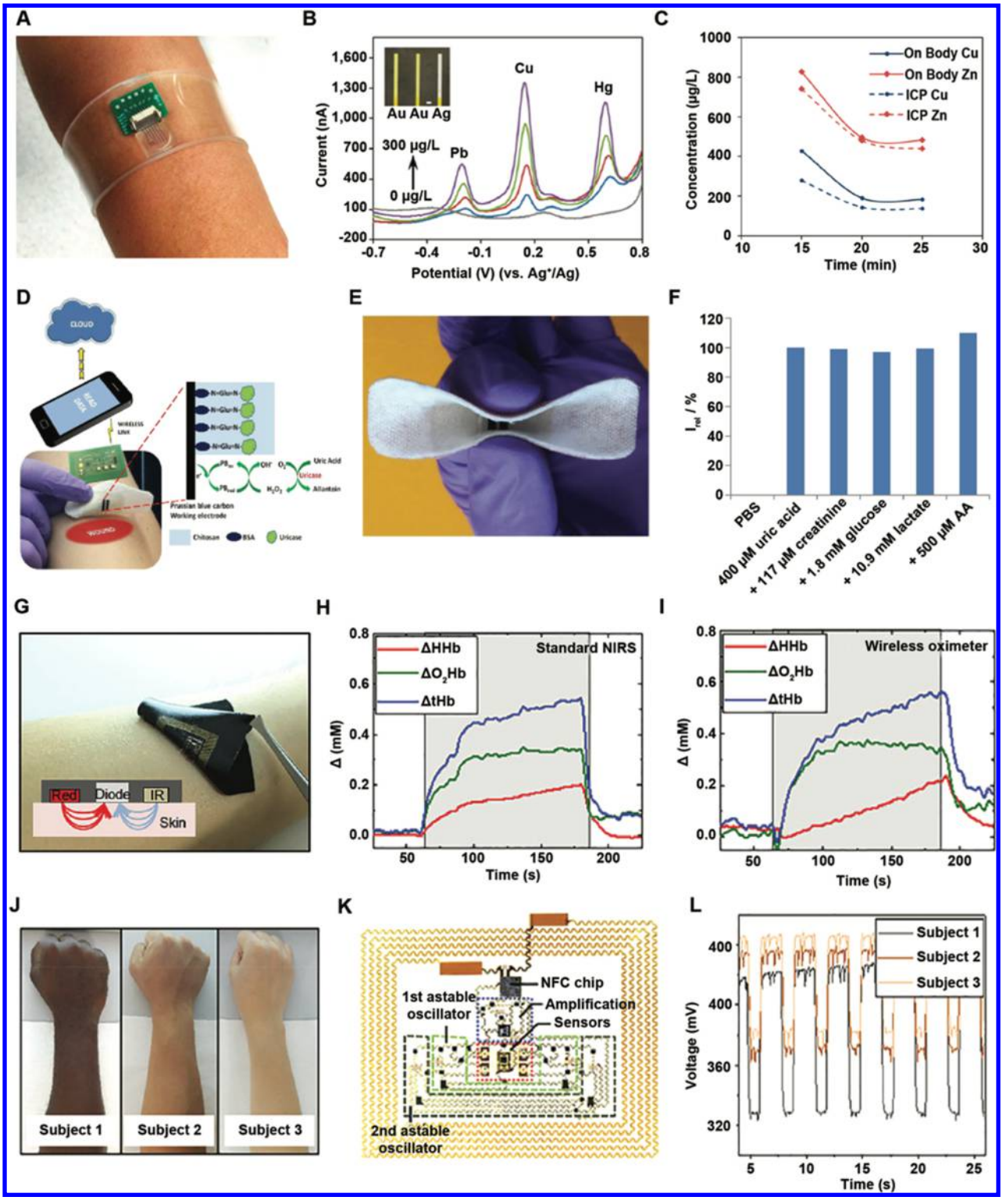

Figure 16. Sensors for miscellaneous biochemical signals. (A) Photograph of a wearable voltammetric sensor for heavy metal detection. (B) Voltammograms generated by the sensor illustrating oxidation peaks corresponding to Pb, Cu, and Hg. (C) Comparison of data recorded by the wearable sensor during human trails and determined by ICP-MS. (A−C) Adapted with permission from ref 543. Copyright 2016 American Chemical Society. (D) Photograph and scheme showing a bandage-based, NFC-powered uric acid sensor for wound healing monitoring. (E) Image of the bandage sensor showing its flexibility. (F) Plot illustrating the selectivity of the sensor toward uric acid in the presence of various potential interfering chemical species. (D−F) Adapted with permission from ref 545. Copyright 2015 Elsevier. (G) Optical image of a epidermal wireless oximeter mounted on the forearm. (H,I) Comparison of measurements simultaneously recorded from a commercial device and from a wireless oximeter. (J) Optical image of volunteer participants with different skin colors and (K) of the wireless spectrometer with four pulsed LEDs. (L) Measurements of different skin colors performed using a skin-integrated wireless platform. (G−L) Adapted with permission from ref 440. Copyright 2016 American Association for the Advancement of Science.

DOI: 10.1021/acs.chemrev.8b00573
Chem. Rev. 2019, 119, 5461−5533

sensing of chloride (Figure 15K). Preparation of the superabsorbent material involves gelation and subsequent drying of sodium polyacrylate (absorbent polymer) and *N*,*N*′-methylenebis(acrylamide) (fast swelling agent) in the presence of sodium metabisulfite (cross-linker). A hydrophobic microchannel separates each reservoir to enable sequential filling. Each reservoir includes three distinct reaction zones (0−75, 75−150, and <150 mM) for sweat chloride detection. The colorimetric assay is a solution of 2,4,6-tris(2-pyridyl)-*s*-triazine (TPTZ, a chelating agent), mercury-(II), Hg^{2+}, and iron-(II), Fe^{2+}, that favors complexation between Hg^{2+} and TPTZ to form colorless $Hg^{[TPTZ]}{}_2$. The addition of chloride induces a reaction with Hg^{2+} to produce mercuric chloride, $HgCl_2$, and release TPTZ, which readily chelates with a stoichiometric equivalence of Fe^{2+}. The $Fe^{[TPTZ]}{}_2$ is blue in color, and the optical density corresponds directly to the chloride concentration (via a calibration curve). Upon initial filling, sweat enters into each of the zones of the first reservoir until it reaches a superabsorbent valve; absorption leads to expansion that closes the inlet to the first reservoir. This process diverts the sweat to the next reservoir to yield a time-sequenced analysis of sweat chloride concentration. Analyzing the color values for each reaction zone enables the quantitative measurement of chloride concentration. On-body tests reveal that sweat chloride concentration increases with time to a concentration range of 40−80 mM and then gradually decreases with decreasing sweat rate at the end of the study (Figure 15L).

Fluorescent sensing offers an additional option for optical readout, of interest due to the rich library of fluorophores for detecting chemical analytes relevant to skin-interfaced applications.[538−540] Recent work leverages this fluorescent methodology for sweat analysis in an epifluidic platform for the analysis of sodium, zinc, and chloride.[541] Here, sweat analytes react with fluorophores located in the microfluidic structure to generate a fluorescent signal with an intensity proportional (or inversely proportional) to the analyte concentration. Quantification of sodium and zinc is via a commercially available fluorescent assay. For chloride, the fluorophore bis-*N*-methylacridinium nitrate reacts with excess Cl^-, resulting in diffusion-limited collisional quenching. A smartphone-based module for exciting and detecting fluorescence facilitates analysis in the field. The inclusion of reference chambers with known fluorophore concentrations (thus fixed fluorescence intensity) enables quantitative concentration analysis. Volunteer human studies reveal high accuracy in comparison to conventional fluorimeters for sweat analysis.

3.2.3. Miscellaneous Biochemical Signals. In addition to electrolytes and metabolites, recent publications report epidermal chemical sensors for other targets, such as heavy metals,[542,543] caffeine (a model analyte for drug detection),[443] and cortisol[544] in sweat, chemical markers for monitoring wound healing,[199,545,546] hemoglobin[222] in blood, and melanin[440] in the skin.

Monitoring essential heavy metals in sweat provides insight into human endurance levels and the ability to recover after high-intensity athletic activities.[470] In addition, sweat represents a physiological route for excreting toxic heavy metals and, therefore, provides a means for rapidly screening for exposure.[547] Examples of skin-interfaced heavy metal sensors utilize stripping voltammetry-based techniques (Figure 16A).[542,543] These sensors include a thin layer of bismuth electrodeposited on carbon or Au electrodes with a coating of tetrafluoroethylene-perfluoro-3,6-dioxa-4-methyl-7-octenesulfonic acid copolymer to improve sensitivity. Bismuth modified electrodes of this type represent low-toxicity alternatives to conventional mercury-coated electrodes.[548] Detection involves a two-step process: (1) heavy metal ion analytes from sweat coat the sensor surface by electrodeposition and (2) stripping of the deposited metals from the surface yields distinct voltammetric oxidation peaks that correspond to a particular heavy metal (e.g., copper, cadmium, zinc, arsenic),[549] with parts per million or even parts per trillion limits of detection (Figure 16B). Characterization of sensor repeatability indicate robust performance even under cyclic mechanical deformation (200 bending cycles, radius of curvature: 3.2 mm). Human studies highlight capabilities for real-time monitoring of heavy metals in sweat, with results that match those of standard chemical analytical tools such as inductively coupled plasma mass spectroscopy (Figure 16C).

Hormones are another class of biochemical markers of interest.[550−552] Cortisol, specifically, is commonly used as an indicator of stress and is present in sweat.[553] A recently reported approach to sensing utilizes a molecularly imprinted polymer (MIP)-based and an organic transistor.[544] Fabricated on a soft, stretchable SEBS elastomer, the device architecture uses a PEDOT:PSS electrochemical transistor with an Ag/AgCl gate electrode functionalized with an acrylate-based MIP as a cortisol recognition layer. The sensing mechanism relies on modulation of the drain current as a result of binding of cortisol to the MIP-functionalized gate electrode. Bench-top studies reveal a linear sensor response to increasing cortisol concentration with a detection limit of 10 nM.

An additional promising direction in skin-interfaced electrochemical sensing focuses on real-time monitoring of wound healing via detection of relevant markers (e.g., pH,[546,554] uric acid[545]). One example integrates a potentiometric polyaniline-based pH sensor on a bandage.[554] Tracking uric acid levels is possible using NFC-based enzymatic electrochemical sensors in a similar form factor (Figure 16D).[545] Screen-printed sensors based on Prussian Blue perform well even when repeatedly bent by 180° for 80 cycles (Figure 16E). The response is linear across the physiologically relevant range concentrations (up to 0.8 mM) with negligible effects from common electroactive species, such as creatinine, lactate, glucose, and ascorbic acid (Figure 16F).

Hemoglobin and bilirubin represent additional classes of biochemical analytes, essential for oxygen transport and skin pigmentation, respectively. Because these species absorb light within the visible regime,[555] optical measurement approaches are possible in skin-like form factors similar to those introduced for PPG measurements in section 3.1.5. Most examples measure hemoglobin in its deoxygenated and oxygenated state,[428] thereby providing both heart rate information[427] as well as both arterial[556] and tissue oxygenation levels.[557] These measurements provide significant information on cardiovascular,[413] myocardial,[414] and overall tissue health.[558] Blood oxygenation can be extracted from the pulsatile component of signals obtained either in transmission or reflection mode at two different wavelengths to yield the oxygenation state of hemoglobin and to enable calculation of arterial oxygenation.[428] Here, as with optical PPG measurements, the reduction of motion artifacts is critical to obtain a high signal fidelity. Devices, such as the highly miniaturized battery-free wireless system shown in (Figure 11N), offer a stable platform for chronic recording. Another key aspect is the conformal interface to the epidermis. Figure 16J−L highlights an example where an opaque

DOI: 10.1021/acs.chemrev.8b00573
Chem. Rev. 2019, 119, 5461−5533

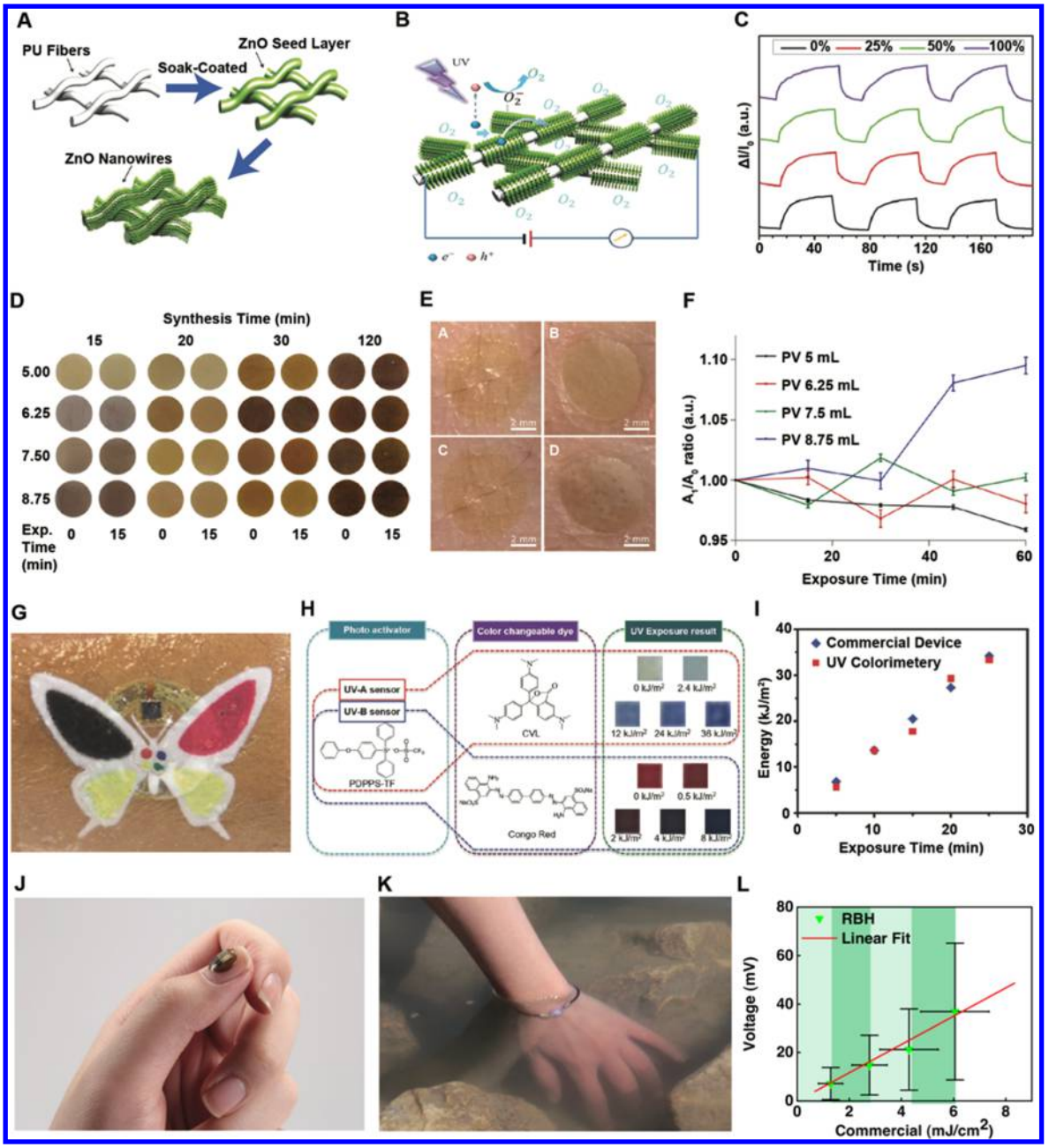

Figure 17. Devices for monitoring light exposure. (A) Schematic illustration of the fabrication process for a fabric-based ZnO UV sensor. (B) Illustration of the sensing mechanism for a ZnO UV sensor. (C) Plot demonstrating the rapid, reversible nature of the UV sensor. (A–C) Adapted with permission from ref 598. Copyright 2016 Wiley-VCH Verlag GmbH & Co. KGaA. (D) Photograph of an array of AgNPs-decorated bacterial cellulose nanopaper after UV exposure for varying time periods. (E) Images of the AgNPs-based UV sensor worn by a human subject and after exposure to sunlight. (F) Correlation of area under the curve (A_1/A_0) of the normalized initial UV–vis spectrum to solar simulator exposure. (D–F) Adapted with permission from ref 578. Copyright 2017 American Chemical Society. (G) A colorimetric UVA and UVB sensor with battery-free NFC capabilities for wireless transmission. (H) Dyes utilized by the sensor for detecting UVA and UVB radiation and their color evolution as a function of radiation intensity. (I) Comparison of the data acquired by the wearable sensor to a commercial UV meter. (G–I) Adapted with permission from ref 599. Copyright 2017 Wiley-VCH Verlag GmbH & Co. KGaA. (J) Optical image of the UVA dosimeter worn on the fingernail and (K) worn on the wrist and submerged in water. (L) Comparison of measurements recorded during afternoon exercise using wireless mm-NFC and commercial dosimeters. (J–L) Adapted with permission from ref 600. Copyright 2018 American Association for Advancement of Science.

elastomeric backing shields the measurement site and constituent battery-free electronic circuitry from ambient light.[440] Beyond blood oxygenation, melanin and bilirubin[559] are other species of interest. Bilirubin serves as an indicator for hyperbilirubinemia[560] and coronary artery health.[561] Skin-interfaced systems that use multiple colors provide spectrometric analysis. Here, time sequenced readout of a target region probed at four different colors (infrared, red, orange, and yellow) using a wireless, battery-free system allows for assessment of subtle changes in skin color.

3.3. Environmental Signals

Signals from interactions of the human body with the surrounding environment can be as important to health monitoring as measurements from the body itself. A wide

DOI: 10.1021/acs.chemrev.8b00573
Chem. Rev. 2019, 119, 5461–5533

range of portable environmental sensors provides key capabilities in monitoring food quality,[562−565] pesticide contamination,[566−568] gaseous pollution,[569,570] and UV radiation exposure[571,572] as well as in collecting forensic evidence.[573−576] Although conventional systems permit on-site, rapid analysis in the field, with minimal sample degradation, their sizes, weights, and overall form factors prevent direct integration with the body, in most cases. Here, the ability of bio-integrated electronics to conform to the skin or fingernails enables precise understanding and quantification of localized exposures to environmental hazards. The following subsections highlight recent progress in epidermal platforms designed for capturing signals from the environment.

3.3.1. Light. The spectral composition of sunlight that reaches Earth's surface consists of ∼8% ultraviolet (UV), ∼46% visible, and ∼46% IR light (by energy flux).[577] Although each component is essential for sustaining life (e.g., illumination, heat), UV light is unique in its impact on human health, where exposures to UVB (280−315 nm) and UVA (315−400 nm) are most physiologically relevant.[578] Exposure is a key component in the production of vitamin D, an essential element in modulating blood pressure and as a vital aspect in maintaining mental well-being.[579,580] However, excessive exposure results in deleterious effects including erythema,[581] cataracts,[582] melanoma,[583] and immune system suppression.[584] Skin cancers are the most common form of cancer, with an excess of 5 million cases of basal cell and squamous cell carcinomas occurring annually, resulting in treatment costs of $8.1 billion.[585] The Skin Cancer Foundation states that 20% of the American population (1 in 5 people) will develop skin cancer during their lifetime.[586] Such risks highlight the critical need for technologies that can accurately measure and alert people to overexposure of UV light. Although commercially available band-based wearable UV sensors seek to fulfill this need, most lack either quantitative accuracy or utilize expensive, rigid components that impede wearability and lead to nonadoption. This section highlights the recent advances in skin-interfaced UV sensors for precise, personalized monitoring of exposure.

Most academic research centers on developing inexpensive, body compliant UV sensors with a primary focus on leveraging the semiconducting properties of ZnO.[587−591] The sensing mechanism relies on the adsorption/desorption of ambient oxygen molecules onto the ZnO sensor surface.[592] The oxygen molecules capture free electrons during absorption, resulting in a surface depletion layer and conductivity reduction. UV light photogenerates electron−hole pairs whereby the resulting holes interact with the adsorbed oxygen ions to form molecular oxygen, thus increasing conductivity. One representative example of a skin-interfaced UV monitor uses poly(*p*-phenylene terephthalamide)-supported ZnO nanowires (ZnO NWs) as the sensing surface.[593] The sensor consists of hydrothermally grown ZnO NWs from an initial sputtered seed layer of ZnO on poly(*p*-phenylene terephthalamide) threads. The ZnO NWs radially cover the thread surface and a subsequent partial overcoat of PDMS enhances the durability of the overall structure. Repeat dosing of the sensor with UV light of varying intensity (0.2−1 mW cm^{-2}) and monitoring the corresponding conductivity changes validates device performance for detecting ambient UV exposure. Interestingly, the conductivity of the UV sensor decreases linearly with increasing light intensity. The report attributes this behavior to the screening/neutralization of the piezoelectric charges on ZnO by the UV light-generated carriers, resulting in a decrease in conductivity.

To reduce fabrication cost and necessity for cleanroom processing, other embodiments leverage established printing and solution processing techniques[31,594−596] to develop flexible, skin-integrated ZnO-based UV sensors.[597] For example, deposition of a ZnO microparticle ink onto flexible PI sheets by inkjet printing results in a highly flexible, yet inexpensive UV sensing device. The sensor performance exhibits negligible performance degradation in response to either the degree (bending radius: 3−10 mm) or number of bends (>500) and offers both a fast response time (∼0.3 s) and high ON/OFF ratio (∼3525).

As with sensing platforms described in other sections, thin, stretchable construction is important for irritation-free integration with the human body.[171,601−603] Recent work describes a ZnO UV sensor based on a highly stretchable PU textile (Figure 17A).[598] Infiltration of the textile with a precursor solution enables in situ, hydrothermal growth of ZnO NWs. As with the NW-based sensors described above, UV light modulates the conductivity of the ZnO (Figure 17B) to enable a reversible response (Figure 17C) with a speed that varies from ∼30 to ∼40 ms upon stretching to ∼125% tensile strain, possibly due to decreasing rate of oxygen diffusion rate in the stretched state.

Colorimetric alternatives to these and related electronic approaches are attractive due to their lightweight, low cost designs and sizes that can be easily miniaturized due to their battery-free operation. One strategy exploits the plasmonic modulation of AgNPs in the presence of UV radiation (Figure 17D).[578] AgNPs undergo photolysis when exposed to UV light,[604,605] thereby changing the nanoparticle size which results in a visible color change with exposure dose. Varying the length of reaction (15−120 min) and volume of $AgNO_3$ (0.1 v/v%; 5−8.75 mL) added to a heated (65 °C) 2 M NaOH solution (15 mL) enables control of AgNP size. A library of 16 different sized AgNPs enables tailoring of device response to UV exposure (Figure 17D,E) in which a single size corresponds to a specific skin pigmentation. Devices have response times of ∼15 min, with color changes optimized to provide rapid, high contrast, visual quantification of UV exposure for high and moderate cancer-prone skin types (skin types I, II, III, and IV) (Figure 17F).

UV-sensitive organic dyes represent other options in colorimetric sensing. One example combines this approach with screen printing and soft lithography to obtain a soft, stretchable, skin-like UV sensing platform for the fast (within 20 s), simultaneous colorimetric measurement of UVA and UVB exposure (Figure 17G).[599] The active material combines photosensitive activators (photoacid generators or photoradical initiators) and a color changeable dye (photochromic dyes) dispersed within a PDMS matrix. This activator/dye combination yields a distinct color change under UV light exposure (Figure 17H) such that quantitative measurement is possible via image analysis with the inclusion of color reference markers and UV filters for differentiation between UVA (0−300 KJ m^{-2}) and UVB (4 KJ m^{-2}) components. This capability is distinct from the preceding examples that only quantify broadband UV exposure. Color analysis of a photo captured by a smartphone provides rapid, accurate measurement of ambient UV radiation with performance rivaling that of commercial UV meters (Figure 17I). Advanced processing algorithms can further improve the accuracy and precision of such a platform.[606]

Electronic sensors offer an alternative option to monitoring UV exposure. A recent noteworthy embodiment[600] utilizes a fully electronic approach in a wireless, battery-free, millimeter-

DOI: 10.1021/acs.chemrev.8b00573
Chem. Rev. 2019, 119, 5461−5533

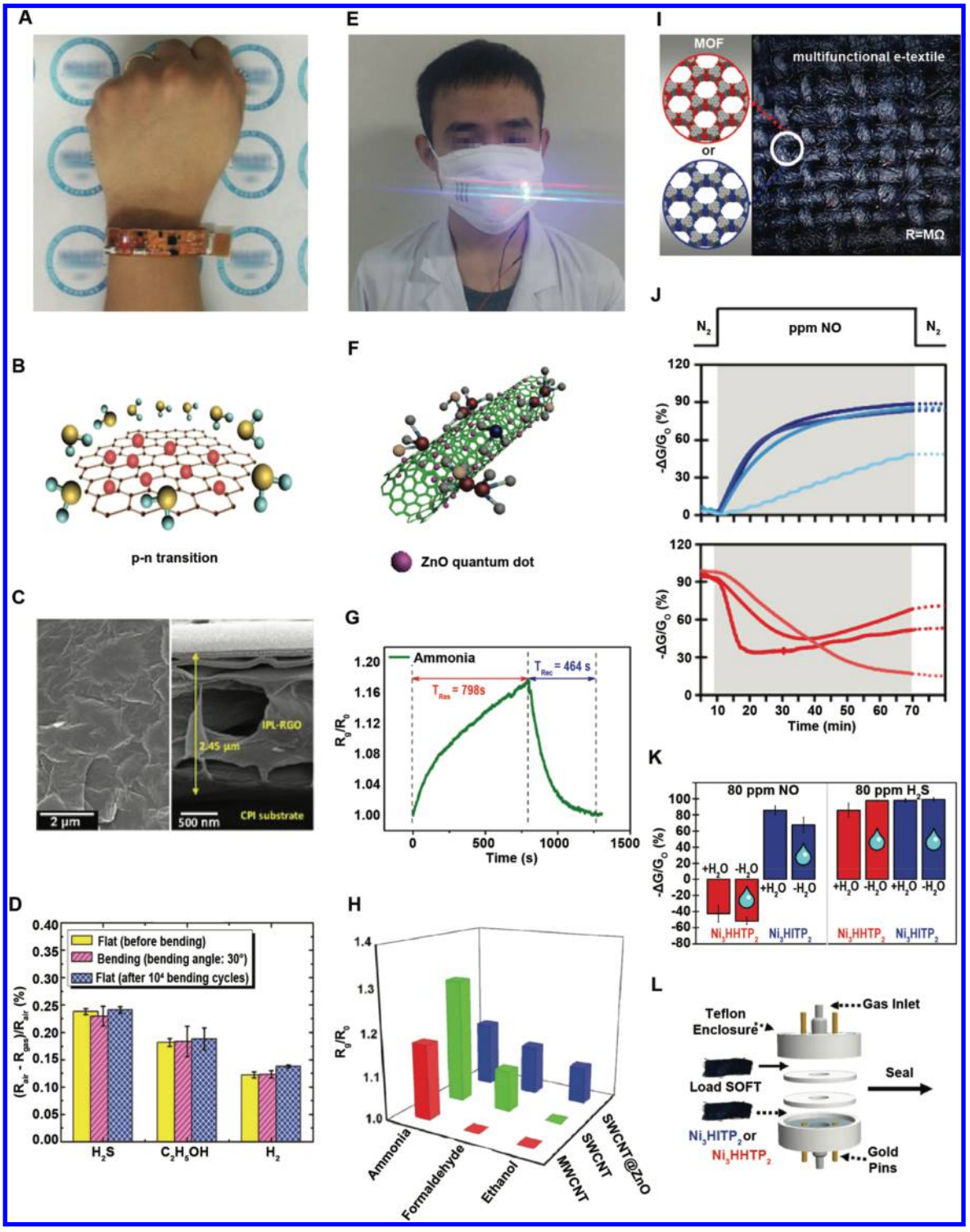

Figure 18. Gas sensors. (A) A wrist-band-based RGO gas sensor. (B) Schematic illustration of the interaction of gas targets with RGO and the resulting modulation of the conductivity of the RGO. (C) SEM micrograph of RGO coated over a PI substrate. (D) Selectivity of the RGO sensor toward hydrogen sulfide, ethanol, and hydrogen gases and effect of bending. (A–D) Adapted with permission from ref 631. Copyright 2016 Springer Nature. (E) Optical image of a ZnO/CNT-based gas sensor embedded in a mask. (F) Illustration of the interaction of ammonia gas with a ZnO/CNT transducer for gas sensing. (G) Real-time response of the sensor during intermittent exposure to ammonia gas. (H) Plot of the selectivity of the sensor. (E–H) Adapted with permission from ref 635. Copyright 2018 Springer Nature. (I) Image of a textile-based Ni metal–organic framework for gas sensing and capture. (J) Sensor response for two different Ni-based metal organic frameworks when exposed to NO with Ni_3HHTP_2 (red, top) and Ni_3HITP_2 (blue, bottom). (K) Sensor response to analytes at saturation levels (80 ppm of NO and H_2S, left to right) for Ni_3HHTP_2 (red) and Ni_3HITP_2 (blue) (dry nitrogen, solid bars; 5000 ppm water–water droplet. (L) Apparatus for membrane testing. (I–L) Adapted with permission from ref 636. Copyright 2017 American Chemical Society.

DOI: 10.1021/acs.chemrev.8b00573
Chem. Rev. 2019, 119, 5461–5533

scale form factor for both the instantaneous, real-time measurement or long-term continuous monitoring of exposure to UVA, UVB, visible, and IR light (Figure 17J). The platform records exposure using photodiodes with narrowband responses in the spectral ranges of interest (e.g., UVA, UVB) to generate photocurrents proportional to the instantaneous exposure intensity and wavelength-dependent quantum efficiencies. Each photodiode continuously charges a supercapacitor during exposure. The integration of a system-on-a-chip (SoC) with NFC capabilities enables the conversion of the supercapacitor voltage to the cumulative exposure dose (via a conversion factor) for subsequent wireless transmission to a smartphone. Full device encapsulation with PDMS provides a waterproof seal (Figure 17K) to support long-term durability as demonstrated by 10 devices, mounted on fabric swatches, remaining functional after washing in a washing machine for 35 min (rotating at 400 rpm with 40 °C water).

This UV sensor, unlike traditional wrist-mounted counterparts, can integrate anywhere on the body for localized sensing of UV-exposure in a way that does not impose any device burden on the user. Such capabilities are important not only for user compliance but also for monitoring exposure in sun-damaged or sensitized areas of the skin in the context of skin cancer and general skin health. Field trials on human volunteers validate superior device performance in recording continuous UV exposure in comparison to a wrist-worn commercial UV sensors (Figure 17L).

Monitoring exposure to visible radiation, specifically blue light (450−495 nm), is of growing scientific and clinical interest. A recent study[607] suggests high intensity blue light exposure (e.g., from electronic devices) accelerates damage to the photoreceptors in the retina; other studies[608−610] indicate blue light exposure affects the human circadian rhythm, influencing sleep quality and alertness. Blue light exposure is also critical in therapeutic applications such as in treatment of hyperbilirubinemia,[611] seasonal affective disorder,[612] or potentially as a means for decreasing systolic blood pressure and arterial stiffness.[613] Few skin-interfaced platforms monitor blue light exposure, with eyeglass-mounted color sensors being the primary form factor.[614,615] The preceding mm-NFC dosimeter platform[600] represents the only truly epidermal device for monitoring exposure to blue light. A clinical study demonstrates device efficacy by monitoring the exposure of jaundiced infants in the neo-natal intensive care unit (NICU) undergoing bili light therapy for treating hyperbilirubinemia.

3.3.2. Gases. The rapid increase in toxic gas emissions due to expanding industrialization can lead to negative impacts on the global biosphere and the local environment.[616−620] As such, toxic gas sensors are of interest both to the general public[621] and to those working in settings that are susceptible to high levels of such gases.[622,623] Portable gas sensors use conducting polymers,[624] carbonaceous nanomaterials,[625] metal oxides,[626] and composites of all three[627] for detection of toxic gases, even at parts per trillion (ppt) levels.[628,629] As in other contexts, skin-interfaced gas sensors for real-time, personalized monitoring of exposure across the body can be important.

Recent advances in polymer chemistry, ceramics, and nanotechnology serve as the foundations of gas sensing that can occur in wearable formats.[630] Most such sensors leverage carbon nanomaterials to transduce the presence of gas via the modulation of the resistivity due to gas adsorption. For example, a strap-based flexible device with a GO transducing layer can rapidly detect hydrogen sulfide, ethanol, and hydrogen in the 5−20 ppm range (Figure 18A).[631] Here, a transparent, colorless PI membrane functionalized with RGO formed by irradiation of GO (via drop casting) with intense pulsed light (1.15 J cm^{-2}; ON/OFF, 15/30 ms) offers enhanced selectivity toward the gaseous targets (Figure 18B). The adsorption of gas molecules (either of the three gases) dramatically changes the resistivity of the RGO (Figure 18C). Principal component analysis of the measurement signals enable differentiation between the three gas targets (Figure 18D). Incorporating RGO within stretchable elastic yarns enables a soft, skin compliant gas sensor embodiment.[632] Using a similar basis of operation, skin-interfaced gas sensors can also exploit conducting polymers to detect target gases.[633,634]

The sensitivity, selectivity, and stability of gas sensors based on carbonaceous nanomaterials and conducting polymers depending on environmental factors such as humidity and on their strong interactions with volatile organic compounds. Although metal oxides offer enhanced sensing characteristics, where gases can induce changes in oxygen stoichiometry and electrically active surface charges, their high operating temperatures (300−400 °C) preclude use in skin-interfaced applications. Metal oxide composites with conducting polymers or carbon nanomaterials, however, combine the high performance of metal oxides with room temperature operation of conducting polymers and carbon nanomaterials.[627]

Similarly, composites of MoS_2 and carbon nanomaterials[637] or conducting polymers[638] offer additional options. For example, integrating a CNT and ZnO-based flexible fiberglass gas sensor into a face mask enables detection of ethanol, ammonia, and formaldehyde (Figure 18E).[635] The device utilizes three separate sensing receptors: MWCNTs, SWCNTs, and ZnO/SWCNTs (Figure 18F). Benchtop analysis reveal an immediate response to target gas exposure (Figure 18G). MWCNTs exhibit the highest response for ammonia; SWCNTs respond well to ammonia and formaldehyde, but not to ethanol, and ZnO/SWCNTs detect all the three gases (Figure 18H). Monitoring each sensor response enables selective detection of the three target gases. In a similar manner, polymer−carbon nanomaterial composites offer superior gas sensing performance as compared to the individual components.[639−641] A fabric-based body-integrated ethanol sensor uses PVA coated CNTs (PVA/CNTs) for selectively sensing ethanol among other interfering vapors such as ammonia, acetone, benzene, cyclohexane, methanol, toluene, and xylene. The PVA/CNT composite exhibits a nearly 13-fold higher response than pristine CNTs, with a response time of ∼25 s.[639]

Metal organic frameworks comprise an additional class of materials in wearable gas sensors.[636,642] Their high porosity, tunable functionality, and wide availability of ligands and nodes make metal organic frameworks ideal candidates for a wide variety of gas sensors.[643,644] Recent work leverages these attributes to develop a fabric-based system for gas sensing, capture, and filtration.[636] Direct synthesis of nickel-based conductive metal organic frameworks on textile surfaces through direct solution-phase self-assembly from simple molecular building blocks forms the sensor (Figure 18I). Two variants of the nickel-based metal organic frameworks, each with nickel as the metallic node and a different organic ligand (2,3,6,7,10,11-hexahydroxytriphenylene or 2,3,6,7,10,11-hexaaminotriphenylene), selectively detect either nitric oxide (limit of detection, 0.16 ppm) or hydrogen sulfide (limit of detection, 0.23 ppm) (Figure 18J). The system operates even under humid conditions (18% relative humidity, 5000 ppm) (Figure 18K) and is suitable

DOI: 10.1021/acs.chemrev.8b00573
Chem. Rev. 2019, 119, 5461−5533

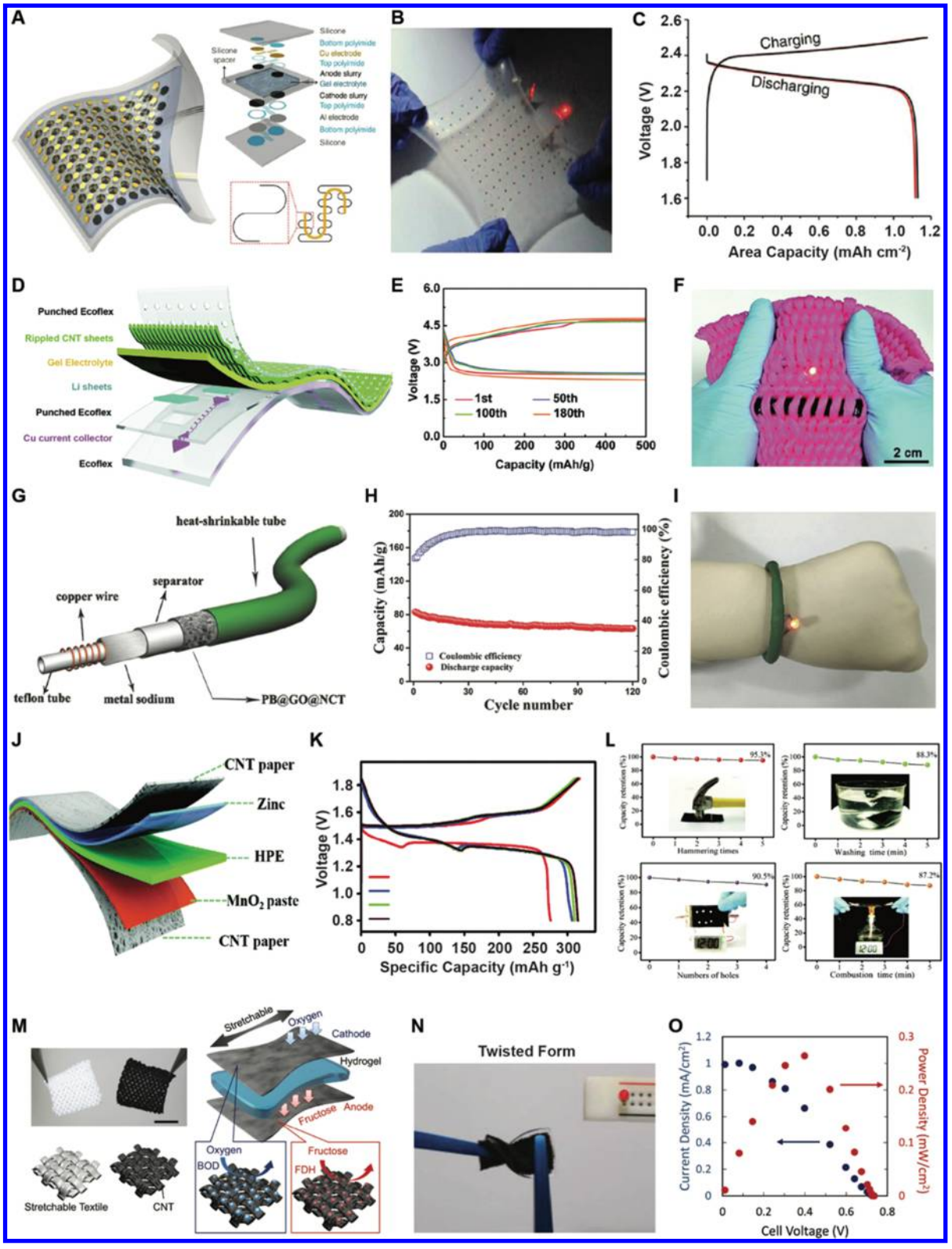

Figure 19. Batteries. (A) Schematic illustration a Li-ion battery utilizing serpentine structures to impart stretchability. (B) Optical image of the battery being stretched while powering a red LED. (C) Plot of the charging/discharging characteristics. (A–C) Adapted with permission from ref 662. Copyright 2013 Springer Nature. (D) Exploded schematic illustration of the different layers of a stretchable lithium–air battery and (E) its charging/discharging properties (F) when embedded in fabric to power an LED. (D–F) Adapted with permission from ref 675. Copyright 2016 Royal Society of Chemistry. (G) Schematic illustration of a sodium–Prussian Blue battery. (H) A plot showing its characteristics and (I) image of the battery powering an LED. (G–I) Adapted with permission from ref 670. Copyright 2017 Wiley-VCH Verlag GmbH & Co. KGaA. (J) Exploded view illustration of different components of a zinc–MnO_2 battery. (K) Plot of the charging/discharging properties and (L) performance under repeated punching, washing, hammering, and exposing to fire. (J–L) Adapted with permission from ref 676. Copyright 2018 Royal Society of Chemistry. (M) A schematic

DOI: 10.1021/acs.chemrev.8b00573
Chem. Rev. 2019, 119, 5461–5533

Figure 19. continued

illustration of a fructose-based biobattery. (N) Image of the biobattery being twisted while powering an LED. (O) Plot illustrating characteristics of the biobattery. (M–O) Adapted with permission from ref 673. Copyright 2015 Elsevier.

for gas capture and filtration (Figure 18L); however, the response time is on the order of minutes (~10–20 min). Metal organic framework/CNT-fiber composites offer an alternative where the CNT-based fibers serve as a highly flexible, conductive substrate and the metal organic frameworks impart gas selectivity.[642]

3.3.3. Miscellaneous Environmental Signals. Skin-interfaced sensors for forensic applications represent another area of active research interest. Gloves are the primary form factor, as many chemical species of interest are either toxic or easily contaminated by skin debris during the sample collection process. Recent demonstrations include sensors for gunshot residue,[645] explosives,[645,646] drugs of abuse,[647] and nerve agents.[646,648,649] Typically, the fabrication utilizes a screen printing process to form sensor electrodes onto the fingertips of gloves. Abrasive electro-analytical techniques[650] enable sample collection and analysis. For the detection of gunshot residue, explosives, and drugs, the sample capture involves rolling a fingertip-based sensor on a surface that supports the sample. Subsequent analysis using voltammetric techniques detects the presence or absence of the species of interest. Field tests demonstrate the capability to detect the presence of gunshot residues[645] and drugs.[647] Wearable sensors for nerve agent detection follow similar protocols with the working electrode functionalized with enzymes for specific nerve agents.[646,648]

Food analysis is of increasing interest for detecting the presence of allergens or contamination by drugs of abuse, yet a nascent area of research for epidermal sensors. The targets of interest are, however, readily adaptable to form factors similar to those employed for forensic applications. A recent demonstration highlights integration of a colorimetric pH sensor onto artificial fingernails for rapid pH analysis of beverages.[651] The sensor utilizes various pH sensitive dyes (bromothymol blue, bromocresol green, and cresol red) encapsulated in a PVC membrane to encompass a working pH range of 3–10. Application of the pH cocktail solution to artificial fingernails enables analysis of the entire range of pH values. Benchtop analysis with standard solutions and common items, such as lemon juice (pH 2.5), tap water (pH 6.5), and baking soda (pH 9), illustrate the use of this platform for rapid pH analysis in a wide pH range.

For both forensic and food analysis applications, bio-integration enables precise, highly localized quantification of targets of interest with respect to various body locations in a manner not possible with conventional "wearable" devices. This type of use represents an underdeveloped area of bio-integrated systems with many opportunities for additional research. Integrating intimate, localized environmental monitoring with the precision physiological monitoring platforms detailed in sections 3.1 and 3.2 offers the potential for unparalleled insight into the overall human health state.

4. POWER

The demanding requirements for thin, soft, lightweight construction in the types of skin-interfaced wearable systems described here create challenges, and associated research opportunities, in power supply and in designs for power efficient operation. The following sections introduce some recent concepts in energy storage and energy harvesting. A subsequent section discusses considerations in system efficiency.

4.1. Energy Storage Technologies

Energy storage systems, in the form of batteries and supercapacitors, comprise the majority of integrated power sources in epidermal applications. This section provides a brief overview of both technologies and highlights key device embodiments representing the current state-of-the-art for integrating energy storage in bio-integrated platforms.

4.1.1. Batteries. The latest in battery-based energy storage systems possess high specific energy densities, fast recharging capabilities, and excellent cycle stabilities, suitable for applications ranging from powering homes[652] and vehicles[653,654] to miniaturized electronics[655] and medical implants.[656] These developments stem primarily from rapid progress in battery materials,[657,658] yet most systems are rigid and bulky, rendering them poorly suited for skin-interfaced devices.[655] The simplest examples use commercial coin cell batteries,[442,463,659] but such components typically dominate the device weight and form factor. Batteries tailored to the requirements of bio-interfaced applications exploit developments in soft materials, active battery chemistries, nanotechnology, biocompatible electrolytes, and design optimization.[35,660,661] The nascent field of stretchable, skin-interfaced batteries primarily includes examples of lithium,[662–666] zinc,[667–669] sodium,[670–672] and enzyme[673,674] based systems, as highlighted in the following.

An early example of a stretchable lithium-ion (Li-ion) battery for epidermal applications exploits optimized microstructures and the materials engineering approaches of section 2.1.2 in serpentine-based stretchable current collector architectures. Doctor blade coating delivers slurries of active anodic (Li_2TiO_3) and cathodic ($LiCoO_2$) materials (Figure 19A)[662] with carbon black (as conductive support), PVDF (as a polymeric binder), and *N*-methyl-2-pyrrolidone (slurry vehicle) to a collection of active regions. Encapsulating the entire system into a silicone elastomer defines the overall soft mechanics of the battery. Reversible deformations to strains of nearly 300% are possible before mechanical failure (Figure 19B) while maintaining capacities of ~1.1 mAh cm^{-2} (>20 cycles, cutoff voltage of 2.5–1.6 V) (Figure 19C).

Fabric-type designs represent an interesting additional class of substrate for bio-integrated energy storage.[660,677] Fabrics possess high specific surface areas, and they can be functionalized to support high loading of active materials per surface area. The fabrication of such textile-based energy storage systems typically begins with the transformation of nonconductive fabrics into conductive formats by coating with carbon-based conductors[678,679] or metals,[680] followed by functionalization with anodic and cathodic active materials. One example[680] involves electroplating of nonconductive commercial polyester fibers with nickel and subsequent coating with anodic and cathodic slurries prepared by mixing carbon black, active materials (Li_2TiO_3 or $LiCoO_2$), and polymeric binder in *N*-methyl-2-pyrrolidone. The binder is a special formulation of PU in which oligomers of polytetramethylene

DOI: 10.1021/acs.chemrev.8b00573
Chem. Rev. 2019, 119, 5461–5533

glycol and polyethylene glycol cross-link with 4,4-diphenylmethane diisocyanate to yield a material that is stretchable (for wearability) and can support hydrogen bonding to enhance battery material adhesion. An ethylene carbonate and dimethyl carbonate mixture serves as the electrolyte. The battery retains ~91.8% of the original capacity (85 mA g^{-1}) after 5500 cycles of folding/unfolding.

Other fabric embodiments utilize conductive yarns directly spun from either neat CNT forests or CNT composites.[681] One example exploits this route in a highly stretchable yarn-based Li-ion battery.[664] Here, conductive MWCNT-based yarns formed from MWCNT forests serve as the substrate material. Coating individual yarns with active battery material slurry forms the anode (Li_2TiO_3) and cathode ($LiMn_2O_4$). The battery comprises a sealed, shrinkable, flexible tube of twisted threads of yarn-based electrodes (a belt separator between electrodes eliminates shorting) and an electrolyte mixture of ethylene carbonate, diethyl carbonate, and dimethyl carbonate. The battery exhibits a volumetric power density of ~0.56 W cm^{-3} and maintains ~84% of its capacity after 200 stretching cycles at 100% strain. As an alternative to these assembly methods, a recent report presents the use of additive manufacturing methods (3D printing) to form yarn-based batteries directly.[668] Custom 3D printers extrude three printable inks, consisting of anodic nanoparticles (Li_2TiO_3, < 200 nm), cathodic nanoparticles ($LiFePO_4$, 50−100 nm), and SWCNTs within a PVDF gel (prepared in *N*-methyl-2-pyrrolidone) to form CNT yarn-based anodes and cathodes. Assembling the battery in a manner similar to the previous example[664] completes the fabrication process. Batteries of this type exhibit high specific capacities (110 mAh g^{-1}) at current densities of 50 mA g^{-1}.

Efforts to further increase the energy densities of wearable batteries involve materials beyond those in Li-ion systems. Lithium−air batteries, in particular, are attractive due to theoretical energy densities that can reach ~5−10 times those of conventional Li-ion batteries.[682−684] A recent report of a stretchable lithium−air battery (Figure 1919D−F) suggests significant enhancements in performance relative to previously explored slurry-based Li-ion systems.[675] The device uses a bonded array of millimeter-wide, thin, flexible lithium sheets as the anode, laminated to a copper spring-based current collector affixed to a soft, stretchable silicone substrate. The cathode is a wrinkled elastomeric composite of a MWCNT thin film on a silicone sheet bonded to a perforated silicone substrate to facilitate access to oxygen from air. A two-part solution, prepared under an argon atmosphere, serves as a gel electrolyte. Solution A is a mixture of lithium bis(trifluoromethane)sulfonamide, succinonitrile, and poly(ethylene oxide) in a solvent mixture of methylene chloride and acetone. Solution B is dissolved poly(vinylidene-fluoride-*co*-hexafluoropropylene) in *N*-methyl-2-pyrrolidinone. The thorough mixing of the two solutions yields the gel electrolyte. The battery energy density (based on the total weight) is ~2540 Wh kg^{-1}, which represents a ~22 times increase over previously reported stretchable Li-ion batteries and a ~110 times increase over stretchable supercapacitors.[685,686]

Although lithium-based batteries are of widespread interest, reliance on toxic components represents a drawback for bio-integrated applications. Less toxic battery systems, such as those based on sodium[687,688] and zinc,[689,690] are, therefore, important to consider. A representative example of a textile-based sodium battery[670] utilizes an anode formed by wrapping a thin copper wire over a Teflon tube and subsequently rolling a sodium foil over the assembly. A two-step process of electroless nickel plating and subsequent dip coating to form an iron(III) ferrocyanide/graphene oxide layer on a fabric support yields a flexible, low-cost cathodic material. The battery structure consists of the cathode, soaked in an electrolyte (sodium hexafluorophosphate in a mixture of ethylene carbonate and dimethyl carbonate), wrapped over the anode and polypropylene separator, and sealed with heat shrink tubing (Figure 19G). This type of environmentally friendly battery exhibits high flexibility, good rate capability (30 C), and cyclic stability (up to 1800 cycles before performance degradation) (Figure 19H). Integration can occur on necklaces or wrist-bands (Figure 19I) for skin-interfaced applications.

Spontaneous ignition or battery detonation due to either thermal runaway[691] or physical damage[692] represents an additional concern for applications considered here. Recent work to address this issue focuses on a damage-proof, highly safe zinc−manganese oxide-based skin-integrated battery design (Figure 19J)[676] that relies upon a tough electrolyte gel that consists of a polyacrylamide-grafted gelatin hydrogel infiltrated within a polyacrylonitrile membrane. The grafting process significantly enhances the mechanical strength and ionic conductivity of the gel, while the polyacrylonitrile fibers improve the mechanical resiliency and reduce the probability for forming electrical shorts. The anode consists of an electroplated zinc/CNT paper composite, and the cathode uses a manganese oxide nanorod/CNT composite printed onto CNT paper. The battery offers impressive charging−discharging characteristics (~2772 mAg^{-1}) (Figure 19K) that marginally decrease under extreme conditions such as repeated hammering, washing, hole punching, and even exposure to fire (Figure 19L).

By comparison to these inorganic materials systems, biobatteries, as defined by systems that rely on enzymatic reactions to generate electricity, offer another option in biocompatible power sources.[673,674,693] Figure 19M exemplifies this approach.[673] This fructose fuel-based platform uses highly stretchable textiles (PI/PU cofibers) coated with SWCNT ink as support substrates. Functionalizing the anode-designated textile with D-fructose dehydrogenase (to selectively oxidize fructose) and immobilizing the cathode-designated textile with bilirubin oxidase (to catalyze oxygen reduction) forms active electrodes. An acrylamide-based polymer gel containing 200 mM fructose acts as a solid-state electrolyte and provides the fuel (fructose) to the biobattery for spontaneous production of electricity. The stretchable underlying fabric architecture is highly durable to axial strain (Figure 19N) and maintains power generation capability of ~0.2 mW cm^{-2} across a 1.2 kΩ load (Figure 19O). Although such biobatteries comprise an interesting class of power source, additional materials research is necessary to overcome their relatively low power densities and open circuit voltages, together with their short shelf life.

4.1.2. Supercapacitors. Supercapacitors exhibit several key advantages over batteries including fast charging/discharging, high power density, and enhanced operational durability for large numbers of charging/discharging cycles.[38,694] These features are of particular interest to skin-interfaced platforms, particularly for their ability in rapid charging, delivering quick bursts of energy and supporting pathways for device miniaturization.[37,695,696] As with batteries, much research on skin-interfaced supercapacitors focus on fabric-based systems due to their high surface areas and favorable mechanics,[695,697−700] with particular emphasis on symmetric carbon-based nanomaterial electrodes.[701−706] Figure 20A−C highlights

DOI: 10.1021/acs.chemrev.8b00573
Chem. Rev. 2019, 119, 5461−5533

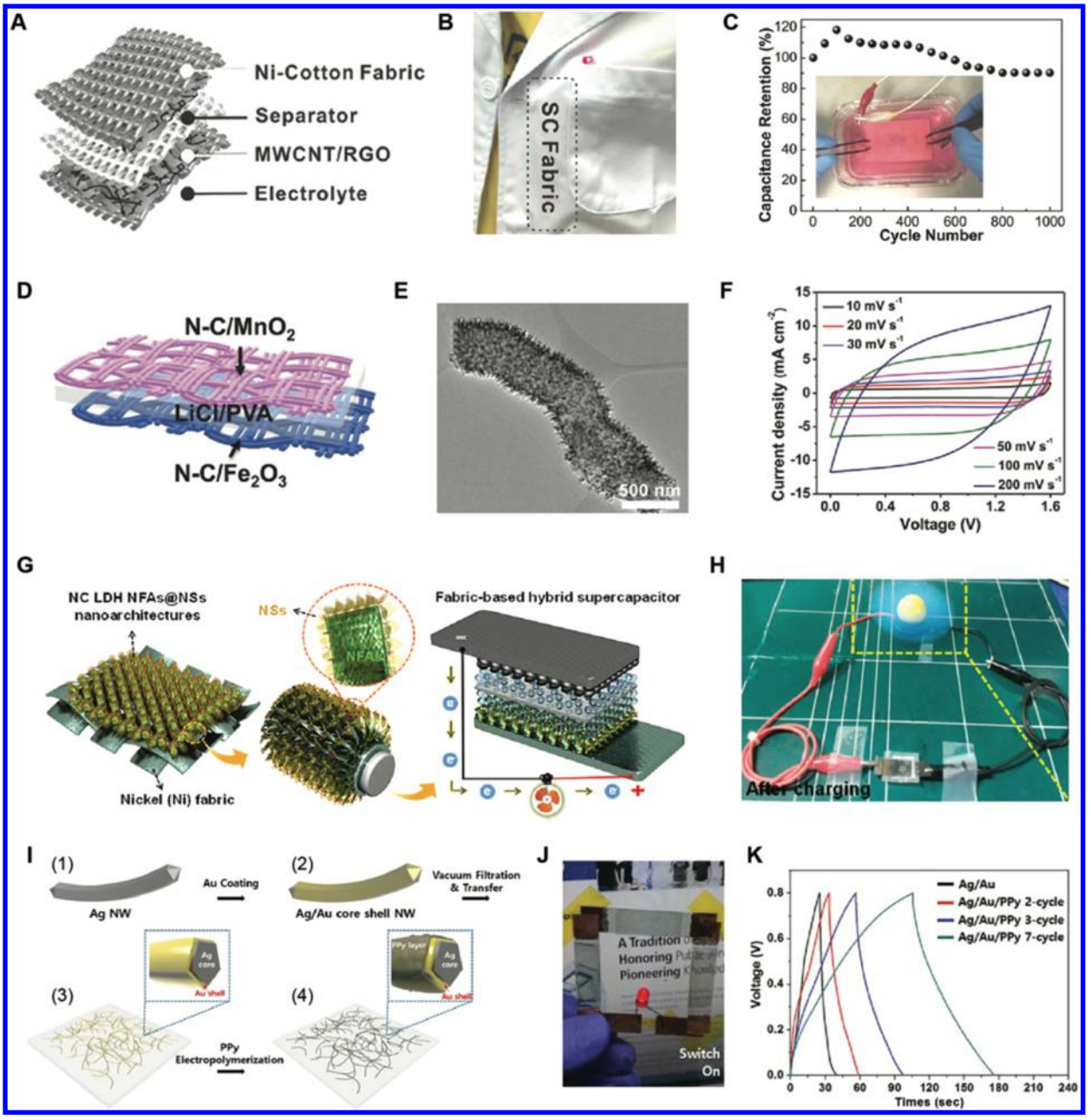

Figure 20. Supercapacitors. (A) Illustration of a CNT/RGO-based textile supercapacitor. (B) Image of the capacitor embedded within a coat for powering an LED. (C) Capacity retention of the supercapacitor when submerged in water. (A–C) Adapted with permission from ref 703. Copyright 2017 Wiley-VCH Verlag GmbH & Co. KGaA. (D) Schematic illustration of an asymmetric textile-based supercapacitor. (E) TEM images of the N-C/Fe_2O_3 nanostructure. (F) Cycling properties of the supercapacitor. (D–F) Adapted with permission from ref 707. Copyright 2018 Wiley-VCH Verlag GmbH & Co. KGaA. (G) Illustration of a supercapacitor that uses a self-branched bimetallic, layered double hydroxide coaxial nanostructure. (H) Image of the device powering an LED. (G,H) Adapted with permission from ref 708. Copyright 2017 American Chemical Society. (I) Illustration of an Ag/Au core–shell NW-based transparent supercapacitor. (J) Image of the transparent power source illuminating an LED. (K) Plots highlighting the charging/discharging properties of the supercapacitor. (I–K) Adapted with permission from ref 709. Copyright 2017 Springer Nature.

a representative example of a waterproof, epidermal carbon-based supercapacitor system with an ultrahigh areal capacitance.[703] The devices uses a nickel-plated, highly porous cotton fabric, coated with alternating layers of RGO and CNTs by a filtration process, as the symmetric electrodes separated by a PVA-based hydrogel layer. A water repellant (polyterafluorethlene agent) overcoat renders the supercapacitor waterproof. The supercapacitor maintains a capacity of 3.2 F cm^{-2} after 10000 charge/discharge cycles, zero capacitive decay after 10000 bending tests, and continuous operation while submerged in water (test spanned a 10 h time period).

Asymmetric supercapacitors can support improved cell voltages as well as energy and power densities.[710] Such systems utilize either a pseudocapacitive or an electrochemical double-layer-based capacitive electrode configuration formed from metal oxides[707,711−713] or metal oxide/conducting polymer composites.[714] Figure 20D,E exemplifies a typical skin-interfaced asymmetric supercapacitor.[707] This platform uses polypyrrole nanowires electrochemically grown on carbon fibers

DOI: 10.1021/acs.chemrev.8b00573
Chem. Rev. 2019, 119, 5461−5533

for electrodes. After carbonization, the electrochemical growth of manganese oxide and iron oxide particles (on two separate substrates) completes the fabrication. Two such electrodes, separated by a PVA gel-based electrolyte, form the final asymmetric supercapacitor structure. Benchtop system characterization (Figure 20F) shows an operation voltage of 1.6 V, delivery of over 60 mF cm^{-2} during an approximate 50 s charging/discharging time, and 30 mF cm^{-2} over an approximate 5 s discharge.

Metal hydroxide-based skin-interfaced asymmetric supercapacitors offer even higher energy densities.[708,715] A recent example incorporates a self-branched bimetallic-layered double hydroxide coaxial nanostructure-based supercapacitor into fabric (Figure 20G,H).[708] The supercapacitor uses an activated carbon cathode and a hierarchically structured anode. The anode consists of a nickel-plated fabric surface coated with arrays of nickel cobalt-layered double hydroxide nanoflakes. A subsequent synthesis step forms nickel cobalt-layered double hydroxide nanosheets on the nanoflake coating. This type of supercapacitor exhibits a large areal capacitance of 1147.23 mF cm^{-2} at 3 mA cm^{-2} and a high energy density of 0.392 mWh cm^{-2} at a power density of 2.353 mW cm^{-2}.

In addition to increasing performance, some research efforts focus on the development of transparent epidermal supercapacitors for improved visual/optical interfaces to the underlying skin.[709] One noteworthy embodiment[709] uses a Ag/Au/polypyrrole core−shell nanowire-based mesh (Figure 20I) on a silicone substrate as the supercapacitor electrode. The chemical reduction of auric ions onto AgNWs with polyvinylpyrrolidone as a capping agent produces Ag/Au core−shell NWs. Vacuum filtration of the Ag/Au NW solution forms mesh electrodes that can be subsequently transferred onto a silicone substrate. Electropolymerization of pyrrole forms a conductive layer of polypyrrole around these NWs. The resulting system offers good transparency across the visible range (73% at 550 nm for 2 layers of the Ag/Au/polypyrrole core−shell NW-based mesh) (Figure 20J) and good charging/discharging cycling properties (580 μF cm^{-2} at current density 5.8 μA cm^{-2}) (Figure 20K).

4.2. Energy Harvesting Technologies

Capabilities in energy harvesting can, in ideal scenarios, allow for operation without the need for batteries or supercapacitors for energy storage; in others, harvesting can reduce storage capacity requirements.[716] Several recent reviews provide excellent summaries of the various technology options.[40,717−722] This section presents a focused overview of approaches specifically tailored for use in skin-interfaced platforms.

4.2.1. Radio Frequency. Harvesting power from RF transmission represents one of the most versatile and scalable means to operate skin-integrated, battery-free sensors.[723] NFC technologies involve RF at 13.56 MHz, originally designed for RF identification tags, authentication, and wireless payments but also capable of use in a mode that provides power transfer to a matched receiving antenna. Recent work demonstrates the ability to use NFC approaches to meet operational power requirements for skin-interfaced devices that have skin-like form factors. An attractive feature is that NFC infrastructure is a ubiquitous and almost universal feature in consumer gadgetry such as smartphones and tablets, thereby enabling wireless links to cloud-based databases and computing power.[724] The magnetic resonant coupling utilized in NFC technology enables not only high-efficiency power transfer[725,726] but also data communication,[727] resulting in passive device architectures capable of moderate data throughput (up to 424 Kbps, ISO 18000-3 standard). With low component count and readily available, integrated commercial solutions, typical implementation strategies require only a connection to an NFC antenna.[222,728] Furthermore, RF in the NFC operating frequency range undergoes negligible absorption in biological tissues, and its transmission is relatively insensitive to the dielectric properties of the surroundings. The main disadvantage is that the near field nature of the technology prevents operation over distances larger than ∼1 m, without additional passive hardware, even with high power transmission systems.

Figure 21 highlights recent examples of NFC-enabled skin-interfaced devices. These systems exploit the materials and engineering design strategies introduced in section 2 to yield skin-like mechanical properties suitable for intimate integration with the human body.[173,728] The devices most typically use thin filamentary metal traces as antennas, patterned by laser ablation or photolithography[220,440,521,599,724,730] or GaIn-based liquid

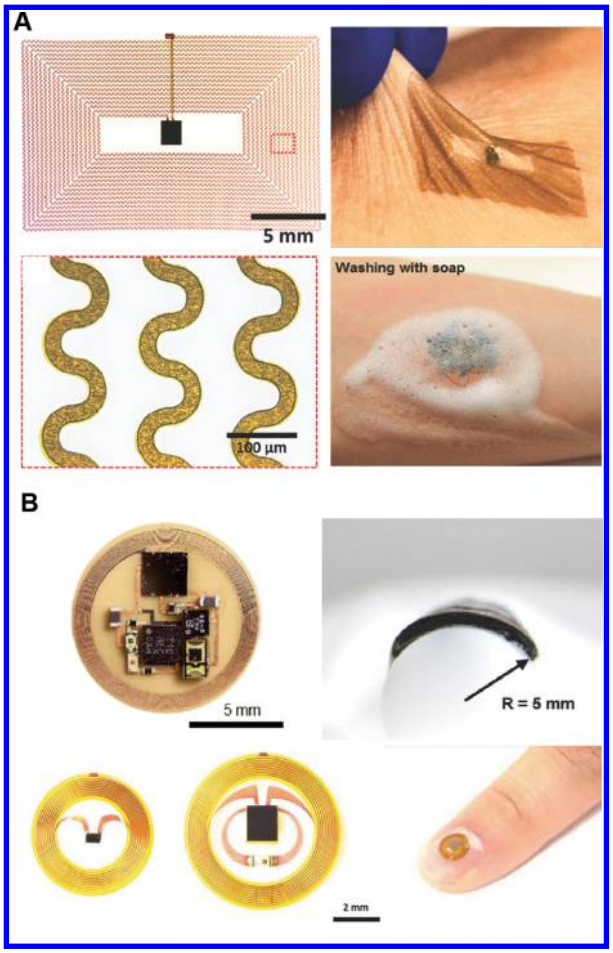

Figure 21. Skin-interfaced wireless devices based on NFC technology. (A) Optical image of an epidermal NFC-based device (left, top) and optical microscope image of the region indicated in red (left, bottom). (Right, top) Optical image of the device conformally interfaced with the skin and (right, bottom) washed with soap/water. Reproduced with permission from ref 728. Copyright 2014 Wiley-VCH Verlag GmbH & Co. KGaA. (B) Representative examples of ultraminiaturized NFC-enabled devices for integration onto the fingernail. (top) Reproduced with permission from ref 222. Copyright 2016 Wiley-VCH Verlag GmbH & Co. KGaA). (bottom) Reproduced with permission from ref 729. Copyright 2015 Wiley-VCH Verlag GmbH & Co. KGaA.

DOI: 10.1021/acs.chemrev.8b00573
Chem. Rev. 2019, 119, 5461−5533

metals[300] in PDMS microchannels. Such designs support high levels of mechanical durability and stretchability for robust on-body performance (Figure 21A).[728] These platforms can incorporate optoelectronic components and silicon-based digital, analogue, and mixed-mode technologies as demonstrated in a recently reported epidermal system for PPG (Figure 11N−Q).[440] Other, related NFC-enabled devices exist for sensing a range of biophysical (pressure,[724] temperature[730]), biochemical (sweat-based electrolytes[220,521]), and environmental (UV[599,600]) signals. Figure 21B highlights examples of ultraminiaturized designs, where overall device diameters are as small as 5.8 mm, suitable for integration onto a fingernail.[729] A wireless device for PPG and pulse oximetry monitoring leverages this form factor for long-term use and overall superior device performance.[222]

Far-field energy harvesting at frequencies of several hundred MHz or several GHz offers an RF option that can support operating ranges of several or many meters (Figure 22).[732] By comparison to NFC, such far-field approaches typically require directional antennas, they can be affected by reflection and absorption from the surroundings, including biological tissues, and they typically demand proper orientation between the transmission and receiving antennas.[734] Current research focuses on purpose-built electronics[735] for far-field skin-interfaced sensors. One example utilizes contact printing assembly processes to fabricate modular devices capable of activating an LED using RF powers within established safety limits (Figure 22A).[731] Other cases use small rigid circuit boards and simple dipole antennas in epidermal form factors (Figure 22B) to harvest power sufficient for transmission of sensor data in a fully passive mode.[732] As Figure 22C shows, the miniaturization offered by far-field systems enables fully stretchable devices with small sizes (~6 cm × 3 cm) and capabilities for powering LEDs.[733]

4.2.2. Photovoltaics. Photovoltaic (PV) harvesting offers another promising strategy. Although requirements for consistent light exposure limit broad utilization in wearable applications, PV approaches can be used synergistically with batteries and other forms of harvesting and storage.[736] This section highlights some recent results in PV harvesting systems, classified as inorganic, organic, and inorganic/organic hybrids,[737−746] in skin-integrated devices.

PV systems based on Si (monocrystalline, polycrystalline, and amorphous), GaAs, cadmium telluride (CdTe), and copper indium gallium selenide (CIGS) dominate industrial scale power generation.[736,747] The materials engineering approaches introduced in section 2.1.2, in particular the island-bridge configuration, enable flexible/stretchable PV harvesters to be constructed from these same materials.[748,749] For example, arrays of dual-junction GaInP/GaAs microscale solar cells with buckled Ti/Au metallic interconnects can form PV systems with ability to biaxially stretch up to 60% and with energy conversion efficiencies and areal fill factors of 19% and 0.85, respectively.[748] More recent work exploits a similar concept in a skin-compatible form factor with a collection of chip-scale, rechargeable lithium-ion batteries, to yield a sustainable power supply for wireless skin thermography (Figure 23A,B).[730] Here, a 2 × 2 array of cells harvests a maximum power of 12.5 mW (areal fill factor of 0.84) with a negligible decrease in performance under biaxial stretching up to 30%.

Organic photovoltaic harvesters (OPVs) are of increasing interest as lightweight, flexible alternatives to inorganic devices.[752] The comparatively poor energy conversion efficiencies and the limited environmental stability remain as challenges for use in epidermal applications. Progress includes reports of advanced materials, such as benzodithiophene- and difluorobenzothiadiazol-based polymers, which when combined with fullerene acceptors, offer conversion efficiencies as high as 11.7%.[753−756] Additionally, certain air-stable polymers and encapsulation strategies improve long-term environmental stability. For example, a recent report[750] highlights a stretchable,

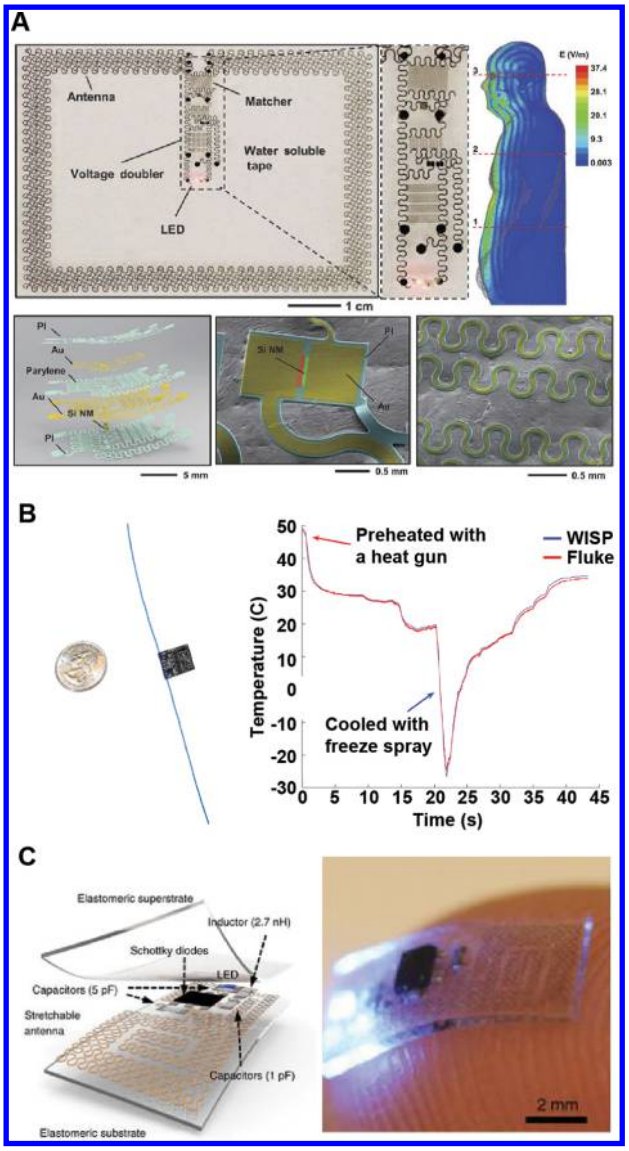

Figure 22. Skin-interfaced devices based on far-field radio frequency technology. (A) Optical image of epidermal far-field RF-based device (top, left), schematic illustration of the device (bottom, right), and SEM micrographs of a silicon nanomembrane RF diode (bottom, center) and a FS parallel plate capacitor on a skin replica (bottom, right). Model of the human body shows the simulated specific absorption rate of an RF source 1.5 m away. Reproduced with permission from ref 731. Copyright 2016 Springer Nature. (B) (left) Optical image of a Wireless Identification and Sensing Platform and (right) demonstration of measurement capabilities in detecting temperature changes. Reproduced with permission from ref 732. Copyright 2008 Institute of Electrical and Electronics Engineers. (C) Demonstration of the miniaturization capabilities of far-field systems through a schematic illustration (left) and optical image (right) of a small, fully stretchable device capable of powering LEDs. Reproduced with permission from ref 733. Copyright 2015 Springer Nature.

DOI: 10.1021/acs.chemrev.8b00573
Chem. Rev. 2019, 119, 5461−5533

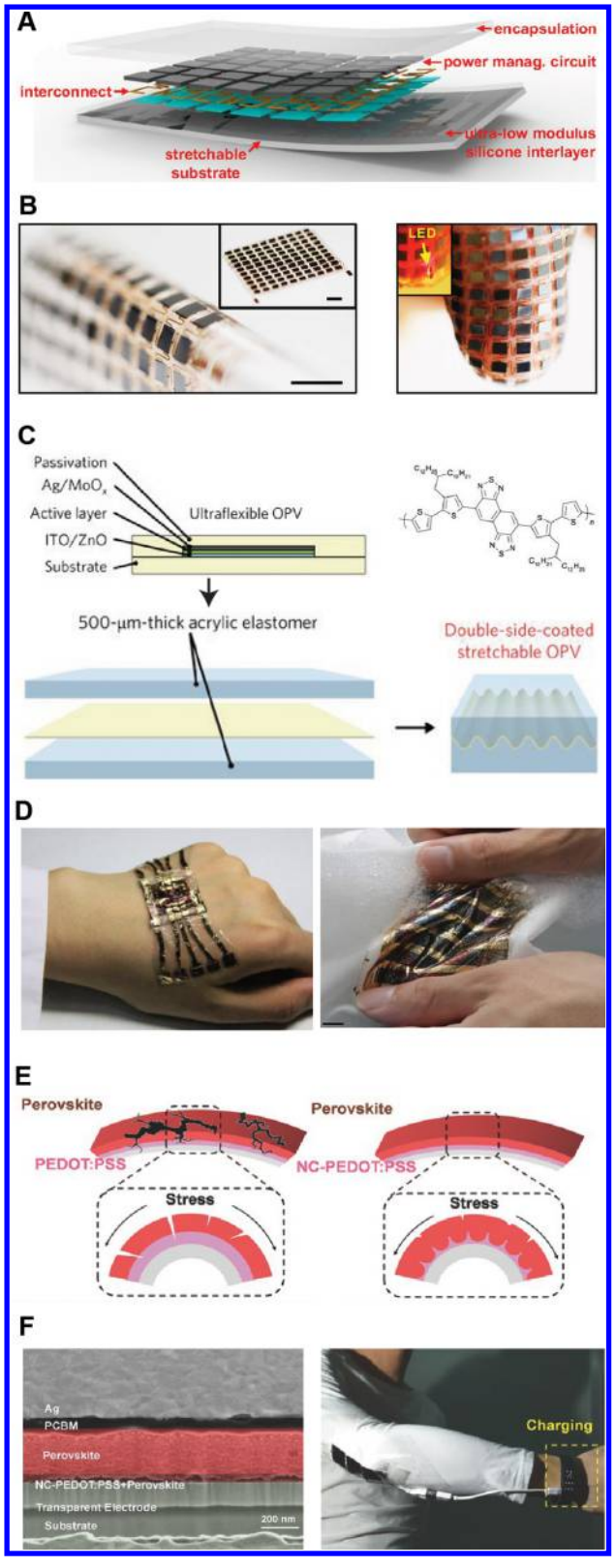

Figure 23. Photovoltaic cells. (A) Schematic illustration of a soft, thin skin-mounted power management system with photovoltaic power supply. (B) Photographs of the device bent around a cylindrical tube and an index finger (scale bar, 5 mm). (A,B) Adapted with permission from ref 730. Copyright 2016 National Academy of Sciences. (C) Schematic illustration of a washable and stretchable organic photovoltaic device. (D) Photographs of the device conforming to the hand and a dress shirt. (C,D) Adapted with permission from ref 750. Copyright 2017 Springer Nature. (E) Schematic illustration of a wearable perovskite photovoltaic device. (F) SEM cross-sectional image of the device and photograph of assembled device on the coat charging an electronic watch. (E,F) Adapted with permission from ref 751. Copyright 2017 Wiley-VCH Verlag GmbH & Co. KGaA.

waterproof elastomer-coated OPV (Figure 23C) in which a composite film of a donor−acceptor polymer with quaterthiophene and naphtho[1,2-*c*:5,6-*c*′]bis[1,2,5]thiadiazole and [6,6]-phenyl C_{71}-butyric acid methyl ester serves as high efficiency, air-stable active layer. This type of OPV is "washable", and exhibits an energy conversion efficiency of 7.9% and stretchability of 52% (Figure 23D). The efficiency drops, however, by 46% after 30 days of exposure to the ambient environment.

Organic−inorganic perovskites exhibit remarkable photophysical properties and are a promising class of materials for skin-interfaced PV harvesting.[757−761] Typical perovskites in PV applications include RAX (RA: MA, FA; X: I, Br) or BX_2 (B: Pb, Sn; X: I, Br, Cl) as described in detail in a recent review.[762] Flexible perovskite PV cells exhibit power conversion efficiencies in excess of 20%[755] with the potential to reach the Shockley−Queisser limit for a single-junction PV cell (33.5%).[763−765] A recent paper reports a flexible, large-scale (>1 cm^2) perovskite PV harvester for use as a skin-interfaced power source with a conversion efficiency of 12.3%.[751] This embodiment utilizes a nanocellular PEDOT:PSS scaffold as an interfacial layer for the perovskite film (PbI_2/MAI/[6,6]-phenyl-C61-butyric acid methyl ester) to mitigate bending-induced mechanical stresses (Figure 23E,F). Infiltration of the perovskite into the scaffold during fabrication (before drying) inhibits crack propagation. The flexible, PV harvester maintains 93% of the pristine conversion efficiency after 1000 bending cycles (2 mm radius of curvature). As with OPVs, the environmental and mechanical stability of perovskite films remain as critical challenges for use in epidermal platforms.[762]

4.2.3. Thermoelectrics. Thermoelectric generators in bio-integrated wearable systems exploit the Seebeck effect to harvest energy from the temperature difference between the skin and the ambient environment. Although the overall power density is relatively low due to modest temperature gradients (typically ~10 μW cm^{-2}), particularly for thin device geometries, this harvesting approach yields a continuous and stable source of power. Such performance is ideal for epidermal sensor platforms designed for long-term continuous monitoring. The detailed performance attributes depend on both the material selections and the structural designs of the generator.[766−768]

The active materials in thermoelectric generators span a large range of both inorganic (primarily Bi, Te, Sb, and Se composites) and organic (conducting polymers, CNTs, and transition metal dichalcogenides) compounds.[769−775] The key performance metric for both classes of devices is the thermoelectric figure of merit, $ZT = \alpha^2\sigma T/k$, where α is the Seebeck coefficient, σ, k are the electrical conductivity and thermal conductivity, respectively, and T is absolute temperature. The power factor, $\alpha^2\sigma$, enables comparison of materials with similar thermal conductivities. In the case of inorganic thermoelectric materials, bismuth telluride (Bi_2Te_3) and antimony telluride (Sb_2Te_3) based alloys are most common due to their high conversion efficiency at room temperature (e.g., power factor of ~4000 μW m^{-1} K^{-2} for a nanostructured p-type $Bi_{0.5}Sb_{1.5}Te_3$

DOI: 10.1021/acs.chemrev.8b00573
Chem. Rev. 2019, 119, 5461−5533

film[776]) and facile integration with standard thin-film processing.[777]

By comparison, organic semiconductors exhibit relatively low power factors, but they are lightweight, intrinsically flexible, solution-processable, low cost, and potentially abundant.[770,778,779] Conducting polymers (polyaniline, polypyrrole, polythiophene, polyacetylene, polycarbazoles, polyphenylenevinylene, and PEDOT:PSS[770,780−782]) are of primary interest, where the power factors can range from 10^{-4} to 10^{3} μW m^{-1} K^{-2} (dependent on doping and molecular conformation of the polymer chains).[770,783−785] Although less common, recent SWCNT-based composites show promise, with a comparable thermoelectric power factor to commercial-grade bismuth telluride.[786,787] For example, composites, comprised of polyaniline, PEDOT:PSS stabilized graphene, and PEDOT:PSS stabilized double-walled CNTs, show a high thermoelectric power factor of 2710 μW m^{-1} K^{-2};[785] however, the absence of thermal conductivity characterization prevents calculation of the ZT value necessary for comparison with inorganic thermoelectric materials.

The conversion efficiency also strongly depends on the structural design of the generator (in-plane or cross-plane), independent of material selection. A device consists of alternating sets of semiconducting elements (n- and p-type), known as legs, connected in series. The most common approach to thin, flexible devices involves legs oriented in an in-plane configuration, even though such an arrangement results in relatively low power generation.[788,789] In a cross-plane structure, the legs lie perpendicular to the substrate. This configuration aligns with heat flow from the skin to the surroundings, resulting in improved voltage and power output, although at the expense of overall thickness. Consideration of the contact area of the generator to the skin is particularly important in epidermal devices as a conformal interface improves performance by minimizing thermal contact resistance.

The most widely reported thermoelectric generators for epidermal applications utilize inorganic materials and a flexible, cross-plane configuration.[22,766] Design guidelines from experimental and computational studies offer insight into optimizing the performance. A quasi-3D computational model[793] defines the interrelationships between the fill factor, leg dimensions, thermal conductivity (both substrate and composite filler), substrate thickness, and dimensions of external heat spreaders for body-worn generators. For epidermal applications, the model suggests that the thermal conductivity of the semiconductor material (rather than the ZT) is a key factor, along with the device fill factor. Complementary work experimentally defines the effects of structure (leg height, fill factor) on output power.[90,794] Both parameters influence the overall power density. Increasing the leg height (from 0.8 to 2.5 mm) yields an approximate 4-fold improvement in power density, decreasing the fill factor (from ∼25% to 15%) results in an increase in power density as the optimum fill factor depends on the surrounding thermal resistance. A demonstration of a skin-interfaced thermoelectric generator with 2.5 mm legs (commercially available), and 15.1% fill factor exhibits a power density of 2.28 μW cm^{-2}, currently the highest reported value for an epidermal generator without an integrated heatsink (Figure 24A).[790]

Using a similar design strategy, a recent report describes liquid metal (EGaIn) channels to connect commercial thermoelectric legs ($Bi_{0.5}Sb_{1.5}Te_3$ P-type and $Bi_2Se_{0.3}Te_{2.7}$ N-type) encapsulated in PDMS to obtain a stretchable generator with an output

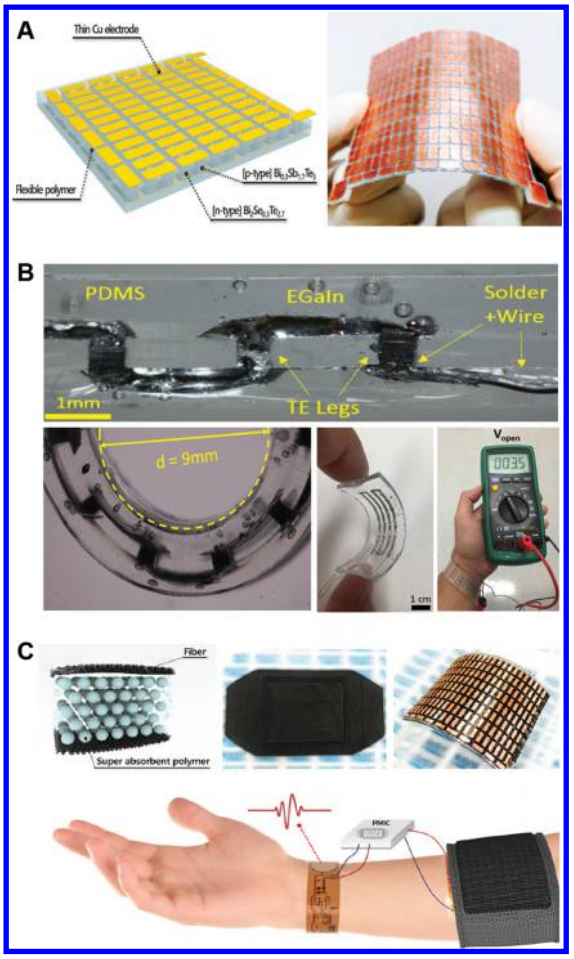

Figure 24. Thermoelectric generators. (A) Schematic diagram and photograph of an inorganic flexible thermoelectric power generator. Adapted with permission from ref 790. Copyright 2018 Elsevier. (B) Optical images of a thermoelectric generator with liquid metal interconnects. Adapted with permission from ref 791. Copyright 2018 Elsevier. (C) Schematic picture and photograph of a wearable thermoelectric generator, powering an ECG sensor. Adapted with permission from ref 792. Copyright 2018 American Chemical Society.

power of 1.48 μW at ΔT = 0.4 K (Figure 24B).[791] Computational modeling predicts that with appropriate optimized designs (increasing the thermal conductivity of the PDMS, and extending the lengths of the legs) could enable power outputs of 29 μW and 7.3 μW cm^{-2}, respectively, at ΔT = 1.6 K, without the use of a heatsink.

By comparison, epidermal embodiments with heatsinks offer significantly higher power densities. A recent report details a flexible, wrist-mounted thermoelectric generator, consisting of 52 pairs of rectangular-shaped P-type ($Bi_{0.5}Sb_{1.5}Te_3$) and N-type ($Bi_2Se_{0.5}Te_{2.5}$) thermoelectric legs and an evanescent polymer-based heat sink, capable of powering a miniaturized accelerometer to monitor body movements (Figure 24C).[792] The flexible heat sink consists of a water-saturated superabsorbent polymer (sodium polyacrylate) encapsulated by xylitol-impregnated fabric such that evaporative water loss induces an enhanced thermal gradient from the endothermic water/xylitol reaction. The device generates a voltage of 6.6 mV at ΔT = 5.8 K with a calculated output power and power density of 192.6 μW and 16.7 μW cm^{-2} at ΔT = 50 K, respectively.

4.2.4. Piezoelectrics. Piezoelectric generators harvest mechanical energy from human motion via the piezoelectric

DOI: 10.1021/acs.chemrev.8b00573
Chem. Rev. 2019, 119, 5461−5533

effect described in section 3.1.2. These generators can continuously power epidermal platforms when coupled with energy storage devices or they can serve as the basis of self-powered sensors (e.g., kinematic or vascular dynamic signals).[795] Such devices use either organic (PVDF, P(VDF-TrFe))[354,796] or, more commonly, inorganic (PZT, $BaTiO_3$, ZnO)[797,798] piezoelectric materials. As the high performance inorganic materials are rigid and brittle, most embodiments exploit materials engineering approaches described previously to achieve the flexible and stretchable form factors necessary for interfaces to the skin.

Early device designs involve fiber-type generators that convert low-frequency (<1 Hz) mechanical movements into electrical power. Figure 25A highlights a representative system of

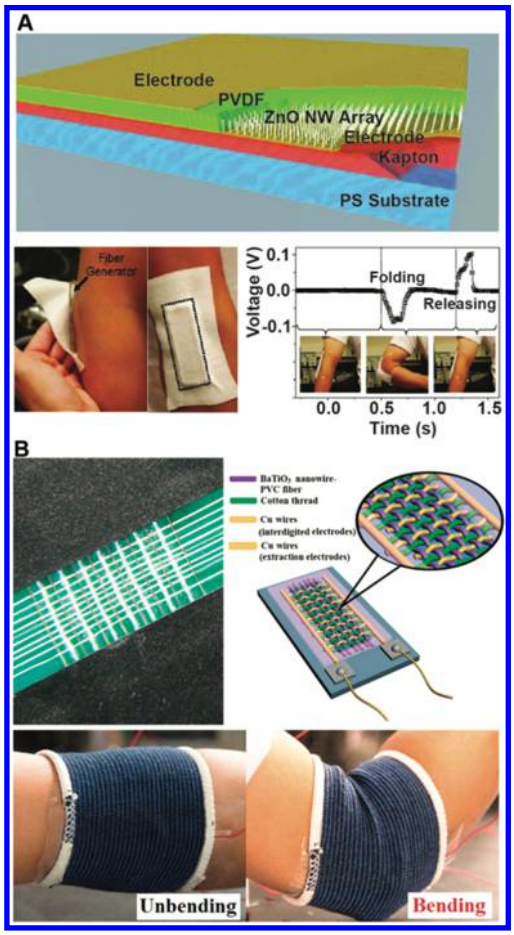

Figure 25. Piezoelectric generators. (A) Schematic illustration and photograph of hybrid-fiber piezoelectric nanogenerator and open-circuit voltage output of the device attached on the elbow. Adapted with permission from ref 797. Copyright 2012 Wiley-VCH Verlag GmbH & Co. KGaA. (B) Schematic picture and photographs of the fabric piezoelectric nanogenerator attached on the elbow. Adapted with permission from ref 799. Copyright 2015 Elsevier.

conductive fibers with a ZnO nanowire/PVDF polymer coating.[797] This hybrid device attaches to the arm and under the folding-release bending cycle of the elbow (to ~90°) produces an output voltage, current density, and volumetric power density of 0.1 V, 10 nA cm^{-2}, 16 μW cm^{-3}, respectively. Figure 25B showcases another hybrid fiber system that consists of aligned $BaTiO_3$ nanowires and PVC polymer.[799] This platform generates an output voltage of 1.9 V and output current of 24 nA, sufficient to power a LED. More advanced designs exploit planar processing techniques for stretchable generators. For example, one demonstration[798] uses a three-layer stack of composite films of highly ordered piezoelectric hemispheres (PZT or ZnO) in a soft PDMS matrix (40% strain). Under an applied normal bending force, a generator of this type can produce an output voltage and current density up to 6 V and 0.2 μA cm^{-2}, respectively. Other work reports highly stretchable (200% strain) piezoelectric generators based on a rubber-based composite with lead magnesium niobate−lead titanate (PMN−PT) and CNTs as piezoelectric fillers and AgNWs (~150 μm in length) as stretchable electrodes.[800] Such a device can generate an output voltage and current up to 4 V and 500 nA, respectively.

The electrical power generated from piezoelectric devices is sufficient for driving small epidermal components with low power consumption, such as LEDs and liquid crystal displays. A key consideration for integrating piezoelectric harvesting into such platforms is the pulsatile, intermittent nature of the generated power. Power management is therefore critical to efficiently utilize piezoelectric generators in epidermal applications.

4.2.5. Triboelectrics. Triboelectric generators offer an alternative approach to piezoelectrics for harvesting mechanical kinetic energy in formats compatible with skin-mounted systems.[801] Such devices produce electrical charges by contact electrification and electrostatic induction during the frictional contact of two surfaces with different polarity of charge separation.[802] The separation of the electrical charges between the two surfaces produces a voltage difference. Triboelectric generators operate primarily in one of two fundamental working modes: contact-mode and sliding-mode.[802] The efficiency largely depends on differences in the electron-attracting ability of the constituent materials and the morphology of the contact surfaces. By comparison to piezoelectric generators, triboelectric devices can exploit a wider array of materials, and they can, in some cases, enable higher output power densities and energy conversion efficiencies. Materials include both organic (PTFE, PET, PI, PDMS, PMMA, CNT, graphene) and inorganic (ITO, Al, Cu, Au, Ti, TiO_2, and Si) compounds.[803−805] Rational design of the contact surfaces, coupled with careful selection of the materials, are important to realizing high conversion efficiencies and energy outputs.[795,806] Arch-shaped macrostructures are common in epidermal contact-mode triboelectric generators due to their easy of fabrication and their relatively high performance.[807,808] Utilization of microstructured surfaces, typically pyramidal shapes, increases the contact area in stretchable epidermal formats, thereby increasing the energy output.[809,810]

One of the earliest experimental demonstrations of an epidermal triboelectric generator uses PDMS and a SWCNT thin film as the active surfaces (Figure 26A−C).[811] Under repeated application of a 2 kPa normal pressure, the system generates an output voltage and current density of 25 V and 8 μA cm^{-2}, respectively, with an estimated power conversion efficiency of 8%. Contact-mode harvesters, on account of the physically separated surfaces, harvest cyclic motion or intermittent impacts. Other designs exploit sliding modes of operation whereby planar motion induces in-plane charge separation. Such sensors exhibit improved performance due to the full constant contact of the active surfaces. For example, one skin-interfaced device uses a sliding-mode triboelectric generator based on two multilayer thin films (AgNWs/PEDOT:PSS/PU) on a PDMS and a poly(ether sulfone)

DOI: 10.1021/acs.chemrev.8b00573
Chem. Rev. 2019, 119, 5461−5533

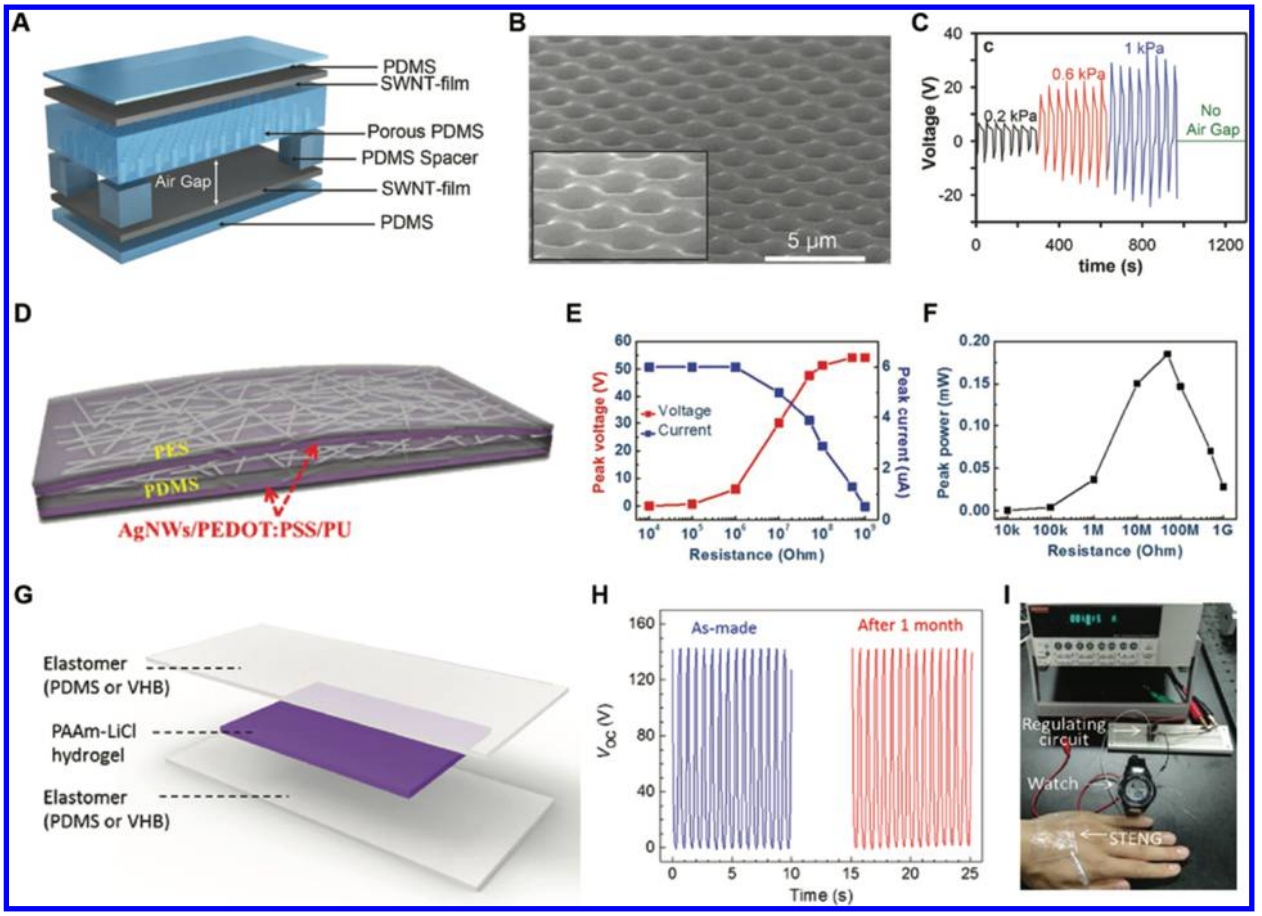

Figure 26. Triboelectric generators. (A) Schematic illustration of a triboelectric energy harvesting e-skin. (B) SEM image of the porous PDMS surface of the device. (C) Open-circuit voltage output. (A–C) Adapted with permission from ref 811. Copyright 2014 Wiley-VCH Verlag GmbH & Co. KGaA. (D) Schematic picture of a transparent stretchable triboelectric generator. (E) Peak voltage and (F) peak power of the device as a function of load resistance. (D–F) Adapted with permission from ref 134. Copyright 2015 American Chemical Society. (G) Schematic diagram of a soft skin-like triboelectric nanogenerator. (H) Voltage output of the device before and after one-month storage. (I) Photograph of the device laminated on the hand, while charging an electronic watch. (G–I) Adapted with permission from ref 812. Copyright 2017 American Association for the Advancement of Science.

(PES) substrate as contact surfaces (Figure 26D–F). The generator output, which when rectified and stored in a supercapacitor, provides sufficient power to an ultralow-power strain sensor for the continuous monitoring of esophageal muscle movements.[134]

A recent noteworthy advance uses a hybrid structure to obtain a highly stretchable (1160%) soft, skin-like triboelectric generator (Figure 26G,H).[812] This device uses an ionic hydrogel (polyacrylamide with LiCl) as the electrode, elastomeric materials (PDMS and conductive adhesives) as electrification layers, and PI as the contact dielectric. The use of the ionic hydrogel enables two harvesting modes: single-electrode and two-electrode. In single-electrode mode, out-of-plane movement of the electrification layers induces movement of ions in the ionic hydrogel. The result is the formation of a layer of excess ions at the interface to balance the static charge. A polarized EDL forms at the interface between the ionic hydrogel and the electrode inducing a current. In single-electrode mode, the generator exhibits an instantaneous output power density of ~3.5 μW cm^{-2}. Replacing the contact dielectric with a second electrode (Al thin film) results in an output power density of 32.8 μW cm^{-2}. A skin-interfaced triboelectric generator of this type (3 cm × 4 cm in size), when integrated with a rectifying capacitor, can power multiple (20) LEDs in series, an LCD display, or an electronic watch (Figure 26I).[812]

4.2.6. Biofuel Cells. Biofuel cells convert biochemical energy present in biofluids to electrical power through redox reactions that use enzymes and/or noble metal-based catalysts. The power density largely depends on the availability of chemical sources in biofluids and the electron transfer efficiency between the enzyme active sites and electrodes. In contrast to other harvesting technologies, epidermal biofuel cells possess a limited power generation rate, low open circuit voltage, and low power density. A key challenge is the stability of operation, which depends on the diffusion rate of biofuels to the enzyme active sites and the overall stability of the enzyme. Additionally, the redox mediators, which facilitate electron transfer, require special consideration not only in stability but also in biocompatibility for skin-interfaced devices.

Biofuel cells require intimate and conformal contact with the human body in order to realize continuous and efficient power extraction from biofluids such as sweat. Stretchability and flexibility can be realized via approaches, such as those introduced in section 2, to accommodate natural movements of the body. Figure 27A,B highlights an example of a highly stretchable (500%) biofuel cell fabricated by a screen printing process.[483] The device uses specially formulated CNT-based

DOI: 10.1021/acs.chemrev.8b00573
Chem. Rev. 2019, 119, 5461–5533

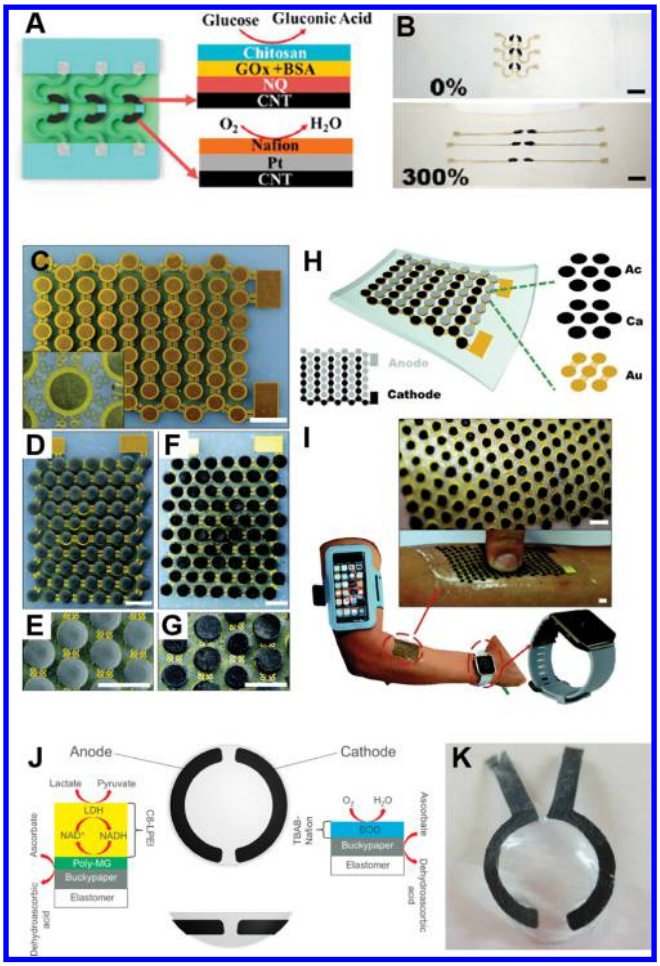

Figure 27. Biofuel cells. (A) Schematic illustration and (B) photographs of stretchable biofuel cells (scale bar, 1 cm). (A,B) Adapted with permission from ref 483. Copyright 2016 American Chemical Society. (C) Photographs of soft, electronic-skin-based biofuel cell before carbon coating, (D,E) after carbon coating, and (F,G) after complete fabrication. (H) Schematic picture of stretchable biofuel cells. (I) Biofuel cells laminated on the forearm to power potential electronics. (C–I) Scale bars, 5 mm. (C–I) Adapted with permission from ref 813. Copyright 2017 The Royal Society of Chemistry. (J) Schematic illustration and (K) photograph of contact lens biofuel cells. (J,K) Adapted with permission from ref 814. Copyright 2015 Elsevier.

stretchable inks and free-standing serpentine interconnects. The ink involves a mixture of CNTs (as the conductive component), mineral oil (as a dispersant), and PU (as the stretchable binder) in tetrahydrofuran. The resulting cell exhibits a maximum power density of ~50 μW cm^{-2} at a voltage of 0.25 V in the presence of 20 mM glucose.

An alternative architecture exploits an island–bridge configuration to further improve the power density. An example, also fabricated by screen printing, bridges islands of densely packed 3D CNT-based electrodes with FS interconnects (Figure 27C–I).[813] In this case, the 3D CNT-based anodes (500 μm in thickness) are a mixture of CNTs (conductive component) and naphthoquinone (redox mediator) in a chitosan (binder) suspension. Bonding the FS-based current collector and functionalizing the 3D electrodes with lactate oxidase completes the anode fabrication process. Cathode fabrication follows in a similar manner using a mixture of CNTs and silver oxide (cathode active material, 30:70 wt/wt ratio) in a tetrafluoroethylene-perfluoro-3,6-dioxa-4-methyl-7-octenesulfonic acid copolymer solution (2 wt %). The resulting system exhibits an open circuit voltage of 0.5 V, a power density of ~1.2 mW cm^{-2} at 0.2 V, and a stable operating performance of 2 days. The biofuel cell, when worn by a human volunteer during exercise, produces ~1 mW power, sufficient for simple electronic components such as power efficient radios and LEDs.

Other notable examples of biofuel cells include ocular-based devices that harvest energy from tears rather than sweat.[814] One device of this type utilizes buckypaper electrodes formed on a silicone elastomer soft contact lens (Figure 27J,K). Operation in synthetic tears yields open circuit voltages of ~0.41 V and maximum power densities of ~8.0 μW cm^{-2}. Additional work will be needed to address the limited operational stability of this system.

4.3. System Efficiency

The power requirements for system operation span a wide range, from relatively high and low levels for active sensors (e.g., optoelectronic methods with high optical output, thermal-actuation recording methods) and passive sensors (e.g., temperature readouts, biopotential electrical recording), respectively. Wireless communication often represents the most significant draw of power. Wireless options that are compatible with existing infrastructures (e.g., WIFI, BLE) have particularly demanding power requirements, especially for operation over a long distances and at high data rates.[43] Although nonstandard low power protocols and application specific system on a chip designs exist,[815] the large scale deployment of such devices requires external, specialized infrastructure that is unlikely to be broadly available in the foreseeable future.[816] The recent standardization of low power protocols may nucleate progress in this direction.[723]

The successful operation of wireless skin-interfaced devices requires consideration of the platform as a complete system from the standpoint of power efficiency, as outlined in Figure 28. Intermittent power sources such as those produced by triboelectric, piezoelectric, and photovoltaic (in the case of on-body interfacing) generators require a buffer to provide constant and sustained power to a device. The addition of supercapacitors or batteries for this purpose requires additional components such as charge controllers and battery management circuits. Furthermore, the finite operational voltage range of most electronic and sensor components necessitates active regulation circuits tailored to application-dependent requirements (e.g., wireless electronics, sensors, power sources). Predicting overall system efficiency in a realistic scenario can be difficult, given the many variables. Each system requires device engineering specifically for the body location, sensor type, and communication method.[817] In aggregate, understanding and accounting for losses throughout the system are essential for effective long-term device operation.

5. SYSTEM LEVEL EMBODIMENTS

The foundational technologies that underpin the skin-like platforms described in this review rely critically on advanced materials, integration/assembly approaches, and unusual device designs to yield a full collection of active and passive components, each with remarkable form factors and mechanical properties. Strategies in combining these building blocks into fully functional, self-contained systems represent an active area of research.[171,196,220,275,488,494,495,504,505,606,818,819]

DOI: 10.1021/acs.chemrev.8b00573
Chem. Rev. 2019, 119, 5461–5533

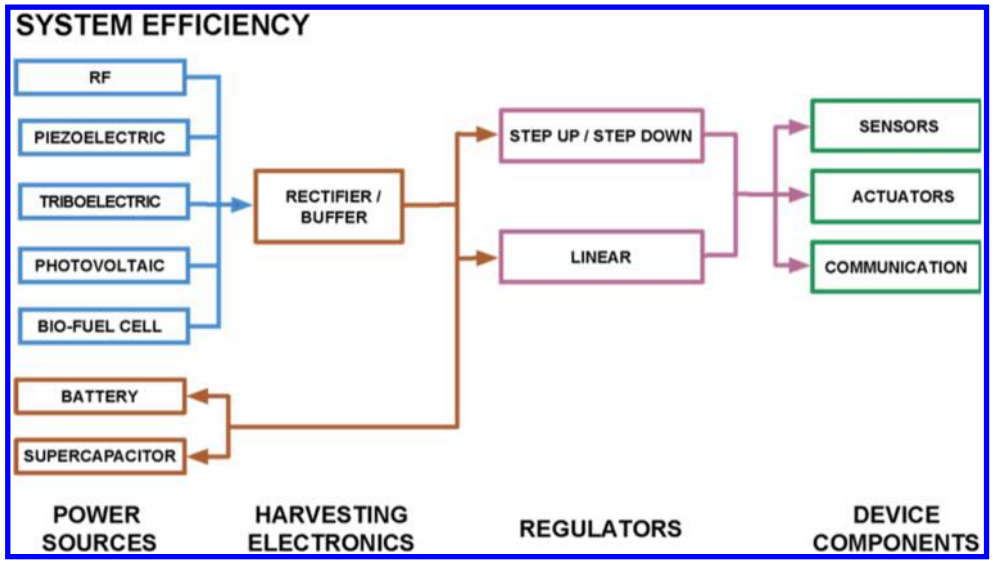

Figure 28. System efficiency. Schematic illustration of the main components that define considerations in system efficiency for bio-integrated wearable devices, delineated according to power sources, harvesting electronics, regulators, and device components.

5.1. Fully Integrated Bio-Integrated Wearable Prototypes

Recent work highlights various options in the assembly of fully integrated skin-interfaced prototypes that incorporate biosensors, elastomeric materials, flexible hybrid electronics (FHEs), and power supply systems to yield impressive levels of functionality. The complexity of these platforms grows with the number of assembly operations, the diversity and spatial distribution of multimodal sensors, and the requirements in wireless connectivity and operating life. Recent demonstrations of soft, skin-interfaced devices range from commercialized wireless systems for multifunctional biophysical measurements of physiological health[221,606,818] to research prototypes for biochemical analysis of sweat (Figure 29).[220,275,488,494]

Figure 29A features, as an example of the latter, an epifluidic system that integrates colorimetric assays and sweat rate sensing capabilities with an NFC electronics module with a smartphone app for image capture and analysis.[220] The electrolyte and metabolite assays exploit existing chemical and enzymatic chemistries for event-based analysis of hydration, electrolyte balance, and recovery. Applications range from real-time analysis of sweat biomarkers and sweat rate to capture/storage of sweat samples for ex situ laboratory evaluation. In both instances, the devices are sufficiently low in cost to allow deployment at high volumes as disposable items. In addition to the colorimetric analysis and sweat microfluidics, routes now exist for integrating on-board electrochemical sensors. A recently described prototype device combines an NFC wireless module with electrochemical sensors.[521] This system supports wireless data transfer and power harvesting from the smartphone (Figure 29B). A separate example combines flexible PCB and soft electrochemical sensors,[494] where the former supports electronic components and sufficient battery capacity for BLE communication, memory, and continuous data transfer (Figure 29C). This hybrid integration approach can also enable actuation and drug delivery. Figure 29D highlights a concept device that senses glucose levels in sweat and, in turn, releases small amounts of drugs transcutaneously in direct response to the glucose read out as part of a closed-loop system.[495]

Taken together, the system level examples in Figure 29 illustrate the overall state of the technology, where soft materials, collections of biosensors, wireless communication modules, electronic processing units, and on-board power supply yield devices that exist in early stage commercial platforms as well as advanced prototypes capable of use in the field.[820] The end applications span across many markets, from consumer to medical applications, where verification testing, validation studies, and cost-effective manufacturing could lead to wide-scale adoption in the relatively near future.

5.2. Fully Integrated Bio-Integrated Wearable Systems in the Market

Several recent bio-integrated wearable systems have transitioned to full scale manufacturing and commercial deployment. These devices incorporate many of the foundational biosensors, wireless connectivity modules, and encapsulation strategies described in earlier sections of this review. Progress relies on integration of elastomer molding techniques, hybrid roll-to-roll and lamination processes, pick and place assembly procedures, and biocompatible skin adhesive interfaces into complete assembly sequences by the most advanced manufacturers in flexible hybrid electronics.

The My Skin Track UV system uses a millimeter-scale, wireless and battery-free device technology that measures multiwavelength electromagnetic radiation in body-integrated forms, including those capable of mounting on the fingernail.[600] Figure 30A shows a UV Sense device in this location (left) and an exploded view schematic illustration of the subcomponents (right), including the encapsulating layer, flexible PCB layer, antenna, LED, super capacitor, and photodetector. The onboard NFC module allows wireless relay of UVA and UVB dosage information, collected in a continuous accumulation mode without external power supply, to a smartphone and recommendations from an engine in the cloud, thereby establishing a system capable of providing actionable feedback to the user to encourage safe exposure to the sun. Similar in overall functionality to the My Skin Track UV system, the My UV Patch is a skin-interfaced device that provides feedback about UV radiation exposure via images taken with a smartphone camera.[600,606] Photochemical dyes patterned along the surface of the device change color in response to UV exposure, thereby providing a visual response that can be

DOI: 10.1021/acs.chemrev.8b00573
Chem. Rev. 2019, 119, 5461−5533

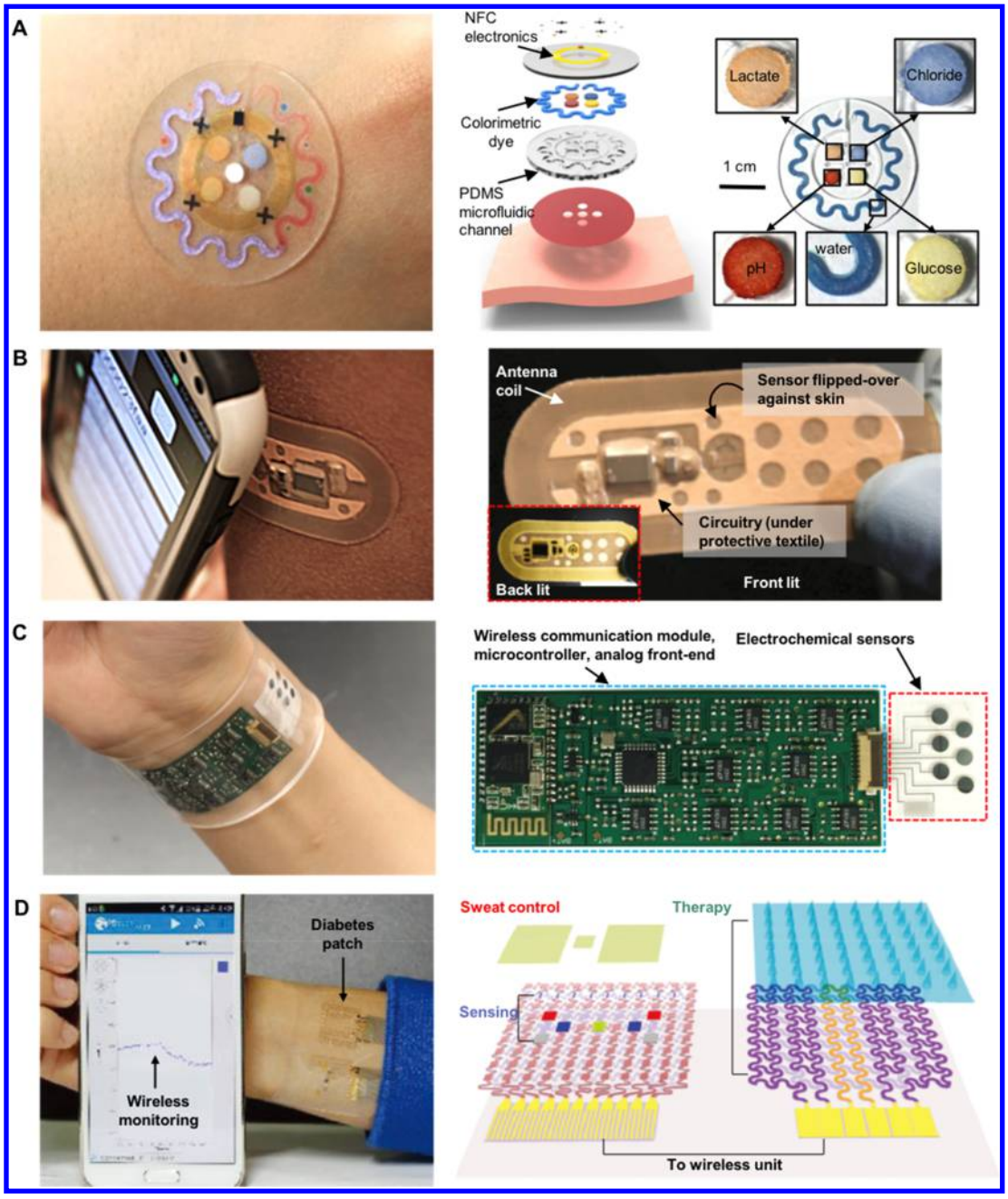

Figure 29. Fully integrated skin-interfaced prototype systems. (A) Optical image of a soft wearable microfluidic device on the skin (left). Magnified view of channels and wells prefilled with colorimetric assays for metabolites and electrolytes (right). Adapted with permission from ref 220. Copyright 2016 American Association for the Advancement of Science. (B) Optical images of smartphone and NFC-enabled electrochemical sensors on the skin (left). Image of an NFC-enabled device highlighting the key electronics components. Adapted with permission from ref 521. Copyright 2015 Institute of Electrical and Electronics Engineers. (C) Optical image of a Bluetooth-enabled wearable device with electrochemical sensors connected to a flexible PCB module on the wrist (left). Image of flexible PCB module electrically coupled to an array of electrochemical sensors for bioanalytes found in sweat (right). Adapted with permission from ref 494. Copyright 2016 Springer Nature. (D) Optical image of smartphone and Bluetooth-enabled wearable devices with electrochemical sensors and actuators used to deliver transdermal drugs and nanoparticles (left). Schematic drawing of stretchable sensing and actuating elements (right). Adapted with permission from ref 495. Copyright 2016 Springer Nature.

captured with a smartphone camera and analyzed in the cloud. Figure 30B shows this type of skin-interfaced device laminated on the back of the hand (left). The exploded view schematic (right) illustrates the subcomponents, including the NFC module and photosensitive dye layers embedded in an ultrathin multilayer stack.[606] The ultrathin form factor and the stretchable/flexible mechanics allow for extreme bending and twisting with normal motions of the human skin, much like a temporary skin tattoo.

While these two devices exploit NFC wireless connectivity and highlight unique battery-free capabilities, other examples of skin-mounted systems exploit miniaturized batteries and BLE connectivity to capture and wirelessly transmit large amounts of physiological data, continuously and without requiring external RF power. The Novii Wireless Patch & Pod System[823] (Figure

DOI: 10.1021/acs.chemrev.8b00573
Chem. Rev. 2019, 119, 5461−5533

Figure 30. Fully integrated body interfaced commercial systems. (A) Optical image of My Skin Track UV device (Wearifi and L'Oréal) on the fingernail (left). Exploded view of My Skin Track UV's battery-free electronics module, optical sensor, and protective encapsulating silicone layer (right). Adapted with permission from ref 821. Copyright 2018 L'Oréal. (B) Optical image of My UV Patch[822] (L'Oréal and mc10 Inc.) adhered to the back surface of the hand. Exploded view of My UV Patch highlighting photosensitive active dyes, epidermal electronics, and hypoallergenic adhesives (right). Adapted with permission from ref 606. Copyright 2018 PLOS. (C) Optical image of Novii pod module instrumented on the abdomen of a pregnant woman (left). The Novii Wireless Patch & Pod System consists of disposable flexible electrodes and a reusable pod containing control circuitry (right). Adapted with permission from ref 823. Copyright 2018 GE Healthcare. (D) Optical image of the Biostamp device,[824] which consists of stretchable electronics, interconnects, and biosensors (left). Schematic drawing of the stretchable electronics and structured elastomeric substrate of this system (right). Adapted with permission from ref 819. Copyright 2018 Springer Nature. (E) Optical image of the Prevent Mouth Guard for monitoring head impacts (left). Schematic drawing of the device showing the flexible electronics and encapsulating layers (right). Adapted with permission from ref 825. Copyright 2018 Prevent Biometrics Inc..

DOI: 10.1021/acs.chemrev.8b00573
Chem. Rev. 2019, 119, 5461−5533

30C) consists of flexible disposable electrodes that magnetically connect to a reusable Novii Pod module, which aquires and processes ECG and EMG signals from the abdomen. The Novii Pod module transmits data in real-time via Bluetooth to an external data acquisition system (The Novii Interface). The Novii System demonstrates the impact of skin-interfaced wearable devices in fetal monitoring. There are several other examples of fully integrated skin-mounted devices that have gained significant traction in related clinical areas including in-hospital patient monitoring (VitalPatch by Vital Connect, Inc.[826]) and remote cardiac rhythm management (Zio Patch by iRhythm, Inc.[827]).

The BioStamp wearable sensing patch (BioStamp nPoint System by mc10 Inc.,[824] Figure 30D) expands on the soft flexible designs and wireless connectivity of these wearable continuous monitoring platforms by utilizing stretchable electronics and elastic interconnect technologies. The Biostamp's stretchable system-level architecture creates a highly conformal interface with several body locations, beyond the torso and abdomen regions, offering continuous clinical grade biometrics to care providers in the clinic and home setting.[221,606] Taken together, the Novii, Zio Patch, VitalPatch, and BioStamp wearable systems represent novel classes of FDA 510(k) cleared wearable medical devices that exploit novel packaging techniques, soft materials, multimodal data streams, wireless connectivity, and conformal electromechanical architectures.

These representative examples of commercially deployed skin-interfaced wearable systems have important design features that have been applied across various other bio-integrated device platforms. For example, the Prevent Mouth Guard[818,825] measures head impacts with high accuracy from inside the oral cavity, in real-time, during contact sports like American football (Figure 30E). Much like the BioStamp, the Prevent Mouth Guard is a fully integrated device, containing multiple accelerometers, wireless charging/data transmission, and associated control circuitry that registers hard impacts and activates visual alerts (via LEDs). However, the dynamic forces exerted during hits, teeth clenching, and repeated swallowing require robust moisture-resistant encapsulating layers to prevent hardware failure modes. These examples of commercially deployed wearable systems highlight the far reaching translational impact of bioelectronics research, from sports performance and patient health monitoring to at-home care, all of which are critical in helping to realize the promise of personalized medicine.

6. CHALLENGES AND FUTURE OUTLOOK

Advances in soft materials, assembly techniques, sensing modalities, power supplies, and system integration strategies summarized in this review provide powerful foundations for new classes of skin-like multifunctional wearable systems, with wide-ranging potential applications across clinical, consumer, and research domains. Recent regulatory approvals and commercial launches of initial generations of devices of this type support important levels of functionality in clinical medicine, cosmetics, and digital health that lie outside the capabilities of traditional electronic systems. While these milestones in translating basic and applied research results out of the laboratory and into the real world are encouraging, many important and interesting challenges remain. Specifically, the materials and the chemistry aspects of devices, such as those highlighted in section 5, will be essential to continued progress in this area of science and technology.

Broadly, the technical challenges[198,443,828,829] in bio-integrated devices span many engineering and materials science disciplines, with an emphasis that depends strongly on the specific requirements, use cases, and user profiles. Most of the recent advances in bio-integrated sensors follow from developments in materials chemistry for detection schemes and form factors that meet needs in bio-interfaced systems. As such, significant attention is on the continued expansion of the existing library of soft, stretchable materials for active electronics, biochemical transduction, passive matrices/encapsulation layers, and power supply. An important aspect of the most impactful work in these areas is a focus on requirements to support a robust, functional biotic/abiotic interface. Establishing materials for linear, stable operation across curvatures and strains that are physiologically relevant, but perhaps not significantly beyond these values, is essential. Because of the intrinsic, time-dynamic nature of biological systems, the devices must operate in rapidly evolving environments where motion-induced artifacts and/or changes the biochemistry of the surrounding environment, pose significant challenges in realizing clinical-grade measurements outside of the clinic or the lab. Development of platforms and materials systems that decouple biophysical/biochemical phenomena from the target signals (e.g., temperature effects from strain effects) in ways that passively or actively suppress noise represents an important direction for continued research.

Some of the most interesting opportunities are in bio-integrated sensors of biochemical signals and the chemistry of the surrounding environment, partly due to difficulties that follow from time dependent effects mentioned above and from requirements in biocompatible form factors.[198,275] Such sensors rely heavily on complex (bio)chemical reactions and/or interactions that are susceptible to varying conditions in the ambient. Moreover, certain sensors require sample preconcentration and/or processes to remove/add certain chemical species and/or adjust pH to maintain optimal performance.[308,830] In conventional devices, such pretreatment procedures and associated calibration steps occur via trained personnel and/or complex automated systems that are largely incompatible with wearable systems. In addition, biofluids, such as sweat, contain a rich, complex array of analytes of interest, with concentrations that can vary significantly across populations and across time, even for a single individual. Developing a comprehensive profile of biochemical and environmental signals of physiological relevance requires highly multiplexed sensor modalities, all with the requirement for biochemical and biomechanical compatibility with the body. Enormous opportunities exist in the creation of materials and chemistries that can serve as the basis for such sensors, where issues in cross-talk, noise from interfering chemical species, and high density integration into arrays are critical considerations. Many applications of skin-interfaced biochemical sensors require detection of exceptionally low concentrations of analytes against this challenging chemical and physical background. Examples include metabolites,[495,831] hormones,[553] vitamins,[832] amino acids,[833] and minerals[834] in sweat and environmental targets such as pollutants,[835] forensic/warfare targets,[836,837] and contraband drugs.[838] The types of expensive, benchtop systems[839] and complex multistep detection processes[840] must be fundamentally transformed to address these challenges and associated opportunities.

Other areas for future work focus mainly on the mechanical properties, from the physical robustness and durability of the

DOI: 10.1021/acs.chemrev.8b00573
Chem. Rev. 2019, 119, 5461−5533

platforms to their ability to support long-duration wear times and extensive cycles of application/removal, to the capacity to operate in highly dynamic environments and under nonidealized conditions (e.g., presence of hair follicles). Typically, skin-mounted sensing platforms utilize soft, low modulus, skin-safe elastomeric materials to achieve conformal interfaces to the epidermis. Achieving such properties in materials systems that are simultaneously physically strong and mechanically tough represent interesting topics in research in chemistry and composite design. The safe integration of such new materials into skin-interfaced platforms also demands an understanding of the biological interactions at the surface of the skin. Optimizing designs to enable breathable interfaces remains an important, but often overlooked, consideration in enabling long-term utilization. Depending on the use case, such devices can be subjected to mechanical stresses from the environment due to damage-inducing impacts and abrasion. Self-healing materials based on polymers,[44,841−848] composites,[849,850] or liquid metal impregnated elastomers[180] represent some ideas that are important in this context.[851,852] Bio-inspired materials engineering approaches that integrate a stretchable reactive or protective layer similar to the flexible dermal armor found in nature (e.g., fish scales, armadillo armor)[53,853−855] are also of interest.

Limitations in power supply are often dominating concerns, especially in the context of requirements in form factor, size, and weight. Although the advances in energy storage and energy harvesting technologies highlighted in section 4 are important, continued progress, and perhaps new directions will be needed to support increasing demands for sampling frequencies, communication bandwidth, operating distances, and lifetimes. Batteries will likely continue to represent the most versatile option, but further reductions in sizes and increases in capacities are needed, and existing materials systems (e.g., Li-ion) may not be sufficient.[655] Supercapacitors are interesting and valuable alternatives to batteries, but their low volumetric energy densities may make them best suited for transient supplies and/or systems to eliminate intermittency associated with energy harvesting approaches.[37] Both technologies will benefit from improvements in mechanical deformability and long-term stable operation, where advanced materials for encapsulation will be particularly important. Energy harvesting offers the potential for self-powered operation to eliminate storage capabilities. RF harvesting can already address many applications, where continuous supply of ~mW levels of power is adequate and proximity to an RF source is feasible. Harvesting based on mechanical motions, thermal gradients, ambient light, and others are promising, but reliable, uninterrupted supply of energy from such sources is typically not possible. Combinations of these types of devices, together with some limited level of on-board storage, may provide an attractive solution. In all cases, advances in materials and chemistry will serve as a primary means for continued progress. Materials will also be essential in ensuring safe, biocompatible construction by eliminating the use of toxic materials in the devices (e.g., As, Cd, Li).

Increasingly key to progress in the field are system-level concerns associated with seamless integration of sensors, power sources, and communications components. The challenges are in heterogeneous materials integration and in fabrication/assembly schemes. For example, robust encapsulation materials are necessary to protect electronic components and battery materials from exposure to the environment. These materials must, at the same time, offer soft, elastic mechanics, thin geometries, biocompatible chemistries, and other properties needed for operation of the overall system. Moreover, human factors related to device attachment, removal, placement, recharging, and disposal add further constraints on materials choices and system designs. Although considerations can be important in research prototypes, they become paramount in systems that must be manufactured efficiently, tested at high throughput for reliability and calibration, designed with appropriate electromechanical properties and in low power architectures, and encapsulated in water-proof constructs that simultaneously allow passage of water vapor and biofluids through selected regions of the platforms. Other considerations, sometimes overlooked, are in the pleasing visual appearances of the devices, to encourage adoption and compliance in usage.[856] Recent work in this direction span a wide range, from rendering the devices into transparent forms (graphene,[857] hydrogel,[858] polymers[859,860]) and transforming them in to fashionable accessories.[220,505]

Skin-interfaced sensors represent a class of technology with powerful potential in personalized medicine and continuous monitoring of the human physiological health state. Successful efforts in this area will address grand challenges for the 21st century, including those in "...the acquisition, management, and use of information in health..." as identified by the National Academy of Engineering, with direct relevance to enhancing the quality and efficiency of medical care and the ability to respond to public health emergencies. Research efforts in the hardware aspects of this area involve an appealing, multidisciplinary mix of chemistry and materials science, along with electrical, mechanical, and biomedical engineering, at the direct interface with medical science. The rich range of topics in fundamental science in the broader context of technologies designed to address urgent societal needs, forms the basis for a vibrant and fruitful area for applied and basic research.

ASSOCIATED CONTENT

Special Issue Paper

This paper is an additional review for *Chem. Rev.* **2019**, volume *119*, issue 1, "Chemical Sensors".

AUTHOR INFORMATION

Corresponding Author

*E-mail: jrogers@northwestern.edu.

ORCID

Jungil Choi: 0000-0002-3659-8978
John A. Rogers: 0000-0002-2980-3961

Author Contributions

∥T.R.R., J.C., and A.J.B. contributed equally to this work.

Notes

The authors declare the following competing financial interest(s): T.R.R., J.C., A.J.B., S.K., P.G., L.T., R.G., and J.A.R. are inventors on patents related to bio-integrated technologies. S.K, T.R.R, and J.A.R. are co-founders of Rhaeos Inc., a company that develops wireless, wearable shunt diagnostic sensors. R.G. and J.A.R. are co-founders of Epicore Biosystems, Inc., a company that develops epidermal sweat sensors, and MC10, a wearable health technology company. J.A.R. is co-founder of several other companies related to bio-integrated technologies including Wearifi, Inc. and Neurolux, Inc.

DOI: 10.1021/acs.chemrev.8b00573
Chem. Rev. 2019, 119, 5461−5533

Biographies

Tyler R. Ray obtained his B.S. and M.S. degrees in Mechanical Engineering from the University of South Carolina in 2008 and 2010. He received his Ph.D. in Mechanical Engineering from the University of California, Santa Barbara, in 2015 and joined the Materials Department at UCSB as a postdoctoral researcher focusing on colloidal assembly of multiscale composite materials. He joined the Rogers Research Group at Northwestern University in 2016 as a postdoctoral research fellow focused on the development of soft, epidermal devices for clinical diagnostics. In 2019, he will join the Department of Mechanical Engineering at the University of Hawai'i at Manoa as an assistant professor. His research interests include the design and fabrication of multifunctional, hierarchical nanocomposite materials, bio-integrated sensing platforms, and micro/nanofabrication with a focus on diagnostic applications.

Jungil Choi received his B.S. in 2007 and M.S. in 2010 in Mechanical and Aerospace Engineering and his Ph.D. in 2015 in Electrical Engineering from Seoul National University. He is currently a postdoctoral researcher within the Materials Science and Engineering Department at Northwestern University. His research interests include microfluidics for biomedical applications, skin-interfaced sensors, and soft material mechanics.

Amay J. Bandodkar received his Integrated Masters in 2011 in Applied Chemistry from Indian Institute of Technology—Banaras Hindu University (India) and his Ph.D. in 2016 in NanoEngineering from University of California, San Diego. He is currently a postdoctoral researcher within Material Science Engineering Department at Northwestern University. His research interest includes wearable and implantable electrochemical systems for sensing and energy applications.

Siddharth Krishnan received his B.S. and M.S. degrees in Mechanical Engineering at Washington University in St. Louis in 2013 and 2014, respectively. He is currently a Ph.D. candidate at the University of Illinois at Urbana−Champaign in the Department of Materials Science and Engineering in Prof. John Rogers' group. He is also a visiting fellow at Northwestern University in the Department of Materials Science and Engineering and the Center for Bio-Integrated Electronics at the Simpson Querrey Institute. His research focuses on wireless bioelectronics for neuroscience, neurosurgery, and dermatology.

Philipp Gutruf received his B.E. degree in Sensorics in 2013 from Karlsruhe University of Applied Sciences in Germany. He obtained his Ph.D. in 2016 from the Royal Melbourne Institute of Technology in Australia. For his postdoctoral work, he joined the Rogers Research Group at the University of Illinois Urbana−Champaign and Northwestern University. Currently, he is an Assistant Professor in the Biomedical Engineering Department at the University of Arizona and leads the Gutruf Lab which is creating devices that seamlessly integrate with biological systems by unifying innovations in soft materials, photonics, and wireless electronics to create systems with broad impact on health diagnostics and neuroscience tools.

Limei Tian obtained her B.S. in Civil Engineering in 2006 and M.S. in Structural Engineering in 2009 from Shandong University, China. She received her Ph.D. in Mechanical Engineering from Washington University in St. Louis in 2014. She was a Beckman Institute Postdoctoral Fellow at the University of Illinois at Urbana−Champaign from 2015 to 2018. Currently, she is an assistant professor in the Department of Biomedical Engineering at Texas A&M University. Her research interests include the design, synthesis, and fabrication of organic/inorganic hybrid materials, wearable and implantable biosensors, responsive and adaptive materials and systems, and unconventional approaches for micro/nanofabrication.

Roozbeh Ghaffari obtained his B.S. and M.E. degrees in Electrical Engineering from the Massachusetts Institute of Technology in 2001 and 2003. He received his Ph.D. degree in Biomedical Engineering from the Harvard Medical School−MIT Program in Health Sciences and Technology in 2008. Roozbeh's Ph.D. research focus was at the intersection of auditory neuroscience, microfluidics, and nanoscale metrology applied to study electromechanical mechanisms in the cochlea. Upon completion of his Ph.D., Roozbeh co-founded MC10 Inc. and served as its Chief Technology Officer (2008−2017). Roozbeh joined the Center for Bio-Integrated Electronics at Northwestern University in May 2017, where he currently serves as Director of Translational Research and Research Associate Professor in the Department of Biomedical Engineering, working at the intersection of basic and translational bioelectronics research.

John A. Rogers obtained B.A. and B.S. degrees in chemistry and in physics from the University of Texas—Austin, in 1989. From MIT, he received S.M. degrees in physics and in chemistry in 1992 and his Ph.D. degree in physical chemistry in 1995. From 1995 to 1997, Rogers was a Junior Fellow in the Harvard University Society of Fellows. He joined Bell Laboratories as a Member of Technical Staff in the Condensed Matter Physics Research Department in 1997 and served as Director of this department from the end of 2000 to 2002. He then spent 13 years on the faculty at University of Illinois, most recently as the Swanlund Chair Professor and Director of the Seitz Materials Research Laboratory. In 2016, he joined Northwestern University as the Louis Simpson and Kimberly Querrey Professor of Materials Science and Engineering, Biomedical Engineering, and Medicine, with affiliate appointments in Mechanical Engineering, Electrical and Computer Engineering, and Chemistry, where he is also Director of the Center for Bio-Integrated Electronics.

REFERENCES

(1) Moore, G. E. Cramming More Components onto Integrated Circuits, Reprinted from Electronics, volume 38, number 8, April 19, 1965, pp.114 ff. *Electronics* **2006**, *11*, 33−35.
(2) Bridgland, H. *CCS Insight Forecast Predicts Apple Watch and Hearables to Fuel Growth in Wearables*; CCS Insight, 2018; https://www.ccsinsight.com/press/company-news/3375-ccs-insight-forecast-predicts-apple-watch-and-hearables-to-fuel-growth-in-wearables (accessed Dec 7, 2018).
(3) Malik, M.; Camm, A. J.; Huikuri, H.; Lombardi, F.; Schmidt, G.; Schwartz, P. J.; Zabel, M. e-Rhythm Study Group of, E. Electronic Gadgets and Their Health-Related Claims. *Int. J. Cardiol.* **2018**, *258*, 163−164.
(4) Stahl, S. E.; An, H.-S.; Dinkel, D. M.; Noble, J. M.; Lee, J.-M. How Accurate Are the Wrist-Based Heart Rate Monitors During Walking and Running Activities? Are They Accurate Enough? *BMJ. Open Sport Exerc. Med.* **2016**, *2*, e000106.
(5) Shcherbina, A.; Mattsson, C. M.; Waggott, D.; Salisbury, H.; Christle, J. W.; Hastie, T.; Wheeler, M. T.; Ashley, E. A. Accuracy in Wrist-Worn, Sensor-Based Measurements of Heart Rate and Energy Expenditure in a Diverse Cohort. *J. Pers. Med.* **2017**, *7*, 3.
(6) Abt, G.; Bray, J.; Benson, A. C. The Validity and Inter-Device Variability of the Apple Watch for Measuring Maximal Heart Rate. *J. Sports Sci.* **2018**, *36*, 1447−1452.
(7) Dooley, E. E.; Golaszewski, N. M.; Bartholomew, J. B. Estimating Accuracy at Exercise Intensities: A Comparative Study of Self-Monitoring Heart Rate and Physical Activity Wearable Devices. *JMIR Mhealth Uhealth* **2017**, *5*, No. e34.
(8) Sartor, F.; Gelissen, J.; van Dinther, R.; Roovers, D.; Papini, G. B.; Coppola, G. Wrist-Worn Optical and Chest Strap Heart Rate Comparison in a Heterogeneous Sample of Healthy Individuals and in Coronary Artery Disease Patients. *BMC Sports Sci. Med. Rehabil.* **2018**, *10*, 10.

DOI: 10.1021/acs.chemrev.8b00573
Chem. Rev. 2019, 119, 5461−5533

(9) Izmailova, E. S.; Wagner, J. A.; Perakslis, E. D. Wearable Devices in Clinical Trials: Hype and Hypothesis. *Clin. Pharmacol. Ther.* **2018**, *104*, 42−52.
(10) Duking, P.; Fuss, F. K.; Holmberg, H. C.; Sperlich, B. Recommendations for Assessment of the Reliability, Sensitivity, and Validity of Data Provided by Wearable Sensors Designed for Monitoring Physical Activity. *JMIR Mhealth Uhealth* **2018**, *6*, No. e102.
(11) Tasnim, F.; Sadraei, A.; Datta, B.; Khan, M.; Choi, K. Y.; Sahasrabudhe, A.; Vega Gálvez, T. A.; Wicaksono, I.; Rosello, O.; Nunez-Lopez, C.; et al. Towards Personalized Medicine: The Evolution of Imperceptible Health-Care Technologies. *Foresight* **2018**, *20*, 589−601.
(12) Wang, X.; Liu, Z.; Zhang, T. Flexible Sensing Electronics for Wearable/Attachable Health Monitoring. *Small* **2017**, *13*, 1602790.
(13) Servati, A.; Zou, L.; Wang, Z. J.; Ko, F.; Servati, P. Novel Flexible Wearable Sensor Materials and Signal Processing for Vital Sign and Human Activity Monitoring. *Sensors* **2017**, *17*, 1622.
(14) Wu, W.; Haick, H. Materials and Wearable Devices for Autonomous Monitoring of Physiological Markers. *Adv. Mater.* **2018**, *30*, 1705024.
(15) Kim, J.; Campbell, A. S.; Wang, J. Wearable Non-Invasive Epidermal Glucose Sensors: A Review. *Talanta* **2018**, *177*, 163−170.
(16) Qian, R. C.; Long, Y. T. Wearable Chemosensors: A Review of Recent Progress. *ChemistryOpen* **2018**, *7*, 118−130.
(17) Yang, Y.; Gao, W. Wearable and Flexible Electronics for Continuous Molecular Monitoring. *Chem. Soc. Rev.* **2019**, DOI: 10.1039/C7CS00730B.
(18) Pappa, A. M.; Parlak, O.; Scheiblin, G.; Mailley, P.; Salleo, A.; Owens, R. M. Organic Electronics for Point-of-Care Metabolite Monitoring. *Trends Biotechnol.* **2018**, *36*, 45−59.
(19) Yetisen, A. K.; Martinez-Hurtado, J. L.; Unal, B.; Khademhosseini, A.; Butt, H. Wearables in Medicine. *Adv. Mater.* **2018**, *30*, 1706910.
(20) Koydemir, H. C.; Ozcan, A. Wearable and Implantable Sensors for Biomedical Applications. *Annu. Rev. Anal. Chem.* **2018**, *11*, 127−146.
(21) Heo, J. S.; Eom, J.; Kim, Y. H.; Park, S. K. Recent Progress of Textile-Based Wearable Electronics: A Comprehensive Review of Materials, Devices, and Applications. *Small* **2018**, *14*, 1703034.
(22) Wang, C.; Wang, C.; Huang, Z.; Xu, S. Materials and Structures toward Soft Electronics. *Adv. Mater.* **2018**, *30*, No. 1801368.
(23) Kamisalic, A.; Fister, I.; Turkanovic, M.; Karakatic, S. Sensors and Functionalities of Non-Invasive Wrist-Wearable Devices: A Review. *Sensors* **2018**, *18*, 1714.
(24) Herbert, R.; Kim, J. H.; Kim, Y. S.; Lee, H. M.; Yeo, W. H. Soft Material-Enabled, Flexible Hybrid Electronics for Medicine, Healthcare, and Human-Machine Interfaces. *Materials* **2018**, *11*, 187.
(25) Lou, Z.; Wang, L.; Shen, G. Recent Advances in Smart Wearable Sensing Systems. *Adv. Mater. Technol.* **2018**, *3*, 1800444.
(26) Chang, T.-H.; Li, K.; Yang, H.; Chen, P.-Y. Multifunctionality and Mechanical Actuation of 2d Materials for Skin-Mimicking Capabilities. *Adv. Mater.* **2018**, *30*, 1802418.
(27) Amjadi, M.; Kyung, K. U.; Park, I.; Sitti, M. Stretchable, Skin-Mountable, and Wearable Strain Sensors and Their Potential Applications: A Review. *Adv. Funct. Mater.* **2016**, *26*, 1678−1698.
(28) Ge, G.; Huang, W.; Shao, J.; Dong, X. Recent Progress of Flexible and Wearable Strain Sensors for Human-Motion Monitoring. *J. Semicond.* **2018**, *39*, No. 011012.
(29) Yang, T. T.; Xie, D.; Li, Z. H.; Zhu, H. W. Recent Advances in Wearable Tactile Sensors: Materials, Sensing Mechanisms, and Device Performance. *Mater. Sci. Eng., R* **2017**, *115*, 1−37.
(30) Bandodkar, A. J.; Jia, W.; Wang, J. Tattoo-Based Wearable Electrochemical Devices: A Review. *Electroanalysis* **2015**, *27*, 562−572.
(31) Kim, J.; Kumar, R.; Bandodkar, A. J.; Wang, J. Advanced Materials for Printed Wearable Electrochemical Devices: A Review. *Adv. Electron. Mater.* **2017**, *3*, 1600260.
(32) Bandodkar, A. J.; Wang, J. Non-Invasive Wearable Electrochemical Sensors: A Review. *Trends Biotechnol.* **2014**, *32*, 363−371.
(33) Economou, A.; Kokkinos, C.; Prodromidis, M. Flexible Plastic, Paper and Textile Lab-on-a Chip Platforms for Electrochemical Biosensing. *Lab Chip* **2018**, *18*, 1812−1830.
(34) Li, Q.; Zhang, L. N.; Tao, X. M.; Ding, X. Review of Flexible Temperature Sensing Networks for Wearable Physiological Monitoring. *Adv. Healthcare Mater.* **2017**, *6*, 1601371.
(35) Yi, F.; Ren, H.; Shan, J.; Sun, X.; Wei, D.; Liu, Z. Wearable Energy Sources Based on 2d Materials. *Chem. Soc. Rev.* **2018**, *47*, 3152−3188.
(36) Dong, L. B.; Xu, C. J.; Li, Y.; Huang, Z. H.; Kang, F. Y.; Yang, Q. H.; Zhao, X. Flexible Electrodes and Supercapacitors for Wearable Energy Storage: A Review by Category. *J. Mater. Chem. A* **2016**, *4*, 4659−4685.
(37) Dubal, D. P.; Chodankar, N. R.; Kim, D. H.; Gomez-Romero, P. Towards Flexible Solid-State Supercapacitors for Smart and Wearable Electronics. *Chem. Soc. Rev.* **2018**, *47*, 2065−2129.
(38) González, A.; Goikolea, E.; Barrena, J. A.; Mysyk, R. Review on Supercapacitors: Technologies and Materials. *Renewable Sustainable Energy Rev.* **2016**, *58*, 1189−1206.
(39) An, T. C.; Cheng, W. L. Recent Progress in Stretchable Supercapacitors. *J. Mater. Chem. A* **2018**, *6*, 15478−15494.
(40) Wu, H.; Huang, Y.; Xu, F.; Duan, Y.; Yin, Z. Energy Harvesters for Wearable and Stretchable Electronics: From Flexibility to Stretchability. *Adv. Mater.* **2016**, *28*, 9881−9919.
(41) Lou, Z.; Li; Wang, L.; Shen, G. Recent Progress of Self-Powered Sensing Systems for Wearable Electronics. *Small* **2017**, *13*, 1701791.
(42) Gonzalez-Solino, C.; Lorenzo, M. D. Enzymatic Fuel Cells: Towards Self-Powered Implantable and Wearable Diagnostics. *Biosensors* **2018**, *8*, 11.
(43) Liang, T.; Yuan, Y. J. Wearable Medical Monitoring Systems Based on Wireless Networks: A Review. *IEEE Sens. J.* **2016**, *16*, 8186−8199.
(44) Wang, S.; Oh, J. Y.; Xu, J.; Tran, H.; Bao, Z. Skin-Inspired Electronics: An Emerging Paradigm. *Acc. Chem. Res.* **2018**, *51*, 1033−1045.
(45) Kim, H. J.; Sim, K.; Thukral, A.; Yu, C. J. Rubbery Electronics and Sensors from Intrinsically Stretchable Elastomeric Composites of Semiconductors and Conductors. *Sci. Adv.* **2017**, *3*, No. e1701114.
(46) Wang, C.; Xia, K.; Wang, H.; Liang, X.; Yin, Z.; Zhang, Y. Advanced Carbon for Flexible and Wearable Electronics. *Adv. Mater.* **2018**, 1801072.
(47) Xiang, L.; Zhang, H.; Hu, Y.; Peng, L.-M. Carbon Nanotube-Based Flexible Electronics. *J. Mater. Chem. C* **2018**, *6*, 7714−7727.
(48) Roy, S.; David-Pur, M.; Hanein, Y. Carbon Nanotube-Based Ion Selective Sensors for Wearable Applications. *ACS Appl. Mater. Interfaces* **2017**, *9*, 35169−35177.
(49) Reina, G.; Gonzalez-Dominguez, J. M.; Criado, A.; Vazquez, E.; Bianco, A.; Prato, M. Promises, Facts and Challenges for Graphene in Biomedical Applications. *Chem. Soc. Rev.* **2017**, *46*, 4400−4416.
(50) Zhao, S.; Tseng, P.; Grasman, J.; Wang, Y.; Li, W.; Napier, B.; Yavuz, B.; Chen, Y.; Howell, L.; Rincon, J.; Omenetto, F. G.; Kaplan, D. L. Programmable Hydrogel Ionic Circuits for Biologically Matched Electronic Interfaces. *Adv. Mater.* **2018**, *30*, No. 1800598.
(51) Lee, H. R.; Kim, C. C.; Sun, J. Y. Stretchable Ionics - a Promising Candidate for Upcoming Wearable Devices. *Adv. Mater.* **2018**, *30*, No. 1704403.
(52) Dickey, M. D. Stretchable and Soft Electronics Using Liquid Metals. *Adv. Mater.* **2017**, *29*, 1606425.
(53) Liu, Y.; He, K.; Chen, G.; Leow, W. R.; Chen, X. Nature-Inspired Structural Materials for Flexible Electronic Devices. *Chem. Rev.* **2017**, *117*, 12893−12941.
(54) Wang, L.; Chen, D.; Jiang, K.; Shen, G. New Insights and Perspectives into Biological Materials for Flexible Electronics. *Chem. Soc. Rev.* **2017**, *46*, 6764−6815.
(55) Cai, P.; Hu, B.; Leow, W. R.; Wang, X.; Loh, X. J.; Wu, Y. L.; Chen, X. Biomechano-Interactive Materials and Interfaces. *Adv. Mater.* **2018**, *30*, No. 1800572.
(56) Nagels, S.; Deferme, W. Fabrication Approaches to Interconnect Based Devices for Stretchable Electronics: A Review. *Materials* **2018**, *11*, 375.

DOI: 10.1021/acs.chemrev.8b00573
Chem. Rev. 2019, 119, 5461−5533

(57) Wang, D.; Zhang, Y.; Lu, X.; Ma, Z.; Xie, C.; Zheng, Z. Chemical Formation of Soft Metal Electrodes for Flexible and Wearable Electronics. *Chem. Soc. Rev.* **2018**, *47*, 4611−4641.
(58) Han, S. T.; Peng, H.; Sun, Q.; Venkatesh, S.; Chung, K. S.; Lau, S. C.; Zhou, Y.; Roy, V. A. L. An Overview of the Development of Flexible Sensors. *Adv. Mater.* **2017**, *29*, 1700375.
(59) Al-Halhouli, A.; Qitouqa, H.; Alashqar, A.; Abu-Khalaf, J. Inkjet Printing for the Fabrication of Flexible/Stretchable Wearable Electronic Devices and Sensors. *Sens. Rev.* **2018**, *38*, 438−452.
(60) Gao, M.; Li, L. H.; Song, Y. L. Inkjet Printing Wearable Electronic Devices. *J. Mater. Chem. C* **2017**, *5*, 2971−2993.
(61) Zhao, J.; Chi, Z.; Yang, Z.; Chen, X.; Arnold, M. S.; Zhang, Y.; Xu, J.; Chi, Z.; Aldred, M. P. Recent Developments of Truly Stretchable Thin Film Electronic and Optoelectronic Devices. *Nanoscale* **2018**, *10*, 5764−5792.
(62) Linghu, C.; Zhang, S.; Wang, C.; Song, J. Transfer Printing Techniques for Flexible and Stretchable Inorganic Electronics. *NPJ. Flexible Electron.* **2018**, *2*, 26.
(63) Rogers, J. A.; Someya, T.; Huang, Y. G. Materials and Mechanics for Stretchable Electronics. *Science* **2010**, *327*, 1603−1607.
(64) Kim, D. H.; Xiao, J.; Song, J.; Huang, Y.; Rogers, J. A. Stretchable, Curvilinear Electronics Based on Inorganic Materials. *Adv. Mater.* **2010**, *22*, 2108−2124.
(65) Zhang, H.; Liu, Y.; Yang, C.; Xiang, L.; Hu, Y.; Peng, L.-M. Wafer-Scale Fabrication of Ultrathin Flexible Electronic Systems Via Capillary-Assisted Electrochemical Delamination. *Adv. Mater.* **2018**, *30*, 1805408.
(66) Lipomi, D. J. Stretchable Figures of Merit in Deformable Electronics. *Adv. Mater.* **2016**, *28*, 4180−4183.
(67) Lee, Y.; Kim, J.; Joo, H.; Raj, M. S.; Ghaffari, R.; Kim, D. H. Wearable Sensing Systems with Mechanically Soft Assemblies of Nanoscale Materials. *Adv. Mater. Technol.* **2017**, *2*, 1700053.
(68) Liu, H. S.; Pan, B. C.; Liou, G. S. Highly Transparent Agnw/Pdms Stretchable Electrodes for Elastomeric Electrochromic Devices. *Nanoscale* **2017**, *9*, 2633−2639.
(69) Hong, S. Y.; Oh, J. H.; Park, H.; Yun, J. Y.; Jin, S. W.; Sun, L.; Zi, G.; Ha, J. S. Polyurethane Foam Coated with a Multi-Walled Carbon Nanotube/Polyaniline Nanocomposite for a Skin-Like Stretchable Array of Multi-Functional Sensors. *NPG Asia Mater.* **2017**, *9*, No. e448.
(70) Chortos, A.; Zhu, C.; Oh, J. Y.; Yan, X.; Pochorovski, I.; To, J. W.; Liu, N.; Kraft, U.; Murmann, B.; Bao, Z. Investigating Limiting Factors in Stretchable All-Carbon Transistors for Reliable Stretchable Electronics. *ACS Nano* **2017**, *11*, 7925−7937.
(71) Lipomi, D. J.; Lee, J. A.; Vosgueritchian, M.; Tee, B. C. K.; Bolander, J. A.; Bao, Z. A. Electronic Properties of Transparent Conductive Films of Pedot:Pss on Stretchable Substrates. *Chem. Mater.* **2012**, *24*, 373−382.
(72) Oh, J. Y.; Kim, S.; Baik, H. K.; Jeong, U. Conducting Polymer Dough for Deformable Electronics. *Adv. Mater.* **2016**, *28*, 4455−4461.
(73) Müller, C.; Goffri, S.; Breiby, D. W.; Andreasen, J. W.; Chanzy, H. D.; Janssen, R. A.; Nielsen, M. M.; Radano, C. P.; Sirringhaus, H.; Smith, P.; Stingelin-Stutzmann, N. Tough, Semiconducting Poly-ethylene-Poly (3-Hexylthiophene) Diblock Copolymers. *Adv. Funct. Mater.* **2007**, *17*, 2674−2679.
(74) Kim, H. J.; Kim, J. H.; Ryu, J. H.; Kim, Y.; Kang, H.; Lee, W. B.; Kim, T. S.; Kim, B. J. Architectural Engineering of Rod-Coil Compatibilizers for Producing Mechanically and Thermally Stable Polymer Solar Cells. *ACS Nano* **2014**, *8*, 10461−10470.
(75) Haque, M. A.; Kurokawa, T.; Gong, J. P. Super Tough Double Network Hydrogels and Their Application as Biomaterials. *Polymer* **2012**, *53*, 1805−1822.
(76) Parida, K.; Kumar, V.; Jiangxin, W.; Bhavanasi, V.; Bendi, R.; Lee, P. S. Highly Transparent, Stretchable, and Self-Healing Ionic-Skin Triboelectric Nanogenerators for Energy Harvesting and Touch Applications. *Adv. Mater.* **2017**, *29*, 1702181.
(77) Cao, Y.; Morrissey, T. G.; Acome, E.; Allec, S. I.; Wong, B. M.; Keplinger, C.; Wang, C. A Transparent, Self-Healing, Highly Stretchable Ionic Conductor. *Adv. Mater.* **2017**, *29*, 1605099.
(78) Sekitani, T.; Noguchi, Y.; Hata, K.; Fukushima, T.; Aida, T.; Someya, T. A Rubberlike Stretchable Active Matrix Using Elastic Conductors. *Science* **2008**, *321*, 1468−1472.
(79) Matsuhisa, N.; Inoue, D.; Zalar, P.; Jin, H.; Matsuba, Y.; Itoh, A.; Yokota, T.; Hashizume, D.; Someya, T. Printable Elastic Conductors by in Situ Formation of Silver Nanoparticles from Silver Flakes. *Nat. Mater.* **2017**, *16*, 834−840.
(80) Savagatrup, S.; Chan, E.; Renteria-Garcia, S. M.; Printz, A. D.; Zaretski, A. V.; O'Connor, T. F.; Rodriquez, D.; Valle, E.; Lipomi, D. J. Plasticization of Pedot:Pss by Common Additives for Mechanically Robust Organic Solar Cells and Wearable Sensors. *Adv. Funct. Mater.* **2015**, *25*, 427−436.
(81) Vosgueritchian, M.; Lipomi, D. J.; Bao, Z. A. Highly Conductive and Transparent Pedot:Pss Films with a Fluorosurfactant for Stretchable and Flexible Transparent Electrodes. *Adv. Funct. Mater.* **2012**, *22*, 421−428.
(82) Wang, Y.; Zhu, C.; Pfattner, R.; Yan, H.; Jin, L.; Chen, S.; Molina-Lopez, F.; Lissel, F.; Liu, J.; Rabiah, N. I.; et al. A Highly Stretchable, Transparent, and Conductive Polymer. *Sci. Adv.* **2017**, *3*, No. e1602076.
(83) Kayser, L. V.; Russell, M. D.; Rodriquez, D.; Abuhamdieh, S. N.; Dhong, C.; Khan, S.; Stein, A. N.; Ramirez, J.; Lipomi, D. J. Raft Polymerization of an Intrinsically Stretchable Water-Soluble Block Copolymer Scaffold for Pedot. *Chem. Mater.* **2018**, *30*, 4459−4468.
(84) Tahk, D.; Lee, H. H.; Khang, D. Y. Elastic Moduli of Organic Electronic Materials by the Buckling Method. *Macromolecules* **2009**, *42*, 7079−7083.
(85) Lang, U.; Naujoks, N.; Dual, J. Mechanical Characterization of Pedot:Pss Thin Films. *Synth. Met.* **2009**, *159*, 473−479.
(86) Wang, S.; Xu, J.; Wang, W.; Wang, G. N.; Rastak, R.; Molina-Lopez, F.; Chung, J. W.; Niu, S.; Feig, V. R.; Lopez, J.; et al. Skin Electronics from Scalable Fabrication of an Intrinsically Stretchable Transistor Array. *Nature* **2018**, *555*, 83−88.
(87) Wang, G. J. N.; Shaw, L.; Xu, J.; Kurosawa, T.; Schroeder, B. C.; Oh, J. Y.; Benight, S. J.; Bao, Z. Inducing Elasticity through Oligo-Siloxane Crosslinks for Intrinsically Stretchable Semiconducting Polymers. *Adv. Funct. Mater.* **2016**, *26*, 7254−7262.
(88) Peng, R.; Pang, B.; Hu, D. Q.; Chen, M. J.; Zhang, G. B.; Wang, X. H.; Lu, H. B.; Cho, K.; Qiu, L. Z. An Aba Triblock Copolymer Strategy for Intrinsically Stretchable Semiconductors. *J. Mater. Chem. C* **2015**, *3*, 3599−3606.
(89) Savagatrup, S.; Printz, A. D.; Rodriquez, D.; Lipomi, D. J. Best of Both Worlds: Conjugated Polymers Exhibiting Good Photovoltaic Behavior and High Tensile Elasticity. *Macromolecules* **2014**, *47*, 1981−1992.
(90) Savagatrup, S.; Zhao, X.; Chan, E.; Mei, J.; Lipomi, D. J. Effect of Broken Conjugation on the Stretchability of Semiconducting Polymers. *Macromol. Rapid Commun.* **2016**, *37*, 1623−1628.
(91) Root, S. E.; Savagatrup, S.; Printz, A. D.; Rodriquez, D.; Lipomi, D. J. Mechanical Properties of Organic Semiconductors for Stretchable, Highly Flexible, and Mechanically Robust Electronics. *Chem. Rev.* **2017**, *117*, 6467−6499.
(92) Printz, A. D.; Lipomi, D. J. Competition between Deformability and Charge Transport in Semiconducting Polymers for Flexible and Stretchable Electronics. *Appl. Phys. Rev.* **2016**, *3*, No. 021302.
(93) Yang, C. H.; Suo, Z. G. *Hydrogel Ionotronics. Nat. Rev. Mater.* **2018**, *3*, 125−142.
(94) Zhao, X. H. Multi-Scale Multi-Mechanism Design of Tough Hydrogels: Building Dissipation into Stretchy Networks. *Soft Matter* **2014**, *10*, 672−687.
(95) Gong, J. P.; Katsuyama, Y.; Kurokawa, T.; Osada, Y. Double-Network Hydrogels with Extremely High Mechanical Strength. *Adv. Mater.* **2003**, *15*, 1155−1158.
(96) Sun, J. Y.; Zhao, X.; Illeperuma, W. R.; Chaudhuri, O.; Oh, K. H.; Mooney, D. J.; Vlassak, J. J.; Suo, Z. Highly Stretchable and Tough Hydrogels. *Nature* **2012**, *489*, 133−136.
(97) Keplinger, C.; Sun, J. Y.; Foo, C. C.; Rothemund, P.; Whitesides, G. M.; Suo, Z. Stretchable, Transparent, Ionic Conductors. *Science* **2013**, *341*, 984−987.

DOI: 10.1021/acs.chemrev.8b00573
Chem. Rev. 2019, 119, 5461−5533

(98) Lei, Z. Y.; Wang, Q. K.; Wu, P. Y. A Multifunctional Skin-Like Sensor Based on a 3d Printed Thermo-Responsive Hydrogel. *Mater. Horiz.* **2017**, *4*, 694−700.
(99) Xu, C. Y.; Li, B. Z.; Xu, C. Y.; Zheng, J. M. A Novel Dielectric Elastomer Actuator Based on Compliant Polyvinyl Alcohol Hydrogel Electrodes. *J. Mater. Sci.: Mater. Electron.* **2015**, *26*, 9213−9218.
(100) Lei, Z.; Wang, Q.; Sun, S.; Zhu, W.; Wu, P. A Bioinspired Mineral Hydrogel as a Self-Healable, Mechanically Adaptable Ionic Skin for Highly Sensitive Pressure Sensing. *Adv. Mater.* **2017**, *29*, 1700321.
(101) Lei, Z.; Wu, P. A Supramolecular Biomimetic Skin Combining a Wide Spectrum of Mechanical Properties and Multiple Sensory Capabilities. *Nat. Commun.* **2018**, *9*, 1134.
(102) Tang, J. D.; Li, J. Y.; Vlassak, J. J.; Suo, Z. G. Adhesion between Highly Stretchable Materials. *Soft Matter* **2016**, *12*, 1093−1099.
(103) Efimenko, K.; Wallace, W. E.; Genzer, J. Surface Modification of Sylgard-184 Poly(Dimethyl Siloxane) Networks by Ultraviolet and Ultraviolet/Ozone Treatment. *J. Colloid Interface Sci.* **2002**, *254*, 306−315.
(104) Wirthl, D.; Pichler, R.; Drack, M.; Kettlguber, G.; Moser, R.; Gerstmayr, R.; Hartmann, F.; Bradt, E.; Kaltseis, R.; Siket, C. M.; et al. Instant Tough Bonding of Hydrogels for Soft Machines and Electronics. *Sci. Adv.* **2017**, *3*, No. e1700053.
(105) Yuk, H.; Zhang, T.; Parada, G. A.; Liu, X.; Zhao, X. Skin-Inspired Hydrogel-Elastomer Hybrids with Robust Interfaces and Functional Microstructures. *Nat. Commun.* **2016**, *7*, 12028.
(106) Liu, Q. H.; Nian, G. D.; Yang, C. H.; Qu, S. X.; Suo, Z. G. Bonding Dissimilar Polymer Networks in Various Manufacturing Processes. *Nat. Commun.* **2018**, *9*, 846.
(107) López-Barrón, C. R.; Chen, R.; Wagner, N. J. Ultrastretchable Iono-Elastomers with Mechanoelectrical Response. *ACS Macro Lett.* **2016**, *5*, 1332−1338.
(108) Xie, Y.; Xie, R.; Yang, H.-C.; Chen, Z.; Hou, J.; López-Barrón, C. R.; Wagner, N. J.; Gao, K.-Z. Iono-Elastomer-Based Wearable Strain Sensor with Real-Time Thermomechanical Dual Response. *ACS Appl. Mater. Interfaces* **2018**, *10*, 32435−32443.
(109) Kim, W.; Kim, W. 3 V Omni-Directionally Stretchable One-Body Supercapacitors Based on a Single Ion-Gel Matrix and Carbon Nanotubes. *Nanotechnology* **2016**, *27*, 225402.
(110) Osada, I.; de Vries, H.; Scrosati, B.; Passerini, S. Ionic-Liquid-Based Polymer Electrolytes for Battery Applications. *Angew. Chem., Int. Ed.* **2016**, *55*, 500−513.
(111) Noshadi, I.; Walker, B. W.; Portillo-Lara, R.; Shirzaei Sani, E.; Gomes, N.; Aziziyan, M. R.; Annabi, N. Engineering Biodegradable and Biocompatible Bio-Ionic Liquid Conjugated Hydrogels with Tunable Conductivity and Mechanical Properties. *Sci. Rep.* **2017**, *7*, 4345.
(112) Li, J.; Ma, P. C.; Chow, W. S.; To, C. K.; Tang, B. Z.; Kim, J. K. Correlations between Percolation Threshold, Dispersion State, and Aspect Ratio of Carbon Nanotubes. *Adv. Funct. Mater.* **2007**, *17*, 3207−3215.
(113) Román, S.; Lund, F.; Bustos, J.; Palza, H. About the Relevance of Waviness, Agglomeration, and Strain on the Electrical Behavior of Polymer Composites Filled with Carbon Nanotubes Evaluated by a Monte-Carlo Simulation. *Mater. Res. Express* **2018**, *5*, No. 015044.
(114) Park, J.; You, I.; Shin, S.; Jeong, U. Material Approaches to Stretchable Strain Sensors. *ChemPhysChem* **2015**, *16*, 1155−1163.
(115) Mutiso, R. M.; Winey, K. I. Electrical Properties of Polymer Nanocomposites Containing Rod-Like Nanofillers. *Prog. Polym. Sci.* **2015**, *40*, 63−84.
(116) Liu, C. Recent Developments in Polymer Mems. *Adv. Mater.* **2007**, *19*, 3783−3790.
(117) Shih, W. P.; Tsao, L. C.; Lee, C. W.; Cheng, M. Y.; Chang, C.; Yang, Y. J.; Fan, K. C. Flexible Temperature Sensor Array Based on a Graphite-Polydimethylsiloxane Composite. *Sensors* **2010**, *10*, 3597−3610.
(118) Lu, N. S.; Lu, C.; Yang, S. X.; Rogers, J. Highly Sensitive Skin-Mountable Strain Gauges Based Entirely on Elastomers. *Adv. Funct. Mater.* **2012**, *22*, 4044−4050.
(119) Su, M.; Li, F.; Chen, S.; Huang, Z.; Qin, M.; Li, W.; Zhang, X.; Song, Y. Nanoparticle Based Curve Arrays for Multirecognition Flexible Electronics. *Adv. Mater.* **2016**, *28*, 1369−1374.
(120) Jiang, C. W.; Ni, I. C.; Tzeng, S. D.; Kuo, W. Nearly Isotropic Piezoresistive Response Due to Charge Detour Conduction in Nanoparticle Thin Films. *Sci. Rep.* **2015**, *5*, 11939.
(121) Gong, S.; Cheng, W. L. One-Dimensional Nanomaterials for Soft Electronics. *Adv. Electron. Mater.* **2017**, *3*, 1600314.
(122) Jung, S.; Lee, J.; Hyeon, T.; Lee, M.; Kim, D. H. Fabric-Based Integrated Energy Devices for Wearable Activity Monitors. *Adv. Mater.* **2014**, *26*, 6329−6334.
(123) Sekitani, T.; Nakajima, H.; Maeda, H.; Fukushima, T.; Aida, T.; Hata, K.; Someya, T. Stretchable Active-Matrix Organic Light-Emitting Diode Display Using Printable Elastic Conductors. *Nat. Mater.* **2009**, *8*, 494−499.
(124) Lipomi, D. J.; Vosgueritchian, M.; Tee, B. C.; Hellstrom, S. L.; Lee, J. A.; Fox, C. H.; Bao, Z. Skin-Like Pressure and Strain Sensors Based on Transparent Elastic Films of Carbon Nanotubes. *Nat. Nanotechnol.* **2011**, *6*, 788−792.
(125) Amjadi, M.; Pichitpajongkit, A.; Lee, S.; Ryu, S.; Park, I. Highly Stretchable and Sensitive Strain Sensor Based on Silver Nanowire-Elastomer Nanocomposite. *ACS Nano* **2014**, *8*, 5154−5163.
(126) Gong, S.; Schwalb, W.; Wang, Y.; Chen, Y.; Tang, Y.; Si, J.; Shirinzadeh, B.; Cheng, W. A Wearable and Highly Sensitive Pressure Sensor with Ultrathin Gold Nanowires. *Nat. Commun.* **2014**, *5*, 3132.
(127) Kim, K. S.; Zhao, Y.; Jang, H.; Lee, S. Y.; Kim, J. M.; Kim, K. S.; Ahn, J. H.; Kim, P.; Choi, J. Y.; Hong, B. H. Large-Scale Pattern Growth of Graphene Films for Stretchable Transparent Electrodes. *Nature* **2009**, *457*, 706−710.
(128) Yan, C.; Wang, J.; Kang, W.; Cui, M.; Wang, X.; Foo, C. Y.; Chee, K. J.; Lee, P. S. Highly Stretchable Piezoresistive Graphene-Nanocellulose Nanopaper for Strain Sensors. *Adv. Mater.* **2014**, *26*, 2022−2027.
(129) Jang, H.; Park, Y. J.; Chen, X.; Das, T.; Kim, M. S.; Ahn, J. H. Graphene-Based Flexible and Stretchable Electronics. *Adv. Mater.* **2016**, *28*, 4184−4202.
(130) Chen, Z.; Ren, W.; Gao, L.; Liu, B.; Pei, S.; Cheng, H. M. Three-Dimensional Flexible and Conductive Interconnected Graphene Networks Grown by Chemical Vapour Deposition. *Nat. Mater.* **2011**, *10*, 424−428.
(131) Shin, M. K.; Oh, J.; Lima, M.; Kozlov, M. E.; Kim, S. J.; Baughman, R. H. Elastomeric Conductive Composites Based on Carbon Nanotube Forests. *Adv. Mater.* **2010**, *22*, 2663−2667.
(132) Kim, K. H.; Vural, M.; Islam, M. F. Single-Walled Carbon Nanotube Aerogel-Based Elastic Conductors. *Adv. Mater.* **2011**, *23*, 2865−2869.
(133) Li, P.; Sun, K.; Ouyang, J. Stretchable and Conductive Polymer Films Prepared by Solution Blending. *ACS Appl. Mater. Interfaces* **2015**, *7*, 18415−18423.
(134) Hwang, B. U.; Lee, J. H.; Trung, T. Q.; Roh, E.; Kim, D. I.; Kim, S. W.; Lee, N. E. Transparent Stretchable Self-Powered Patchable Sensor Platform with Ultrasensitive Recognition of Human Activities. *ACS Nano* **2015**, *9*, 8801−8810.
(135) Someya, T.; Bao, Z.; Malliaras, G. G. The Rise of Plastic Bioelectronics. *Nature* **2016**, *540*, 379−385.
(136) Matsuhisa, N.; Kaltenbrunner, M.; Yokota, T.; Jinno, H.; Kuribara, K.; Sekitani, T.; Someya, T. Printable Elastic Conductors with a High Conductivity for Electronic Textile Applications. *Nat. Commun.* **2015**, *6*, 7461.
(137) Lin, L.; Liu, S.; Fu, S.; Zhang, S.; Deng, H.; Fu, Q. Fabrication of Highly Stretchable Conductors Via Morphological Control of Carbon Nanotube Network. *Small* **2013**, *9*, 3620−3629.
(138) Li, Y. J.; Shimizu, H. Toward a Stretchable, Elastic, and Electrically Conductive Nanocomposite: Morphology and Properties of Poly[Styrene-B-(Ethylene-Co-Butylene)-B-Styrene]/Multiwalled Carbon Nanotube Composites Fabricated by High-Shear Processing. *Macromolecules* **2009**, *42*, 2587−2593.

DOI: 10.1021/acs.chemrev.8b00573
Chem. Rev. 2019, 119, 5461−5533

(139) Chen, M.; Tao, T.; Zhang, L.; Gao, W.; Li, C. Highly Conductive and Stretchable Polymer Composites Based on Graphene/Mwcnt Network. *Chem. Commun.* **2013**, *49*, 1612−1614.
(140) Chen, M.; Zhang, L.; Duan, S.; Jing, S.; Jiang, H.; Li, C. Highly Stretchable Conductors Integrated with a Conductive Carbon Nanotube/Graphene Network and 3d Porous Poly(Dimethylsiloxane). *Adv. Funct. Mater.* **2014**, *24*, 7548−7556.
(141) Kim, J.; Lee, M. S.; Jeon, S.; Kim, M.; Kim, S.; Kim, K.; Bien, F.; Hong, S. Y.; Park, J. U. Highly Transparent and Stretchable Field-Effect Transistor Sensors Using Graphene−Nanowire Hybrid Nanostructures. *Adv. Mater.* **2015**, *27*, 3292−3297.
(142) Yan, C.; Cho, J. H.; Ahn, J. H. Graphene-Based Flexible and Stretchable Thin Film Transistors. *Nanoscale* **2012**, *4*, 4870−4882.
(143) Chortos, A.; Koleilat, G. I.; Pfattner, R.; Kong, D.; Lin, P.; Nur, R.; Lei, T.; Wang, H.; Liu, N.; Lai, Y. C.; et al. Mechanically Durable and Highly Stretchable Transistors Employing Carbon Nanotube Semiconductor and Electrodes. *Adv. Mater.* **2016**, *28*, 4441−4448.
(144) Zhu, Y.; Xu, F. Buckling of Aligned Carbon Nanotubes as Stretchable Conductors: A New Manufacturing Strategy. *Adv. Mater.* **2012**, *24*, 1073−1077.
(145) Yu, C.; Masarapu, C.; Rong, J.; Wei, B.; Jiang, H. Stretchable Supercapacitors Based on Buckled Single-Walled Carbon-Nanotube Macrofilms. *Adv. Mater.* **2009**, *21*, 4793−4797.
(146) Khang, D. Y.; Xiao, J.; Kocabas, C.; MacLaren, S.; Banks, T.; Jiang, H.; Huang, Y. Y.; Rogers, J. A. Molecular Scale Buckling Mechanics in Individual Aligned Single-Wall Carbon Nanotubes on Elastomeric Substrates. *Nano Lett.* **2008**, *8*, 124−130.
(147) Park, M.; Im, J.; Shin, M.; Min, Y.; Park, J.; Cho, H.; Park, S.; Shim, M. B.; Jeon, S.; Chung, D. Y.; et al. Highly Stretchable Electric Circuits from a Composite Material of Silver Nanoparticles and Elastomeric Fibres. *Nat. Nanotechnol.* **2012**, *7*, 803−809.
(148) Hu, M.; Cai, X.; Guo, Q.; Bian, B.; Zhang, T.; Yang, J. Direct Pen Writing of Adhesive Particle-Free Ultrahigh Silver Salt-Loaded Composite Ink for Stretchable Circuits. *ACS Nano* **2016**, *10*, 396−404.
(149) Lee, P.; Lee, J.; Lee, H.; Yeo, J.; Hong, S.; Nam, K. H.; Lee, D.; Lee, S. S.; Ko, S. H. Highly Stretchable and Highly Conductive Metal Electrode by Very Long Metal Nanowire Percolation Network. *Adv. Mater.* **2012**, *24*, 3326−3332.
(150) Liang, J.; Tong, K.; Pei, Q. A Water-Based Silver-Nanowire Screen-Print Ink for the Fabrication of Stretchable Conductors and Wearable Thin-Film Transistors. *Adv. Mater.* **2016**, *28*, 5986−5996.
(151) Choi, S.; Park, J.; Hyun, W.; Kim, J.; Kim, J.; Lee, Y. B.; Song, C.; Hwang, H. J.; Kim, J. H.; Hyeon, T.; et al. Stretchable Heater Using Ligand-Exchanged Silver Nanowire Nanocomposite for Wearable Articular Thermotherapy. *ACS Nano* **2015**, *9*, 6626−6633.
(152) Ho, X. N.; Tey, J. N.; Liu, W. J.; Cheng, C. K.; Wei, J. Biaxially Stretchable Silver Nanowire Transparent Conductors. *J. Appl. Phys.* **2013**, *113*, No. 044311.
(153) Ho, M. D.; Ling, Y.; Yap, L. W.; Wang, Y.; Dong, D.; Zhao, Y.; Cheng, W. Percolating Network of Ultrathin Gold Nanowires and Silver Nanowires toward "Invisible" Wearable Sensors for Detecting Emotional Expression and Apexcardiogram. *Adv. Funct. Mater.* **2017**, *27*, 1700845.
(154) Xu, F.; Zhu, Y. Highly Conductive and Stretchable Silver Nanowire Conductors. *Adv. Mater.* **2012**, *24*, 5117−5122.
(155) Kim, Y.; Zhu, J.; Yeom, B.; Di Prima, M.; Su, X.; Kim, J. G.; Yoo, S. J.; Uher, C.; Kotov, N. A. Stretchable Nanoparticle Conductors with Self-Organized Conductive Pathways. *Nature* **2013**, *500*, 59−63.
(156) Chen, S.; Wei, Y.; Yuan, X.; Lin, Y.; Liu, L. A Highly Stretchable Strain Sensor Based on a Graphene/Silver Nanoparticle Synergic Conductive Network and a Sandwich Structure. *J. Mater. Chem. C* **2016**, *4*, 4304−4311.
(157) Chun, K. Y.; Oh, Y.; Rho, J.; Ahn, J. H.; Kim, Y. J.; Choi, H. R.; Baik, S. Highly Conductive, Printable and Stretchable Composite Films of Carbon Nanotubes and Silver. *Nat. Nanotechnol.* **2010**, *5*, 853−857.
(158) Choi, T. Y.; Hwang, B. U.; Kim, B. Y.; Trung, T. Q.; Nam, Y. H.; Kim, D. N.; Eom, K.; Lee, N. E. Stretchable, Transparent, and Stretch-Unresponsive Capacitive Touch Sensor Array with Selectively Patterned Silver Nanowires/Reduced Graphene Oxide Electrodes. *ACS Appl. Mater. Interfaces* **2017**, *9*, 18022−18030.
(159) Roh, E.; Hwang, B. U.; Kim, D.; Kim, B. Y.; Lee, N. E. Stretchable, Transparent, Ultrasensitive, and Patchable Strain Sensor for Human-Machine Interfaces Comprising a Nanohybrid of Carbon Nanotubes and Conductive Elastomers. *ACS Nano* **2015**, *9*, 6252−6261.
(160) Liu, K.; Pan, X. F.; Chen, L. H.; Huang, L. L.; Ni, Y. H.; Liu, J.; Cao, S. L.; Wang, H. P. Ultrasoft Self-Healing Nanoparticle-Hydrogel Composites with Conductive and Magnetic Properties. *ACS Sustainable Chem. Eng.* **2018**, *6*, 6395−6403.
(161) Choi, W. M.; Song, J.; Khang, D. Y.; Jiang, H.; Huang, Y. Y.; Rogers, J. A. Biaxially Stretchable "Wavy" Silicon Nanomembranes. *Nano Lett.* **2007**, *7*, 1655−1663.
(162) Kim, D. H.; Ahn, J. H.; Choi, W. M.; Kim, H. S.; Kim, T. H.; Song, J.; Huang, Y. Y.; Liu, Z.; Lu, C.; Rogers, J. A. Stretchable and Foldable Silicon Integrated Circuits. *Science* **2008**, *320*, 507−511.
(163) Kim, D. H.; Song, J.; Choi, W. M.; Kim, H. S.; Kim, R. H.; Liu, Z.; Huang, Y. Y.; Hwang, K. C.; Zhang, Y. W.; Rogers, J. A. Materials and Noncoplanar Mesh Designs for Integrated Circuits with Linear Elastic Responses to Extreme Mechanical Deformations. *Proc. Natl. Acad. Sci. U. S. A.* **2008**, *105*, 18675−18680.
(164) Fan, J. A.; Yeo, W. H.; Su, Y.; Hattori, Y.; Lee, W.; Jung, S. Y.; Zhang, Y.; Liu, Z.; Cheng, H.; Falgout, L.; et al. Fractal Design Concepts for Stretchable Electronics. *Nat. Commun.* **2014**, *5*, 3266.
(165) Jang, K. I.; Li, K.; Chung, H. U.; Xu, S.; Jung, H. N.; Yang, Y.; Kwak, J. W.; Jung, H. H.; Song, J.; Yang, C.; et al. Self-Assembled Three Dimensional Network Designs for Soft Electronics. *Nat. Commun.* **2017**, *8*, 15894.
(166) Someya, T.; Kato, Y.; Sekitani, T.; Iba, S.; Noguchi, Y.; Murase, Y.; Kawaguchi, H.; Sakurai, T. Conformable, Flexible, Large-Area Networks of Pressure and Thermal Sensors with Organic Transistor Active Matrixes. *Proc. Natl. Acad. Sci. U. S. A.* **2005**, *102*, 12321−12325.
(167) Lanzara, G.; Salowitz, N.; Guo, Z.; Chang, F. K. A Spider-Web-Like Highly Expandable Sensor Network for Multifunctional Materials. *Adv. Mater.* **2010**, *22*, 4643−4648.
(168) Kim, H. J.; Son, C.; Ziaie, B. A Multiaxial Stretchable Interconnect Using Liquid-Alloy-Filled Elastomeric Microchannels. *Appl. Phys. Lett.* **2008**, *92*, No. 011904.
(169) Yoon, J.; Hong, S. Y.; Lim, Y.; Lee, S. J.; Zi, G.; Ha, J. S. Design and Fabrication of Novel Stretchable Device Arrays on a Deformable Polymer Substrate with Embedded Liquid-Metal Interconnections. *Adv. Mater.* **2014**, *26*, 6580−6586.
(170) Li, T.; Suo, Z. G.; Lacour, S. P.; Wagner, S. Compliant Thin Film Patterns of Stiff Materials as Platforms for Stretchable Electronics. *J. Mater. Res.* **2005**, *20*, 3274−3277.
(171) Mohan, A. M. V.; Kim, N.; Gu, Y.; Bandodkar, A. J.; You, J.-M.; Kumar, R.; Kurniawan, J. F.; Xu, S.; Wang, J. Merging of Thin- and Thick-Film Fabrication Technologies: Toward Soft Stretchable "Island-Bridge" Devices. *Adv. Mater. Technol.* **2017**, *2*, 1600284.
(172) Sim, K.; Li, Y.; Song, J.; Yu, C. Biaxially Stretchable Ultrathin Si Enabled by Serpentine Structures on Prestrained Elastomers. *Adv. Mater. Technol.* **2019**, *4*, 1800489.
(173) Kim, D. H.; Lu, N.; Ma, R.; Kim, Y. S.; Kim, R. H.; Wang, S.; Wu, J.; Won, S. M.; Tao, H.; Islam, A.; et al. Epidermal Electronics. *Science* **2011**, *333*, 838−843.
(174) Ma, Y.; Feng, X.; Rogers, J. A.; Huang, Y.; Zhang, Y. Design and Application of 'J-Shaped' Stress-Strain Behavior in Stretchable Electronics: A Review. *Lab Chip* **2017**, *17*, 1689−1704.
(175) Ma, Q.; Cheng, H.; Jang, K. I.; Luan, H.; Hwang, K. C.; Rogers, J. A.; Huang, Y.; Zhang, Y. A Nonlinear Mechanics Model of Bio-Inspired Hierarchical Lattice Materials Consisting of Horseshoe Microstructures. *J. Mech. Phys. Solids* **2016**, *90*, 179−202.
(176) Jang, K. I.; Chung, H. U.; Xu, S.; Lee, C. H.; Luan, H.; Jeong, J.; Cheng, H.; Kim, G. T.; Han, S. Y.; Lee, J. W.; et al. Soft Network Composite Materials with Deterministic and Bio-Inspired Designs. *Nat. Commun.* **2015**, *6*, 6566.
(177) Dickey, M. D.; Chiechi, R. C.; Larsen, R. J.; Weiss, E. A.; Weitz, D. A.; Whitesides, G. M. Eutectic Gallium-Indium (Egain): A Liquid

DOI: 10.1021/acs.chemrev.8b00573
Chem. Rev. 2019, 119, 5461−5533

Metal Alloy for the Formation of Stable Structures in Microchannels at Room Temperature. *Adv. Funct. Mater.* **2008**, *18*, 1097−1104.
(178) Zhu, S.; So, J. H.; Mays, R.; Desai, S.; Barnes, W. R.; Pourdeyhimi, B.; Dickey, M. D. Ultrastretchable Fibers with Metallic Conductivity Using a Liquid Metal Alloy Core. *Adv. Funct. Mater.* **2013**, *23*, 2308−2314.
(179) Cooper, C. B.; Arutselvan, K.; Liu, Y.; Armstrong, D.; Lin, Y. L.; Khan, M. R.; Genzer, J.; Dickey, M. D. Stretchable Capacitive Sensors of Torsion, Strain, and Touch Using Double Helix Liquid Metal Fibers. *Adv. Funct. Mater.* **2017**, *27*, 1605630.
(180) Markvicka, E. J.; Bartlett, M. D.; Huang, X.; Majidi, C. An Autonomously Electrically Self-Healing Liquid Metal-Elastomer Composite for Robust Soft-Matter Robotics and Electronics. *Nat. Mater.* **2018**, *17*, 618−624.
(181) Kwak, M. K.; Jeong, H. E.; Suh, K. Y. Rational Design and Enhanced Biocompatibility of a Dry Adhesive Medical Skin Patch. *Adv. Mater.* **2011**, *23*, 3949−3953.
(182) Stauffer, F.; Thielen, M.; Sauter, C.; Chardonnens, S.; Bachmann, S.; Tybrandt, K.; Peters, C.; Hierold, C.; Voros, J. Skin Conformal Polymer Electrodes for Clinical Ecg and Eeg Recordings. *Adv. Healthcare Mater.* **2018**, *7*, 1700994.
(183) Lee, S.; Inoue, Y.; Kim, D.; Reuveny, A.; Kuribara, K.; Yokota, T.; Reeder, J.; Sekino, M.; Sekitani, T.; Abe, Y.; et al. A Strain-Absorbing Design for Tissue-Machine Interfaces Using a Tunable Adhesive Gel. *Nat. Commun.* **2014**, *5*, 5898.
(184) Bihar, E.; Roberts, T.; Ismailova, E.; Saadaoui, M.; Isik, M.; Sanchez-Sanchez, A.; Mecerreyes, D.; Herve, T.; De Graaf, J. B.; Malliaras, G. G. Fully Printed Electrodes on Stretchable Textiles for Long-Term Electrophysiology. *Adv. Mater. Technol.* **2017**, *2*, 1600251.
(185) Yao, S. S.; Zhu, Y. Nanomaterial-Enabled Dry Electrodes for Electrophysiological Sensing: A Review. *JOM* **2016**, *68*, 1145−1155.
(186) Miyamoto, A.; Lee, S.; Cooray, N. F.; Lee, S.; Mori, M.; Matsuhisa, N.; Jin, H.; Yoda, L.; Yokota, T.; Itoh, A.; et al. Inflammation-Free, Gas-Permeable, Lightweight, Stretchable on-Skin Electronics with Nanomeshes. *Nat. Nanotechnol.* **2017**, *12*, 907−913.
(187) Wang, F.; Liu, S.; Shu, L.; Tao, X. M. Low-Dimensional Carbon Based Sensors and Sensing Network for Wearable Health and Environmental Monitoring. *Carbon* **2017**, *121*, 353−367.
(188) Vinardell, M. P.; Llanas, H.; Marics, L.; Mitjans, M. In Vitro Comparative Skin Irritation Induced by Nano and Non-Nano Zinc Oxide. *Nanomaterials* **2017**, *7*, 56.
(189) Hussain, S. M.; Warheit, D. B.; Ng, S. P.; Comfort, K. K.; Grabinski, C. M.; Braydich-Stolle, L. K. At the Crossroads of Nanotoxicology in Vitro: Past Achievements and Current Challenges. *Toxicol. Sci.* **2015**, *147*, 5−16.
(190) Gulson, B.; McCall, M. J.; Bowman, D. M.; Pinheiro, T. A Review of Critical Factors for Assessing the Dermal Absorption of Metal Oxide Nanoparticles from Sunscreens Applied to Humans, and a Research Strategy to Address Current Deficiencies. *Arch. Toxicol.* **2015**, *89*, 1909−1930.
(191) Pietroiusti, A.; Stockmann-Juvala, H.; Lucaroni, F.; Savolainen, K. Nanomaterial Exposure, Toxicity, and Impact on Human Health. *Wires Nanomed. Nanobi.* **2018**, *10*, No. e1513.
(192) Larese Filon, F.; Mauro, M.; Adami, G.; Bovenzi, M.; Crosera, M. Nanoparticles Skin Absorption: New Aspects for a Safety Profile Evaluation. *Regul. Toxicol. Pharmacol.* **2015**, *72*, 310−322.
(193) Kim, J. H.; Kim, S.; So, J. H.; Kim, K.; Koo, H. J. Cytotoxicity of Gallium-Indium Liquid Metal in an Aqueous Environment. *ACS Appl. Mater. Interfaces* **2018**, *10*, 17448−17454.
(194) Gao, B.; Wang, X.; Li, T.; Feng, Z.; Wang, C.; Gu, Z. Gecko-Inspired Paper Artificial Skin for Intimate Skin Contact and Multisensing. *Adv. Mater. Technol.* **2019**, *4*, 1800392.
(195) Kim, T.; Park, J.; Sohn, J.; Cho, D.; Jeon, S. Bioinspired, Highly Stretchable, and Conductive Dry Adhesives Based on 1d-2d Hybrid Carbon Nanocomposites for All-in-One Ecg Electrodes. *ACS Nano* **2016**, *10*, 4770−4778.
(196) Lee, S. P.; Ha, G.; Wright, D. E.; Ma, Y.; Sen-Gupta, E.; Haubrich, N. R.; Branche, P. C.; Li, W.; Huppert, G. L.; Johnson, M.; et al. Highly Flexible, Wearable, and Disposable Cardiac Biosensors for Remote and Ambulatory Monitoring. *NPJ. Digit. Med.* **2018**, *1*, 2.
(197) Majumder, S.; Mondal, T.; Deen, M. J. Wearable Sensors for Remote Health Monitoring. *Sensors* **2017**, *17*, 130.
(198) Bandodkar, A. J.; Jeerapan, I.; Wang, J. Wearable Chemical Sensors: Present Challenges and Future Prospects. *ACS Sens.* **2016**, *1*, 464−482.
(199) Mirani, B.; Pagan, E.; Currie, B.; Siddiqui, M. A.; Hosseinzadeh, R.; Mostafalu, P.; Zhang, Y. S.; Ghahary, A.; Akbari, M. An Advanced Multifunctional Hydrogel-Based Dressing for Wound Monitoring and Drug Delivery. *Adv. Healthcare Mater.* **2017**, *6*, 1700718.
(200) Chi, Y. M.; Jung, T. P.; Cauwenberghs, G. Dry-Contact and Noncontact Biopotential Electrodes: Methodological Review. *IEEE Rev. Biomed. Eng.* **2010**, *3*, 106−119.
(201) Bai, W. B.; Kuang, T. R.; Chitrakar, C.; Yang, R. G.; Li, S. L.; Zhu, D. H.; Chang, L. Q. Patchable Micro/Nanodevices Interacting with Skin. *Biosens. Bioelectron.* **2018**, *122*, 189−204.
(202) Choi, M. K.; Park, O. K.; Choi, C.; Qiao, S. T.; Ghaffari, R.; Kim, J.; Lee, D. J.; Kim, M.; Hyun, W.; Kim, S. J.; et al. Cephalopod-Inspired Miniaturized Suction Cups for Smart Medical Skin. *Adv. Healthcare Mater.* **2016**, *5*, 80−87.
(203) Zeng, L. A.; Lie, S. A.; Chong, S. Y. Comparison of Medical Adhesive Tapes in Patients at Risk of Facial Skin Trauma under Anesthesia. *Anesthesiol. Res. Pract.* **2016**, *2016*, 4878246.
(204) Ratliff, C. R. Descriptive Study of the Frequency of Medical Adhesive-Related Skin Injuries in a Vascular Clinic. *J. Vasc. Nurs.* **2017**, *35*, 86−89.
(205) Peng, R.; Sonner, Z.; Hauke, A.; Wilder, E.; Kasting, J.; Gaillard, T.; Swaille, D.; Sherman, F.; Mao, X.; Hagen, J.; et al. A New Oil/Membrane Approach for Integrated Sweat Sampling and Sensing: Sample Volumes Reduced from Ul's to Nl's and Reduction of Analyte Contamination from Skin. *Lab Chip* **2016**, *16*, 4415−4423.
(206) Sun, B.; McCay, R. N.; Goswami, S.; Xu, Y.; Zhang, C.; Ling, Y.; Lin, J.; Yan, Z. Gas-Permeable, Multifunctional on-Skin Electronics Based on Laser-Induced Porous Graphene and Sugar-Templated Elastomer Sponges. *Adv. Mater.* **2018**, *30*, 1804327.
(207) Hwang, I.; Kim, H. N.; Seong, M.; Lee, S. H.; Kang, M.; Yi, H.; Bae, W. G.; Kwak, M. K.; Jeong, H. E. Multifunctional Smart Skin Adhesive Patches for Advanced Health Care. *Adv. Healthcare Mater.* **2018**, *7*, 1800275.
(208) Bihar, E.; Roberts, T.; Zhang, Y.; Ismailova, E.; Herve, T.; Malliaras, G. G.; De Graaf, J. B.; Inal, S.; Saadaoui, M. Fully Printed All-Polymer Tattoo/Textile Electronics for Electromyography. *Flex. Print. Electron.* **2018**, *3*, No. 034004.
(209) Yeo, W. H.; Kim, Y. S.; Lee, J.; Ameen, A.; Shi, L.; Li, M.; Wang, S.; Ma, R.; Jin, S. H.; Kang, Z.; et al. Multifunctional Epidermal Electronics Printed Directly onto the Skin. *Adv. Mater.* **2013**, *25*, 2773−2778.
(210) Webb, R. C.; Bonifas, A. P.; Behnaz, A.; Zhang, Y.; Yu, K. J.; Cheng, H.; Shi, M.; Bian, Z.; Liu, Z.; Kim, Y. S.; et al. Ultrathin Conformal Devices for Precise and Continuous Thermal Characterization of Human Skin. *Nat. Mater.* **2013**, *12*, 938−944.
(211) Dagdeviren, C.; Su, Y.; Joe, P.; Yona, R.; Liu, Y.; Kim, Y. S.; Huang, Y.; Damadoran, A. R.; Xia, J.; Martin, L. W.; et al. Conformable Amplified Lead Zirconate Titanate Sensors with Enhanced Piezoelectric Response for Cutaneous Pressure Monitoring. *Nat. Commun.* **2014**, *5*, 4496.
(212) Pang, C.; Koo, J. H.; Nguyen, A.; Caves, J. M.; Kim, M. G.; Chortos, A.; Kim, K.; Wang, P. J.; Tok, J. B.; Bao, Z. Highly Skin-Conformal Microhairy Sensor for Pulse Signal Amplification. *Adv. Mater.* **2015**, *27*, 634−640.
(213) Sekine, T.; Sugano, R.; Tashiro, T.; Sato, J.; Takeda, Y.; Matsui, H.; Kumaki, D.; Domingues Dos Santos, F.; Miyabo, A.; Tokito, S. Fully Printed Wearable Vital Sensor for Human Pulse Rate Monitoring Using Ferroelectric Polymer. *Sci. Rep.* **2018**, *8*, 4442.
(214) Park, D. Y.; Joe, D. J.; Kim, D. H.; Park, H.; Han, J. H.; Jeong, C. K.; Park, H.; Park, J. G.; Joung, B.; Lee, K. J. Self-Powered Real-Time Arterial Pulse Monitoring Using Ultrathin Epidermal Piezoelectric Sensors. *Adv. Mater.* **2017**, *29*, 1702308.

DOI: 10.1021/acs.chemrev.8b00573
Chem. Rev. 2019, 119, 5461−5533

(215) Lochner, C. M.; Khan, Y.; Pierre, A.; Arias, A. C. All-Organic Optoelectronic Sensor for Pulse Oximetry. *Nat. Commun.* **2014**, *5*, 5745.
(216) Schwartz, G.; Tee, B. C.; Mei, J.; Appleton, A. L.; Kim, D. H.; Wang, H.; Bao, Z. Flexible Polymer Transistors with High Pressure Sensitivity for Application in Electronic Skin and Health Monitoring. *Nat. Commun.* **2013**, *4*, 1859.
(217) Khan, Y.; Ostfeld, A. E.; Lochner, C. M.; Pierre, A.; Arias, A. C. Monitoring of Vital Signs with Flexible and Wearable Medical Devices. *Adv. Mater.* **2016**, *28*, 4373−4395.
(218) Pang, C.; Lee, G. Y.; Kim, T. I.; Kim, S. M.; Kim, H. N.; Ahn, S. H.; Suh, K. Y. A Flexible and Highly Sensitive Strain-Gauge Sensor Using Reversible Interlocking of Nanofibres. *Nat. Mater.* **2012**, *11*, 795−801.
(219) Parrilla, M.; Canovas, R.; Jeerapan, I.; Andrade, F. J.; Wang, J. A Textile-Based Stretchable Multi-Ion Potentiometric Sensor. *Adv. Healthcare Mater.* **2016**, *5*, 996−1001.
(220) Koh, A.; Kang, D.; Xue, Y.; Lee, S.; Pielak, R. M.; Kim, J.; Hwang, T.; Min, S.; Banks, A.; Bastien, P.; et al. A Soft, Wearable Microfluidic Device for the Capture, Storage, and Colorimetric Sensing of Sweat. *Sci. Transl. Med.* **2016**, *8*, 366ra165.
(221) Martin, A.; Kim, J.; Kurniawan, J. F.; Sempionatto, J. R.; Moreto, J. R.; Tang, G.; Campbell, A. S.; Shin, A.; Lee, M. Y.; Liu, X.; et al. Epidermal Microfluidic Electrochemical Detection System: Enhanced Sweat Sampling and Metabolite Detection. *ACS Sens.* **2017**, *2*, 1860−1868.
(222) Kim, J.; Gutruf, P.; Chiarelli, A. M.; Heo, S. Y.; Cho, K.; Xie, Z.; Banks, A.; Han, S.; Jang, K. I.; Lee, J. W.; et al. Miniaturized Battery-Free Wireless Systems for Wearable Pulse Oximetry. *Adv. Funct. Mater.* **2017**, *27*, 1604373.
(223) Lee, J. H.; Hwang, J. Y.; Zhu, J.; Hwang, H. R.; Lee, S. M.; Cheng, H.; Lee, S. H.; Hwang, S. W. Flexible Conductive Composite Integrated with Personal Earphone for Wireless, Real-Time Monitoring of Electrophysiological Signs. *ACS Appl. Mater. Interfaces* **2018**, *10*, 21184−21190.
(224) Goverdovsky, V.; von Rosenberg, W.; Nakamura, T.; Looney, D.; Sharp, D. J.; Papavassiliou, C.; Morrell, M. J.; Mandic, D. P. Hearables: Multimodal Physiological in-Ear Sensing. *Sci. Rep.* **2017**, *7*, 6948.
(225) Sempionatto, J. R.; Nakagawa, T.; Pavinatto, A.; Mensah, S. T.; Imani, S.; Mercier, P.; Wang, J. Eyeglasses Based Wireless Electrolyte and Metabolite Sensor Platform. *Lab Chip* **2017**, *17*, 1834−1842.
(226) Yan, Q.; Peng, B.; Su, G.; Cohan, B. E.; Major, T. C.; Meyerhoff, M. E. Measurement of Tear Glucose Levels with Amperometric Glucose Biosensor/Capillary Tube Configuration. *Anal. Chem.* **2011**, *83*, 8341−8346.
(227) Yao, H.; Liao, Y.; Lingley, A. R.; Afanasiev, A.; Lahdesmaki, I.; Otis, B. P.; Parviz, B. A. A Contact Lens with Integrated Telecommunication Circuit and Sensors for Wireless and Continuous Tear Glucose Monitoring. *J. Micromech. Microeng.* **2012**, *22*, No. 075007.
(228) Thomas, N.; Lahdesmaki, I.; Parviz, B. A. A Contact Lens with an Integrated Lactate Sensor. *Sens. Actuators, B* **2012**, *162*, 128−134.
(229) Yao, H.; Shum, A. J.; Cowan, M.; Lahdesmaki, I.; Parviz, B. A. A Contact Lens with Embedded Sensor for Monitoring Tear Glucose Level. *Biosens. Bioelectron.* **2011**, *26*, 3290−3296.
(230) Kim, J.; Kim, M.; Lee, M. S.; Kim, K.; Ji, S.; Kim, Y. T.; Park, J.; Na, K.; Bae, K. H.; Kyun Kim, H.; et al. Wearable Smart Sensor Systems Integrated on Soft Contact Lenses for Wireless Ocular Diagnostics. *Nat. Commun.* **2017**, *8*, 14997.
(231) Kim, J.; Imani, S.; de Araujo, W. R.; Warchall, J.; Valdes-Ramirez, G.; Paixao, T. R.; Mercier, P. P.; Wang, J. Wearable Salivary Uric Acid Mouthguard Biosensor with Integrated Wireless Electronics. *Biosens. Bioelectron.* **2015**, *74*, 1061−1068.
(232) *Dash Pro*; Bragi, 2018; https://www.bragi.com/thedashpro/ (accessed Dec 7, 2018).
(233) *Joule Earring Backing*; Biosensive Technologies Inc., 2018; https://shopjoule.com (accessed Dec 7, 2018).
(234) *Sensimed Triggerfish*; Sensimed, 2018; https://www.sensimed.ch/sensimed-triggerfish (accessed Dec 7, 2018).
(235) Ha, S.; Kim, C.; Chi, Y. M.; Akinin, A.; Maier, C.; Ueno, A.; Cauwenberghs, G. Integrated Circuits and Electrode Interfaces for Noninvasive Physiological Monitoring. *IEEE Trans. Biomed. Eng.* **2014**, *61*, 1522−1537.
(236) Xu, S.; Zhang, Y.; Jia, L.; Mathewson, K. E.; Jang, K. I.; Kim, J.; Fu, H.; Huang, X.; Chava, P.; Wang, R.; et al. Soft Microfluidic Assemblies of Sensors, Circuits, and Radios for the Skin. *Science* **2014**, *344*, 70−74.
(237) Ameri, S. K.; Kim, M.; Kuang, I. A.; Perera, W. K.; Alshiekh, M.; Jeong, H.; Topcu, U.; Akinwande, D.; Lu, N. S. Imperceptible Electrooculography Graphene Sensor System for Human-Robot Interface. *NPJ. 2D Mater. Appl.* **2018**, *2*, 19.
(238) Lee, S. M.; Byeon, H. J.; Lee, J. H.; Baek, D. H.; Lee, K. H.; Hong, J. S.; Lee, S. H. Self-Adhesive Epidermal Carbon Nanotube Electronics for Tether-Free Long-Term Continuous Recording of Biosignals. *Sci. Rep.* **2014**, *4*, 6074.
(239) Jeong, J. W.; Kim, M. K.; Cheng, H.; Yeo, W. H.; Huang, X.; Liu, Y.; Zhang, Y.; Huang, Y.; Rogers, J. A. Capacitive Epidermal Electronics for Electrically Safe, Long-Term Electrophysiological Measurements. *Adv. Healthcare Mater.* **2014**, *3*, 642−648.
(240) Leleux, P.; Badier, J. M.; Rivnay, J.; Benar, C.; Herve, T.; Chauvel, P.; Malliaras, G. G. Conducting Polymer Electrodes for Electroencephalography. *Adv. Healthcare Mater.* **2014**, *3*, 490−493.
(241) Lopez-Gordo, M. A.; Sanchez-Morillo, D.; Pelayo Valle, F. Dry Eeg Electrodes. *Sensors* **2014**, *14*, 12847−12870.
(242) Mathewson, K. E.; Harrison, T. J.; Kizuk, S. A. High and Dry? Comparing Active Dry Eeg Electrodes to Active and Passive Wet Electrodes. *Psychophysiology* **2017**, *54*, 74−82.
(243) Wang, Y.; Qiu, Y.; Ameri, S. K.; Jang, H.; Dai, Z.; Huang, Y.; Lu, N. Low-Cost, um-Thick, Tape-Free Electronic Tattoo Sensors with Minimized Motion and Sweat Artifacts. *NPJ. Flexible Electron.* **2018**, *2*, 6.
(244) Nawrocki, R. A.; Jin, H.; Lee, S.; Yokota, T.; Sekino, M.; Someya, T. Self-Adhesive and Ultra-Conformable, Sub-300 Nm Dry Thin-Film Electrodes for Surface Monitoring of Biopotentials. *Adv. Funct. Mater.* **2018**, *28*, 1803279.
(245) Grozea, C.; Voinescu, C. D.; Fazli, S. Bristle-Sensors—Low-Cost Flexible Passive Dry Eeg Electrodes for Neurofeedback and Bci Applications. *J. Neural. Eng.* **2011**, *8*, No. 025008.
(246) Ruffini, G.; Dunne, S.; Fuentemilla, L.; Grau, C.; Farres, E.; Marco-Pallares, J.; Watts, P. C. P.; Silva, S. R. P. First Human Trials of a Dry Electrophysiology Sensor Using a Carbon Nanotube Array Interface. *Sens. Actuators, A* **2008**, *144*, 275−279.
(247) Jung, H. C.; Moon, J. H.; Baek, D. H.; Lee, J. H.; Choi, Y. Y.; Hong, J. S.; Lee, S. H. Cnt/Pdms Composite Flexible Dry Electrodes for Long-Term Ecg Monitoring. *IEEE Trans. Biomed. Eng.* **2012**, *59*, 1472−1479.
(248) Myers, A. C.; Huang, H.; Zhu, Y. Wearable Silver Nanowire Dry Electrodes for Electrophysiological Sensing. *RSC Adv.* **2015**, *5*, 11627−11632.
(249) Mostafalu, P.; Sonkusale, S. A High-Density Nanowire Electrode on Paper for Biomedical Applications. *RSC Adv.* **2015**, *5*, 8680−8687.
(250) Varadan, V. K.; Oh, S.; Kwon, H.; Hankins, P. Wireless Point-of-Care Diagnosis for Sleep Disorder with Dry Nanowire Electrodes. *J. Nanotechnol. Eng. Med.* **2010**, *1*, No. 031012.
(251) Yapici, M. K.; Alkhidir, T.; Samad, Y. A.; Liao, K. Graphene-Clad Textile Electrodes for Electrocardiogram Monitoring. *Sens. Actuators, B* **2015**, *221*, 1469−1474.
(252) Jin, G. J.; Uddin, M. J.; Shim, J. S. Biomimetic Cilia-Patterned Rubber Electrode Using Ultra Conductive Polydimethylsiloxane. *Adv. Funct. Mater.* **2018**, *28*, 1804351.
(253) Kim, J. H.; Kim, S. R.; Kil, H. J.; Kim, Y. C.; Park, J. W. Highly Conformable, Transparent Electrodes for Epidermal Electronics. *Nano Lett.* **2018**, *18*, 4531−4540.
(254) Fan, Y. J.; Li, X.; Kuang, S. Y.; Zhang, L.; Chen, Y. H.; Liu, L.; Zhang, K.; Ma, S. W.; Liang, F.; Wu, T.; et al. Highly Robust, Transparent, and Breathable Epidermal Electrode. *ACS Nano* **2018**, *12*, 9326.

DOI: 10.1021/acs.chemrev.8b00573
Chem. Rev. 2019, 119, 5461−5533

(255) Jang, K. I.; Jung, H. N.; Lee, J. W.; Xu, S.; Liu, Y. H.; Ma, Y.; Jeong, J. W.; Song, Y. M.; Kim, J.; Kim, B. H.; et al. Ferromagnetic, Folded Electrode Composite as a Soft Interface to the Skin for Long-Term Electrophysiological Recording. *Adv. Funct. Mater.* **2016**, *26*, 7281−7290.
(256) Jeong, J. W.; Yeo, W. H.; Akhtar, A.; Norton, J. J.; Kwack, Y. J.; Li, S.; Jung, S. Y.; Su, Y.; Lee, W.; Xia, J.; et al. Materials and Optimized Designs for Human-Machine Interfaces Via Epidermal Electronics. *Adv. Mater.* **2013**, *25*, 6839−6846.
(257) Norton, J. J.; Lee, D. S.; Lee, J. W.; Lee, W.; Kwon, O.; Won, P.; Jung, S. Y.; Cheng, H.; Jeong, J. W.; Akce, A.; et al. Soft, Curved Electrode Systems Capable of Integration on the Auricle as a Persistent Brain-Computer Interface. *Proc. Natl. Acad. Sci. U. S. A.* **2015**, *112*, 3920−3925.
(258) Kabiri Ameri, S.; Ho, R.; Jang, H.; Tao, L.; Wang, Y.; Wang, L.; Schnyer, D. M.; Akinwande, D.; Lu, N. Graphene Electronic Tattoo Sensors. *ACS Nano* **2017**, *11*, 7634−7641.
(259) Leleux, P.; Johnson, C.; Strakosas, X.; Rivnay, J.; Herve, T.; Owens, R. M.; Malliaras, G. G. Ionic Liquid Gel-Assisted Electrodes for Long-Term Cutaneous Recordings. *Adv. Healthcare Mater.* **2014**, *3*, 1377−1380.
(260) Isik, M.; Lonjaret, T.; Sardon, H.; Marcilla, R.; Herve, T.; Malliaras, G. G.; Ismailova, E.; Mecerreyes, D. Cholinium-Based Ion Gels as Solid Electrolytes for Long-Term Cutaneous Electrophysiology. *J. Mater. Chem. C* **2015**, *3*, 8942−8948.
(261) Lin, B. S.; Chou, W.; Wang, H. Y.; Huang, Y. J.; Pan, J. S. Development of Novel Non-Contact Electrodes for Mobile Electrocardiogram Monitoring System. *IEEE J. Transl. Eng. Health Med.* **2013**, *1*, 2700108.
(262) Gandhi, N.; Khe, C.; Chung, D.; Chi, Y. M.; Cauwenberghs, G. Properties of Dry and Non-Contact Electrodes for Wearable Physiological Sensors. *2011 International Conference on Body Sensor Networks, May 23−25*, 2011; pp 107−112.
(263) Torres, F.; das Graças Mota Melo, M.; Tosti, A. Management of Contact Dermatitis Due to Nickel Allergy: An Update. *Clin., Cosmet. Invest. Dermatol.* **2009**, *2*, 39−48.
(264) Son, D.; Lee, J.; Qiao, S.; Ghaffari, R.; Kim, J.; Lee, J. E.; Song, C.; Kim, S. J.; Lee, D. J.; Jun, S. W.; et al. Multifunctional Wearable Devices for Diagnosis and Therapy of Movement Disorders. *Nat. Nanotechnol.* **2014**, *9*, 397−404.
(265) Findlow, A.; Goulermas, J. Y.; Nester, C.; Howard, D.; Kenney, L. P. J. Predicting Lower Limb Joint Kinematics Using Wearable Motion Sensors. *Gait Posture* **2008**, *28*, 120−126.
(266) Lee, S.-W.; Mase, K.; Kogure, K. Detection of Spatio-Temporal Gait Parameters by Using Wearable Motion Sensors. *2006 IEEE Engineering in Medicine and Biology 27th Annual Conference, Shanghai*, 2006; 6836−6839.
(267) Tao, W.; Liu, T.; Zheng, R.; Feng, H. Gait Analysis Using Wearable Sensors. *Sensors* **2012**, *12*, 2255−2283.
(268) Dobkin, B. H. Wearable Motion Sensors to Continuously Measure Real-World Physical Activities. *Curr. Opin. Neurol.* **2013**, *26*, 602−608.
(269) Jeon, H.; Hong, S. K.; Kim, M. S.; Cho, S. J.; Lim, G. Omni-Purpose Stretchable Strain Sensor Based on a Highly Dense Nanocracking Structure for Whole-Body Motion Monitoring. *ACS Appl. Mater. Interfaces* **2017**, *9*, 41712−41721.
(270) Yamada, T.; Hayamizu, Y.; Yamamoto, Y.; Yomogida, Y.; Izadi-Najafabadi, A.; Futaba, D. N.; Hata, K. A Stretchable Carbon Nanotube Strain Sensor for Human-Motion Detection. *Nat. Nanotechnol.* **2011**, *6*, 296−301.
(271) Drack, M.; Graz, I.; Sekitani, T.; Someya, T.; Kaltenbrunner, M.; Bauer, S. An Imperceptible Plastic Electronic Wrap. *Adv. Mater.* **2015**, *27*, 34−40.
(272) Reeder, J.; Kaltenbrunner, M.; Ware, T.; Arreaga-Salas, D.; Avendano-Bolivar, A.; Yokota, T.; Inoue, Y.; Sekino, M.; Voit, W.; Sekitani, T.; et al. Mechanically Adaptive Organic Transistors for Implantable Electronics. *Adv. Mater.* **2014**, *26*, 4967−4973.
(273) Kaltenbrunner, M.; Sekitani, T.; Reeder, J.; Yokota, T.; Kuribara, K.; Tokuhara, T.; Drack, M.; Schwodiauer, R.; Graz, I.; Bauer-Gogonea, S.; et al. An Ultra-Lightweight Design for Imperceptible Plastic Electronics. *Nature* **2013**, *499*, 458−463.
(274) Tiwana, M. I.; Redmond, S. J.; Lovell, N. H. A Review of Tactile Sensing Technologies with Applications in Biomedical Engineering. *Sens. Actuators, A* **2012**, *179*, 17−31.
(275) Heikenfeld, J.; Jajack, A.; Rogers, J.; Gutruf, P.; Tian, L.; Pan, T.; Li, R.; Khine, M.; Kim, J.; Wang, J.; et al. Wearable Sensors: Modalities, Challenges, and Prospects. *Lab Chip* **2018**, *18*, 217−248.
(276) Trung, T. Q.; Lee, N. E. Flexible and Stretchable Physical Sensor Integrated Platforms for Wearable Human-Activity Monitoringand Personal Healthcare. *Adv. Mater.* **2016**, *28*, 4338−4372.
(277) Yao, S.; Swetha, P.; Zhu, Y. Nanomaterial-Enabled Wearable Sensors for Healthcare. *Adv. Healthcare Mater.* **2018**, *7*, 1700889.
(278) Yang, C. C.; Hsu, Y. L. A Review of Accelerometry-Based Wearable Motion Detectors for Physical Activity Monitoring. *Sensors* **2010**, *10*, 7772−7788.
(279) Iosa, M.; Picerno, P.; Paolucci, S.; Morone, G. Wearable Inertial Sensors for Human Movement Analysis. *Expert Rev. Med. Devices* **2016**, *13*, 641−659.
(280) You, I.; Kim, B.; Park, J.; Koh, K.; Shin, S.; Jung, S.; Jeong, U. Stretchable E-Skin Apexcardiogram Sensor. *Adv. Mater.* **2016**, *28*, 6359−6364.
(281) Gao, Y.; Ota, H.; Schaler, E. W.; Chen, K.; Zhao, A.; Gao, W.; Fahad, H. M.; Leng, Y.; Zheng, A.; Xiong, F.; et al. Wearable Microfluidic Diaphragm Pressure Sensor for Health and Tactile Touch Monitoring. *Adv. Mater.* **2017**, *29*, 1701985.
(282) Won, S. M.; Kim, H. S.; Lu, N. S.; Kim, D. G.; Del Solar, C.; Duenas, T.; Ameen, A.; Rogers, J. A. Piezoresistive Strain Sensors and Multiplexed Arrays Using Assemblies of Single-Crystalline Silicon Nanoribbons on Plastic Substrates. *IEEE Trans. Electron Devices* **2011**, *58*, 4074−4078.
(283) Kwon, D.; Lee, T. I.; Shim, J.; Ryu, S.; Kim, M. S.; Kim, S.; Kim, T. S.; Park, I. Highly Sensitive, Flexible, and Wearable Pressure Sensor Based on a Giant Piezocapacitive Effect of Three-Dimensional Microporous Elastomeric Dielectric Layer. *ACS Appl. Mater. Interfaces* **2016**, *8*, 16922−16931.
(284) Zhou, J.; Gu, Y.; Fei, P.; Mai, W.; Gao, Y.; Yang, R.; Bao, G.; Wang, Z. L. Flexible Piezotronic Strain Sensor. *Nano Lett.* **2008**, *8*, 3035−3040.
(285) Sun, Q.; Seung, W.; Kim, B. J.; Seo, S.; Kim, S. W.; Cho, J. H. Active Matrix Electronic Skin Strain Sensor Based on Piezopotential-Powered Graphene Transistors. *Adv. Mater.* **2015**, *27*, 3411−3417.
(286) Bao, R.; Wang, C.; Dong, L.; Yu, R.; Zhao, K.; Wang, Z. L.; Pan, C. Flexible and Controllable Piezo-Phototronic Pressure Mapping Sensor Matrix by Zno Nw/P-Polymer Led Array. *Adv. Funct. Mater.* **2015**, *25*, 2884−2891.
(287) Wang, X.; Zhang, H.; Dong, L.; Han, X.; Du, W.; Zhai, J.; Pan, C.; Wang, Z. L. Self-Powered High-Resolution and Pressure-Sensitive Triboelectric Sensor Matrix for Real-Time Tactile Mapping. *Adv. Mater.* **2016**, *28*, 2896−2903.
(288) Lee, S. W.; Park, J. J.; Park, B. H.; Mun, S. C.; Park, Y. T.; Liao, K.; Seo, T. S.; Hyun, W. J.; Park, O. O. Enhanced Sensitivity of Patterned Graphene Strain Sensors Used for Monitoring Subtle Human Body Motions. *ACS Appl. Mater. Interfaces* **2017**, *9*, 11176−11183.
(289) Wang, Y.; Wang, L.; Yang, T. T.; Li, X.; Zang, X. B.; Zhu, M.; Wang, K. L.; Wu, D. H.; Zhu, H. W. Wearable and Highly Sensitive Graphene Strain Sensors for Human Motion Monitoring. *Adv. Funct. Mater.* **2014**, *24*, 4666−4670.
(290) Zhang, H.; Niu, W.; Zhang, S. Extremely Stretchable, Stable, and Durable Strain Sensors Based on Double-Network Organogels. *ACS Appl. Mater. Interfaces* **2018**, *10*, 32640.
(291) Wang, X.; Gu, Y.; Xiong, Z.; Cui, Z.; Zhang, T. Silk-Molded Flexible, Ultrasensitive, and Highly Stable Electronic Skin for Monitoring Human Physiological Signals. *Adv. Mater.* **2014**, *26*, 1336−1342.
(292) Ge, J.; Sun, L.; Zhang, F. R.; Zhang, Y.; Shi, L. A.; Zhao, H. Y.; Zhu, H. W.; Jiang, H. L.; Yu, S. H. A Stretchable Electronic Fabric Artificial Skin with Pressure-, Lateral Strain-, and Flexion-Sensitive Properties. *Adv. Mater.* **2016**, *28*, 722−728.

DOI: 10.1021/acs.chemrev.8b00573
Chem. Rev. 2019, 119, 5461−5533

(293) Sangeetha, N. M.; Decorde, N.; Viallet, B.; Viau, G.; Ressier, L. Nanoparticle-Based Strain Gauges Fabricated by Convective Self Assembly: Strain Sensitivity and Hysteresis with Respect to Nanoparticle Sizes. *J. Phys. Chem. C* **2013**, *117*, 1935−1940.
(294) Kramer, R. K.; Majidi, C.; Wood, R. J. Wearable Tactile Keypad with Stretchable Artificial Skin. *2011 IEEE International Conference on Robotics and Automation, May 9−13*, 2011; pp 1103−1107.
(295) Kramer, R. K.; Majidi, C.; Sahai, R.; Wood, R. J. Soft Curvature Sensors for Joint Angle Proprioception. *2011 IEEE/RSJ. International Conference on Intelligent Robots and Systems, Sep 25−30*, 2011; pp 1919−1926.
(296) Khan, M. R.; Eaker, C. B.; Bowden, E. F.; Dickey, M. D. Giant and Switchable Surface Activity of Liquid Metal Via Surface Oxidation. *Proc. Natl. Acad. Sci. U. S. A.* **2014**, *111*, 14047−14051.
(297) Egry, I.; Ricci, E.; Novakovic, R.; Ozawa, S. Surface Tension of Liquid Metals and Alloys–Recent Developments. *Adv. Colloid Interface Sci.* **2010**, *159*, 198−212.
(298) Kim, D.; Lee, D. W.; Choi, W.; Lee, J. B. A Super-Lyophobic 3-D Pdms Channel as a Novel Microfluidic Platform to Manipulate Oxidized Galinstan. *J. Microelectromech. Syst.* **2013**, *22*, 1267−1275.
(299) Scharmann, F.; Cherkashinin, G.; Breternitz, V.; Knedlik, C.; Hartung, G.; Weber, T.; Schaefer, J. A. Viscosity Effect on Gainsn Studied by Xps. *Surf. Interface Anal.* **2004**, *36*, 981−985.
(300) Jeong, Y. R.; Kim, J.; Xie, Z. Q.; Xue, Y. G.; Won, S. M.; Lee, G.; Jin, S. W.; Hong, S. Y.; Feng, X.; Huang, Y. G.; et al. A Skin-Attachable, Stretchable Integrated System Based on Liquid Gainsn for Wireless Human Motion Monitoring with Multi-Site Sensing Capabilities. *NPG Asia Mater.* **2017**, *9*, No. e443.
(301) Cho, D.; Park, J.; Kim, J.; Kim, T.; Kim, J.; Park, I.; Jeon, S. Three-Dimensional Continuous Conductive Nanostructure for Highly Sensitive and Stretchable Strain Sensor. *ACS Appl. Mater. Interfaces* **2017**, *9*, 17369−17378.
(302) Park, M.; Park, Y. J.; Chen, X.; Park, Y. K.; Kim, M. S.; Ahn, J. H. Mos2 -Based Tactile Sensor for Electronic Skin Applications. *Adv. Mater.* **2016**, *28*, 2556−2562.
(303) Kang, D.; Pikhitsa, P. V.; Choi, Y. W.; Lee, C.; Shin, S. S.; Piao, L.; Park, B.; Suh, K. Y.; Kim, T. I.; Choi, M. Ultrasensitive Mechanical Crack-Based Sensor Inspired by the Spider Sensory System. *Nature* **2014**, *516*, 222−226.
(304) Nur, R.; Matsuhisa, N.; Jiang, Z.; Nayeem, M. O. G.; Yokota, T.; Someya, T. A Highly Sensitive Capacitive-Type Strain Sensor Using Wrinkled Ultrathin Gold Films. *Nano Lett.* **2018**, *18*, 5610.
(305) Rim, Y. S.; Bae, S. H.; Chen, H.; De Marco, N.; Yang, Y. Recent Progress in Materials and Devices toward Printable and Flexible Sensors. *Adv. Mater.* **2016**, *28*, 4415−4440.
(306) Yang, S.; Lu, N. Gauge Factor and Stretchability of Silicon-on-Polymer Strain Gauges. *Sensors* **2013**, *13*, 8577−8594.
(307) Ying, M.; Bonifas, A. P.; Lu, N.; Su, Y.; Li, R.; Cheng, H.; Ameen, A.; Huang, Y.; Rogers, J. A. Silicon Nanomembranes for Fingertip Electronics. *Nanotechnology* **2012**, *23*, 344004.
(308) Wang, X.; Li, J.; Song, H.; Huang, H.; Gou, J. Highly Stretchable and Wearable Strain Sensor Based on Printable Carbon Nanotube Layers/Polydimethylsiloxane Composites with Adjustable Sensitivity. *ACS Appl. Mater. Interfaces* **2018**, *10*, 7371−7380.
(309) Lu, Y.; Biswas, M. C.; Guo, Z.; Jeon, J. W.; Wujcik, E. K. Recent Developments in Bio-Monitoring Via Advanced Polymer Nanocomposite-Based Wearable Strain Sensors. *Biosens. Bioelectron.* **2019**, *123*, 167.
(310) Kanoun, O.; Muller, C.; Benchirouf, A.; Sanli, A.; Dinh, T. N.; Al-Hamry, A.; Bu, L.; Gerlach, C.; Bouhamed, A. Flexible Carbon Nanotube Films for High Performance Strain Sensors. *Sensors* **2014**, *14*, 10042−10071.
(311) Larimi, S. R.; Rezaei Nejad, H.; Oyatsi, M.; O'Brien, A.; Hoorfar, M.; Najjaran, H. Low-Cost Ultra-Stretchable Strain Sensors for Monitoring Human Motion and Bio-Signals. *Sens. Actuators, A* **2018**, *271*, 182−191.
(312) Shi, G.; Zhao, Z. H.; Pai, J. H.; Lee, I.; Zhang, L. Q.; Stevenson, C.; Ishara, K.; Zhang, R. J.; Zhu, H. W.; Ma, J. Highly Sensitive, Wearable, Durable Strain Sensors and Stretchable Conductors Using Graphene/Silicon Rubber Composites. *Adv. Funct. Mater.* **2016**, *26*, 7614−7625.
(313) Li, Q.; Ullah, Z.; Li, W.; Guo, Y.; Xu, J.; Wang, R.; Zeng, Q.; Chen, M.; Liu, C.; Liu, L. Wide-Range Strain Sensors Based on Highly Transparent and Supremely Stretchable Graphene/Ag-Nanowires Hybrid Structures. *Small* **2016**, *12*, 5058−5065.
(314) Park, J. J.; Hyun, W. J.; Mun, S. C.; Park, Y. T.; Park, O. O. Highly Stretchable and Wearable Graphene Strain Sensors with Controllable Sensitivity for Human Motion Monitoring. *ACS Appl. Mater. Interfaces* **2015**, *7*, 6317−6324.
(315) Tian, H.; Shu, Y.; Cui, Y. L.; Mi, W. T.; Yang, Y.; Xie, D.; Ren, T. L. Scalable Fabrication of High-Performance and Flexible Graphene Strain Sensors. *Nanoscale* **2014**, *6*, 699−705.
(316) Gong, S.; Lai, D. T.; Su, B.; Si, K. J.; Ma, Z.; Yap, L. W.; Guo, P.; Cheng, W. Highly Stretchy Black Gold E-Skin Nanopatches as Highly Sensitive Wearable Biomedical Sensors. *Adv. Electron. Mater.* **2015**, *1*, 1400063.
(317) Park, B.; Kim, J.; Kang, D.; Jeong, C.; Kim, K. S.; Kim, J. U.; Yoo, P. J.; Kim, T. I. Dramatically Enhanced Mechanosensitivity and Signal-to-Noise Ratio of Nanoscale Crack-Based Sensors: Effect of Crack Depth. *Adv. Mater.* **2016**, *28*, 8130−8137.
(318) Liu, Y.; Norton, J. J.; Qazi, R.; Zou, Z.; Ammann, K. R.; Liu, H.; Yan, L.; Tran, P. L.; Jang, K. I.; Lee, J. W.; et al. Epidermal Mechano-Acoustic Sensing Electronics for Cardiovascular Diagnostics and Human-Machine Interfaces. *Sci. Adv.* **2016**, *2*, No. e1601185.
(319) Cohen, D. J.; Mitra, D.; Peterson, K.; Maharbiz, M. M. A Highly Elastic, Capacitive Strain Gauge Based on Percolating Nanotube Networks. *Nano Lett.* **2012**, *12*, 1821−1825.
(320) Cai, L.; Song, L.; Luan, P.; Zhang, Q.; Zhang, N.; Gao, Q.; Zhao, D.; Zhang, X.; Tu, M.; Yang, F.; et al. Super-Stretchable, Transparent Carbon Nanotube-Based Capacitive Strain Sensors for Human Motion Detection. *Sci. Rep.* **2013**, *3*, 3048.
(321) Yao, S. S.; Zhu, Y. Wearable Multifunctional Sensors Using Printed Stretchable Conductors Made of Silver Nanowires. *Nanoscale* **2014**, *6*, 2345−2352.
(322) Woo, S. J.; Kong, J. H.; Kim, D. G.; Kim, J. M. A Thin All-Elastomeric Capacitive Pressure Sensor Array Based on Micro-Contact Printed Elastic Conductors. *J. Mater. Chem. C* **2014**, *2*, 4415−4422.
(323) Park, S.; Vosguerichian, M.; Bao, Z. A Review of Fabrication and Applications of Carbon Nanotube Film-Based Flexible Electronics. *Nanoscale* **2013**, *5*, 1727−1752.
(324) Hu, W. L.; Niu, X. F.; Zhao, R.; Pei, Q. B. Elastomeric Transparent Capacitive Sensors Based on an Interpenetrating Composite of Silver Nanowires and Polyurethane. *Appl. Phys. Lett.* **2013**, *102*, No. 083303.
(325) Kim, S. R.; Kim, J. H.; Park, J. W. Wearable and Transparent Capacitive Strain Sensor with High Sensitivity Based on Patterned Ag Nanowire Networks. *ACS Appl. Mater. Interfaces* **2017**, *9*, 26407−26416.
(326) Pang, Y.; Zhang, K.; Yang, Z.; Jiang, S.; Ju, Z.; Li, Y.; Wang, X.; Wang, D.; Jian, M.; Zhang, Y.; et al. Epidermis Microstructure Inspired Graphene Pressure Sensor with Random Distributed Spinosum for High Sensitivity and Large Linearity. *ACS Nano* **2018**, *12*, 2346−2354.
(327) Kim, S. Y.; Park, S.; Park, H. W.; Park, D. H.; Jeong, Y.; Kim, D. H. Highly Sensitive and Multimodal All-Carbon Skin Sensors Capable of Simultaneously Detecting Tactile and Biological Stimuli. *Adv. Mater.* **2015**, *27*, 4178−4185.
(328) Kenry; Yeo, J. C.; Lim, C. T. Emerging Flexible and Wearable Physical Sensing Platforms for Healthcare and Biomedical Applications. *Microsyst. Nanoeng.* **2016**, *2*, 16043.
(329) Choong, C. L.; Shim, M. B.; Lee, B. S.; Jeon, S.; Ko, D. S.; Kang, T. H.; Bae, J.; Lee, S. H.; Byun, K. E.; Im, J.; et al. Highly Stretchable Resistive Pressure Sensors Using a Conductive Elastomeric Composite on a Micropyramid Array. *Adv. Mater.* **2014**, *26*, 3451−3458.
(330) Zhu, Y. S.; Li, J. W.; Cai, H. B.; Wu, Y. M.; Ding, H. Y.; Pan, N.; Wang, X. P. Highly Sensitive and Skin-Like Pressure Sensor Based on Asymmetric Double-Layered Structures of Reduced Graphite Oxide. *Sens. Actuators, B* **2018**, *255*, 1262−1267.

DOI: 10.1021/acs.chemrev.8b00573
Chem. Rev. 2019, 119, 5461−5533

(331) Zhu, B.; Niu, Z.; Wang, H.; Leow, W. R.; Wang, H.; Li, Y.; Zheng, L.; Wei, J.; Huo, F.; Chen, X. Microstructured Graphene Arrays for Highly Sensitive Flexible Tactile Sensors. *Small* **2014**, *10*, 3625−3631.
(332) Bae, G. Y.; Pak, S. W.; Kim, D.; Lee, G.; Kim, D. H.; Chung, Y.; Cho, K. Linearly and Highly Pressure-Sensitive Electronic Skin Based on a Bioinspired Hierarchical Structural Array. *Adv. Mater.* **2016**, *28*, 5300−5306.
(333) Pan, L.; Chortos, A.; Yu, G.; Wang, Y.; Isaacson, S.; Allen, R.; Shi, Y.; Dauskardt, R.; Bao, Z. An Ultra-Sensitive Resistive Pressure Sensor Based on Hollow-Sphere Microstructure Induced Elasticity in Conducting Polymer Film. *Nat. Commun.* **2014**, *5*, 3002.
(334) Park, J.; Lee, Y.; Hong, J.; Lee, Y.; Ha, M.; Jung, Y.; Lim, H.; Kim, S. Y.; Ko, H. Tactile-Direction-Sensitive and Stretchable Electronic Skins Based on Human-Skin-Inspired Interlocked Microstructures. *ACS Nano* **2014**, *8*, 12020−12029.
(335) Park, J.; Lee, Y.; Hong, J.; Ha, M.; Jung, Y. D.; Lim, H.; Kim, S. Y.; Ko, H. Giant Tunneling Piezoresistance of Composite Elastomers with Interlocked Microdome Arrays for Ultrasensitive and Multimodal Electronic Skins. *ACS Nano* **2014**, *8*, 4689−4697.
(336) Kim, K. H.; Hong, S. K.; Jang, N. S.; Ha, S. H.; Lee, H. W.; Kim, J. M. Wearable Resistive Pressure Sensor Based on Highly Flexible Carbon Composite Conductors with Irregular Surface Morphology. *ACS Appl. Mater. Interfaces* **2017**, *9*, 17499−17507.
(337) Shi, J.; Wang, L.; Dai, Z.; Zhao, L.; Du, M.; Li, H.; Fang, Y. Multiscale Hierarchical Design of a Flexible Piezoresistive Pressure Sensor with High Sensitivity and Wide Linearity Range. *Small* **2018**, *14*, No. 1800819.
(338) Park, S. J.; Kim, J.; Chu, M.; Khine, M. Flexible Piezoresistive Pressure Sensor Using Wrinkled Carbon Nanotube Thin Films for Human Physiological Signals. *Adv. Mater. Technol.* **2018**, *3*, 1700158.
(339) Pang, Y.; Tian, H.; Tao, L.; Li, Y.; Wang, X.; Deng, N.; Yang, Y.; Ren, T. L. Flexible, Highly Sensitive, and Wearable Pressure and Strain Sensors with Graphene Porous Network Structure. *ACS Appl. Mater. Interfaces* **2016**, *8*, 26458−26462.
(340) Jung, S.; Kim, J. H.; Kim, J.; Choi, S.; Lee, J.; Park, I.; Hyeon, T.; Kim, D. H. Reverse-Micelle-Induced Porous Pressure-Sensitive Rubber for Wearable Human-Machine Interfaces. *Adv. Mater.* **2014**, *26*, 4825−4830.
(341) Yao, H. B.; Ge, J.; Wang, C. F.; Wang, X.; Hu, W.; Zheng, Z. J.; Ni, Y.; Yu, S. H. A Flexible and Highly Pressure-Sensitive Graphene-Polyurethane Sponge Based on Fractured Microstructure Design. *Adv. Mater.* **2013**, *25*, 6692−6698.
(342) Chen, H. T.; Miao, L. M.; Su, Z. M.; Song, Y.; Han, M. D.; Chen, X. X.; Cheng, X. L.; Chen, D. M.; Zhang, H. X. Fingertip-Inspired Electronic Skin Based on Triboelectric Sliding Sensing and Porous Piezoresistive Pressure Detection. *Nano Energy* **2017**, *40*, 65−72.
(343) Ding, Y.; Yang, J.; Tolle, C. R.; Zhu, Z. Flexible and Compressible Pedot:Pss@Melamine Conductive Sponge Prepared Via One-Step Dip Coating as Piezoresistive Pressure Sensor for Human Motion Detection. *ACS Appl. Mater. Interfaces* **2018**, *10*, 16077−16086.
(344) Hou, C.; Wang, H.; Zhang, Q.; Li, Y.; Zhu, M. Highly Conductive, Flexible, and Compressible All-Graphene Passive Electronic Skin for Sensing Human Touch. *Adv. Mater.* **2014**, *26*, 5018−5024.
(345) Zhao, X. L.; Hua, Q. L.; Yu, R. M.; Zhang, Y.; Pan, C. F. Flexible, Stretchable and Wearable Multifunctional Sensor Array as Artificial Electronic Skin for Static and Dynamic Strain Mapping. *Adv. Electron. Mater.* **2015**, *1*, 1500142.
(346) Mannsfeld, S. C.; Tee, B. C.; Stoltenberg, R. M.; Chen, C. V.; Barman, S.; Muir, B. V.; Sokolov, A. N.; Reese, C.; Bao, Z. Highly Sensitive Flexible Pressure Sensors with Microstructured Rubber Dielectric Layers. *Nat. Mater.* **2010**, *9*, 859−864.
(347) Park, K. I.; Son, J. H.; Hwang, G. T.; Jeong, C. K.; Ryu, J.; Koo, M.; Choi, I.; Lee, S. H.; Byun, M.; Wang, Z. L.; et al. Highly-Efficient, Flexible Piezoelectric Pzt Thin Film Nanogenerator on Plastic Substrates. *Adv. Mater.* **2014**, *26*, 2514−2520.
(348) Zhu, G.; Yang, R.; Wang, S.; Wang, Z. L. Flexible High-Output Nanogenerator Based on Lateral Zno Nanowire Array. *Nano Lett.* **2010**, *10*, 3151−3155.
(349) Xin, Y.; Sun, H. S.; Tian, H. Y.; Guo, C.; Li, X.; Wang, S. H.; Wang, C. The Use of Polyvinylidene Fluoride (Pvdf) Films as Sensors for Vibration Measurement: A Brief Review. *Ferroelectrics* **2016**, *502*, 28−42.
(350) Wang, G.; Liu, T.; Sun, X.-C.; Li, P.; Xu, Y.-S.; Hua, J.-G.; Yu, Y.-H.; Li, S.-X.; Dai, Y.-Z.; Song, X.-Y.; et al. Flexible Pressure Sensor Based on Pvdf Nanofiber. *Sens. Actuators, A* **2018**, *280*, 319−325.
(351) Trung, T. Q.; Tien, N. T.; Seol, Y. G.; Lee, N. E. Transparent and Flexible Organic Field-Effect Transistor for Multi-Modal Sensing. *Org. Electron.* **2012**, *13*, 533−540.
(352) Dagdeviren, C.; Joe, P.; Tuzman, O. L.; Park, K. I.; Lee, K. J.; Shi, Y.; Huang, Y. G.; Rogers, J. A. Recent Progress in Flexible and Stretchable Piezoelectric Devices for Mechanical Energy Harvesting, Sensing and Actuation. *Extreme Mech Lett.* **2016**, *9*, 269−281.
(353) Zhang, W. G.; Zhu, R.; Nguyen, V.; Yang, R. S. Highly Sensitive and Flexible Strain Sensors Based on Vertical Zinc Oxide Nanowire Arrays. *Sens. Actuators, A* **2014**, *205*, 164−169.
(354) Persano, L.; Dagdeviren, C.; Su, Y.; Zhang, Y.; Girardo, S.; Pisignano, D.; Huang, Y.; Rogers, J. A. High Performance Piezoelectric Devices Based on Aligned Arrays of Nanofibers of Poly-(Vinylidenefluoride-Co-Trifluoroethylene). *Nat. Commun.* **2013**, *4*, 1633.
(355) Kennedy, D. A.; Lee, T.; Seely, D. A Comparative Review of Thermography as a Breast Cancer Screening Technique. *Integr. Cancer Ther.* **2009**, *8*, 9−16.
(356) Barnes, R. B. Thermography of the Human Body. *Science* **1963**, *140*, 870−877.
(357) Lahiri, B. B.; Bagavathiappan, S.; Jayakumar, T.; Philip, J. Medical Applications of Infrared Thermography: A Review. *Infrared Phys. Technol.* **2012**, *55*, 221−235.
(358) Dowding, D.; Freeman, S.; Nimmo, S.; Smith, D.; Wisniewski, M. An Investigation into the Accuracy of Different Types of Thermometers. *Prof. Nurse* **2002**, *18*, 166−168.
(359) Webb, R. C.; Krishnan, S.; Rogers, J. A. Ultrathin, Skin-Like Devices for Precise, Continuous Thermal Property Mapping of Human Skin and Soft Tissues. In *Stretchable Bioelectronics for Medical Devices and Systems*; Rogers, J., Ghaffari, R., Kim, D.-H., Eds.; Springer, 2016; pp 117−132.
(360) Krishnan, S. R.; Ray, T. R.; Ayer, A. B.; Ma, Y.; Gutruf, P.; Lee, K.; Lee, J. Y.; Wei, C.; Feng, X.; Ng, B.; et al. Epidermal Electronics for Noninvasive, Wireless, Quantitative Assessment of Ventricular Shunt Function in Patients with Hydrocephalus. *Sci. Transl. Med.* **2018**, *10*, No. eaat8437.
(361) Jeon, J.; Lee, H. B.; Bao, Z. Flexible Wireless Temperature Sensors Based on Ni Microparticle-Filled Binary Polymer Composites. *Adv. Mater.* **2013**, *25*, 850−855.
(362) Hong, S. Y.; Lee, Y. H.; Park, H.; Jin, S. W.; Jeong, Y. R.; Yun, J.; You, I.; Zi, G.; Ha, J. S. Stretchable Active Matrix Temperature Sensor Array of Polyaniline Nanofibers for Electronic Skin. *Adv. Mater.* **2016**, *28*, 930−935.
(363) Hanif, A.; Trung, T. Q.; Siddiqui, S.; Toi, P. T.; Lee, N. E. Stretchable, Transparent, Tough, Ultrathin, and Self-Limiting Skin-Like Substrate for Stretchable Electronics. *ACS Appl. Mater. Interfaces* **2018**, *10*, 27297−27307.
(364) Wang, Q.; Yu, Y.; Yang, J.; Liu, J. Fast Fabrication of Flexible Functional Circuits Based on Liquid Metal Dual-Trans Printing. *Adv. Mater.* **2015**, *27*, 7109−7116.
(365) Zhu, C.; Chortos, A.; Wang, Y.; Pfattner, R.; Lei, T.; Hinckley, A. C.; Pochorovski, I.; Yan, X.; To, J. W.-F.; Oh, J. Y.; Tok, J. B.-H.; Bao, Z.; Murmann, B. Stretchable Temperature-Sensing Circuits with Strain Suppression Based on Carbon Nanotube Transistors. *Nat. Electron.* **2018**, *1*, 183−190.
(366) Bendi, R.; Bhavanasi, V.; Parida, K.; Nguyen, V. C.; Sumboja, A.; Tsukagoshi, K.; Lee, P. S. Self-Powered Graphene Thermistor. *Nano Energy* **2016**, *26*, 586−594.

DOI: 10.1021/acs.chemrev.8b00573
Chem. Rev. 2019, 119, 5461−5533

(367) Kong, D.; Le, L. T.; Li, Y.; Zunino, J. L.; Lee, W. Temperature-Dependent Electrical Properties of Graphene Inkjet-Printed on Flexible Materials. *Langmuir* **2012**, *28*, 13467−13472.
(368) Yan, C.; Wang, J.; Lee, P. S. Stretchable Graphene Thermistor with Tunable Thermal Index. *ACS Nano* **2015**, *9*, 2130−2137.
(369) Yang, J.; Wei, D. P.; Tang, L. L.; Song, X. F.; Luo, W.; Chu, J.; Gao, T. P.; Shi, H. F.; Du, C. L. Wearable Temperature Sensor Based on Graphene Nanowalls. *RSC Adv.* **2015**, *5*, 25609−25615.
(370) Trung, T. Q.; Ramasundaram, S.; Hwang, B. U.; Lee, N. E. An All-Elastomeric Transparent and Stretchable Temperature Sensor for Body-Attachable Wearable Electronics. *Adv. Mater.* **2016**, *28*, 502−509.
(371) Agarwal, R.; Mazhari, B. An Organic Temperature Sensor Based on Asymmetric Metal Insulator Semiconductor Capacitor with Electrically Tunable Sensing Area. *IEEE Sens. Lett.* **2018**, *2*, 1−4.
(372) Wang, C.; Xia, K.; Zhang, M.; Jian, M.; Zhang, Y. An All-Silk-Derived Dual-Mode E-Skin for Simultaneous Temperature-Pressure Detection. *ACS Appl. Mater. Interfaces* **2017**, *9*, 39484−39492.
(373) Yamamoto, Y.; Yamamoto, D.; Takada, M.; Naito, H.; Arie, T.; Akita, S.; Takei, K. Efficient Skin Temperature Sensor and Stable Gel-Less Sticky Ecg Sensor for a Wearable Flexible Healthcare Patch. *Adv. Healthcare Mater.* **2017**, *6*, 1700495.
(374) Choe, A.; Yeom, J.; Shanker, R.; Kim, M. P.; Kang, S.; Ko, H. Stretchable and Wearable Colorimetric Patches Based on Thermoresponsive Plasmonic Microgels Embedded in a Hydrogel Film. *NPG Asia Mater.* **2018**, *10*, 912−922.
(375) Bian, Z. G.; Song, J. Z.; Webb, R. C.; Bonifas, A. P.; Rogers, J. A.; Huang, Y. G. Thermal Analysis of Ultrathin, Compliant Sensors for Characterization of the Human Skin. *RSC Adv.* **2014**, *4*, 5694−5697.
(376) Zhang, Y.; Webb, R. C.; Luo, H.; Xue, Y.; Kurniawan, J.; Cho, N. H.; Krishnan, S.; Li, Y.; Huang, Y.; Rogers, J. A. Theoretical and Experimental Studies of Epidermal Heat Flux Sensors for Measurements of Core Body Temperature. *Adv. Healthcare Mater.* **2016**, *5*, 119−127.
(377) Yokota, T.; Inoue, Y.; Terakawa, Y.; Reeder, J.; Kaltenbrunner, M.; Ware, T.; Yang, K.; Mabuchi, K.; Murakawa, T.; Sekino, M.; et al. Ultraflexible, Large-Area, Physiological Temperature Sensors for Multipoint Measurements. *Proc. Natl. Acad. Sci. U. S. A.* **2015**, *112*, 14533−14538.
(378) Gao, L.; Zhang, Y.; Malyarchuk, V.; Jia, L.; Jang, K. I.; Webb, R. C.; Fu, H.; Shi, Y.; Zhou, G.; Shi, L.; et al. Epidermal Photonic Devices for Quantitative Imaging of Temperature and Thermal Transport Characteristics of the Skin. *Nat. Commun.* **2014**, *5*, 4938.
(379) Lundberg, B.; Sundqvist, B. Resistivity of a Composite Conducting Polymer as a Function of Temperature, Pressure, and Environment - Applications as a Pressure and Gas Concentration Transducer. *J. Appl. Phys.* **1986**, *60*, 1074−1079.
(380) Pertijs, M. A. P.; Makinwa, K. A. A.; Huijsing, J. H. A Cmos Smart Temperature Sensor with a 3 Sigma Inaccuracy of ± 0.1 Degrees C from −55 Degrees C to 125 Degrees C. *IEEE J. Solid-State Circuits* **2005**, *40*, 2805−2815.
(381) Salowitz, N. P.; Guo, Z. Q.; Kim, S. J.; Li, Y. H.; Lanzara, G.; Chang, F. K. Microfabricated Expandable Sensor Networks for Intelligent Sensing Materials. *IEEE Sens. J.* **2014**, *14*, 2138−2144.
(382) Elias, P. M. The Skin Barrier as an Innate Immune Element. *Semin. Immunopathol.* **2007**, *29*, 3−14.
(383) Rawlings, A. V.; Harding, C. R. Moisturization and Skin Barrier Function. *Dermatol. Ther.* **2004**, *17*, 43−48.
(384) Walters, K. A.; Roberts, M. S. The Structure and Function of Skin. *Drugs and the Pharmaceutical Sciences* **2002**, *119*, 1−40.
(385) Gustafsson, S. E. Transient Plane Source Techniques for Thermal-Conductivity and Thermal-Diffusivity Measurements of Solid Materials. *Rev. Sci. Instrum.* **1991**, *62*, 797−804.
(386) Webb, R. C.; Ma, Y.; Krishnan, S.; Li, Y.; Yoon, S.; Guo, X.; Feng, X.; Shi, Y.; Seidel, M.; Cho, N. H.; et al. Epidermal Devices for Noninvasive, Precise, and Continuous Mapping of Macrovascular and Microvascular Blood Flow. *Sci. Adv.* **2015**, *1*, No. e1500701.
(387) Cahill, D. G. Thermal Conductivity Measurement from 30 to 750 K: The 3ω Method. *Rev. Sci. Instrum.* **1990**, *61*, 802−808.
(388) Tian, L.; Li, Y.; Webb, R. C.; Krishnan, S.; Bian, Z.; Song, J.; Ning, X.; Crawford, K.; Kurniawan, J.; Bonifas, A.; et al. Sensors: Flexible and Stretchable 3ω Sensors for Thermal Characterization of Human Skin. *Adv. Funct. Mater.* **2017**, *27*, 1701282.
(389) Krishnan, S. R.; Su, C.-J.; Xie, Z.; Patel, M.; Madhvapathy, S. R.; Xu, Y.; Freudman, J.; Ng, B.; Heo, S. Y.; Wang, H.; et al. Wireless, Battery-Free Epidermal Electronics for Continuous, Quantitative, Multimodal Thermal Characterization of Skin. *Small* **2018**, *14*, 1803192.
(390) Dagdeviren, C.; Shi, Y.; Joe, P.; Ghaffari, R.; Balooch, G.; Usgaonkar, K.; Gur, O.; Tran, P. L.; Crosby, J. R.; Meyer, M.; et al. Conformal Piezoelectric Systems for Clinical and Experimental Characterization of Soft Tissue Biomechanics. *Nat. Mater.* **2015**, *14*, 728−736.
(391) Takenouchi, M.; Suzuki, H.; Tagami, H. Hydration Characteristics of Pathologic Stratum Corneum−Evaluation of Bound Water. *J. Invest. Dermatol.* **1986**, *87*, 574−576.
(392) Clarys, P.; Clijsen, R.; Taeymans, J.; Barel, A. O. Hydration Measurements of the Stratum Corneum: Comparison between the Capacitance Method (Digital Version of the Corneometer Cm 825®) and the Impedance Method (Skicon-200ex®). *Skin Res. Technol.* **2012**, *18*, 316−323.
(393) Frödin, T.; Helander, P.; Molin, L.; Skogh, M. Hydration of Human Stratum Corneum Studied in Vivo by Optothermal Infrared Spectrometry, Electrical Capacitance Measurement, and Evaporimetry. *Acta Derm. Venereol.* **1987**, *68*, 461−467.
(394) Batt, M. D.; Fairhurst, E. Hydration of the Stratum Corneum. *Int. J. Cosmet. Sci.* **1986**, *8*, 253−264.
(395) Querleux, B.; Richard, S.; Bittoun, J.; Jolivet, O.; Idy-Peretti, I.; Bazin, R.; Leveque, J. L. In Vivo Hydration Profile in Skin Layers by High-Resolution Magnetic Resonance Imaging. *Skin Pharmacol.* **2004**, *7*, 210−216.
(396) Schafer, P.; Bewick-Sonntag, C.; Capri, M. G.; Berardesca, E. Physiological Changes in Skin Barrier Function in Relation to Occlusion Level, Exposure Time and Climatic Conditions. *Skin Pharmacol. Appl. Skin Physiol.* **2002**, *15*, 7−19.
(397) Tang, H.; Blankschtein, D.; Langer, R. Prediction of Steady-State Skin Permeabilities of Polar and Nonpolar Permeants across Excised Pig Skin Based on Measurements of Transient Diffusion: Characterization of Hydration Effects on the Skin Porous Pathway. *J. Pharm. Sci.* **2002**, *91*, 1891−1907.
(398) Verdier-Sevrain, S.; Bonte, F. Skin Hydration: A Review on Its Molecular Mechanisms. *J. Cosmet. Dermatol.* **2007**, *6*, 75−82.
(399) Yamamoto, T.; Yamamoto, Y. Electrical Properties of the Epidermal Stratum Corneum. *Med. Biol. Eng.* **1976**, *14*, 151−158.
(400) Blank, I. H.; Moloney, J.; Emslie, A. G.; Simon, I.; Apt, C. The Diffusion of Water across the Stratum-Corneum as a Function of Its Water-Content. *J. Invest. Dermatol.* **1984**, *82*, 188−194.
(401) Blank, I. H. Factors Which Influence the Water Content of the Stratum Corneum. *J. Invest. Dermatol.* **1952**, *18*, 433−440.
(402) Krishnan, S.; Shi, Y. Z.; Webb, R. C.; Ma, Y. J.; Bastien, P.; Crawford, K. E.; Wang, A.; Feng, X.; Manco, M.; Kurniawan, J.; et al. Multimodal Epidermal Devices for Hydration Monitoring. *Microsyst. Nanoeng.* **2017**, *3*, 17014.
(403) Huang, X.; Yeo, W. H.; Liu, Y.; Rogers, J. A. Epidermal Differential Impedance Sensor for Conformal Skin Hydration Monitoring. *Biointerphases* **2012**, *7*, 52.
(404) Alanen, E.; Nuutinen, J.; Nicklen, K.; Lahtinen, T.; Monkkonen, J. Measurement of Hydration in the Stratum Corneum with the Moisturemeter and Comparison with the Corneometer. *Skin Res. Technol.* **2004**, *10*, 32−37.
(405) Huang, X.; Cheng, H.; Chen, K.; Zhang, Y.; Zhang, Y.; Liu, Y.; Zhu, C.; Ouyang, S. C.; Kong, G. W.; Yu, C.; Rogers, J. A. Epidermal Impedance Sensing Sheets for Precision Hydration Assessment and Spatial Mapping. *IEEE Trans. Biomed. Eng.* **2013**, *60*, 2848−2857.
(406) Madhvapathy, S. R.; Ma, Y. J.; Patel, M.; Krishnan, S.; Wei, C.; Li, Y. J.; Xu, S.; Feng, X.; Huang, Y. G.; Rogers, J. A. Epidermal Electronic Systems for Measuring the Thermal Properties of Human

DOI: 10.1021/acs.chemrev.8b00573
Chem. Rev. 2019, 119, 5461−5533

Skin at Depths of up to Several Millimeters. *Adv. Funct. Mater.* **2018**, *28*, 1802083.
(407) Pawlaczyk, M.; Lelonkiewicz, M.; Wieczorowski, M. Age-Dependent Biomechanical Properties of the Skin. *Postep. Derm. Alergol.* **2013**, *30*, 302−306.
(408) Thacker, J. G.; Stalnecker, M. C.; Allaire, P. E.; Edgerton, M. T.; Rodeheaver, G. T.; Edlich, R. F. Practical Applications of Skin Biomechanics. *Clin. Plast. Surg.* **1977**, *4*, 167−171.
(409) Balbir-Gurman, A.; Denton, C. P.; Nichols, B.; Knight, C. J.; Nahir, A. M.; Martin, G.; Black, C. M. Non-Invasive Measurement of Biomechanical Skin Properties in Systemic Sclerosis. *Ann. Rheum. Dis.* **2002**, *61*, 237−241.
(410) Shi, Y.; Dagdeviren, C.; Rogers, J. A.; Gao, C. F.; Huang, Y. An Analytic Model for Skin Modulus Measurement Via Conformal Piezoelectric Systems. *J. Appl. Mech.* **2015**, *82*, No. 091007.
(411) Michard, F. A Sneak Peek into Digital Innovations and Wearable Sensors for Cardiac Monitoring. *J. Clin. Monit. Comput.* **2017**, *31*, 253−259.
(412) Doutreleau, S.; Canuet, M.; Enache, I.; Di Marco, P.; Lonsdorfer, E.; Oswald-Mammoser, M.; Charloux, A. Right Heart Hemodynamics in Pulmonary Hypertension- an Echocardiography and Catheterization Study. *Circ. J.* **2016**, *80*, 2019−2025.
(413) Wren, C.; Reinhardt, Z.; Khawaja, K. Twenty-Year Trends in Diagnosis of Life-Threatening Neonatal Cardiovascular Malformations. *Arch. Dis. Child. Fetal Neonatal Ed.* **2008**, *93*, F33−35.
(414) Jobsis, F. F. Noninvasive, Infrared Monitoring of Cerebral and Myocardial Oxygen Sufficiency and Circulatory Parameters. *Science* **1977**, *198*, 1264−1267.
(415) Jeong, Y. R.; Park, H.; Jin, S. W.; Hong, S. Y.; Lee, S. S.; Ha, J. S. Highly Stretchable and Sensitive Strain Sensors Using Fragmentized Graphene Foam. *Adv. Funct. Mater.* **2015**, *25*, 4228−4236.
(416) Park, J.; Kim, M.; Lee, Y.; Lee, H. S.; Ko, H. Fingertip Skin-Inspired Microstructured Ferroelectric Skins Discriminate Static/Dynamic Pressure and Temperature Stimuli. *Sci. Adv.* **2015**, *1*, No. e1500661.
(417) Luo, N.; Dai, W.; Li, C.; Zhou, Z.; Lu, L.; Poon, C. C. Y.; Chen, S.-C.; Zhang, Y.; Zhao, N. Flexible Piezoresistive Sensor Patch Enabling Ultralow Power Cuffless Blood Pressure Measurement. *Adv. Funct. Mater.* **2016**, *26*, 1178−1187.
(418) Sharma, M.; Barbosa, K.; Ho, V.; Griggs, D.; Ghirmai, T.; Krishnan, S. K.; Hsiai, T. K.; Chiao, J. C.; Cao, H. Cuff-Less and Continuous Blood Pressure Monitoring: A Methodological Review. *Technologies* **2017**, *5*, 21.
(419) Zhu, Z.; Li, R.; Pan, T. Imperceptible Epidermal-Iontronic Interface for Wearable Sensing. *Adv. Mater.* **2018**, *30*, 1705122.
(420) Flammer, A. J.; Anderson, T.; Celermajer, D. S.; Creager, M. A.; Deanfield, J.; Ganz, P.; Hamburg, N. M.; Luscher, T. F.; Shechter, M.; Taddei, S.; et al. The Assessment of Endothelial Function: From Research into Clinical Practice. *Circulation* **2012**, *126*, 753−767.
(421) Petrofsky, J. S. Resting Blood Flow in the Skin: Does It Exist, and What Is the Influence of Temperature, Aging, and Diabetes? *J. Diabetes Sci. Technol.* **2012**, *6*, 674−685.
(422) Fiala, D.; Lomas, K. J.; Stohrer, M. A Computer Model of Human Thermoregulation for a Wide Range of Environmental Conditions: The Passive System. *J. Appl. Physiol.* **1999**, *87*, 1957−1972.
(423) Charkoudian, N. Skin Blood Flow in Adult Human Thermoregulation: How It Works, When It Does Not, and Why. *Mayo Clin. Proc.* **2003**, *78*, 603−612.
(424) Ganz, W.; Swan, H. J. Measurement of Blood Flow by Thermodilution. *Am. J. Cardiol.* **1972**, *29*, 241−246.
(425) Valvano, J. W.; Allen, J. T.; Bowman, H. F. The Simultaneous Measurement of Thermal Conductivity, Thermal Diffusivity, and Perfusion in Small Volumes of Tissue. *J. Biomech. Eng.* **1984**, *106*, 192−197.
(426) Yang, D.; Converse, M. C.; Mahvi, D. M.; Webster, J. G. Expanding the Bioheat Equation to Include Tissue Internal Water Evaporation During Heating. *IEEE Trans. Biomed. Eng.* **2007**, *54*, 1382−1388.
(427) Allen, J. Photoplethysmography and Its Application in Clinical Physiological Measurement. *Physiol. Meas.* **2007**, *28*, R1−39.
(428) Tremper, K. K. Pulse Oximetry. *Chest* **1989**, *95*, 713−715.
(429) Mendelson, Y. Pulse Oximetry: Theory and Applications for Noninvasive Monitoring. *Clin. Chem.* **1992**, *38*, 1601−1607.
(430) Yelderman, M.; New, W. Evaluation of Pulse Oximetry. *Anesthesiology* **1983**, *59*, 349−351.
(431) Xu, H. H.; Liu, J.; Zhang, J.; Zhou, G. D.; Luo, N. Q.; Zhao, N. Flexible Organic/Inorganic Hybrid near-Infrared Photoplethysmogram Sensor for Cardiovascular Monitoring. *Adv. Mater.* **2017**, *29*, 1700975.
(432) Watthanawisuth, N.; Lomas, T.; Wisitsoraat, A.; Tuantranont, A. Wireless Wearable Pulse Oximeter for Health Monitoring Using Zigbee Wireless Sensor Network. *2010 International Conference on Electrical Engineering/Electronics Computer Telecommunications and Information Technology (ECTI-CON)*, 2010; pp 575−579.
(433) Asada, H. H.; Shaltis, P.; Reisner, A.; Rhee, S.; Hutchinson, R. C. Mobile Monitoring with Wearable Photoplethysmographic Biosensors. *IEEE Eng. Med. Biol. Mag.* **2003**, *22*, 28−40.
(434) Moron, M. J.; Casilari, E.; Luque, R.; Gázquez, J. A. A Wireless Monitoring System for Pulse-Oximetry Sensors. *2005 Systems Communications Proceedings*, 2005; pp 79−84.
(435) Yan, Y. S.; Poon, C. C.; Zhang, Y. T. Reduction of Motion Artifact in Pulse Oximetry by Smoothed Pseudo Wigner-Ville Distribution. *J. Neuroeng. Rehabil.* **2005**, *2*, 3.
(436) Relente, A.; Sison, L. Characterization and Adaptive Filtering of Motion Artifacts in Pulse Oximetry Using Accelerometers. *Proceedings of the Second Joint Engineering in Medicine and Biology, 2002: 24th Annual Conference and the Annual Fall Meeting of the Biomedical Engineering Society EMBS/BMES Conference*, 2002; pp 1769−1770,
(437) Mendelson, Y.; Pujary, C. Measurement Site and Photodetector Size Considerations in Optimizing Power Consumption of a Wearable Reflectance Pulse Oximeter. *2003 Proceedings of the 25th Annual International Conference of the IEEE Engineering in Medicine and Biology Society*, 2003; pp 3016−3019.
(438) Yokota, T.; Zalar, P.; Kaltenbrunner, M.; Jinno, H.; Matsuhisa, N.; Kitanosako, H.; Tachibana, Y.; Yukita, W.; Koizumi, M.; Someya, T. Ultraflexible Organic Photonic Skin. *Sci. Adv.* **2016**, *2*, No. e1501856.
(439) Khan, Y.; Han, D.; Pierre, A.; Ting, J.; Wang, X.; Lochner, C. M.; Bovo, G.; Yaacobi-Gross, N.; Newsome, C.; Wilson, R.; et al. A Flexible Organic Reflectance Oximeter Array. *Proc. Natl. Acad. Sci. U. S. A.* **2018**, *115*, E11015−E11024.
(440) Kim, J.; Salvatore, G. A.; Araki, H.; Chiarelli, A. M.; Xie, Z.; Banks, A.; Sheng, X.; Liu, Y.; Lee, J. W.; Jang, K. I.; et al. Battery-Free, Stretchable Optoelectronic Systems for Wireless Optical Characterization of the Skin. *Sci. Adv.* **2016**, *2*, No. e1600418.
(441) Kim, S. B.; Zhang, Y.; Won, S. M.; Bandodkar, A. J.; Sekine, Y.; Xue, Y.; Koo, J.; Harshman, S. W.; Martin, J. A.; Park, J. M.; et al. Super-Absorbent Polymer Valves and Colorimetric Chemistries for Time-Sequenced Discrete Sampling and Chloride Analysis of Sweat Via Skin-Mounted Soft Microfluidics. *Small* **2018**, *14*, 1703334.
(442) Bandodkar, A. J.; Molinnus, D.; Mirza, O.; Guinovart, T.; Windmiller, J. R.; Valdes-Ramirez, G.; Andrade, F. J.; Schoning, M. J.; Wang, J. Epidermal Tattoo Potentiometric Sodium Sensors with Wireless Signal Transduction for Continuous Non-Invasive Sweat Monitoring. *Biosens. Bioelectron.* **2014**, *54*, 603−609.
(443) Tai, L. C.; Gao, W.; Chao, M. H.; Bariya, M.; Ngo, Q. P.; Shahpar, Z.; Nyein, H. Y. Y.; Park, H.; Sun, J.; Jung, Y.; et al. Methylxanthine Drug Monitoring with Wearable Sweat Sensors. *Adv. Mater.* **2018**, *30*, No. 1707442.
(444) Matzeu, G.; Florea, L.; Diamond, D. Advances in Wearable Chemical Sensor Design for Monitoring Biological Fluids. *Sens. Actuators, B* **2015**, *211*, 403−418.
(445) Barfield, M.; Spooner, N.; Lad, R.; Parry, S.; Fowles, S. Application of Dried Blood Spots Combined with Hplc-Ms/Ms for the Quantification of Acetaminophen in Toxicokinetic Studies. *J. Chromatogr. B: Anal. Technol. Biomed. Life Sci.* **2008**, *870*, 32−37.
(446) Talwar, D.; Davidson, H.; Cooney, J.; O'Reilly, D. S. J. Vitamin B-I Status Assessed by Direct Measurement of Thiamin Pyrophosphate

DOI: 10.1021/acs.chemrev.8b00573
Chem. Rev. 2019, 119, 5461−5533

in Erythrocytes or Whole Blood by HPLC: Comparison with Erythrocyte Transketolase Activation Assay. *Clin. Chem.* **2000**, *46*, 704−710.
(447) Ohno, T.; Shinohara, A.; Kohge, I.; Chiba, M.; Hirata, T. Isotopic Analysis of Fe in Human Red Blood Cells by Multiple Collector-Icp-Mass Spectrometry. *Anal. Sci.* **2004**, *20*, 617−621.
(448) Toffaletti, J.; Hammes, M. E.; Gray, R.; Lineberry, B.; Abrams, B. Lactate Measured in Diluted and Undiluted Whole Blood and Plasma: Comparison of Methods and Effect of Hematocrit. *Clin. Chem.* **1992**, *38*, 2430−2434.
(449) Young, C. C. Evolution of Blood Chemistry Analyzers Based on Ion Selective Electrodes. *J. Chem. Educ.* **1997**, *74*, 177−182.
(450) Davison, R. C.; Coleman, D.; Balmer, J.; Nunn, M.; Theakston, S.; Burrows, M.; Bird, S. Assessment of Blood Lactate: Practical Evaluation of the Biosen 5030 Lactate Analyzer. *Med. Sci. Sports Exercise* **2000**, *32*, 243−247.
(451) Clarke, W. L.; Cox, D.; Gonder-Frederick, L. A.; Carter, W.; Pohl, S. L. Evaluating Clinical Accuracy of Systems for Self-Monitoring of Blood Glucose. *Diabetes Care* **1987**, *10*, 622−628.
(452) Bandodkar, A. J.; Imani, S.; Nunez-Flores, R.; Kumar, R.; Wang, C.; Mohan, A. M. V.; Wang, J.; Mercier, P. P. Re-Usable Electrochemical Glucose Sensors Integrated into a Smartphone Platform. *Biosens. Bioelectron.* **2018**, *101*, 181−187.
(453) Wagner, J.; Malchoff, C.; Abbott, G. Invasiveness as a Barrier to Self-Monitoring of Blood Glucose in Diabetes. *Diabetes Technol. Ther.* **2005**, *7*, 612−619.
(454) Joseph, J. I.; Hipszer, B.; Mraovic, B.; Chervoneva, I.; Joseph, M.; Grunwald, Z. Clinical Need for Continuous Glucose Monitoring in the Hospital. *J. Diabetes Sci. Technol.* **2009**, *3*, 1309−1318.
(455) Godek, S. F.; Peduzzi, C.; Burkholder, R.; Condon, S.; Dorshimer, G.; Bartolozzi, A. R. Sweat Rates, Sweat Sodium Concentrations, and Sodium Losses in 3 Groups of Professional Football Players. *J. Athl. Train.* **2010**, *45*, 364−371.
(456) Holmes, N. A.; Miller, V. S.; Schneider, J.; Hasan, O.; Bates, G. P. Plasma Sodium Levels and Dietary Sodium Intake in Manual Workers in the Middle East. *Ann. Occup. Hyg.* **2011**, *55*, 397−402.
(457) Hussain, M. A.; Khan, P.; Kwak Kyung, S. WSN Research Activities for Military Application. *11th International Conference on Advanced Communication Technology, Feb 15−18*, 2009; pp 271−274.
(458) Gibson, L. E.; Cooke, R. E. A Test for Concentration of Electrolytes in Sweat in Cystic Fibrosis of the Pancreas Utilizing Pilocarpine by Iontophoresis. *Pediatrics* **1959**, *23*, 545−549.
(459) Montain, S. J.; Sawka, M. N.; Wenger, C. B. Hyponatremia Associated with Exercise: Risk Factors and Pathogenesis. *Exercise Sport Sci. Rev.* **2001**, *29*, 113−117.
(460) Dill, D. B.; Hall, F. G.; Van Beaumont, W. Sweat Chloride Concentration: Sweat Rate, Metabolic Rate, Skin Temperature, and Age. *J. Appl. Physiol.* **1966**, *21*, 99−106.
(461) Sakharov, D. A.; Shkurnikov, M. U.; Vagin, M. Y.; Yashina, E. I.; Karyakin, A. A.; Tonevitsky, A. G. Relationship between Lactate Concentrations in Active Muscle Sweat and Whole Blood. *Bull. Exp. Biol. Med.* **2010**, *150*, 83−85.
(462) Jia, W.; Bandodkar, A. J.; Valdes-Ramirez, G.; Windmiller, J. R.; Yang, Z.; Ramirez, J.; Chan, G.; Wang, J. Electrochemical Tattoo Biosensors for Real-Time Noninvasive Lactate Monitoring in Human Perspiration. *Anal. Chem.* **2013**, *85*, 6553−6560.
(463) Imani, S.; Bandodkar, A. J.; Mohan, A. M.; Kumar, R.; Yu, S.; Wang, J.; Mercier, P. P. A Wearable Chemical-Electrophysiological Hybrid Biosensing System for Real-Time Health and Fitness Monitoring. *Nat. Commun.* **2016**, *7*, 11650.
(464) Khodagholy, D.; Curto, V. F.; Fraser, K. J.; Gurfinkel, M.; Byrne, R.; Diamond, D.; Malliaras, G. G.; Benito-Lopez, F.; Owens, R. M. Organic Electrochemical Transistor Incorporating an Ionogel as a Solid State Electrolyte for Lactate Sensing. *J. Mater. Chem.* **2012**, *22*, 4440−4443.
(465) Garcia, S. O.; Ulyanova, Y. V.; Figueroa-Teran, R.; Bhatt, K. H.; Singhal, S.; Atanassov, P. Wearable Sensor System Powered by a Biofuel Cell for Detection of Lactate Levels in Sweat. *ECS J. Solid State Sci. Technol.* **2016**, *5*, M3075−M3081.
(466) Alam, F.; RoyChoudhury, S.; Jalal, A. H.; Umasankar, Y.; Forouzanfar, S.; Akter, N.; Bhansali, S.; Pala, N. Lactate Biosensing: The Emerging Point-of-Care and Personal Health Monitoring. *Biosens. Bioelectron.* **2018**, *117*, 818−829.
(467) Polliack, A.; Taylor, R.; Bader, D. Sweat Analysis Following Pressure Ischaemia in a Group of Debilitated Subjects. *J. Rehabil. Res. Dev.* **1997**, *34*, 303−308.
(468) Waller, M. F.; Haymes, E. M. The Effects of Heat and Exercise on Sweat Iron Loss. *Med. Sci. Sports Exercise* **1996**, *28*, 197−203.
(469) DeRuisseau, K. C.; Cheuvront, S. N.; Haymes, E. M.; Sharp, R. G. Sweat Iron and Zinc Losses During Prolonged Exercise. *Int. J. Sport Nutr. Exercise Metab.* **2002**, *12*, 428−437.
(470) Cordova, A.; Navas, F. J. Effect of Training on Zinc Metabolism: Changes in Serum and Sweat Zinc Concentrations in Sportsmen. *Ann. Nutr. Metab.* **1998**, *42*, 274−282.
(471) Emaminejad, S.; Gao, W.; Wu, E.; Davies, Z. A.; Yin Yin Nyein, H.; Challa, S.; Ryan, S. P.; Fahad, H. M.; Chen, K.; Shahpar, Z.; et al. Autonomous Sweat Extraction and Analysis Applied to Cystic Fibrosis and Glucose Monitoring Using a Fully Integrated Wearable Platform. *Proc. Natl. Acad. Sci. U. S. A.* **2017**, *114*, 4625−4630.
(472) Abellan-Llobregat, A.; Jeerapan, I.; Bandodkar, A.; Vidal, L.; Canals, A.; Wang, J.; Morallon, E. A Stretchable and Screen-Printed Electrochemical Sensor for Glucose Determination in Human Perspiration. *Biosens. Bioelectron.* **2017**, *91*, 885−891.
(473) Lee, H.; Hong, Y. J.; Baik, S.; Hyeon, T.; Kim, D. H. Enzyme-Based Glucose Sensor: From Invasive to Wearable Device. *Adv. Healthcare Mater.* **2018**, *7*, 1701150.
(474) Hong, Y. J.; Lee, H.; Kim, J.; Lee, M.; Choi, H. J.; Hyeon, T.; Kim, D.-H. Multifunctional Wearable System That Integrates Sweat-Based Sensing and Vital-Sign Monitoring to Estimate Pre-/Post-Exercise Glucose Levels. *Adv. Funct. Mater.* **2018**, *28*, 1805754.
(475) Aguirre, A.; Testa-Weintraub, L. A.; Banderas, J. A.; Haraszthy, G. G.; Reddy, M. S.; Levine, M. J. Sialochemistry: A Diagnostic Tool? *Crit. Rev. Oral Biol. Med.* **1993**, *4*, 343−350.
(476) Mitsubayashi, K.; Arakawa, T. Cavitas Sensors: Contact Lens Type Sensors & Mouthguard Sensors. *Electroanalysis* **2016**, *28*, 1170−1187.
(477) Liu, Q.; Liu, Y.; Wu, F.; Cao, X.; Li, Z.; Alharbi, M.; Abbas, A. N.; Amer, M. R.; Zhou, C. Highly Sensitive and Wearable In2o3 Nanoribbon Transistor Biosensors with Integrated on-Chip Gate for Glucose Monitoring in Body Fluids. *ACS Nano* **2018**, *12*, 1170−1178.
(478) Currano, L. J.; Sage, F. C.; Hagedon, M.; Hamilton, L.; Patrone, J.; Gerasopoulos, K. Wearable Sensor System for Detection of Lactate in Sweat. *Sci. Rep.* **2018**, *8*, 15890.
(479) Xuan, X.; Yoon, H. S.; Park, J. Y. A Wearable Electrochemical Glucose Sensor Based on Simple and Low-Cost Fabrication Supported Micro-Patterned Reduced Graphene Oxide Nanocomposite Electrode on Flexible Substrate. *Biosens. Bioelectron.* **2018**, *109*, 75−82.
(480) Yoon, H.; Xuan, X.; Jeong, S.; Park, J. Y. Wearable, Robust, Non-Enzymatic Continuous Glucose Monitoring System and Its in Vivo Investigation. *Biosens. Bioelectron.* **2018**, *117*, 267−275.
(481) Malhotra, B. D.; Chaubey, A. Biosensors for Clinical Diagnostics Industry. *Sens. Actuators, B* **2003**, *91*, 117−127.
(482) Park, S.; Boo, H.; Chung, T. D. Electrochemical Non-Enzymatic Glucose Sensors. *Anal. Chim. Acta* **2006**, *556*, 46−57.
(483) Bandodkar, A. J.; Jeerapan, I.; You, J. M.; Nunez-Flores, R.; Wang, J. Highly Stretchable Fully-Printed Cnt-Based Electrochemical Sensors and Biofuel Cells: Combining Intrinsic and Design-Induced Stretchability. *Nano Lett.* **2016**, *16*, 721−727.
(484) Windmiller, J. R.; Wang, J. Wearable Electrochemical Sensors and Biosensors: A Review. *Electroanalysis* **2013**, *25*, 29−46.
(485) Coyle, S.; Lau, K. T.; Moyna, N.; O'Gorman, D.; Diamond, D.; Di Francesco, F.; Costanzo, D.; Salvo, P.; Trivella, M. G.; De Rossi, D. E.; et al. Biotex–Biosensing Textiles for Personalised Healthcare Management. *IEEE Trans. Inf. Technol. Biomed.* **2010**, *14*, 364−370.
(486) Modali, A.; Vanjari, S. R. K.; Dendukuri, D. Wearable Woven Electrochemical Biosensor Patch for Non-Invasive Diagnostics. *Electroanalysis* **2016**, *28*, 1276−1282.

DOI: 10.1021/acs.chemrev.8b00573
Chem. Rev. 2019, 119, 5461−5533

(487) Cho, E.; Mohammadifar, M.; Choi, S. A Self-Powered Sensor Patch for Glucose Monitoring in Sweat. *IEEE 30th International Conference on Micro Electro Mechanical Systems (MEMS), Jan 22−26*, 2017; pp 366−369.
(488) Lee, H.; Song, C.; Hong, Y. S.; Kim, M. S.; Cho, H. R.; Kang, T.; Shin, K.; Choi, S. H.; Hyeon, T.; Kim, D. H. Wearable/Disposable Sweat-Based Glucose Monitoring Device with Multistage Transdermal Drug Delivery Module. *Sci. Adv.* **2017**, *3*, e1601314.
(489) Arakawa, T.; Kuroki, Y.; Nitta, H.; Chouhan, P.; Toma, K.; Sawada, S.; Takeuchi, S.; Sekita, T.; Akiyoshi, K.; Minakuchi, S.; et al. Mouthguard Biosensor with Telemetry System for Monitoring of Saliva Glucose: A Novel Cavitas Sensor. *Biosens. Bioelectron.* **2016**, *84*, 106−111.
(490) Zeng, S. W.; Yong, K. T.; Roy, I.; Dinh, X. Q.; Yu, X.; Luan, F. A Review on Functionalized Gold Nanoparticles for Biosensing Applications. *Plasmonics* **2011**, *6*, 491−506.
(491) Shao, Y. Y.; Wang, J.; Wu, H.; Liu, J.; Aksay, I. A.; Lin, Y. H. Graphene Based Electrochemical Sensors and Biosensors: A Review. *Electroanalysis* **2010**, *22*, 1027−1036.
(492) Matharu, Z.; Daggumati, P.; Wang, L.; Dorofeeva, T. S.; Li, Z.; Seker, E. Nanoporous-Gold-Based Electrode Morphology Libraries for Investigating Structure-Property Relationships in Nucleic Acid Based Electrochemical Biosensors. *ACS Appl. Mater. Interfaces* **2017**, *9*, 12959−12966.
(493) Wildgoose, G. G.; Banks, C. E.; Compton, R. G. Metal Nanoparticles and Related Materials Supported on Carbon Nanotubes: Methods and Applications. *Small* **2006**, *2*, 182−193.
(494) Gao, W.; Emaminejad, S.; Nyein, H. Y. Y.; Challa, S.; Chen, K.; Peck, A.; Fahad, H. M.; Ota, H.; Shiraki, H.; Kiriya, D.; et al. Fully Integrated Wearable Sensor Arrays for Multiplexed in Situ Perspiration Analysis. *Nature* **2016**, *529*, 509−514.
(495) Lee, H.; Choi, T. K.; Lee, Y. B.; Cho, H. R.; Ghaffari, R.; Wang, L.; Choi, H. J.; Chung, T. D.; Lu, N.; Hyeon, T.; et al. A Graphene-Based Electrochemical Device with Thermoresponsive Microneedles for Diabetes Monitoring and Therapy. *Nat. Nanotechnol.* **2016**, *11*, 566−572.
(496) Oh, S. Y.; Hong, S. Y.; Jeong, Y. R.; Yun, J.; Park, H.; Jin, S. W.; Lee, G.; Oh, J. H.; Lee, H.; Lee, S.-S.; et al. Skin-Attachable, Stretchable Electrochemical Sweat Sensor for Glucose and Ph Detection. *ACS Appl. Mater. Interfaces* **2018**, *10*, 13729−13740.
(497) Bariya, M.; Nyein, H. Y. Y.; Javey, A. Wearable Sweat Sensors. *Nat. Electron.* **2018**, *1*, 160−171.
(498) Faria, T. Q.; Mingote, A.; Siopa, F.; Ventura, R.; Maycock, C.; Santos, H. Design of New Enzyme Stabilizers Inspired by Glycosides of Hyperthermophilic Microorganisms. *Carbohydr. Res.* **2008**, *343*, 3025−3033.
(499) Kaushik, J. K.; Bhat, R. Why Is Trehalose an Exceptional Protein Stabilizer? An Analysis of the Thermal Stability of Proteins in the Presence of the Compatible Osmolyte Trehalose. *J. Biol. Chem.* **2003**, *278*, 26458−26465.
(500) Simmers, P.; Li, S. K.; Kasting, G.; Heikenfeld, J. Prolonged and Localized Sweat Stimulation by Iontophoretic Delivery of the Slowly-Metabolized Cholinergic Agent Carbachol. *J. Dermatol. Sci.* **2018**, *89*, 40−51.
(501) Kim, J.; Jeerapan, I.; Imani, S.; Cho, T. N.; Bandodkar, A.; Cinti, S.; Mercier, P. P.; Wang, J. Noninvasive Alcohol Monitoring Using a Wearable Tattoo-Based Iontophoretic-Biosensing System. *ACS Sens.* **2016**, *1*, 1011−1019.
(502) Hauke, A.; Simmers, P.; Ojha, Y. R.; Cameron, B. D.; Ballweg, R.; Zhang, T.; Twine, N.; Brothers, M.; Gomez, E.; Heikenfeld, J. Complete Validation of a Continuous and Blood-Correlated Sweat Biosensing Device with Integrated Sweat Stimulation. *Lab Chip* **2018**, *18*, 3750−3759.
(503) Choi, J.; Xue, Y.; Xia, W.; Ray, T. R.; Reeder, J. T.; Bandodkar, A. J.; Kang, D.; Xu, S.; Huang, Y.; Rogers, J. A. Soft, Skin-Mounted Microfluidic Systems for Measuring Secretory Fluidic Pressures Generated at the Surface of the Skin by Eccrine Sweat Glands. *Lab Chip* **2017**, *17*, 2572−2580.
(504) Choi, J.; Kang, D.; Han, S.; Kim, S. B.; Rogers, J. A. Thin, Soft, Skin-Mounted Microfluidic Networks with Capillary Bursting Valves for Chrono-Sampling of Sweat. *Adv. Healthcare Mater.* **2017**, *6*, 1601355.
(505) Choi, J.; Ghaffari, R.; Baker, L. B.; Rogers, J. A. Skin-Interfaced Systems for Sweat Collection and Analytics. *Sci. Adv.* **2018**, *4*, No. eaar3921.
(506) Park, J.; Kim, J.; Kim, S. Y.; Cheong, W. H.; Jang, J.; Park, Y. G.; Na, K.; Kim, Y. T.; Heo, J. H.; Lee, C. Y.; et al. Soft, Smart Contact Lenses with Integrations of Wireless Circuits, Glucose Sensors, and Displays. *Sci. Adv.* **2018**, *4*, No. eaap9841.
(507) Iguchi, S.; Mitsubayashi, K.; Uehara, T.; Ogawa, M. A Wearable Oxygen Sensor for Transcutaneous Blood Gas Monitoring at the Conjunctiva. *Sens. Actuators, B* **2005**, *108*, 733−737.
(508) Kagie, A.; Bishop, D. K.; Burdick, J.; La Belle, J. T.; Dymond, R.; Felder, R.; Wang, J. Flexible Rolled Thick-Film Miniaturized Flow-Cell for Minimally Invasive Amperometric Sensing. *Electroanalysis* **2008**, *20*, 1610−1614.
(509) Kudo, H.; Sawada, T.; Kazawa, E.; Yoshida, H.; Iwasaki, Y.; Mitsubayashi, K. A Flexible and Wearable Glucose Sensor Based on Functional Polymers with Soft-Mems Techniques. *Biosens. Bioelectron.* **2006**, *22*, 558−562.
(510) Liao, Y.-T.; Yao, H.; Lingley, A.; Parviz, B.; Otis, B. P. A 3-Mw Cmos Glucose Sensor for Wireless Contact-Lens Tear Glucose Monitoring. *IEEE J. Solid-State Circuits* **2012**, *47*, 335−344.
(511) Mannoor, M. S.; Tao, H.; Clayton, J. D.; Sengupta, A.; Kaplan, D. L.; Naik, R. R.; Verma, N.; Omenetto, F. G.; McAlpine, M. C. Graphene-Based Wireless Bacteria Detection on Tooth Enamel. *Nat. Commun.* **2012**, *3*, 763.
(512) Kim, J.; Valdes-Ramirez, G.; Bandodkar, A. J.; Jia, W.; Martinez, A. G.; Ramirez, J.; Mercier, P.; Wang, J. Non-Invasive Mouthguard Biosensor for Continuous Salivary Monitoring of Metabolites. *Analyst* **2014**, *139*, 1632−1636.
(513) Mitsubayashi, K. Cavitas Sensors and Sniff-Cam for Biomonitoring: Soft Contact Lens & Mouthguard Sensors, Optical Bio-Sniffing of Human Vocs. *2016 IEEE Sensors, Orlando, FL, Oct 30−Nov 3*, 2016; pp 1−3.
(514) Minamitani, H.; Suzuki, Y.; Iijima, A.; Nagao, T. A Denture Base Type of Sensor System for Simultaneous Monitoring of Hydrogen Ion Concentration Ph and Tissue Temperature in the Oral Cavity. *IEICE Trans. Inf. Syst.* **2002**, *E85-D*, 22−29.
(515) Glennon, T.; O'Quigley, C.; McCaul, M.; Matzeu, G.; Beirne, S.; Wallace, G. G.; Stroiescu, F.; O'Mahoney, N.; White, P.; Diamond, D. 'Sweatch': A Wearable Platform for Harvesting and Analysing Sweat Sodium Content. *Electroanalysis* **2016**, *28*, 1283−1289.
(516) Evans, A. *Potentiometry and Ion Selective Electrodes*; John Wiley and Sons Inc.: New York, 1987.
(517) Zhang, X. J.; Ogorevc, B.; Wang, J. Solid-State Ph Nanoelectrode Based on Polyaniline Thin Film Electrodeposited onto Ion-Beam Etched Carbon Fiber. *Anal. Chim. Acta* **2002**, *452*, 1−10.
(518) Yue, F.; Ngin, T. S.; Hailin, G. A Novel Paper Ph Sensor Based on Polypyrrole. *Sens. Actuators, B* **1996**, *32*, 33−39.
(519) Bobacka, J. Potential Stability of All-Solid-State Ion-Selective Electrodes Using Conducting Polymers as Ion-to-Electron Transducers. *Anal. Chem.* **1999**, *71*, 4932−4937.
(520) Bobacka, J. Conducting Polymer-Based Solid-State Ion-Selective Electrodes. *Electroanalysis* **2006**, *18*, 7−18.
(521) Rose, D. P.; Ratterman, M. E.; Griffin, D. K.; Hou, L.; Kelley-Loughnane, N.; Naik, R. R.; Hagen, J. A.; Papautsky, I.; Heikenfeld, J. C. Adhesive Rfid Sensor Patch for Monitoring of Sweat Electrolytes. *IEEE Trans. Biomed. Eng.* **2015**, *62*, 1457−1465.
(522) Wang, S.; Wu, Y.; Gu, Y.; Li, T.; Luo, H.; Li, L. H.; Bai, Y.; Li, L.; Liu, L.; Cao, Y.; et al. Wearable Sweatband Sensor Platform Based on Gold Nanodendrite Array as Efficient Solid Contact of Ion-Selective Electrode. *Anal. Chem.* **2017**, *89*, 10224−10231.
(523) Curto, V. F.; Fay, C.; Coyle, S.; Byrne, R.; O'Toole, C.; Barry, C.; Hughes, S.; Moyna, N.; Diamond, D.; Benito-Lopez, F. Real-Time Sweat Ph Monitoring Based on a Wearable Chemical Barcode Micro-

DOI: 10.1021/acs.chemrev.8b00573
Chem. Rev. 2019, 119, 5461−5533

Fluidic Platform Incorporating Ionic Liquids. *Sens. Actuators, B* **2012**, *171*, 1327−1334.
(524) Schazmann, B.; Morris, D.; Slater, C.; Beirne, S.; Fay, C.; Reuveny, R.; Moyna, N.; Diamond, D. A Wearable Electrochemical Sensor for the Real-Time Measurement of Sweat Sodium Concentration. *Anal. Methods* **2010**, *2*, 342−348.
(525) Guinovart, T.; Bandodkar, A. J.; Windmiller, J. R.; Andrade, F. J.; Wang, J. A Potentiometric Tattoo Sensor for Monitoring Ammonium in Sweat. *Analyst* **2013**, *138*, 7031−7038.
(526) Bandodkar, A. J.; Hung, V. W.; Jia, W.; Valdes-Ramirez, G.; Windmiller, J. R.; Martinez, A. G.; Ramirez, J.; Chan, G.; Kerman, K.; Wang, J. Tattoo-Based Potentiometric Ion-Selective Sensors for Epidermal Ph Monitoring. *Analyst* **2013**, *138*, 123−128.
(527) Nyein, H. Y.; Gao, W.; Shahpar, Z.; Emaminejad, S.; Challa, S.; Chen, K.; Fahad, H. M.; Tai, L. C.; Ota, H.; Davis, R. W.; et al. A Wearable Electrochemical Platform for Noninvasive Simultaneous Monitoring of Ca(2+) and Ph. *ACS Nano* **2016**, *10*, 7216−7224.
(528) Nakata, S.; Shiomi, M.; Fujita, Y.; Arie, T.; Akita, S.; Takei, K. A Wearable Ph Sensor with High Sensitivity Based on a Flexible Charge-Coupled Device. *Nat. Electron.* **2018**, *1*, 596−603.
(529) Hulanicki, A.; Michalska, A. All-Solid-State Chloride-Selective Electrode with Poly(Pyrrole) Solid Contact. *Electroanalysis* **1995**, *7*, 692−693.
(530) Mousavi, Z.; Teter, A.; Lewenstam, A.; Maj-Zurawska, M.; Ivaska, A.; Bobacka, J. Comparison of Multi-Walled Carbon Nanotubes and Poly(3-Octylthiophene) as Ion-to-Electron Transducers in All-Solid-State Potassium Ion-Selective Electrodes. *Electroanalysis* **2011**, *23*, 1352−1358.
(531) Jaworska, E.; Lewandowski, W.; Mieczkowski, J.; Maksymiuk, K.; Michalska, A. Simple and Disposable Potentiometric Sensors Based on Graphene or Multi-Walled Carbon Nanotubes–Carbon-Plastic Potentiometric Sensors. *Analyst* **2013**, *138*, 2363−2371.
(532) Vázquez, M.; Danielsson, P.; Bobacka, J.; Lewenstam, A.; Ivaska, A. Solution-Cast Films of Poly(3,4-Ethylenedioxythiophene) as Ion-to-Electron Transducers in All-Solid-State Ion-Selective Electrodes. *Sens. Actuators, B* **2004**, *97*, 182−189.
(533) Crespo, G. A.; Macho, S.; Rius, F. X. Ion-Selective Electrodes Using Carbon Nanotubes as Ion-to-Electron Transducers. *Anal. Chem.* **2008**, *80*, 1316−1322.
(534) Ping, J. F.; Wang, Y. X.; Wu, J.; Ying, Y. B. Development of an All-Solid-State Potassium Ion-Selective Electrode Using Graphene as the Solid-Contact Transducer. *Electrochem. Commun.* **2011**, *13*, 1529−1532.
(535) Hoekstra, R.; Blondeau, P.; Andrade, F. J. Ionsens: A Wearable Potentiometric Sensor Patch for Monitoring Total Ion Content in Sweat. *Electroanalysis* **2018**, *30*, 1536−1544.
(536) Gonzalo-Ruiz, J.; Mas, R.; de Haro, C.; Cabruja, E.; Camero, R.; Alonso-Lomillo, M. A.; Munoz, F. J. Early Determination of Cystic Fibrosis by Electrochemical Chloride Quantification in Sweat. *Biosens. Bioelectron.* **2009**, *24*, 1788−1791.
(537) Li, Z.; Askim, J. R.; Suslick, K. S. The Optoelectronic Nose: Colorimetric and Fluorometric Sensor Arrays. *Chem. Rev.* **2019**, *119*, 231.
(538) Valeur, B.; Leray, I. Design Principles of Fluorescent Molecular Sensors for Cation Recognition. *Coord. Chem. Rev.* **2000**, *205*, 3−40.
(539) Carter, K. P.; Young, A. M.; Palmer, A. E. Fluorescent Sensors for Measuring Metal Ions in Living Systems. *Chem. Rev.* **2014**, *114*, 4564−4601.
(540) Carstea, E. M.; Bridgeman, J.; Baker, A.; Reynolds, D. M. Fluorescence Spectroscopy for Wastewater Monitoring: A Review. *Water Res.* **2016**, *95*, 205−219.
(541) Sekine, Y.; Kim, S. B.; Zhang, Y.; Bandodkar, A. J.; Xu, S.; Choi, J.; Irie, M.; Ray, T. R.; Kohli, P.; Kozai, N.; et al. A Fluorometric Skin-Interfaced Microfluidic Device and Smartphone Imaging Module for in Situ Quantitative Analysis of Sweat Chemistry. *Lab Chip* **2018**, *18*, 2178−2186.
(542) Kim, J.; de Araujo, W. R.; Samek, I. A.; Bandodkar, A. J.; Jia, W. Z.; Brunetti, B.; Paixao, T. R. L. C.; Wang, J. Wearable Temporary Tattoo Sensor for Real-Time Trace Metal Monitoring in Human Sweat. *Electrochem. Commun.* **2015**, *51*, 41−45.
(543) Gao, W.; Nyein, H. Y. Y.; Shahpar, Z.; Fahad, H. M.; Chen, K.; Emaminejad, S.; Gao, Y. J.; Tai, L. C.; Ota, H.; Wu, E.; et al. Wearable Microsensor Array for Multiplexed Heavy Metal Monitoring of Body Fluids. *ACS Sens.* **2016**, *1*, 866−874.
(544) Parlak, O.; Keene, S. T.; Marais, A.; Curto, V. F.; Salleo, A. Molecularly Selective Nanoporous Membrane-Based Wearable Organic Electrochemical Device for Noninvasive Cortisol Sensing. *Sci. Adv.* **2018**, *4*, No. eaar2904.
(545) Kassal, P.; Kim, J.; Kumar, R.; de Araujo, W. R.; Steinberg, I. M.; Steinberg, M. D.; Wang, J. Smart Bandage with Wireless Connectivity for Uric Acid Biosensing as an Indicator of Wound Status. *Electrochem. Commun.* **2015**, *56*, 6−10.
(546) Lyu, B.; Punjiya, M.; Matharu, Z.; Sonkusale, S. An Improved pH Mapping Bandage with Thread-Based Sensors for Chronic Wound Monitoring. *2018 IEEE International Symposium on Circuits and Systems (ISCAS), May 27−30*, 2018; pp 1−4.
(547) Sears, M. E.; Kerr, K. J.; Bray, R. I. Arsenic, Cadmium, Lead, and Mercury in Sweat: A Systematic Review. *J. Environ. Public Health* **2012**, *2012*, 184745.
(548) Wang, J.; Lu, J.; Hocevar, S. B.; Farias, P. A.; Ogorevc, B. Bismuth-Coated Carbon Electrodes for Anodic Stripping Voltammetry. *Anal. Chem.* **2000**, *72*, 3218−3222.
(549) Duinker, J. C.; Kramer, C. J. M. An Experimental Study on the Speciation of Dissolved Zinc, Cadmium, Lead and Copper in River Rhine and North Sea Water, by Differential Pulsed Anodic Stripping Voltammetry. *Mar. Chem.* **1977**, *5*, 207−228.
(550) Ghaly, M.; Teplitz, D. The Biologic Effects of Grounding the Human Body During Sleep as Measured by Cortisol Levels and Subjective Reporting of Sleep, Pain, and Stress. *J. Altern. Complement. Med.* **2004**, *10*, 767−776.
(551) Gann, P. H.; Hennekens, C. H.; Ma, J.; Longcope, C.; Stampfer, M. J. Prospective Study of Sex Hormone Levels and Risk of Prostate Cancer. *J. Natl. Cancer Inst.* **1996**, *88*, 1118−1126.
(552) Klein, I.; Ojamaa, K. Thyroid Hormone and the Cardiovascular System. *N. Engl. J. Med.* **2001**, *344*, 501−509.
(553) Russell, E.; Koren, G.; Rieder, M.; Van Uum, S. H. The Detection of Cortisol in Human Sweat: Implications for Measurement of Cortisol in Hair. *Ther. Drug Monit.* **2014**, *36*, 30−34.
(554) Guinovart, T.; Valdes-Ramirez, G.; Windmiller, J. R.; Andrade, F. J.; Wang, J. Bandage-Based Wearable Potentiometric Sensor for Monitoring Wound Ph. *Electroanalysis* **2014**, *26*, 1345−1353.
(555) Chedekel, M. Photophysics and Photochemistry of Melanin. *J. Invest. Dermatol.* **1994**, *102*, 264.
(556) Severinghaus, J. W. Takuo Aoyagi: Discovery of Pulse Oximetry. *Anesth. Analg.* **2007**, *105*, S1−S4.
(557) Millikan, G. A. The Oximeter, an Instrument for Measuring Continuously the Oxygen Saturation of Arterial Blood in Man. *Rev. Sci. Instrum.* **1942**, *13*, 434−444.
(558) Thorniley, M. S.; Sinclair, J.; Barnett, N.; Shurey, C.; Green, C. The Use of near-Infrared Spectroscopy for Assessing Flap Viability During Reconstructive Surgery. *Br. J. Plast. Surg.* **1998**, *51*, 218−226.
(559) Malloy, H. T.; Evelyn, K. A. The Determination of Bilirubin with the Photoelectric Colorimeter. *J. Biol. Chem.* **1937**, *119*, 481−490.
(560) Bhutani, V. K.; Johnson, L.; Sivieri, E. M. Predictive Ability of a Predischarge Hour-Specific Serum Bilirubin for Subsequent Significant Hyperbilirubinemia in Healthy Term and near-Term Newborns. *Pediatrics* **1999**, *103*, 6−14.
(561) Hopkins, P. N.; Wu, L. L.; Hunt, S. C.; James, B. C.; Vincent, G. M.; Williams, R. R. Higher Serum Bilirubin Is Associated with Decreased Risk for Early Familial Coronary Artery Disease. *Arterioscler., Thromb., Vasc. Biol.* **1996**, *16*, 250−255.
(562) Liang, R. N.; Zhang, R. M.; Qin, W. Potentiometric Sensor Based on Molecularly Imprinted Polymer for Determination of Melamine in Milk. *Sens. Actuators, B* **2009**, *141*, 544−550.
(563) Brunetti, B.; Desimoni, E. Voltammetric Determination of Vitamin B6 in Food Samples and Dietary Supplements. *J. Food Compos. Anal.* **2014**, *33*, 155−160.

DOI: 10.1021/acs.chemrev.8b00573
Chem. Rev. 2019, 119, 5461−5533

(564) Mohan, A. M.; Brunetti, B.; Bulbarello, A.; Wang, J. *Analyst* **2015**, *140*, 7522−7526.
(565) Baldwin, E. A.; Bai, J.; Plotto, A.; Dea, S. Electronic Noses and Tongues: Applications for the Food and Pharmaceutical Industries. *Sensors* **2011**, *11*, 4744−4766.
(566) Hossain, S. M.; Luckham, R. E.; McFadden, M. J.; Brennan, J. D. Reagentless Bidirectional Lateral Flow Bioactive Paper Sensors for Detection of Pesticides in Beverage and Food Samples. *Anal. Chem.* **2009**, *81*, 9055−9064.
(567) Liu, G.; Lin, Y. Electrochemical Sensor for Organophosphate Pesticides and Nerve Agents Using Zirconia Nanoparticles as Selective Sorbents. *Anal. Chem.* **2005**, *77*, 5894−5901.
(568) Vo-Dinh, T. Sers Chemical Sensors and Biosensors - New Tools for Environmental and Biological Analysis. *Sens. Actuators, B* **1995**, *29*, 183−189.
(569) Lin, C.; Gillespie, J.; Schuder, M. D.; Duberstein, W.; Beverland, I. J.; Heal, M. R. Evaluation and Calibration of Aeroqual Series 500 Portable Gas Sensors for Accurate Measurement of Ambient Ozone and Nitrogen Dioxide. *Atmos. Environ.* **2015**, *100*, 111−116.
(570) Massie, C.; Stewart, G.; McGregor, G.; Gilchrist, J. R. Design of a Portable Optical Sensor for Methane Gas Detection. *Sens. Actuators, B* **2006**, *113*, 830−836.
(571) Chai, G. Y.; Lupan, O.; Chow, L.; Heinrich, H. Crossed Zinc Oxide Nanorods for Ultraviolet Radiation Detection. *Sens. Actuators, A* **2009**, *150*, 184−187.
(572) Diffey, B. L. Sources and Measurement of Ultraviolet Radiation. *Methods* **2002**, *28*, 4−13.
(573) Singh, S. Sensors–an Effective Approach for the Detection of Explosives. *J. Hazard. Mater.* **2007**, *144*, 15−28.
(574) O'Mahony, A. M.; Windmiller, J. R.; Samek, I. A.; Bandodkar, A. J.; Wang, J. Swipe and Scan": Integration of Sampling and Analysis of Gunshot Metal Residues at Screen-Printed Electrodes. *Electrochem. Commun.* **2012**, *23*, 52−55.
(575) Liu, P.; Yeung, S. H.; Crenshaw, K. A.; Crouse, C. A.; Scherer, J. R.; Mathies, R. A. Real-Time Forensic DNA Analysis at a Crime Scene Using a Portable Microchip Analyzer. *Forensic Sci. Int.: Genet.* **2008**, *2*, 301−309.
(576) O'Mahony, A. M.; Wang, J. Electrochemical Detection of Gunshot Residue for Forensic Analysis: A Review. *Electroanalysis* **2013**, *25*, 1341−1358.
(577) Qahtan, A.; Rao, S. P.; Keumala, N. The Effectiveness of the Sustainable Flowing Water Film in Improving the Solar-Optical Properties of Glazing in the Tropics. *Energ Buildings* **2014**, *77*, 247−255.
(578) Barajas-Carmona, J. G.; Francisco-Aldana, L.; Morales-Narváez, E. Wearable Nanoplasmonic Patch Detecting Sun/UV Exposure. *Anal. Chem.* **2017**, *89*, 13589−13595.
(579) Holick, M. F. Sunlight and Vitamin D for Bone Health and Prevention of Autoimmune Diseases, Cancers, and Cardiovascular Disease. *Am. J. Clin. Nutr.* **2004**, *80*, 1678S−1688S.
(580) Webb, A. R.; Engelsen, O. Calculated Ultraviolet Exposure Levels for a Healthy Vitamin D Status. *Photochem. Photobiol.* **2006**, *82*, 1697−1703.
(581) Fitzpatrick, T. B. The Validity and Practicality of Sun-Reactive Skin Types I through Vi. *Arch. Dermatol.* **1988**, *124*, 869−871.
(582) Taylor, H. R.; West, S. K.; Rosenthal, F. S.; Munoz, B.; Newland, H. S.; Abbey, H.; Emmett, E. A. Effect of Ultraviolet Radiation on Cataract Formation. *N. Engl. J. Med.* **1988**, *319*, 1429−1433.
(583) Urbach, F. Ultraviolet Radiation and Skin Cancer of Humans. *J. Photochem. Photobiol., B* **1997**, *40*, 3−7.
(584) Selgrade, M. K.; Repacholi, M. H.; Koren, H. S. Ultraviolet Radiation-Induced Immune Modulation: Potential Consequences for Infectious, Allergic, and Autoimmune Disease. *Environ. Health Perspect.* **1997**, *105*, 332−334.
(585) Guy, G. P.; Machlin, S. R.; Ekwueme, D. U.; Yabroff, K. R. Prevalence and Costs of Skin Cancer Treatment in the Us, 2002−2006 and 2007−2011. *Am. J. Prev. Med.* **2015**, *48*, 183−187.
(586) Stern, R. S. Prevalence of a History of Skin Cancer in 2007: Results of an Incidence-Based Model. *Arch. Dermatol.* **2010**, *146*, 279−282.
(587) Yun, J.; Lim, Y.; Lee, H.; Lee, G.; Park, H.; Hong, S. Y.; Jin, S. W.; Lee, Y. H.; Lee, S.-S.; Ha, J. S. A Patterned Graphene/Zno Uv Sensor Driven by Integrated Asymmetric Micro-Supercapacitors on a Liquid Metal Patterned Foldable Paper. *Adv. Funct. Mater.* **2017**, *27*, 1700135.
(588) Zhou, J.; Gu, Y.; Hu, Y.; Mai, W.; Yeh, P. H.; Bao, G.; Sood, A. K.; Polla, D. L.; Wang, Z. L. Gigantic Enhancement in Response and Reset Time of Zno Uv Nanosensor by Utilizing Schottky Contact and Surface Functionalization. *Appl. Phys. Lett.* **2009**, *94*, 191103.
(589) Gedamu, D.; Paulowicz, I.; Kaps, S.; Lupan, O.; Wille, S.; Haidarschin, G.; Mishra, Y. K.; Adelung, R. Rapid Fabrication Technique for Interpenetrated Zno Nanotetrapod Networks for Fast Uv Sensors. *Adv. Mater.* **2014**, *26*, 1541−1550.
(590) Gutruf, P.; Zeller, E.; Walia, S.; Nili, H.; Sriram, S.; Bhaskaran, M. Stretchable and Tunable Microtectonic Zno-Based Sensors and Photonics. *Small* **2015**, *11*, 4532−4539.
(591) Gutruf, P.; Walia, S.; Sriram, S.; Bhaskaran, M. Visible-Blind Uv Imaging with Oxygen-Deficient Zinc Oxide Flexible Devices. *Adv. Electron. Mater.* **2015**, *1*, 1500264.
(592) Li, Q. H.; Gao, T.; Wang, Y. G.; Wang, T. H. Adsorption and Desorption of Oxygen Probed from Zno Nanowire Films by Photocurrent Measurements. *Appl. Phys. Lett.* **2005**, *86*, 123117.
(593) Zhang, L.; Bai, S.; Su, C.; Zheng, Y.; Qin, Y.; Xu, C.; Wang, Z. L. A High-Reliability Kevlar Fiber-Zno Nanowires Hybrid Nanogenerator and Its Application on Self-Powered Uv Detection. *Adv. Funct. Mater.* **2015**, *25*, 5794−5798.
(594) Krebs, F. C. Fabrication and Processing of Polymer Solar Cells: A Review of Printing and Coating Techniques. *Sol. Energy Mater. Sol. Cells* **2009**, *93*, 394−412.
(595) Nie, W.; Tsai, H.; Asadpour, R.; Blancon, J. C.; Neukirch, A. J.; Gupta, G.; Crochet, J. J.; Chhowalla, M.; Tretiak, S.; Alam, M. A.; et al. Solar Cells. High-Efficiency Solution-Processed Perovskite Solar Cells with Millimeter-Scale Grains. *Science* **2015**, *347*, 522−525.
(596) Azarova, N. A.; Owen, J. W.; McLellan, C. A.; Grimminger, M. A.; Chapman, E. K.; Anthony, J. E.; Jurchescu, O. D. Fabrication of Organic Thin-Film Transistors by Spray-Deposition for Low-Cost, Large-Area Electronics. *Org. Electron.* **2010**, *11*, 1960−1965.
(597) Tran, V. T.; Wei, Y.; Yang, H.; Zhan, Z.; Du, H. All-Inkjet-Printed Flexible ZnO Micro Photodetector for a Wearable Uv Monitoring Device. *Nanotechnology* **2017**, *28*, No. 095204.
(598) Liao, X.; Liao, Q.; Zhang, Z.; Yan, X.; Liang, Q.; Wang, Q.; Li, M.; Zhang, Y. A Highly Stretchable Zno@Fiber-Based Multifunctional Nanosensor for Strain/Temperature/Uv Detection. *Adv. Funct. Mater.* **2016**, *26*, 3074−3081.
(599) Araki, H.; Kim, J.; Zhang, S. N.; Banks, A.; Crawford, K. E.; Sheng, X.; Gutruf, P.; Shi, Y. Z.; Pielak, R. M.; Rogers, J. A. Materials and Device Designs for an Epidermal Uv Colorimetric Dosimeter with near Field Communication Capabilities. *Adv. Funct. Mater.* **2017**, *27*, 1604465.
(600) Heo, S. Y.; Kim, J.; Gutruf, P.; Banks, A.; Wei, P.; Pielak, R.; Balooch, G.; Shi, Y.; Araki, H.; Rollo, D.; et al. Wireless, Battery-Free, Miniaturized Dosimeters for Monitoring Exposure to Solar Radiation. *Sci. Transl. Med.* **2018**, *10*, No. eaau1643.
(601) Jing, X.; Mi, H. Y.; Lin, Y. J.; Enriquez, E.; Peng, X. F.; Turng, L. S. Highly Stretchable and Biocompatible Strain Sensors Based on Mussel-Inspired Super-Adhesive Self-Healing Hydrogels for Human Motion Monitoring. *ACS Appl. Mater. Interfaces* **2018**, *10*, 20897−20909.
(602) Xu, H.; Yin, L.; Liu, C.; Sheng, X.; Zhao, N. Recent Advances in Biointegrated Optoelectronic Devices. *Adv. Mater.* **2018**, *30*, No. 1800156.
(603) Bandodkar, A. J.; Nunez-Flores, R.; Jia, W.; Wang, J. All-Printed Stretchable Electrochemical Devices. *Adv. Mater.* **2015**, *27*, 3060−3065.

DOI: 10.1021/acs.chemrev.8b00573
Chem. Rev. 2019, 119, 5461−5533

(604) Cheng, Y. W.; Yin, L. Y.; Lin, S. H.; Wiesner, M.; Bernhardt, E.; Liu, J. Toxicity Reduction of Polymer-Stabilized Silver Nanoparticles by Sunlight. *J. Phys. Chem. C* **2011**, *115*, 4425−4432.
(605) Gorham, J. M.; MacCuspie, R. I.; Klein, K. L.; Fairbrother, D. H.; Holbrook, R. D. Uv-Induced Photochemical Transformations of Citrate-Capped Silver Nanoparticle Suspensions. *J. Nanopart. Res.* **2012**, *14*, 1139.
(606) Shi, Y.; Manco, M.; Moyal, D.; Huppert, G.; Araki, H.; Banks, A.; Joshi, H.; McKenzie, R.; Seewald, A.; Griffin, G.; et al. Soft, Stretchable, Epidermal Sensor with Integrated Electronics and Photochemistry for Measuring Personal Uv Exposures. *PLoS One* **2018**, *13*, No. e0190233.
(607) Vicente-Tejedor, J.; Marchena, M.; Ramirez, L.; Garcia-Ayuso, D.; Gomez-Vicente, V.; Sanchez-Ramos, C.; de la Villa, P.; Germain, F. Removal of the Blue Component of Light Significantly Decreases Retinal Damage after High Intensity Exposure. *PLoS One* **2018**, *13*, No. e0194218.
(608) Lockley, S. W.; Evans, E. E.; Scheer, F. A. J. L.; Brainard, G. C.; Czeisler, C. A.; Aeschbach, D. Short-Wavelength Sensitivity for the Direct Effects of Light on Alertness, Vigilance, and the Waking Electroencephalogram in Humans. *Sleep* **2006**, *29*, 161−168.
(609) Lockley, S. W.; Brainard, G. C.; Czeisler, C. A. High Sensitivity of the Human Circadian Melatonin Rhythm to Resetting by Short Wavelength Light. *J. Clin. Endocrinol. Metab.* **2003**, *88*, 4502−4505.
(610) Stevens, R. G.; Brainard, G. C.; Blask, D. E.; Lockley, S. W.; Motta, M. E. Breast Cancer and Circadian Disruption from Electric Lighting in the Modern World. *Ca-Cancer J. Clin.* **2014**, *64*, 207−218.
(611) American Academy of Pediatrics Subcommittee on Hyperbilirubinemia. Management of Hyperbilirubinemia in the Newborn Infant 35 or More Weeks of Gestation. *Pediatrics* **2004**, *114*, 297.
(612) Strong, R. E.; Marchant, B. K.; Reimherr, F. W.; Williams, E.; Soni, P.; Mestas, R. Narrow-Band Blue-Light Treatment of Seasonal Affective Disorder in Adults and the Influence of Additional Nonseasonal Symptoms. *Depression Anxiety* **2009**, *26*, 273−278.
(613) Stern, M.; Broja, M.; Sansone, R.; Grone, M.; Skene, S. S.; Liebmann, J.; Suschek, C. V.; Born, M.; Kelm, M.; Heiss, C. Blue Light Exposure Decreases Systolic Blood Pressure, Arterial Stiffness, and Improves Endothelial Function in Humans. *Eur. J. Prev. Cardiol.* **2018**, *25*, 1875−1883.
(614) Wahl, F.; Freund, M.; Amft, O. Wiseglass: Smart Eyeglasses Recognising Context. *Proceedings of the 10th EAI International Conference on Body Area Networks, Sydney, New South Wales, Australia*, 2015; pp 11−17.
(615) Wahl, F.; Kasbauer, J.; Amft, O. Computer Screen Use Detection Using Smart Eyeglasses. *Front. ICT* **2017**, *4*, 8.
(616) Borgerson, S. G. Arctic Meltdown—The Economic and Security Implications of Global Warming. *Foreign Affairs* **2008**, *87*, 63−77.
(617) Visser, P. M.; Verspagen, J. M. H.; Sandrini, G.; Stal, L. J.; Matthijs, H. C. P.; Davis, T. W.; Paerl, H. W.; Huisman, J. How Rising Co2 and Global Warming May Stimulate Harmful Cyanobacterial Blooms. *Harmful Algae* **2016**, *54*, 145−159.
(618) Wiedinmyer, C.; Yokelson, R. J.; Gullett, B. K. Global Emissions of Trace Gases, Particulate Matter, and Hazardous Air Pollutants from Open Burning of Domestic Waste. *Environ. Sci. Technol.* **2014**, *48*, 9523−9530.
(619) Aldy, J. E. Policy Surveillance in the G-20 Fossil Fuel Subsidies Agreement: Lessons for Climate Policy. *Clim. Change* **2017**, *144*, 97−110.
(620) Perera, F. P. Multiple Threats to Child Health from Fossil Fuel Combustion: Impacts of Air Pollution and Climate Change. *Environ. Health Perspect.* **2017**, *125*, 141−148.
(621) Adgate, J. L.; Goldstein, B. D.; McKenzie, L. M. Potential Public Health Hazards, Exposures and Health Effects from Unconventional Natural Gas Development. *Environ. Sci. Technol.* **2014**, *48*, 8307−8320.
(622) Finkelman, R. B.; Tian, L. W. The Health Impacts of Coal Use in China. *Int. Geol. Rev.* **2018**, *60*, 579−589.
(623) Mousa, H. A. Short-Term Effects of Subchronic Low-Level Hydrogen Sulfide Exposure on Oil Field Workers. *Environ. Health Prev. Med.* **2015**, *20*, 12−17.
(624) Fratoddi, I.; Venditti, I.; Cametti, C.; Russo, M. V. Chemiresistive Polyaniline-Based Gas Sensors: A Mini Review. *Sens. Actuators, B* **2015**, *220*, 534−548.
(625) Toda, K.; Furue, R.; Hayami, S. Recent Progress in Applications of Graphene Oxide for Gas Sensing: A Review. *Anal. Chim. Acta* **2015**, *878*, 43−53.
(626) Mirzaei, A.; Leonardi, S. G.; Neri, G. Detection of Hazardous Volatile Organic Compounds (Vocs) by Metal Oxide Nanostructures-Based Gas Sensors: A Review. *Ceram. Int.* **2016**, *42*, 15119−15141.
(627) Kaushik, A.; Kumar, R.; Arya, S. K.; Nair, M.; Malhotra, B. D.; Bhansali, S. Organic-Inorganic Hybrid Nanocomposite-Based Gas Sensors for Environmental Monitoring. *Chem. Rev.* **2015**, *115*, 4571−4606.
(628) Bogue, R. Terrorism and Military Actions Pose the Ultimate Challenge to Gas Sensing. *Sens. Rev.* **2011**, *31*, 6−12.
(629) Lim, T.-C. *Nanosensors: Theory and Applications in Industry, Healthcare and Defense*; CRC Press, 2016.
(630) Singh, E.; Meyyappan, M.; Nalwa, H. S. Flexible Graphene-Based Wearable Gas and Chemical Sensors. *ACS Appl. Mater. Interfaces* **2017**, *9*, 34544−34586.
(631) Choi, S.-J.; Kim, S.-J.; Kim, I.-D. Ultrafast Optical Reduction of Graphene Oxide Sheets on Colorless Polyimide Film for Wearable Chemical Sensors. *NPG Asia Mater.* **2016**, *8*, No. e315.
(632) Yun, Y. J.; Kim, D. Y.; Hong, W. G.; Ha, D. H.; Jun, Y.; Lee, H.-K. Highly Stretchable, Mechanically Stable, and Weavable Reduced Graphene Oxide Yarn with High No 2 Sensitivity for Wearable Gas Sensors. *RSC Adv.* **2018**, *8*, 7615−7621.
(633) Huang, W.; Besar, K.; Zhang, Y.; Yang, S.; Wiedman, G.; Liu, Y.; Guo, W.; Song, J.; Hemker, K.; Hristova, K.; et al. A High-Capacitance Salt-Free Dielectric for Self-Healable, Printable, and Flexible Organic Field Effect Transistors and Chemical Sensor. *Adv. Funct. Mater.* **2015**, *25*, 3745−3755.
(634) Cai, G. F.; Wang, J. X.; Lin, M. F.; Chen, J. W.; Cui, M. Q.; Qian, K.; Li, S. H.; Cui, P.; Lee, P. S. A Semitransparent Snake-Like Tactile and Olfactory Bionic Sensor with Reversibly Stretchable Properties. *NPG Asia Mater.* **2017**, *9*, No. e437.
(635) Gao, Z. Y.; Lou, Z.; Chen, S.; Li, L.; Jiang, K.; Fu, Z. L.; Han, W.; Shen, G. Z. Fiber Gas Sensor-Integrated Smart Face Mask for Room-Temperature Distinguishing of Target Gases. *Nano Res.* **2018**, *11*, 511−519.
(636) Smith, M. K.; Mirica, K. A. Self-Organized Frameworks on Textiles (Soft): Conductive Fabrics for Simultaneous Sensing, Capture, and Filtration of Gases. *J. Am. Chem. Soc.* **2017**, *139*, 16759−16767.
(637) Yun, Y. J.; Hong, W. G.; Kim, D. Y.; Kim, H. J.; Jun, Y.; Lee, H. K. E-Textile Gas Sensors Composed of Molybdenum Disulfide and Reduced Graphene Oxide for High Response and Reliability. *Sens. Actuators, B* **2017**, *248*, 829−835.
(638) Wang, T.; Guo, Y.; Wan, P.; Sun, X.; Zhang, H.; Yu, Z.; Chen, X. A Flexible Transparent Colorimetric Wrist Strap Sensor. *Nanoscale* **2017**, *9*, 869−874.
(639) Maity, D.; Rajavel, K.; Kumar, R. T. R. Polyvinyl Alcohol Wrapped Multiwall Carbon Nanotube (Mwcnts) Network on Fabrics for Wearable Room Temperature Ethanol Sensor. *Sens. Actuators, B* **2018**, *261*, 297−306.
(640) Li, L.; Fu, C. W.; Lou, Z.; Chen, S.; Han, W.; Jiang, K.; Chen, D.; Shen, G. Z. Flexible Planar Concentric Circular Micro-Supercapacitor Arrays for Wearable Gas Sensing Application. *Nano Energy* **2017**, *41*, 261−268.
(641) Chiou, J. C.; Wu, C. C. A Wearable and Wireless Gas-Sensing System Using Flexible Polymer/Multi-Walled Carbon Nanotube Composite Films. *Polymers* **2017**, *9*, 457.
(642) Rui, K.; Wang, X.; Du, M.; Zhang, Y.; Wang, Q.; Ma, Z.; Zhang, Q.; Li, D.; Huang, X.; Sun, G.; et al. Dual-Function Metal-Organic Framework-Based Wearable Fibers for Gas Probing and Energy Storage. *ACS Appl. Mater. Interfaces* **2018**, *10*, 2837−2842.

DOI: 10.1021/acs.chemrev.8b00573
Chem. Rev. 2019, 119, 5461−5533

(643) Stock, N.; Biswas, S. Synthesis of Metal-Organic Frameworks (Mofs): Routes to Various Mof Topologies, Morphologies, and Composites. *Chem. Rev.* **2012**, *112*, 933−969.
(644) Zhou, H.-C.; Long, J. R.; Yaghi, O. M. Introduction to Metal−Organic Frameworks. *Chem. Rev.* **2012**, *112*, 673−674.
(645) Bandodkar, A. J.; O'Mahony, A. M.; Ramirez, J.; Samek, I. A.; Anderson, S. M.; Windmiller, J. R.; Wang, J. Solid-State Forensic Finger Sensor for Integrated Sampling and Detection of Gunshot Residue and Explosives: Towards 'Lab-on-a-Finger'. *Analyst* **2013**, *138*, 5288−5295.
(646) Sempionatto, J. R.; Mishra, R. K.; Martin, A.; Tang, G.; Nakagawa, T.; Lu, X.; Campbell, A. S.; Lyu, K. M.; Wang, J. Wearable Ring-Based Sensing Platform for Detecting Chemical Threats. *ACS Sens.* **2017**, *2*, 1531−1538.
(647) de Jong, M.; Sleegers, N.; Kim, J.; Van Durme, F.; Samyn, N.; Wang, J.; De Wael, K. Electrochemical Fingerprint of Street Samples for Fast on-Site Screening of Cocaine in Seized Drug Powders. *Chem. Sci.* **2016**, *7*, 2364−2370.
(648) Mishra, R. K.; Martin, A.; Nakagawa, T.; Barfidokht, A.; Lu, X.; Sempionatto, J. R.; Lyu, K. M.; Karajic, A.; Musameh, M. M.; Kyratzis, I. L.; et al. Detection of Vapor-Phase Organophosphate Threats Using Wearable Conformable Integrated Epidermal and Textile Wireless Biosensor Systems. *Biosens. Bioelectron.* **2018**, *101*, 227−234.
(649) Zhu, R.; Azzarelli, J. M.; Swager, T. M. Wireless Hazard Badges to Detect Nerve-Agent Simulants. *Angew. Chem., Int. Ed.* **2016**, *55*, 9662−9666.
(650) Scholz, F.; Lange, B. Abrasive Stripping Voltammetry - an Electrochemical Solid-State Spectroscopy of Wide Applicability. *TrAC, Trends Anal. Chem.* **1992**, *11*, 359−367.
(651) Kim, J.; Cho, T. N.; Valdes-Ramirez, G.; Wang, J. A Wearable Fingernail Chemical Sensing Platform: Ph Sensing at Your Fingertips. *Talanta* **2016**, *150*, 622−628.
(652) Kanamura, K. Large-Scale Batteries for Green Energy Society. In *Electrochemical Science for a Sustainable Society*; Springer, 2017; pp 175−195.
(653) Jaguemont, J.; Boulon, L.; Dube, Y. A Comprehensive Review of Lithium-Ion Batteries Used in Hybrid and Electric Vehicles at Cold Temperatures. *Appl. Energy* **2016**, *164*, 99−114.
(654) Gao, X. Z.; Hou, Z. X.; Guo, Z.; Chen, X. Q. Reviews of Methods to Extract and Store Energy for Solar-Powered Aircraft. *Renewable Sustainable Energy Rev.* **2015**, *44*, 96−108.
(655) Wang, Y. X.; Liu, B.; Li, Q. Y.; Cartmell, S.; Ferrara, S.; Deng, Z. Q. D.; Xiao, J. Lithium and Lithium Ion Batteries for Applications in Microelectronic Devices: A Review. *J. Power Sources* **2015**, *286*, 330−345.
(656) Montgomery, J. A.; Ellis, C. R. Longevity of Cardiovascular Implantable Electronic Devices. *Card. Electrophysiol. Clin.* **2018**, *10*, 1−9.
(657) He, Y. H.; Matthews, B.; Wang, J. Y.; Song, L.; Wang, X. X.; Wu, G. Innovation and Challenges in Materials Design for Flexible Rechargeable Batteries: From 1d to 3d. *J. Mater. Chem. A* **2018**, *6*, 735−753.
(658) Gu, P.; Zheng, M. B.; Zhao, Q. X.; Xiao, X.; Xue, H. G.; Pang, H. Rechargeable Zinc-Air Batteries: A Promising Way to Green Energy. *J. Mater. Chem. A* **2017**, *5*, 7651−7666.
(659) Nyein, H. Y. Y.; Tai, L. C.; Ngo, Q. P.; Chao, M.; Zhang, G. B.; Gao, W.; Bariya, M.; Bullock, J.; Kim, H.; Fahad, H. M.; et al. A Wearable Microfluidic Sensing Patch for Dynamic Sweat Secretion Analysis. *ACS Sens.* **2018**, *3*, 944−952.
(660) Jost, K.; Dion, G.; Gogotsi, Y. Textile Energy Storage in Perspective. *J. Mater. Chem. A* **2014**, *2*, 10776−10787.
(661) Du, C. F.; Liang, Q. H.; Luo, Y. B.; Zheng, Y.; Yan, Q. Y. Recent Advances in Printable Secondary Batteries. *J. Mater. Chem. A* **2017**, *5*, 22442−22458.
(662) Xu, S.; Zhang, Y.; Cho, J.; Lee, J.; Huang, X.; Jia, L.; Fan, J. A.; Su, Y.; Su, J.; Zhang, H.; et al. Stretchable Batteries with Self-Similar Serpentine Interconnects and Integrated Wireless Recharging Systems. *Nat. Commun.* **2013**, *4*, 1543.
(663) Liu, X.; Zhao, K.; Wang, Z. L.; Yang, Y. Unity Convoluted Design of Solid Li-Ion Battery and Triboelectric Nanogenerator for Self-Powered Wearable Electronics. *Adv. Energy Mater.* **2017**, *7*, 1701629.
(664) Ren, J.; Zhang, Y.; Bai, W.; Chen, X.; Zhang, Z.; Fang, X.; Weng, W.; Wang, Y.; Peng, H. Elastic and Wearable Wire-Shaped Lithium-Ion Battery with High Electrochemical Performance. *Angew. Chem., Int. Ed.* **2014**, *53*, 7864−7869.
(665) Liu, T.; Xu, J. J.; Liu, Q. C.; Chang, Z. W.; Yin, Y. B.; Yang, X. Y.; Zhang, X. B. Ultrathin, Lightweight, and Wearable Li-O2 Battery with High Robustness and Gravimetric/Volumetric Energy Density. *Small* **2017**, *13*, 1602952.
(666) Wang, Y.; Chen, C.; Xie, H.; Gao, T.; Yao, Y.; Pastel, G.; Han, X.; Li, Y.; Zhao, J.; Fu, K. K.; Hu, L. 3d-Printed All-Fiber Li-Ion Battery toward Wearable Energy Storage. *Adv. Funct. Mater.* **2017**, *27*, 1703140.
(667) Kumar, R.; Shin, J.; Yin, L.; You, J. M.; Meng, Y. S.; Wang, J. All-Printed, Stretchable Zn-Ag2o Rechargeable Battery Via Hyperelastic Binder for Self-Powering Wearable Electronics. *Adv. Energy Mater.* **2017**, *7*, 1602096.
(668) Zamarayeva, A. M.; Ostfeld, A. E.; Wang, M.; Duey, J. K.; Deckman, I.; Lechene, B. P.; Davies, G.; Steingart, D. A.; Arias, A. C. Flexible and Stretchable Power Sources for Wearable Electronics. *Sci. Adv.* **2017**, *3*, No. e1602051.
(669) Berchmans, S.; Bandodkar, A. J.; Jia, W. Z.; Ramirez, J.; Meng, Y. S.; Wang, J. An Epidermal Alkaline Rechargeable Ag-Zn Printable Tattoo Battery for Wearable Electronics. *J. Mater. Chem. A* **2014**, *2*, 15788−15795.
(670) Zhu, Y. H.; Yuan, S.; Bao, D.; Yin, Y. B.; Zhong, H. X.; Zhang, X. B.; Yan, J. M.; Jiang, Q. Decorating Waste Cloth Via Industrial Wastewater for Tube-Type Flexible and Wearable Sodium-Ion Batteries. *Adv. Mater.* **2017**, *29*, 1603719.
(671) Chen, Q.; Sun, S.; Zhai, T.; Yang, M.; Zhao, X.; Xia, H. Yolk−Shell Nis2 Nanoparticle-Embedded Carbon Fibers for Flexible Fiber-Shaped Sodium Battery. *Adv. Energy Mater.* **2018**, *8*, 1800054.
(672) Wei, Y.; Hu, Q.; Cao, Y. H.; Fang, D.; Xu, W. L.; Jiang, M.; Huang, J.; Liu, H.; Fan, X. Polypyrrole Nanotube Arrays on Carbonized Cotton Textile for Aqueous Sodium Battery. *Org. Electron.* **2017**, *46*, 211−217.
(673) Ogawa, Y.; Takai, Y.; Kato, Y.; Kai, H.; Miyake, T.; Nishizawa, M. Stretchable Biofuel Cell with Enzyme-Modified Conductive Textiles. *Biosens. Bioelectron.* **2015**, *74*, 947−952.
(674) Pang, S.; Gao, Y.; Choi, S. Flexible and Stretchable Biobatteries: Monolithic Integration of Membrane-Free Microbial Fuel Cells in a Single Textile Layer. *Adv. Energy Mater.* **2018**, *8*, 1702261.
(675) Wang, L.; Zhang, Y.; Pan, J.; Peng, H. S. Stretchable Lithium-Air Batteries for Wearable Electronics. *J. Mater. Chem. A* **2016**, *4*, 13419−13424.
(676) Li, H. F.; Han, C. P.; Huang, Y.; Huang, Y.; Zhu, M. S.; Pei, Z. X.; Xue, Q.; Wang, Z. F.; Liu, Z. X.; Tang, Z. J.; et al. An Extremely Safe and Wearable Solid-State Zinc Ion Battery Based on a Hierarchical Structured Polymer Electrolyte. *Energy Environ. Sci.* **2018**, *11*, 941−951.
(677) Hansora, D. P.; Shimpi, N. G.; Mishra, S. Performance of Hybrid Nanostructured Conductive Cotton Materials as Wearable Devices: An Overview of Materials, Fabrication, Properties and Applications. *RSC Adv.* **2015**, *5*, 107716−107770.
(678) Stoppa, M.; Chiolerio, A. Wearable Electronics and Smart Textiles: A Critical Review. *Sensors* **2014**, *14*, 11957−11992.
(679) Zeng, W.; Shu, L.; Li, Q.; Chen, S.; Wang, F.; Tao, X. M. Fiber-Based Wearable Electronics: A Review of Materials, Fabrication, Devices, and Applications. *Adv. Mater.* **2014**, *26*, 5310−5336.
(680) Lee, Y. H.; Kim, J. S.; Noh, J.; Lee, I.; Kim, H. J.; Choi, S.; Seo, J.; Jeon, S.; Kim, T. S.; Lee, J. Y.; et al. Wearable Textile Battery Rechargeable by Solar Energy. *Nano Lett.* **2013**, *13*, 5753−5761.
(681) Foroughi, J.; Spinks, G. M.; Antiohos, D.; Mirabedini, A.; Gambhir, S.; Wallace, G. G.; Ghorbani, S. R.; Peleckis, G.; Kozlov, M. E.; Lima, M. D.; et al. Highly Conductive Carbon Nanotube-Graphene Hybrid Yarn. *Adv. Funct. Mater.* **2014**, *24*, 5859−5865.
(682) Chen, Y. H.; Freunberger, S. A.; Peng, Z. Q.; Fontaine, O.; Bruce, P. G. Charging a Li-O-2 Battery Using a Redox Mediator. *Nat. Chem.* **2013**, *5*, 489−494.

DOI: 10.1021/acs.chemrev.8b00573
Chem. Rev. 2019, 119, 5461−5533

(683) Luntz, A. C.; McCloskey, B. D. Nonaqueous Li-Air Batteries: A Status Report. *Chem. Rev.* **2014**, *114*, 11721−11750.
(684) Xia, C.; Kwok, C. Y.; Nazar, L. F. A High-Energy-Density Lithium-Oxygen Battery Based on a Reversible Four-Electron Conversion to Lithium Oxide. *Science* **2018**, *361*, 777−781.
(685) Xie, Y. Z.; Liu, Y.; Zhao, Y. D.; Tsang, Y. H.; Lau, S. P.; Huang, H. T.; Chai, Y. Stretchable All-Solid-State Supercapacitor with Wavy Shaped Polyaniline/Graphene Electrode. *J. Mater. Chem. A* **2014**, *2*, 9142−9149.
(686) Liu, W.; Chen, Z.; Zhou, G.; Sun, Y.; Lee, H. R.; Liu, C.; Yao, H.; Bao, Z.; Cui, Y. 3d Porous Sponge-Inspired Electrode for Stretchable Lithium-Ion Batteries. *Adv. Mater.* **2016**, *28*, 3578−3583.
(687) Slater, M. D.; Kim, D.; Lee, E.; Johnson, C. S. Sodium-Ion Batteries. *Adv. Funct. Mater.* **2013**, *23*, 947−958.
(688) Yabuuchi, N.; Kubota, K.; Dahbi, M.; Komaba, S. Research Development on Sodium-Ion Batteries. *Chem. Rev.* **2014**, *114*, 11636−11682.
(689) Li, Y.; Dai, H. Recent Advances in Zinc-Air Batteries. *Chem. Soc. Rev.* **2014**, *43*, 5257−5275.
(690) Fu, J.; Cano, Z. P.; Park, M. G.; Yu, A.; Fowler, M.; Chen, Z. Electrically Rechargeable Zinc-Air Batteries: Progress, Challenges, and Perspectives. *Adv. Mater.* **2017**, *29*, 1604685.
(691) Wang, Q. S.; Ping, P.; Zhao, X. J.; Chu, G. Q.; Sun, J. H.; Chen, C. H. Thermal Runaway Caused Fire and Explosion of Lithium Ion Battery. *J. Power Sources* **2012**, *208*, 210−224.
(692) Lamb, J.; Orendorff, C. J. Evaluation of Mechanical Abuse Techniques in Lithium Ion Batteries. *J. Power Sources* **2014**, *247*, 189−196.
(693) Ogawa, Y.; Kato, K.; Miyake, T.; Nagamine, K.; Ofuji, T.; Yoshino, S.; Nishizawa, M. Organic Transdermal Iontophoresis Patch with Built-in Biofuel Cell. *Adv. Healthcare Mater.* **2015**, *4*, 506−510.
(694) Zhao, C. M.; Zheng, W. T. A Review for Aqueous Electrochemical Supercapacitors. *Front. Energy Res.* **2015**, *3*, 23.
(695) Wen, Z.; Yeh, M. H.; Guo, H.; Wang, J.; Zi, Y.; Xu, W.; Deng, J.; Zhu, L.; Wang, X.; Hu, C.; et al. Self-Powered Textile for Wearable Electronics by Hybridizing Fiber-Shaped Nanogenerators, Solar Cells, and Supercapacitors. *Sci. Adv.* **2016**, *2*, No. e1600097.
(696) Zhu, J.; Tang, S.; Wu, J.; Shi, X.; Zhu, B.; Meng, X. Wearable High-Performance Supercapacitors Based on Silver-Sputtered Textiles with Feco2s4−Nico2s4 Composite Nanotube-Built Multitripod Architectures as Advanced Flexible Electrodes. *Adv. Energy Mater.* **2017**, *7*, 1601234.
(697) Meng, Y.; Zhao, Y.; Hu, C.; Cheng, H.; Hu, Y.; Zhang, Z.; Shi, G.; Qu, L. All-Graphene Core-Sheath Microfibers for All-Solid-State, Stretchable Fibriform Supercapacitors and Wearable Electronic Textiles. *Adv. Mater.* **2013**, *25*, 2326−2331.
(698) Hu, L.; Pasta, M.; La Mantia, F.; Cui, L.; Jeong, S.; Deshazer, H. D.; Choi, J. W.; Han, S. M.; Cui, Y. Stretchable, Porous, and Conductive Energy Textiles. *Nano Lett.* **2010**, *10*, 708−714.
(699) Zhang, D.; Miao, M.; Niu, H.; Wei, Z. Core-Spun Carbon Nanotube Yarn Supercapacitors for Wearable Electronic Textiles. *ACS Nano* **2014**, *8*, 4571−4579.
(700) Jost, K.; Stenger, D.; Perez, C. R.; McDonough, J. K.; Lian, K.; Gogotsi, Y.; Dion, G. Knitted and Screen Printed Carbon-Fiber Supercapacitors for Applications in Wearable Electronics. *Energy Environ. Sci.* **2013**, *6*, 2698−2705.
(701) Wu, G.; Tan, P.; Wu, X.; Peng, L.; Cheng, H.; Wang, C. F.; Chen, W.; Yu, Z.; Chen, S. High-Performance Wearable Micro-Supercapacitors Based on Microfluidic-Directed Nitrogen-Doped Graphene Fiber Electrodes. *Adv. Funct. Mater.* **2017**, *27*, 1702493.
(702) Song, Z. Q.; Fan, Y. Y.; Sun, Z. H.; Han, D. X.; Bao, Y.; Niu, L. A New Strategy for Integrating Superior Mechanical Performance and High Volumetric Energy Density into a Janus Graphene Film for Wearable Solid-State Supercapacitors. *J. Mater. Chem. A* **2017**, *5*, 20797−20807.
(703) Yang, Y.; Huang, Q.; Niu, L.; Wang, D.; Yan, C.; She, Y.; Zheng, Z. Waterproof, Ultrahigh Areal-Capacitance, Wearable Supercapacitor Fabrics. *Adv. Mater.* **2017**, *29*, 1606679.
(704) Dong, K.; Wang, Y. C.; Deng, J.; Dai, Y.; Zhang, S. L.; Zou, H.; Gu, B.; Sun, B.; Wang, Z. L. A Highly Stretchable and Washable All-Yarn-Based Self-Charging Knitting Power Textile Composed of Fiber Triboelectric Nanogenerators and Supercapacitors. *ACS Nano* **2017**, *11*, 9490−9499.
(705) Liu, L.; Yu, Y.; Yan, C.; Li, K.; Zheng, Z. Wearable Energy-Dense and Power-Dense Supercapacitor Yarns Enabled by Scalable Graphene-Metallic Textile Composite Electrodes. *Nat. Commun.* **2015**, *6*, 7260.
(706) Shen, C.; Xie, Y.; Zhu, B.; Sanghadasa, M.; Tang, Y.; Lin, L. Wearable Woven Supercapacitor Fabrics with High Energy Density and Load-Bearing Capability. *Sci. Rep.* **2017**, *7*, 14324.
(707) Fu, W. B.; Zhao, E. B.; Ren, X. L.; Magasinski, A.; Yushin, G. Hierarchical Fabric Decorated with Carbon Nanowire/Metal Oxide Nanocomposites for 1.6 V Wearable Aqueous Supercapacitors. *Adv. Energy Mater.* **2018**, *8*, 1703454.
(708) Nagaraju, G.; Chandra Sekhar, S.; Krishna Bharat, L.; Yu, J. S. Wearable Fabrics with Self-Branched Bimetallic Layered Double Hydroxide Coaxial Nanostructures for Hybrid Supercapacitors. *ACS Nano* **2017**, *11*, 10860−10874.
(709) Moon, H.; Lee, H.; Kwon, J.; Suh, Y. D.; Kim, D. K.; Ha, I.; Yeo, J.; Hong, S.; Ko, S. H. Ag/Au/Polypyrrole Core-Shell Nanowire Network for Transparent, Stretchable and Flexible Supercapacitor in Wearable Energy Devices. *Sci. Rep.* **2017**, *7*, 41981.
(710) Choudhary, N.; Li, C.; Moore, J.; Nagaiah, N.; Zhai, L.; Jung, Y.; Thomas, J. Asymmetric Supercapacitor Electrodes and Devices. *Adv. Mater.* **2017**, *29*, 1605336.
(711) Ma, W. J.; Chen, S. H.; Yang, S. Y.; Chen, W. P.; Weng, W.; Cheng, Y. H.; Zhu, M. F. Flexible All-Solid-State Asymmetric Supercapacitor Based on Transition Metal Oxide Nanorods/Reduced Graphene Oxide Hybrid Fibers with High Energy Density. *Carbon* **2017**, *113*, 151−158.
(712) Sun, J.; Man, P.; Zhang, Q. C.; He, B.; Zhou, Z. Y.; Li, C. W.; Wang, X. N.; Guo, J. B.; Zhao, J. X.; Xie, L. Y.; et al. Hierarchically-Structured Co3o4 Nanowire Arrays Grown on Carbon Nanotube Fibers as Novel Cathodes for High-Performance Wearable Fiber-Shaped Asymmetric Supercapacitors. *Appl. Surf. Sci.* **2018**, *447*, 795−801.
(713) Yang, Y.; Zhang, N.; Zhang, B.; Zhang, Y.; Tao, C.; Wang, J.; Fan, X. Highly-Efficient Dendritic Cable Electrodes for Flexible Supercapacitive Fabric. *ACS Appl. Mater. Interfaces* **2017**, *9*, 40207−40214.
(714) Wang, J.; Dong, L.; Xu, C.; Ren, D.; Ma, X.; Kang, F. Polymorphous Supercapacitors Constructed from Flexible Three-Dimensional Carbon Network/Polyaniline/Mno2 Composite Textiles. *ACS Appl. Mater. Interfaces* **2018**, *10*, 10851−10859.
(715) Gong, X. F.; Li, S. H.; Lee, P. S. A Fiber Asymmetric Supercapacitor Based on Feooh/Ppy on Carbon Fibers as an Anode Electrode with High Volumetric Energy Density for Wearable Applications. *Nanoscale* **2017**, *9*, 10794−10801.
(716) Eriksson, R.; Kose, J.; Tacke, A. How Does Intrinsic Motivation Moderate The Effect of The Sustained Use of Wearable Fitness Technology?: A Quantitative Study. Master's Thesis. Linnaeus University, 2017.
(717) Proto, A.; Penhaker, M.; Conforto, S.; Schmid, M. Nanogenerators for Human Body Energy Harvesting. *Trends Biotechnol.* **2017**, *35*, 610−624.
(718) Wang, Z. L.; Wu, W. Nanotechnology-Enabled Energy Harvesting for Self-Powered Micro-/Nanosystems. *Angew. Chem., Int. Ed.* **2012**, *51*, 11700−11721.
(719) Radousky, H. B.; Liang, H. Energy Harvesting: An Integrated View of Materials, Devices and Applications. *Nanotechnology* **2012**, *23*, 502001.
(720) Sue, C. Y.; Tsai, N. C. Human Powered Mems-Based Energy Harvest Devices. *Appl. Energy* **2012**, *93*, 390−403.
(721) Misra, V.; Bozkurt, A.; Calhoun, B.; Jackson, T. N.; Jur, J. S.; Lach, J.; Lee, B.; Muth, J.; Oralkan, O.; Ozturk, M.; et al. Flexible Technologies for Self-Powered Wearable Health and Environmental Sensing. *Proc. IEEE* **2015**, *103*, 665−681.

DOI: 10.1021/acs.chemrev.8b00573
Chem. Rev. 2019, 119, 5461−5533

(722) Sun, H.; Zhang, Y.; Zhang, J.; Sun, X. M.; Peng, H. S. Energy Harvesting and Storage in 1d Devices. *Nat. Rev. Mater.* **2017**, *2*, 17023.
(723) Andreev, S.; Galinina, O.; Pyattaev, A.; Gerasimenko, M.; Tirronen, T.; Torsner, J.; Sachs, J.; Dohler, M.; Koucheryavy, Y. Understanding the Iot Connectivity Landscape: A Contemporary M2m Radio Technology Roadmap. *IEEE Commun. Mag.* **2015**, *53*, 32−40.
(724) Han, S.; Kim, J.; Won, S. M.; Ma, Y.; Kang, D.; Xie, Z.; Lee, K. T.; Chung, H. U.; Banks, A.; Min, S.; et al. Battery-Free, Wireless Sensors for Full-Body Pressure and Temperature Mapping. *Sci. Transl. Med.* **2018**, *10*, No. eaan4950.
(725) Kurs, A.; Karalis, A.; Moffatt, R.; Joannopoulos, J. D.; Fisher, P.; Soljacic, M. Wireless Power Transfer Via Strongly Coupled Magnetic Resonances. *Science* **2007**, *317*, 83−86.
(726) Cannon, B. L.; Hoburg, J. F.; Stancil, D. D.; Goldstein, S. C. Magnetic Resonant Coupling as a Potential Means for Wireless Power Transfer to Multiple Small Receivers. *IEEE Trans. Power Electron.* **2009**, *24*, 1819−1825.
(727) Fischer, J. Nfc in Cell Phones: The New Paradigm for an Interactive World [near-Field Communications]. *IEEE Commun. Mag.* **2009**, *47*, 22−28.
(728) Kim, J.; Banks, A.; Cheng, H.; Xie, Z.; Xu, S.; Jang, K. I.; Lee, J. W.; Liu, Z.; Gutruf, P.; Huang, X.; et al. Epidermal Electronics with Advanced Capabilities in near-Field Communication. *Small* **2015**, *11*, 906−912.
(729) Kim, J.; Banks, A.; Xie, Z.; Heo, S. Y.; Gutruf, P.; Lee, J. W.; Xu, S.; Jang, K. I.; Liu, F.; Brown, G.; et al. Miniaturized Flexible Electronic Systems with Wireless Power and near-Field Communication Capabilities. *Adv. Funct. Mater.* **2015**, *25*, 4761−4767.
(730) Lee, J. W.; Xu, R.; Lee, S.; Jang, K. I.; Yang, Y.; Banks, A.; Yu, K. J.; Kim, J.; Xu, S.; Ma, S.; et al. Soft, Thin Skin-Mounted Power Management Systems and Their Use in Wireless Thermography. *Proc. Natl. Acad. Sci. U. S. A.* **2016**, *113*, 6131−6136.
(731) Huang, X.; Liu, Y. H.; Kong, G. W.; Seo, J. H.; Ma, Y. J.; Jang, K. I.; Fan, J. A.; Mao, S. M.; Chen, Q. W.; Li, D. Z.; et al. Epidermal Radio Frequency Electronics for Wireless Power Transfer. *Microsyst. Nanoeng.* **2016**, *2*, 16052.
(732) Sample, A. P.; Yeager, D. J.; Powledge, P. S.; Mamishev, A. V.; Smith, J. R. Design of an Rfid-Based Battery-Free, Programmable Sensing Platform. *IEEE Trans. Instrum. Meas.* **2008**, *57*, 2608−2615.
(733) Park, S. I.; Brenner, D. S.; Shin, G.; Morgan, C. D.; Copits, B. A.; Chung, H. U.; Pullen, M. Y.; Noh, K. N.; Davidson, S.; Oh, S. J.; et al. Soft, Stretchable, Fully Implantable Miniaturized Optoelectronic Systems for Wireless Optogenetics. *Nat. Biotechnol.* **2015**, *33*, 1280−1286.
(734) Huang, K. B.; Zhou, X. Y. Cutting the Last Wires for Mobile Communications by Microwave Power Transfer. *IEEE Commun. Mag.* **2015**, *53*, 86−93.
(735) Hussain, A. M.; Ghaffar, F. A.; Park, S. I.; Rogers, J. A.; Shamim, A.; Hussain, M. M. Metal/Polymer Based Stretchable Antenna for Constant Frequency Far-Field Communication in Wearable Electronics. *Adv. Funct. Mater.* **2015**, *25*, 6565−6575.
(736) Ostfeld, A. E.; Arias, A. C. Flexible Photovoltaic Power Systems: Integration Opportunities, Challenges and Advances. *Flex. Print. Electron.* **2017**, *2*, No. 013001.
(737) Tsai, H.; Nie, W.; Blancon, J. C.; Stoumpos, C. C.; Asadpour, R.; Harutyunyan, B.; Neukirch, A. J.; Verduzco, R.; Crochet, J. J.; Tretiak, S.; et al. High-Efficiency Two-Dimensional Ruddlesden-Popper Perovskite Solar Cells. *Nature* **2016**, *536*, 312−316.
(738) Bernechea, M.; Miller, N. C.; Xercavins, G.; So, D.; Stavrinadis, A.; Konstantatos, G. Solution-Processed Solar Cells Based on Environmentally Friendly Agbis2 Nanocrystals. *Nat. Photonics* **2016**, *10*, 521−525.
(739) Sun, Y.; Welch, G. C.; Leong, W. L.; Takacs, C. J.; Bazan, G. C.; Heeger, A. J. Solution-Processed Small-Molecule Solar Cells with 6.7% Efficiency. *Nat. Mater.* **2012**, *11*, 44−48.
(740) Zhang, Q.; Kan, B.; Liu, F.; Long, G.; Wan, X.; Chen, X.; Zuo, Y.; Ni, W.; Zhang, H.; Li, M.; et al. Small-Molecule Solar Cells with Efficiency over 9%. *Nat. Photonics* **2015**, *9*, 35−41.
(741) Duan, C.; Zhang, K.; Zhong, C.; Huang, F.; Cao, Y. Recent Advances in Water/Alcohol-Soluble Pi-Conjugated Materials: New Materials and Growing Applications in Solar Cells. *Chem. Soc. Rev.* **2013**, *42*, 9071−9104.
(742) Peet, J.; Heeger, A. J.; Bazan, G. C. "Plastic" Solar Cells: Self-Assembly of Bulk Heterojunction Nanomaterials by Spontaneous Phase Separation. *Acc. Chem. Res.* **2009**, *42*, 1700−1708.
(743) Kaltenbrunner, M.; Adam, G.; Glowacki, E. D.; Drack, M.; Schwodiauer, R.; Leonat, L.; Apaydin, D. H.; Groiss, H.; Scharber, M. C.; White, M. S.; et al. Flexible High Power-Per-Weight Perovskite Solar Cells with Chromium Oxide-Metal Contacts for Improved Stability in Air. *Nat. Mater.* **2015**, *14*, 1032−1039.
(744) Mathew, S.; Yella, A.; Gao, P.; Humphry-Baker, R.; Curchod, B. F.; Ashari-Astani, N.; Tavernelli, I.; Rothlisberger, U.; Nazeeruddin, M. K.; Gratzel, M. Dye-Sensitized Solar Cells with 13% Efficiency Achieved through the Molecular Engineering of Porphyrin Sensitizers. *Nat. Chem.* **2014**, *6*, 242−247.
(745) Gunes, S.; Neugebauer, H.; Sariciftci, N. S. Conjugated Polymer-Based Organic Solar Cells. *Chem. Rev.* **2007**, *107*, 1324−1338.
(746) Chung, I.; Lee, B.; He, J.; Chang, R. P.; Kanatzidis, M. G. All-Solid-State Dye-Sensitized Solar Cells with High Efficiency. *Nature* **2012**, *485*, 486−489.
(747) Shah, A.; Torres, P.; Tscharner, R.; Wyrsch, N.; Keppner, H. Photovoltaic Technology: The Case for Thin-Film Solar Cells. *Science* **1999**, *285*, 692−698.
(748) Lee, J.; Wu, J.; Ryu, J. H.; Liu, Z.; Meitl, M.; Zhang, Y. W.; Huang, Y.; Rogers, J. A. Stretchable Semiconductor Technologies with High Areal Coverages and Strain-Limiting Behavior: Demonstration in High-Efficiency Dual-Junction Gainp/Gaas Photovoltaics. *Small* **2012**, *8*, 1851−1856.
(749) Nam, J.; Lee, Y.; Choi, W.; Kim, C. S.; Kim, H.; Kim, J.; Kim, D.-H.; Jo, S. Transfer Printed Flexible and Stretchable Thin Film Solar Cells Using a Water-Soluble Sacrificial Layer. *Adv. Energy Mater.* **2016**, *6*, 1601269.
(750) Jinno, H.; Fukuda, K.; Xu, X. M.; Park, S.; Suzuki, Y.; Koizumi, M.; Yokota, T.; Osaka, I.; Takimiya, K.; Someya, T. Stretchable and Waterproof Elastomer-Coated Organic Photovoltaics for Washable Electronic Textile Applications. *Nat. Energy* **2017**, *2*, 780−785.
(751) Hu, X.; Huang, Z.; Zhou, X.; Li, P.; Wang, Y.; Huang, Z.; Su, M.; Ren, W.; Li, F.; Li, M.; et al. Wearable Large-Scale Perovskite Solar-Power Source Via Nanocellular Scaffold. *Adv. Mater.* **2017**, *29*, 1703236.
(752) Park, S.; Heo, S. W.; Lee, W.; Inoue, D.; Jiang, Z.; Yu, K.; Jinno, H.; Hashizume, D.; Sekino, M.; Yokota, T.; et al. Self-Powered Ultra-Flexible Electronics Via Nano-Grating-Patterned Organic Photovoltaics. *Nature* **2018**, *561*, 516−521.
(753) He, Z. C.; Xiao, B.; Liu, F.; Wu, H. B.; Yang, Y. L.; Xiao, S.; Wang, C.; Russell, T. P.; Cao, Y. Single-Junction Polymer Solar Cells with High Efficiency and Photovoltage. *Nat. Photonics* **2015**, *9*, 174−179.
(754) Liao, S. H.; Jhuo, H. J.; Yeh, P. N.; Cheng, Y. S.; Li, Y. L.; Lee, Y. H.; Sharma, S.; Chen, S. A. Single Junction Inverted Polymer Solar Cell Reaching Power Conversion Efficiency 10.31% by Employing Dual-Doped Zinc Oxide Nano-Film as Cathode Interlayer. *Sci. Rep.* **2015**, *4*, 6813.
(755) Zhao, J. B.; Li, Y. K.; Yang, G. F.; Jiang, K.; Lin, H. R.; Ade, H.; Ma, W.; Yan, H. Efficient Organic Solar Cells Processed from Hydrocarbon Solvents. *Nat. Energy* **2016**, *1*, 15027.
(756) Liu, Y.; Zhao, J.; Li, Z.; Mu, C.; Ma, W.; Hu, H.; Jiang, K.; Lin, H.; Ade, H.; Yan, H. Aggregation and Morphology Control Enables Multiple Cases of High-Efficiency Polymer Solar Cells. *Nat. Commun.* **2014**, *5*, 5293.
(757) Yaffe, O.; Chernikov, A.; Norman, Z. M.; Zhong, Y.; Velauthapillai, A.; van der Zande, A.; Owen, J. S.; Heinz, T. F. Excitons in Ultrathin Organic-Inorganic Perovskite Crystals. *Phys. Rev. B: Condens. Matter Mater. Phys.* **2015**, *92*, No. e045414.
(758) Wang, G.; Li, D.; Cheng, H. C.; Li, Y.; Chen, C. Y.; Yin, A.; Zhao, Z.; Lin, Z.; Wu, H.; He, Q.; et al. Wafer-Scale Growth of Large

DOI: 10.1021/acs.chemrev.8b00573
Chem. Rev. 2019, 119, 5461−5533

Arrays of Perovskite Microplate Crystals for Functional Electronics and Optoelectronics. *Sci. Adv.* **2015**, *1*, No. e1500613.
(759) deQuilettes, D. W.; Vorpahl, S. M.; Stranks, S. D.; Nagaoka, H.; Eperon, G. E.; Ziffer, M. E.; Snaith, H. J.; Ginger, D. S. Ginger, D. S. Solar Cells. Impact of Microstructure on Local Carrier Lifetime in Perovskite Solar Cells. *Science* **2015**, *348*, 683−686.
(760) Yin, W. J.; Shi, T.; Yan, Y. Unique Properties of Halide Perovskites as Possible Origins of the Superior Solar Cell Performance. *Adv. Mater.* **2014**, *26*, 4653−4658.
(761) Stranks, S. D.; Eperon, G. E.; Grancini, G.; Menelaou, C.; Alcocer, M. J.; Leijtens, T.; Herz, L. M.; Petrozza, A.; Snaith, H. J. Electron-Hole Diffusion Lengths Exceeding 1 Micrometer in an Organometal Trihalide Perovskite Absorber. *Science* **2013**, *342*, 341−344.
(762) Wu, Z. W.; Li, P.; Zhang, Y. K.; Zheng, Z. J. Flexible and Stretchable Perovskite Solar Cells: Device Design and Development Methods. *Small Methods* **2018**, *2*, 1800031.
(763) Saliba, M.; Orlandi, S.; Matsui, T.; Aghazada, S.; Cavazzini, M.; Correa-Baena, J. P.; Gao, P.; Scopelliti, R.; Mosconi, E.; Dahmen, K. H.; et al. A Molecularly Engineered Hole-Transporting Material for Efficient Perovskite Solar Cells. *Nat. Energy* **2016**, *1*, 15017.
(764) Yang, W. S.; Noh, J. H.; Jeon, N. J.; Kim, Y. C.; Ryu, S.; Seo, J.; Seok, S. I. Solar Cells. High-Performance Photovoltaic Perovskite Layers Fabricated through Intramolecular Exchange. *Science* **2015**, *348*, 1234−1237.
(765) Shockley, W.; Queisser, H. J. Detailed Balance Limit of Efficiency of P-N Junction Solar Cells. *J. Appl. Phys.* **1961**, *32*, 510−519.
(766) Siddique, A. R. M.; Mahmud, S.; Van Heyst, B. A Review of the State of the Science on Wearable Thermoelectric Power Generators (Tegs) and Their Existing Challenges. *Renewable Sustainable Energy Rev.* **2017**, *73*, 730−744.
(767) Huynh, T. P.; Haick, H. Autonomous Flexible Sensors for Health Monitoring. *Adv. Mater.* **2018**, *30*, No. 1802337.
(768) Thielen, M.; Sigrist, L.; Magno, M.; Hierold, C.; Benini, L. Human Body Heat for Powering Wearable Devices: From Thermal Energy to Application. *Energy Convers. Manage.* **2017**, *131*, 44−54.
(769) Siddique, A. R. M.; Rabari, R.; Mahmud, S.; Van Heyst, B. Thermal Energy Harvesting from the Human Body Using Flexible Thermoelectric Generator (Fteg) Fabricated by a Dispenser Printing Technique. *Energy* **2016**, *115*, 1081−1091.
(770) Bubnova, O.; Khan, Z. U.; Malti, A.; Braun, S.; Fahlman, M.; Berggren, M.; Crispin, X. Optimization of the Thermoelectric Figure of Merit in the Conducting Polymer Poly(3,4-Ethylenedioxythiophene). *Nat. Mater.* **2011**, *10*, 429−433.
(771) Wei, Q. S.; Mukaida, M.; Kirihara, K.; Naitoh, Y.; Ishida, T. Polymer Thermoelectric Modules Screen-Printed on Paper. *RSC Adv.* **2014**, *4*, 28802−28806.
(772) Ito, M.; Koizumi, T.; Kojima, H.; Saito, T.; Nakamura, M. From Materials to Device Design of a Thermoelectric Fabric for Wearable Energy Harvesters. *J. Mater. Chem. A* **2017**, *5*, 12068−12072.
(773) Oh, J. Y.; Lee, J. H.; Han, S. W.; Chae, S. S.; Bae, E. J.; Kang, Y. H.; Choi, W. J.; Cho, S. Y.; Lee, J. O.; Baik, H. K.; et al. Chemically Exfoliated Transition Metal Dichalcogenide Nanosheet-Based Wearable Thermoelectric Generators. *Energy Environ. Sci.* **2016**, *9*, 1696−1705.
(774) Wan, C. L.; Tian, R. M.; Azizi, A. B.; Huang, Y. J.; Wei, Q. S.; Sasai, R.; Wasusate, S.; Ishida, T.; Koumoto, K. Flexible Thermoelectric Foil for Wearable Energy Harvesting. *Nano Energy* **2016**, *30*, 840−845.
(775) Tian, R. M.; Wan, C. L.; Wang, Y. F.; Wei, Q. S.; Ishida, T.; Yamamoto, A.; Tsuruta, A.; Shin, W. S.; Li, S.; Koumoto, K. A Solution-Processed Tis2/Organic Hybrid Superlattice Film Towards Flexible Thermoelectric Devices. *J. Mater. Chem. A* **2017**, *5*, 564−570.
(776) Poudel, B.; Hao, Q.; Ma, Y.; Lan, Y.; Minnich, A.; Yu, B.; Yan, X.; Wang, D.; Muto, A.; Vashaee, D.; et al. High-Thermoelectric Performance of Nanostructured Bismuth Antimony Telluride Bulk Alloys. *Science* **2008**, *320*, 634−638.
(777) Francioso, L.; De Pascali, C.; Farella, I.; Martucci, C.; Creti, P.; Siciliano, P.; Perrone, A. Flexible Thermoelectric Generator for Ambient Assisted Living Wearable Biometric Sensors. *J. Power Sources* **2011**, *196*, 3239−3243.
(778) Aich, R. B.; Blouin, N.; Bouchard, A.; Leclerc, M. Electrical and Thermoelectric Properties of Poly(2,7-Carbazole) Derivatives. *Chem. Mater.* **2009**, *21*, 751−757.
(779) Blackburn, J. L.; Ferguson, A. J.; Cho, C.; Grunlan, J. C. Carbon-Nanotube-Based Thermoelectric Materials and Devices. *Adv. Mater.* **2018**, *30*, 1704386.
(780) Lee, K.; Cho, S.; Park, S. H.; Heeger, A. J.; Lee, C. W.; Lee, S. H. Metallic Transport in Polyaniline. *Nature* **2006**, *441*, 65−68.
(781) Nardes, A. M.; Kemerink, M.; Janssen, R. A. J.; Bastiaansen, J. A. M.; Kiggen, N. M. M.; Langeveld, B. M. W.; van Breemen, A. J. J. M.; de Kok, M. M. Microscopic Understanding of the Anisotropic Conductivity of Pedot: Pss Thin Films. *Adv. Mater.* **2007**, *19*, 1196−1200.
(782) Eftekhari, A.; Kazemzad, M.; Keyanpour-Rad, M. Significant Effect of Dopant Size on Nanoscale Fractal Structure of Polypyrrole Film. *Polym. J.* **2006**, *38*, 781−785.
(783) Kim, G. H.; Shao, L.; Zhang, K.; Pipe, K. P. Engineered Doping of Organic Semiconductors for Enhanced Thermoelectric Efficiency. *Nat. Mater.* **2013**, *12*, 719−723.
(784) He, M.; Zhao, L.; Wang, J.; Han, W.; Yang, Y.; Qiu, F.; Lin, Z. Self-Assembly of All-Conjugated Poly(3-Alkylthiophene) Diblock Copolymer Nanostructures from Mixed Selective Solvents. *ACS Nano* **2010**, *4*, 3241−3247.
(785) Zhang, Q.; Sun, Y.; Xu, W.; Zhu, D. Organic Thermoelectric Materials: Emerging Green Energy Materials Converting Heat to Electricity Directly and Efficiently. *Adv. Mater.* **2014**, *26*, 6829−6851.
(786) Avery, A. D.; Zhou, B. H.; Lee, J.; Lee, E. S.; Miller, E. M.; Ihly, R.; Wesenberg, D.; Mistry, K. S.; Guillot, S. L.; Zink, B. L.; et al. Tailored Semiconducting Carbon Nanotube Networks with Enhanced Thermoelectric Properties. *Nat. Energy* **2016**, *1*, 16033.
(787) Cho, C.; Wallace, K. L.; Tzeng, P.; Hsu, J. H.; Yu, C.; Grunlan, J. C. Outstanding Low Temperature Thermoelectric Power Factor from Completely Organic Thin Films Enabled by Multidimensional Conjugated Nanomaterials. *Adv. Energy Mater.* **2016**, *6*, 1502168.
(788) Rojas, J. P.; Conchouso, D.; Arevalo, A.; Singh, D.; Foulds, I. G.; Hussain, M. M. Paper-Based Origami Flexible and Foldable Thermoelectric Nanogenerator. *Nano Energy* **2017**, *31*, 296−301.
(789) Madan, D.; Wang, Z. Q.; Wright, P. K.; Evans, J. W. Printed Flexible Thermoelectric Generators for Use on Low Levels of Waste Heat. *Appl. Energy* **2015**, *156*, 587−592.
(790) Kim, C. S.; Lee, G. S.; Choi, H.; Kim, Y. J.; Yang, H. M.; Lim, S. H.; Lee, S. G.; Cho, B. J. Structural Design of a Flexible Thermoelectric Power Generator for Wearable Applications. *Appl. Energy* **2018**, *214*, 131−138.
(791) Suarez, F.; Parekh, D. P.; Ladd, C.; Vashaee, D.; Dickey, M. D.; Ozturk, M. C. Flexible Thermoelectric Generator Using Bulk Legs and Liquid Metal Interconnects for Wearable Electronics. *Appl. Energy* **2017**, *202*, 736−745.
(792) Kim, C. S.; Yang, H. M.; Lee, J.; Lee, G. S.; Choi, H.; Kim, Y. J.; Lim, S. H.; Cho, S. H.; Cho, B. J. Self-Powered Wearable Electrocardiography Using a Wearable Thermoelectric Power Generator. *ACS Energy Lett.* **2018**, *3*, 501−507.
(793) Suarez, F.; Nozariasbmarz, A.; Vashaee, D.; Ozturk, M. C. Designing Thermoelectric Generators for Self-Powered Wearable Electronics. *Energy Environ. Sci.* **2016**, *9*, 2099−2113.
(794) Kim, S. J.; We, J. H.; Cho, B. J. A Wearable Thermoelectric Generator Fabricated on a Glass Fabric. *Energy Environ. Sci.* **2014**, *7*, 1959−1965.
(795) Dagdeviren, C.; Li, Z.; Wang, Z. L. Energy Harvesting from the Animal/Human Body for Self-Powered Electronics. *Annu. Rev. Biomed. Eng.* **2017**, *19*, 85−108.
(796) Huang, Y. A.; Ding, Y. J.; Bian, J.; Su, Y. W.; Zhou, J.; Duan, Y. Q.; Yin, Z. P. Hyper-Stretchable Self-Powered Sensors Based on Electrohydrodynamically Printed, Self-Similar Piezoelectric Nano/Microfibers. *Nano Energy* **2017**, *40*, 432−439.
(797) Lee, M.; Chen, C. Y.; Wang, S.; Cha, S. N.; Park, Y. J.; Kim, J. M.; Chou, L. J.; Wang, Z. L. A Hybrid Piezoelectric Structure for

DOI: 10.1021/acs.chemrev.8b00573
Chem. Rev. 2019, 119, 5461−5533

Wearable Nanogenerators (Vol 24, Pg 1759, 2012). *Adv. Mater.* **2012**, *24*, 5283−5283.
(798) Chun, J.; Kang, N. R.; Kim, J. Y.; Noh, M. S.; Kang, C. Y.; Choi, D.; Kim, S. W.; Wang, Z. L.; Baik, J. M. Highly Anisotropic Power Generation in Piezoelectric Hemispheres Composed Stretchable Composite Film for Self-Powered Motion Sensor. *Nano Energy* **2015**, *11*, 1−10.
(799) Zhang, M.; Gao, T.; Wang, J. S.; Liao, J. J.; Qiu, Y. Q.; Yang, Q.; Xue, H.; Shi, Z.; Zhao, Y.; Xiong, Z. X.; et al. A Hybrid Fibers Based Wearable Fabric Piezoelectric Nanogenerator for Energy Harvesting Application. *Nano Energy* **2015**, *13*, 298−305.
(800) Jeong, C. K.; Lee, J.; Han, S.; Ryu, J.; Hwang, G. T.; Park, D. Y.; Park, J. H.; Lee, S. S.; Byun, M.; Ko, S. H.; et al. A Hyper-Stretchable Elastic-Composite Energy Harvester. *Adv. Mater.* **2015**, *27*, 2866−2875.
(801) Zheng, Q.; Shi, B.; Li, Z.; Wang, Z. L. Recent Progress on Piezoelectric and Triboelectric Energy Harvesters in Biomedical Systems. *Adv. Sci.* **2017**, *4*, 1700029.
(802) Niu, S. M.; Wang, Z. L. Theoretical Systems of Triboelectric Nanogenerators. *Nano Energy* **2015**, *14*, 161−192.
(803) Wang, Z. L. Triboelectric Nanogenerators as New Energy Technology and Self-Powered Sensors - Principles, Problems and Perspectives. *Faraday Discuss.* **2014**, *176*, 447−458.
(804) Kim, S.; Gupta, M. K.; Lee, K. Y.; Sohn, A.; Kim, T. Y.; Shin, K. S.; Kim, D.; Kim, S. K.; Lee, K. H.; Shin, H. J.; et al. Transparent Flexible Graphene Triboelectric Nanogenerators. *Adv. Mater.* **2014**, *26*, 3918−3925.
(805) Chandrashekar, B. N.; Deng, B.; Smitha, A. S.; Chen, Y.; Tan, C.; Zhang, H.; Peng, H.; Liu, Z. Roll-to-Roll Green Transfer of Cvd Graphene onto Plastic for a Transparent and Flexible Triboelectric Nanogenerator. *Adv. Mater.* **2015**, *27*, 5210−5216.
(806) Chen, S.; Huang, T.; Zuo, H.; Qian, S.; Guo, Y.; Sun, L.; Lei, D.; Wu, Q.; Zhu, B.; He, C.; et al. A Single Integrated 3d-Printing Process Customizes Elastic and Sustainable Triboelectric Nanogenerators for Wearable Electronics. *Adv. Funct. Mater.* **2018**, *28*, 1805108.
(807) Wang, S.; Lin, L.; Wang, Z. L. Nanoscale Triboelectric-Effect-Enabled Energy Conversion for Sustainably Powering Portable Electronics. *Nano Lett.* **2012**, *12*, 6339−6346.
(808) Tang, W.; Zhou, T.; Zhang, C.; Fan, F. R.; Han, C. B.; Wang, Z. L. A Power-Transformed-and-Managed Triboelectric Nanogenerator and Its Applications in a Self-Powered Wireless Sensing Node. *Nanotechnology* **2014**, *25*, 225402.
(809) Zhao, L. M.; Zheng, Q.; Ouyang, H.; Li, H.; Yan, L.; Shi, B. J.; Li, Z. A Size-Unlimited Surface Microstructure Modification Method for Achieving High Performance Triboelectric Nanogenerator. *Nano Energy* **2016**, *28*, 172−178.
(810) Lin, L.; Xie, Y.; Wang, S.; Wu, W.; Niu, S.; Wen, X.; Wang, Z. L. Triboelectric Active Sensor Array for Self-Powered Static and Dynamic Pressure Detection and Tactile Imaging. *ACS Nano* **2013**, *7*, 8266−8274.
(811) Park, S.; Kim, H.; Vosgueritchian, M.; Cheon, S.; Kim, H.; Koo, J. H.; Kim, T. R.; Lee, S.; Schwartz, G.; Chang, H.; et al. Stretchable Energy-Harvesting Tactile Electronic Skin Capable of Differentiating Multiple Mechanical Stimuli Modes. *Adv. Mater.* **2014**, *26*, 7324−7332.
(812) Pu, X.; Liu, M.; Chen, X.; Sun, J.; Du, C.; Zhang, Y.; Zhai, J.; Hu, W.; Wang, Z. L. Ultrastretchable, Transparent Triboelectric Nanogenerator as Electronic Skin for Biomechanical Energy Harvesting and Tactile Sensing. *Sci. Adv.* **2017**, *3*, No. e1700015.
(813) Bandodkar, A. J.; You, J. M.; Kim, N. H.; Gu, Y.; Kumar, R.; Mohan, A. M. V.; Kurniawan, J.; Imani, S.; Nakagawa, T.; Parish, B.; et al. Soft, Stretchable, High Power Density Electronic Skin-Based Biofuel Cells for Scavenging Energy from Human Sweat. *Energy Environ. Sci.* **2017**, *10*, 1581−1589.
(814) Reid, R. C.; Minteer, S. D.; Gale, B. K. Contact Lens Biofuel Cell Tested in a Synthetic Tear Solution. *Biosens. Bioelectron.* **2015**, *68*, 142−148.
(815) Wang, H.; Wang, X. Y.; Barfidokht, A.; Park, J.; Wang, J.; Mercier, P. P. A Battery-Powered Wireless Ion Sensing System Consuming 5.5 Nw of Average Power. *IEEE J. Solid-State Circuits* **2018**, *53*, 2043−2053.
(816) Zhang, X.; Zhang, Z.; Li, Y.; Liu, C.; Guo, Y. X.; Lian, Y. A 2.89 uW Dry-Electrode Enabled Clockless Wireless Ecg Soc for Wearable Applications. *IEEE J. Solid-State Circuits* **2016**, *51*, 2287−2298.
(817) Shaikh, F. K.; Zeadally, S. Energy Harvesting in Wireless Sensor Networks: A Comprehensive Review. *Renewable Sustainable Energy Rev.* **2016**, *55*, 1041−1054.
(818) Bartsch, A.; Samorezov, S.; Benzel, E.; Miele, V.; Brett, D. Validation of an "Intelligent Mouthguard" Single Event Head Impact Dosimeter. *SAE Tech. Pap. Ser.* **2014**, *58*, 1.
(819) Liu, Y.; Tian, L.; Raj, M. S.; Cotton, M.; Ma, Y.; Ma, S.; McGrane, B.; Pendharkar, A. V.; Dahaleh, N.; Olson, L.; et al. Intraoperative Monitoring of Neuromuscular Function with Soft, Skin-Mounted Wireless Devices. *NPJ. Digit. Med.* **2018**, *1*, 19.
(820) Rogers, J. A.; Malliaras, G. G.; Someya, T. Biomedial Devices Go Wild. *Sci. Adv.* **2018**, *4*, eaav1889.
(821) *L'Oréal Advances Its Commitment to Promoting Sun Safety with La Roche-Posay UV Sense, the First Battery-Free Wearable Electronic UV Sensor*; L'Oréal, 2018; http://www.lorealusa.com/media/press-releases/2018/january/uv-sense (accessed Dec 7, 2018).
(822) *My UV Patch*; L'Oréal, 2019; https://www.laroche-posay.us/my-uv-patch (accessed Dec 7, 2018).
(823) *Monica Novii Wireless Patch System*; General Electric Company, 2018; https://www.gehealthcare.com/en/products/maternal-infant-care/fetal-monitors/monica-novii-wireless-patch-system (accessed Dec 7, 2018).
(824) *Biostamp nPoint*; mc10; 2018; https://www.mc10inc.com (accessed Dec 7, 2018).
(825) *The Prevent System*; Prevent Biometrics, 2018; https://preventbiometrics.com/the-system (accessed Dec 7, 2018).
(826) *Vital Patch Home Page*; VitalConnect, 2018; https://vitalconnect.com/solutions/vitalpatch/, (accessed Dec 7, 2018).
(827) *Why Zio*; iRhythm Technologies, Inc., 2018; https://www.irhythmtech.com/professionals/why-zio (accessed Dec 7, 2018).
(828) Coyle, S.; Curto, V. F.; Benito-Lopez, F.; Florea, L.; Diamond, D. Wearable Bio and Chemical Sensors. In *Wearable Sensors*; Elsevier, 2015; 65−83.
(829) Imani, S.; Mercier, P. P.; Bandodkar, A. J.; Kim, J.; Wang, J. Wearable Chemical Sensors: Opportunities and Challenges. *2016 IEEE International Symposium on Circuits and Systems (ISCAS)*, 2016; pp 1122−1125.
(830) Manz, A.; Graber, N.; Widmer, H. M. Miniaturized Total Chemical-Analysis Systems - a Novel Concept for Chemical Sensing. *Sens. Actuators, B* **1990**, *1*, 244−248.
(831) Liu, Y.-L.; Liu, R.; Qin, Y.; Qiu, Q.-F.; Chen, Z.; Cheng, S.-B.; Huang, W.-H. Flexible Electrochemical Urea Sensor Based on Surface Molecularly Imprinted Nanotubes for Detection of Human Sweat. *Anal. Chem.* **2018**, *90*, 13081−13087.
(832) Lugg, J. W. H.; Ellis, F. P. Some Water-Soluble Vitamins in the Sweat of Tropically Acclimatized European Men. *Br. J. Nutr.* **1954**, *8*, 71−77.
(833) Hadorn, B.; Hanimann, F.; Anders, P.; Curtius, H. C.; Halverson, R. Free Amino-Acids in Human Sweat from Different Parts of the Body. *Nature* **1967**, *215*, 416−417.
(834) Chinevere, T. D.; Kenefick, R. W.; Cheuvront, S. N.; Lukaski, H. C.; Sawka, M. N. Effect of Heat Acclimation on Sweat Minerals. *Med. Sci. Sports Exercise* **2008**, *40*, 886−891.
(835) Lu, R.; Li, W. W.; Mizaikoff, B.; Katzir, A.; Raichlin, Y.; Sheng, G. P.; Yu, H. Q. High-Sensitivity Infrared Attenuated Total Reflectance Sensors for in Situ Multicomponent Detection of Volatile Organic Compounds in Water. *Nat. Protoc.* **2016**, *11*, 377−386.
(836) Loyprasert, S.; Hedstrom, M.; Thavarungkul, P.; Kanatharana, P.; Mattiasson, B. Sub-Attomolar Detection of Cholera Toxin Using a Label-Free Capacitive Immunosensor. *Biosens. Bioelectron.* **2010**, *25*, 1977−1983.
(837) Wang, J. Electrochemical Sensing of Explosives. In *Counter-terrorist Detection Techniques of Explosives*; Elsevier, 2007; pp 91−107.

DOI: 10.1021/acs.chemrev.8b00573
Chem. Rev. 2019, 119, 5461−5533

(838) Emrani, A. S.; Danesh, N. M.; Ramezani, M.; Taghdisi, S. M.; Abnous, K. A Novel Fluorescent Aptasensor Based on Hairpin Structure of Complementary Strand of Aptamer and Nanoparticles as a Signal Amplification Approach for Ultrasensitive Detection of Cocaine. *Biosens. Bioelectron.* **2016**, *79*, 288−293.
(839) Musso, J.; Buchmann, W.; Gonnet, F.; Jarroux, N.; Bellon, S.; Frydman, C.; Brunet, D. L.; Daniel, R. Biomarkers Probed in Saliva by Surface Plasmon Resonance Imaging Coupled to Matrix-Assisted Laser Desorption/Ionization Mass Spectrometry in Array Format. *Anal. Bioanal. Chem.* **2015**, *407*, 1285−1294.
(840) Matharu, Z.; Bandodkar, A. J.; Gupta, V.; Malhotra, B. D. Fundamentals and Application of Ordered Molecular Assemblies to Affinity Biosensing. *Chem. Soc. Rev.* **2012**, *41*, 1363−1402.
(841) Palleau, E.; Reece, S.; Desai, S. C.; Smith, M. E.; Dickey, M. D. Self-Healing Stretchable Wires for Reconfigurable Circuit Wiring and 3d Microfluidics. *Adv. Mater.* **2013**, *25*, 1589−1592.
(842) Cai, G.; Wang, J.; Qian, K.; Chen, J.; Li, S.; Lee, P. S. Extremely Stretchable Strain Sensors Based on Conductive Self-Healing Dynamic Cross-Links Hydrogels for Human-Motion Detection. *Adv. Sci.* **2017**, *4*, 1600190.
(843) Cho, S. H.; White, S. R.; Braun, P. V. Self-Healing Polymer Coatings. *Adv. Mater.* **2009**, *21*, 645−649.
(844) Lin, S.; Yuk, H.; Zhang, T.; Parada, G. A.; Koo, H.; Yu, C.; Zhao, X. Stretchable Hydrogel Electronics and Devices. *Adv. Mater.* **2016**, *28*, 4497−4505.
(845) Blaiszik, B. J.; Kramer, S. L. B.; Olugebefola, S. C.; Moore, J. S.; Sottos, N. R.; White, S. R. Self-Healing Polymers and Composites. *Annu. Rev. Mater. Res.* **2010**, *40*, 179−211.
(846) Liu, Y. J.; Cao, W. T.; Ma, M. G.; Wan, P. Ultrasensitive Wearable Soft Strain Sensors of Conductive, Self-Healing, and Elastic Hydrogels with Synergistic "Soft and Hard" Hybrid Networks. *ACS Appl. Mater. Interfaces* **2017**, *9*, 25559−25570.
(847) Cao, P. F.; Li, B. R.; Hong, T.; Townsend, J.; Qiang, Z.; Xing, K. Y.; Vogiatzis, K. D.; Wang, Y. Y.; Mays, J. W.; Sokolov, A. P.; et al. Superstretchable, Self-Healing Polymeric Elastomers with Tunable Properties. *Adv. Funct. Mater.* **2018**, *28*, 1800741.
(848) Son, D.; Kang, J.; Vardoulis, O.; Kim, Y.; Matsuhisa, N.; Oh, J. Y.; To, J. W. F.; Mun, J. W.; Katsumata, T.; Liu, Y. X.; et al. An Integrated Self-Healable Electronic Skin System Fabricated Via Dynamic Reconstruction of a Nanostructured Conducting Network. *Nat. Nanotechnol.* **2018**, *13*, 1057−1065.
(849) Liu, X. H.; Lu, C. H.; Wu, X. D.; Zhang, X. X. Self-Healing Strain Sensors Based on Nanostructured Supramolecular Conductive Elastomers. *J. Mater. Chem. A* **2017**, *5*, 9824−9832.
(850) Zhu, C.; Fu, Y.; Liu, C.; Liu, Y.; Hu, L.; Liu, J.; Bello, I.; Li, H.; Liu, N.; Guo, S.; et al. Carbon Dots as Fillers Inducing Healing/Self-Healing and Anticorrosion Properties in Polymers. *Adv. Mater.* **2017**, *29*, 1701399.
(851) Huynh, T. P.; Sonar, P.; Haick, H. Advanced Materials for Use in Soft Self-Healing Devices. *Adv. Mater.* **2017**, *29*, 1604973.
(852) Sun, J.; Pu, X.; Liu, M.; Yu, A.; Du, C.; Zhai, J.; Hu, W.; Wang, Z. L. Self-Healable, Stretchable, Transparent Triboelectric Nanogenerators as Soft Power Sources. *ACS Nano* **2018**, *12*, 6147−6155.
(853) Yang, W.; Chen, I. H.; Mckittrick, J.; Meyers, M. A. Flexible Dermal Armor in Nature. *JOM* **2012**, *64*, 475−485.
(854) Naleway, S. E.; Porter, M. M.; McKittrick, J.; Meyers, M. A. Structural Design Elements in Biological Materials: Application to Bioinspiration. *Adv. Mater.* **2015**, *27*, 5455−5476.
(855) Kim, S.; Su, Y.; Mihi, A.; Lee, S.; Liu, Z.; Bhandakkar, T. K.; Wu, J.; Geddes, J. B., 3rd; Johnson, H. T.; Zhang, Y.; et al. Imbricate Scales as a Design Construct for Microsystem Technologies. *Small* **2012**, *8*, 901−906 785. .
(856) Yang, H.; Yu, J.; Zo, H.; Choi, M. User Acceptance of Wearable Devices: An Extended Perspective of Perceived Value. *Telemat Inform* **2016**, *33*, 256−269.
(857) Pang, S.; Hernandez, Y.; Feng, X.; Mullen, K. Graphene as Transparent Electrode Material for Organic Electronics. *Adv. Mater.* **2011**, *23*, 2779−2795.
(858) Gilshteyn, E. P.; Lin, S.; Kondrashov, V. A.; Kopylova, D. S.; Tsapenko, A. P.; Anisimov, A. S.; Hart, A. J.; Zhao, X.; Nasibulin, A. G. A One-Step Method of Hydrogel Modification by Single-Walled Carbon Nanotubes for Highly Stretchable and Transparent Electronics. *ACS Appl. Mater. Interfaces* **2018**, *10*, 28069−28075.
(859) Zhou, Q. T.; Park, J. G.; Kim, K. N.; Thokchom, A. K.; Bae, J.; Baik, J. M.; Kim, T. Transparent-Flexible-Multimodal Triboelectric Nanogenerators for Mechanical Energy Harvesting and Self-Powered Sensor Applications. *Nano Energy* **2018**, *48*, 471−480.
(860) Fan, F. R.; Lin, L.; Zhu, G.; Wu, W.; Zhang, R.; Wang, Z. L. Transparent Triboelectric Nanogenerators and Self-Powered Pressure Sensors Based on Micropatterned Plastic Films. *Nano Lett.* **2012**, *12*, 3109−3114.

DOI: 10.1021/acs.chemrev.8b00573
Chem. Rev. 2019, 119, 5461−5533